Ligand design and its influence on the photophysical and structural properties of dinuclear and tetranuclear copper and silver complexes

by

Jordan Robert Gipper

A.S., Highland Community College (IL), 2016
B.S., University of Wyoming, 2018

AN ABSTRACT OF A DISSERTATION

submitted in partial fulfillment of the requirements for the degree

DOCTOR OF PHILOSOPHY

Department of Chemistry
College of Arts and Sciences

KANSAS STATE UNIVERSITY
Manhattan, Kansas

2025

Abstract

Fluorescent molecules are used in a vast range of applications such as in organic light-emitting diodes (OLEDs) and thermally activated delayed fluorescence (TADF) emitters; however, many promising candidates lack the ability to fluoresce in the solid state which is needed in the manufacturing of these materials. Herein, the synthesis of a novel bidentate ligand, 2-methyl-*N*-((5-(2-(thiophen-2-yl)propan-2-yl)-1*H*-pyrrol-2-yl)methyl)propan-2-amine or **SNNH^{t}Bu,** and the corresponding dinuclear copper (I) and silver (I) complexes are reported with metal-metal bond interactions of 2.686 Å for **[CuSNNH^{t}Bu]$_2$** and 2.88 Å for **[AgSNNH^{t}Bu]$_2$**.

OLEDs and thermally activated delayed fluorescent (TADF) emitters are becoming a more common feature used in display technologies. A desire to move away from heavy and rare earth metals has made Copper (I) or Cu^I a desirable alternative. However, fine tuning of the excitation and emission properties of these complexes is of high importance. As such, we report the structural modification of a previously reported thiophene containing SNN dincuclear Cu^I complex. The synthesis, characterization, and fluorescent properties of two new ligands are investigated. Coordination of these two new ligands along with **NNH^{t}Bu** to Cu^I are conducted. These three new dinuclear Cu^I complexes are synthesized, characterized and their fluorescent and structural properties are compared and contrasted against themselves and the parent compound of **[CuSNNH^{t}Bu]$_2$**.

Copper assemblies play a vital role in biologal and synthetic processes alike. A recent advancement in extended metal chain assemblies has received significant attention due to their application in small molecule activation, in multielectron processes, and fluorescence. Schiff-base calix[2]pyrrole complexes for nickel (II) and palladium (II) have been previously reported

for their use in hydrogen evolution. Herein, the utilization of symmetrical and unsymmetrical Schiff-base calix[2]pyrroles for coordination of Cu (I) to synthesize tetranuclear complexes is explored. By varying the substituents at the quaternary carbon, it was found that two different assemblies, either a distorted square-planar or a bent tetranuclear linear chain assembly were formed. Investigations also include looking into the effects of the imine on the system.

Ligand design and its influence on the photophysical and structural properties of dinuclear and tetranuclear copper and silver complexes

by

Jordan Robert Gipper

A.S., Highland Community College (IL), 2016
B.S., University of Wyoming, 2018

A DISSERTATION

submitted in partial fulfillment of the requirements for the degree

DOCTOR OF PHILOSOPHY

Department of Chemistry
College of Arts and Science

KANSAS STATE UNIVERSITY
Manhattan, Kansas

2025

Approved by:

Major Professor
Dr. Ryan Rafferty

Copyright

Abstract

Fluorescent molecules are used in a vast range of applications such as in organic light-emitting diodes (OLEDs) and thermally activated delayed fluorescence (TADF) emitters; however, many promising candidates lack the ability to fluoresce in the solid state which is needed in the manufacturing of these materials. Herein, the synthesis of a novel bidentate ligand, 2-methyl-*N*-((5-(2-(thiophen-2-yl)propan-2-yl)-1*H*-pyrrol-2-yl)methyl)propan-2-amine or **SNNH^{t}Bu,** and the corresponding dinuclear copper (I) and silver (I) complexes are reported with metal-metal bond interactions of 2.686 Å for **[CuSNNH^{t}Bu]$_2$** and 2.88 Å for **[AgSNNH^{t}Bu]$_2$**.

OLEDs and thermally activated delayed fluorescent (TADF) emitters are becoming a more common feature used in display technologies. A desire to move away from heavy and rare earth metals has made Copper (I) or Cu^{I} a desirable alternative. However, fine tuning of the excitation and emission properties of these complexes is of high importance. As such, we report the structural modification of a previously reported thiophene containing SNN dincuclear Cu^{I} complex. The synthesis, characterization, and fluorescent properties of two new ligands are investigated. Coordination of these two new ligands along with **NNH^{t}Bu** to Cu^{I} are conducted. These three new dinuclear Cu^{I} complexes are synthesized, characterized and their fluorescent and structural properties are compared and contrasted against themselves and the parent compound of **[CuSNNH^{t}Bu]$_2$**.

Copper assemblies play a vital role in biologal and synthetic processes alike. A recent advancement in extended metal chain assemblies has received significant attention due to their application in small molecule activation, in multielectron processes, and fluorescence. Schiff-base calix[2]pyrrole complexes for nickel (II) and palladium (II) have been previously reported

for their use in hydrogen evolution. Herein, the utilization of symmetrical and unsymmetrical Schiff-base calix[2]pyrroles for coordination of Cu (I) to synthesize tetranuclear complexes is explored. By varying the substituents at the quaternary carbon, it was found that two different assemblies, either a distorted square-planar or a bent tetranuclear linear chain assembly were formed. Investigations also include looking into the effects of the imine on the system.

Table of Contents

List of Figures

List of Tables

List of Schemes

Acknowledgements

I would like to acknowledge the two professors that helped me through this Professor Peter Sues and Professor Ryan Rafferty. I like to thank my wonderful girlfriend Dr. Ivina Mali for all her help and support. I truly couldn't have done this without her. I would also like to thank all of my friends and family that have been with me through this colorful time at K-State. Finally, I would like to acknowledge Dr. Logan Trowbridge, Dr. Arnaldo Hernandez, Dr. Boris Averkiev, Bart Bath, and, last but not least, Jim Hodgson. Due to their daily jokes and shenanigans, they made K-State a mildly tolerable place.

Chapter 1 - Luminescent Dinuclear Cuprophilic Complexes

1.1. Introduction

Light has captivated humanity and scientists since the dawn of early history and of rational thought. From first recordings of being studied in ancient Greece to modern-day, scientists have unraveled many of the mysteries surrounding this fundamental aspect of our universe.[1] As a form of electromagnetic radiation, light is generally defined as the electromagnetic spectrum which can be perceived by the eye in the visible region (400-700 nm). Not only contributing to the colors we perceive, but light also influences numerous biological processes such as photosynthesis,[2–4] circadian rhythms,[5–7] and vitamin D synthesis.[8–11] Understanding light's properties has paved the way for significant scientific discoveries, advances, and applications.

1.1.1. Luminescence

Two intriguing phenomenon associated with light are fluorescence and phosphorescence: a process in which a substance absorbs light at a specific wavelength and then re-emits it at a longer wavelength. Chemicals or materials that possess the ability to emit light in this fashion are often referred to as lumiphores. These phenomenon are often represented and depicted graphically by what is known as a Jablonski diagram (**Figure 1.1.**) which shows a molecule's electronic states and the transitions between those states.[12,13] While the Jablonski diagram is typically used to depict electronic and vibronic states and transitions between these states in both the singlet and triplet for simple organic molecules, it can also be used for general representation of inorganic complexes.[14] Most lumiphores are typically in a singlet ground state ($\mathbf{S_0}$) meaning that all of their electrons are paired, and the resulting total spin angular momentum is zero. When energy in the form of a photon is absorbed by a lumiphore, an electron, typically in the highest occupied molecular orbital (HOMO) or $\mathbf{S_0}$, can be excited to a higher energy unoccupied orbital ($\mathbf{S_1}$ or $\mathbf{S_2}$) where $\mathbf{S_1}$ is

commonly referred to as the lowest unoccupied molecular orbital (LUMO). From these states, various transitions can occur such as nonradiative relaxation (wavy lines representing vibrational relaxation) or radiative transitions (dotted lines representing internal conversion (IC) or intersystem crossing (ISC)). If the excited electron remains in an excited singlet state and relaxes radiatively to $\mathbf{S_0}$, light is emitted in the form of fluorescence. However, if the excited electron undergoes ISC to a triplet state ($\mathbf{T_1}$) followed by a radiative relaxation, light will be emitted as phosphorescence. One of the key differences between fluorescence and phosphorescence is that when a fluorescent material stops being excited, the emission will stop almost immediately. That is to say the lifespan of the excited state is short lived, typically in the order of nanoseconds for fluorescence or microseconds to milliseconds for phosphorescence. On the other hand, phosphorescent materials will typically continue to glow for a noticeable period of time afterwards due to the spin-forbidden nature of the transition.

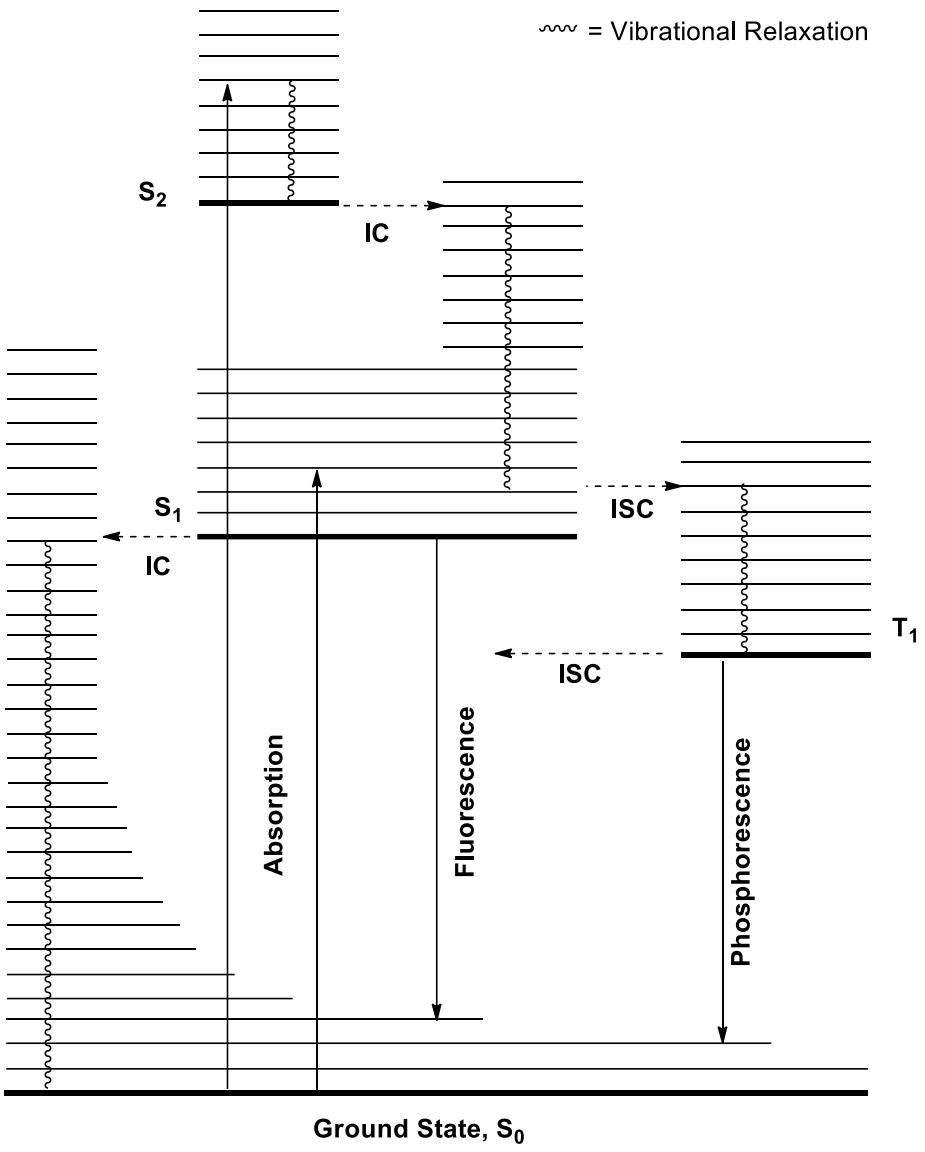

Figure 1.1. Jablonski Diagram

1.1.2. Application of Lumiphores

Many lumiphores have found applications as biological imaging agents, diagnostic tools, fluorescent and phosphorescent dyes or markers, and their use in visualization and studying of complex systems.[15–18] Another important area of application for lumiphores is in light sources, optoelectronic devices and displays. Since the first functional organic light-emitting diodes (OLED) were introduced by Tang and Van Slyke in 1987, OLEDs have seen a significant amount

of interest and growth.[19,20] With an initial quantum efficiency (QE) of 1%, much attention has been put into improving the efficiency and selectivity of output color of these systems.

The QE is defined as the number of photons emitted by a material divided by the number of photons absorbed. To understand why many lumiphores often have poor QE, it is important to first discuss the concept of spin statistics governed by the Boltzmann distribution. According to quantum mechanics, one combination of paired electrons is possible giving a singlet; however, there are three combinations of these electrons that give a triplet. Therefore, in terms of statistical limits, 25% of the excited electrons are in the singlet state while 75% are in the triplet state.[21] For simple organic molecules, they can only harvest the singlet electrons since the transition from triplet to singlet is spin forbidden resulting in these triplet electrons undergoing non-radiative transitions.

The early strategies to increase QE were the incorporation of transition metals as they often have stronger spin-orbit coupling that allows for more efficient intersystem crossing and can harvest the excited electrons either as singlets or as triplets. This has allowed for some metal complexes to achieve near 100% QE even at ambient temperatures.[22–24] Although these lumiphores have high QE, they typically utilize heavy, rare, expensive and toxic transition metals such as iridium,[22–28] osmium,[29] or platinum (**Figure 1.2.**). [30–32] Recent advancement and research in the field have concentrated on developing alternatives to traditional heavy metal complexes. One promising innovation in this regard is the emergence of thermally activated delayed fluorescence (TADF) emitters.

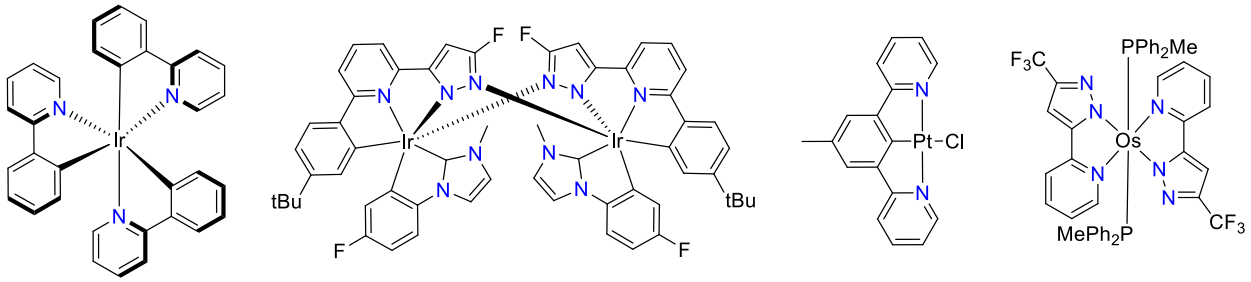

Figure 1.2. Select examples of Iridium, Platinum, and Osmium phosphorescent complexes.

TADF-emitters are designed to have a small energy splitting between $\mathbf{S_1}$ and $\mathbf{T_1}$. This allows ISC and reverse ISC (rISC) from $\mathbf{T_1}$ to $\mathbf{S_1}$ at ambient temperatures resulting in what appears as a delayed fluorescence. Beyond energy splitting, a key difference between the phosphorescent metal complex and TADF-emitters is that TADF-emitters primarily harvest their excited electrons typically in the singlet state, rather than from both triplet and singlet state. Two important classes of compounds and materials have been seen to have TADF-emitting properties: purely organic molecules[33] and Cu^{I} emitters (**Figure 1.3.**).[34–36] While the purely organic TADF-emitters allow for a high degree of tunability, they suffer long emission decay times which can cause problems in applications to OLEDs.[37]

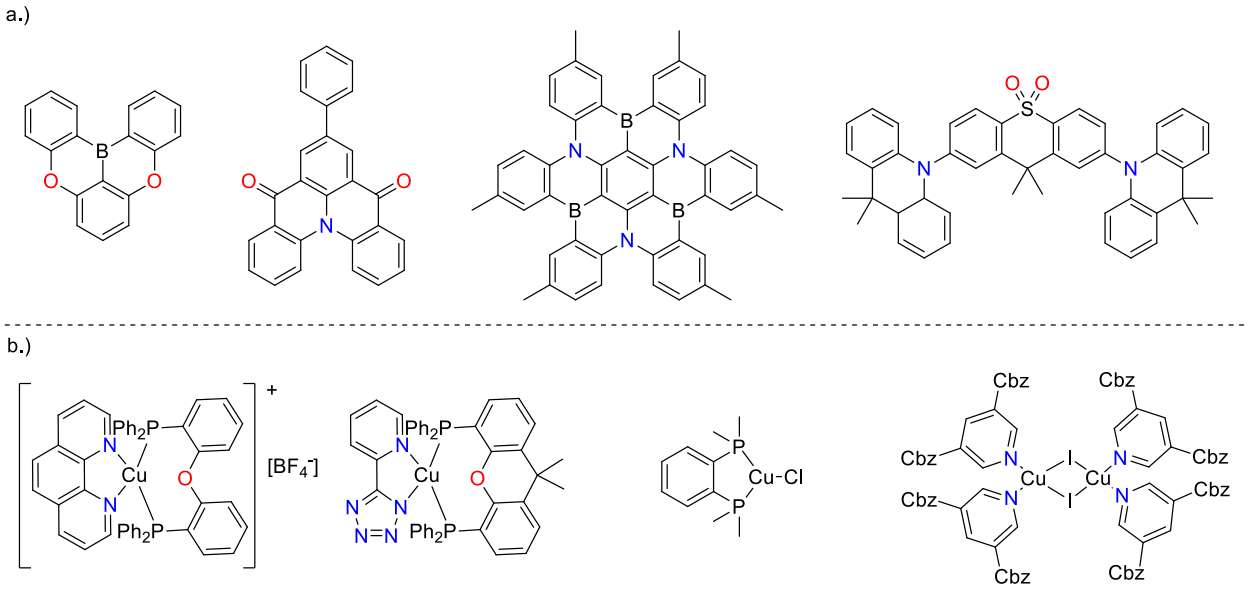

Figure 1.3. a.) Select examples of purely organic TADF-emitters and b.) select examples of mono- and dinuclear Cu^{I} TADF-emitters. Cbz = Carbazole.

Cu^{I} TADF-emitters, on the other hand, have a much faster ISC resulting in faster decay due to spin-orbit coupling induced by the Cu^{I} center. Currently, Cu^{I} TADF-emitters can be broken down into two main categories: mononuclear and dinuclear complexes.[34–36] Mononuclear Cu^{I} complexes, which are the most prevalent in the field, typically adopt a four-coordinate tetrahedral geometry. Similarly, dinuclear Cu^{I} complexes, often featuring bridging halides, also exhibit a tetrahedral structure around the Cu^{I} center. Although there are examples of mono- and dinuclear three-coordinate complexes, they are less common.[38] This tetrahedral structure makes them prone to weak emission due to excited-state Psuedo Jahn-Teller flattening distortions that accelerate non-radiative decay (**Figure 1.4.**).[35,38] This is also why many Cu^{II} lumiphores are not typically found or applied to this field.[38] Research has demonstrated that two- and three-coordinate species outperform these complexes.[39]

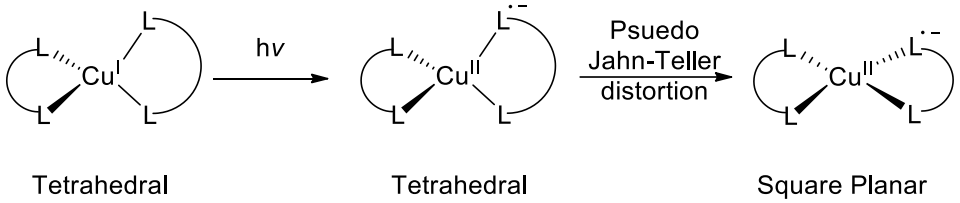

Figure 1.4. Representation of Psuedo Jahn-Teller flattening distortion upon excitation of a tetrahedral Cu^{I} lumiphore.

One class of Cu^{I} lumiphores that has received little attention are those that have cuprophilic interactions. Cuprophilic interactions are derived from the more general name of metallophilic interactions coined to represent attractive interactions between metal atoms with closed-shell configurations.[40] These interactions are often seen with silver and gold complexes where the metal-metal distance is less than that of the van der Waals radii of the two atoms. While less developed than the other coinage metals, there are many examples of cuprophilic complexes.[41] Although not all cuprophilic complexes show luminescent properties, select examples of dinuclear cuprophilic complexes that demonstrate luminescent properties will be discussed with emphasis on the Cu^{I}-Cu^{I} interaction, their luminescent, and how ligand modification affects both.

1.2. Luminescent Dinuclear Cu^{I} Complexes

1.2.1 Anionic Nitrogen Donating Dinuclear Cu^{I} Complexes

The first dinuclear Cu^{I} complex, 1,3-bis(phenyl)triazenide Cu^{I} or diazoaminobenzene Cu^{I} (**1**), was structurally determined in 1960[42], its fluorescent properties were discovered in 1995[43] despite being synthesized in 1900. From the structural characterization, **1** was found to have a Cu^{I}-Cu^{I} distance of 2.4405(10) Å, well within that of the Van der Waals radii.[42] Spectroscopic investigations undertaken by Harvey revealed UV-vis absorption of a solution of **1** in 2-MeTHF and a max absorption at 392 nm (ε = 7,720 M^{-1} cm^{-1}).[43] By looking at the excitation and emission of **1** (**Figure 1.5.a.**), it was determined that **1** fluoresced with no phosphorescence being detected.

The excitation spectrum measured at 600 nm showed a major peak at 500 nm with a shoulder around 540 nm. For the emission spectrum (λ_{exc} = 500 nm), a major peak was seen around 560 nm and a shouldering peak at 600 nm. The fluorescence studies suggested that the emission (600 nm) is polarized parallel to the absorption (500 nm) indicating that the symmetry of the Franck-Condon active modes is the same along the spectrum. Extended Hückel molecular orbital (EHMO) calculations were also conducted and found that the HOMO was mainly comprised of π-bonding system distributed in the phenyl and N_3 groups with a small contribution from the d_{xy} of the Cu atoms. The LUMO on the other hand mainly consists of the antibonding orbitals of N_3 backbone with little Cu contribution. These results along with the experimental fluorescence spectra suggest that the lowest energy excitation comes from an intraligand π system involving some of the metal atomic orbitals to a π* system almost entirely localized in the nitrogen frame with some weak metal-to-ligand charge transfer character. Using time-dependent Heller's theory, theoretical and experimental fluorescence and excitation spectra matched well and strongly suggested a 0-0 band at 550 nm right where the excitation and emission spectrum overlap. Various 1,3-bis(aryl)triazenides have also been synthesized; however, their fluorescence properties still remain uninvestigated.[44,45]

A structurally related class of ligands to 1,3-bis(aryl)triazenides are the 1,3-bis(aryl)amidinate ligands, in which the central nitrogen is replaced with carbon. The first dinuclear complex of this class was synthesized by *Cotton et al.* in 1988.[46] This seminal paper primarily compared the dinuclear Cu^I and Ag^I *N*,*N*'-di-p-tolylformamidinato complexes (**2**) based upon the crystal structure and computational calculations, but did have a Cu^I-Cu^I distance of 2.497(2) Å, and only slightly larger than that of compound **1**. The UV-vis absorption spectrum of **2** was recorded in CH_2Cl_2 showing absorbance at 324 (ε = 34,300 M^{-1} cm^{-1}), and 258 nm (ε =

37,720 M^{-1} cm^{-1}). Compared to the UV-vis absorption of **1** in 2-MeTHF, a clear blue shift of about 70 nm in absorption is observed.

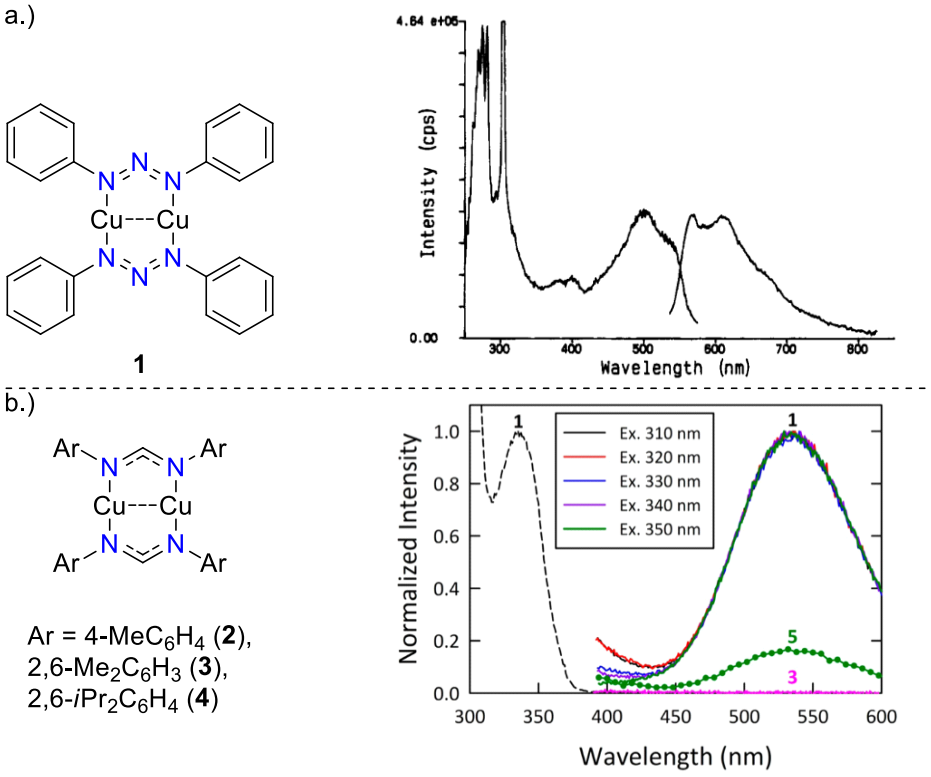

Figure 1.5. a.) Chemical structure of **1** and the excitation and emission spectra of **1** in 2-MeTHF. Reprinted with permission from Harvey, P. D. The $Cu_2(C_6H_5NNNC_6H_5)_2$ Dimer. Theoretical and Spectroscopic Investigations of the First Example of a Fluorescent D10-D10 Complex. Inorg Chem **1995**, 34 (8), 2019–2024. Copyright 1995 American Chemical Society. and b.) Structure of **2-4** and the excitation, broken line, and the emission spectra of **3**, **4**, and **Ag-4** in THF. Adapted with permission from Lane, A. C. et al. Multinuclear Copper(I) and Silver(I) Amidinate Complexes: Synthesis, Luminescence, and CS2 Insertion Reactivity. Inorg Chem **2014**, 53 (21), 11357–11366. Copyright 2014 American Chemical Society.

Since this first publication by *Cotton et al*, many different dinuclear bis(aryl)amidinate Cu^I complexes have been synthesized and crystal structures elucidated.[47–50] Despite the aryl or amininate substitution, these complexes have a small range of 2.4571(2)-2.548(1) Å for their Cu^I-Cu^I distances. However, it wasn't until 2014 when *Lane et al.* first examined the fluorescence properties of two different aryl-amidinate Cu^I complexes (**3** and **4**).[49] From these studies, the UV-vis absorption of both were taken showing a maxima at 255 nm (ε = 20,650 M^{-1} cm^{-1} for **3**) in THF. When looking at the fluorescence of **3** in THF (**Figure 1.5.b.**), it showed non-Franck-Condon fluorescence with an excitation maximum at 330 nm (λ_{ems} = 535 nm) while having a consistent emission peak at 535 nm despite being excited over a wide range, suggestive of ground-state homogeneity (e.g., one emitting species). Compound **4** uniquely showed no fluorescence characteristics while the silver variation (**Ag-4**) showed a slight emission around 540 nm.

When comparing **3** to **1**, it can be seen that **3** has a larger Cu^I-Cu^I distance at 2.548(1) Å as compared to 2.4405(10) Å. This distance is likely due to the steric bulk and repulsion of the 2,6-dimethyl groups found on the aromatic rings of **3** instead of the replacement of the central nitrogen for carbon as **2** has a Cu^I-Cu^I distance of 2.497(2)Å. The fluorescence of **3** is drastically different than that of **1**. While **1** showed a Frank-Codon spectrum, **3** did not. Another key difference is that **3** absorbs and is excited at 330 nm while **1** had an excitation wavelength around 300 nm which is drastically blue-shifted.

1.2.2. NHC-Supported Dinuclear Cu^I Complexes

While the previously mentioned complexes have N-donor atoms from the ligand and are neutral, another important ligand class involves N-heterocyclic carbenes (NHC). While some NHC containing cuprophilic molecules have either not been studied for their fluorescent properties or do not show fluorescence,[51] a series of phenanthrolinyl-functionalized NHCs synthesized by Bo

Liu *et al*. do.[52] **5-16** were synthesized by mixing the corresponding half-ligand imidazolium PF_6 salt, [HL](PF_6), with Cu powder in acetonitrile at room temperature exposed to air to afford the corresponding dinuclear Cu^I dimers (**Figure 1.6.**). From the crystal structure, **5-11** showed the ligands arranged in a head-to-tail fashion with each Cu^I center being three coordinate bound to one NHC and the phenanthrolinyl group of another ligand. The Cu^I-Cu^I distances were in a very narrow range of 2.707-2.736 Å suggesting that the bulk of the imidazolium played little role in the metal-metal interaction; however, in solution, **10** and **11** showed an isomerization between the head-to-tail and a head-to-head arrangement where both phenanthrolinyl groups are bound to a four-coordinate Cu^I and the two NHCs are bound a two-coordinate Cu^I. When the steric bulk is further increased to 2,6-$^i Pr_2C_6H_3$ (Dipp) this head-to-head arrangement around the Cu^I centers was observed in the crystal structure as seen in **12** with a shortened Cu^I-Cu^I distance of 2.653 Å. Additionally, if the PF_6 anion was substituted for a halide [X^- = Cl (**13**), Br (**14**), and I (**15**)], the head-to-tail configuration was conserved, but it was also found that the two Cu^I centers were now bridged by a single halide atom making each Cu^I center four-coordinate. The Cu^I-Cu^I distances were 2.611, 2.606, and 2.598 Å, respectively, with the change in distance attributed to the size of the halide. Finally, **16** showed a similar structure to **13-15**, but instead of a bridging halide, it contained a bridging acetonitrile along with the head-to-tail arrangement of the ligands and had a Cu^I-Cu^I distance of 2.676 Å.

Despite the wide range of structural modifications represented by **5-16**, these complexes showed similar UV-vis absorption spectra having two main absorption peaks at 220-230 nm and 270-280nm at room temperature in acetonitrile, similar to that of the ligand precursor. Despite **9**, **11**, and **12**, these complexes showed weak emission when excited with 290 nm light when in a solution of acetonitrile. They exhibited double emission bands in the regions of 350-355 nm and

365-370 nm which is again similar to the ligand precursor. As such, the fluorescence of these complexes is likely due to the ligands and not the Cu^{I}-Cu^{I} interaction.

a.)

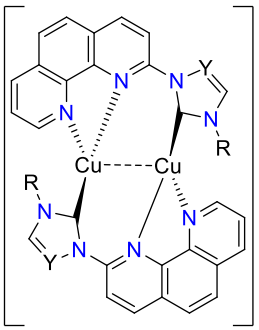

Y = CH, R = Me (**5**), allyl (**6**), *n*Bu (**7**), *i*Pr (**8**), *t*Bu (**9**),Mes (**10**); Y= N, R = allyl (**11**)

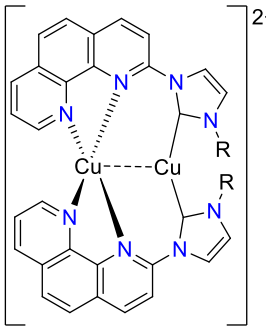

R = Dipp (**12**)

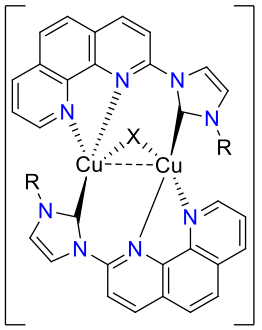

R = Mes, X = Cl (**13**), Br (**14**), I (**15**)

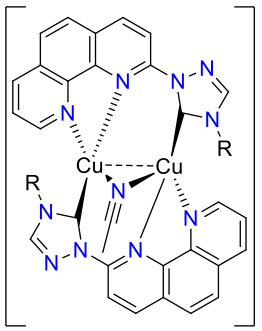

R = Bn (**16**)

b.)

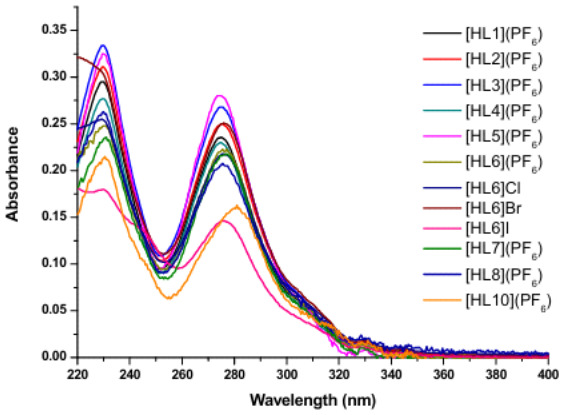

c.)

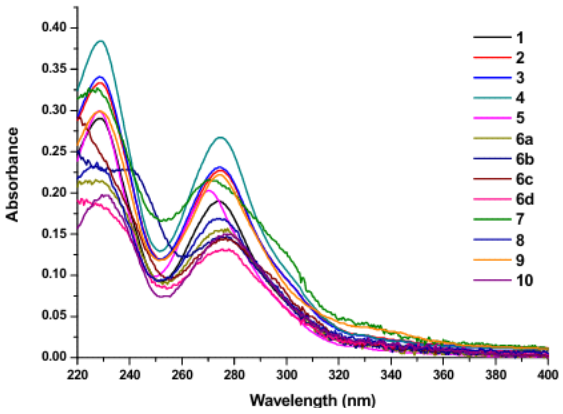

d.)

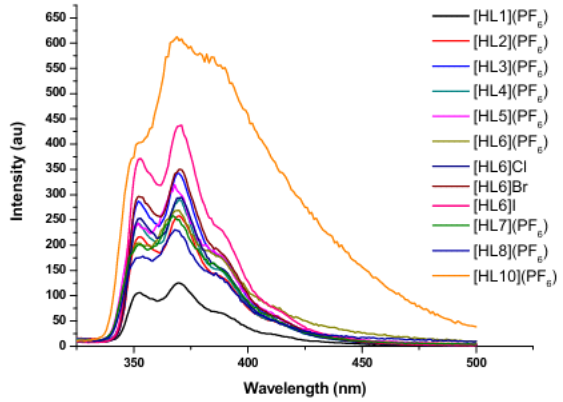

e.)

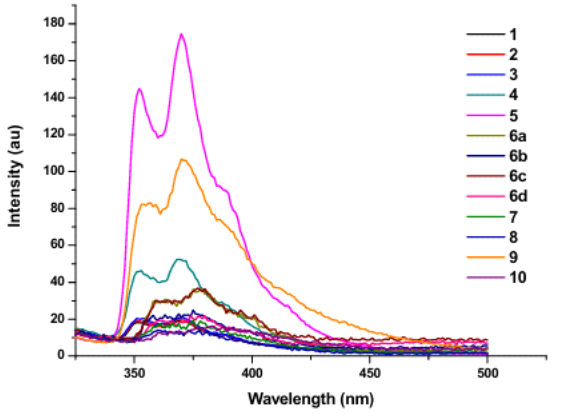

Figure 1.6. a.) Chemical structures of **5**-**16**, b.) UV-vis absorption spectra of NHC precursors at 298 K in acetonitrile (6.6 x 10^{-6}M) solution, c.) UV-vis absorption spectra of Cu^{I}- NHC complexes at 298 K in acetonitrile (3.3 x 10^{-6}M) solution, d.) emission spectra of NHC precursors at 298 K in acetonitrile (6.6 x 10^{-6}M) solution, and e.) emission spectra of Cu^{I}-NHC complexes at 298 K in acetonitrile (3.3 x 10^{-6}M) solution. Adapted with permission from Liu, B. et al. Dinuclear Copper(I) Complexes of Phenanthrolinyl-Functionalized NHC Ligands. Organometallics **2013**, 32 (19), 5451–5460. Copyright 2013 American Chemical Society.

A similar series of complexes were synthesized by Jorn Nitsch *et al* where instead of a phenanthrolinlyl-group these complexes contained a pyridine-functionalized NHC.[53] These complexes were synthesized by mixing the corresponding imidazolium chloride with CuCl in ammonia water. Complexes **17**-**20** demonstrated a similar head-to-tail ligand arrangement as the phenanthrolinlyl-functionalized NHCs. However, each Cu^{I} center was also ligated by a chloride making each Cu^{I} three-coordinate. The Cu^{I}-Cu^{I} distances for these complexes were in the range of 2.5226(8)-2.5744(9) Å with increasing distance as the R-group became more electron donating. When the mesityl-group on the imidazolium was substituted for the bulkier Dipp-group, a polymeric structure was observed with **21** which showed no Cu^{I}-Cu^{I} interaction.

It was realized that these complexes showed a bright greenish emission under near-UV excitation (**Figure 1.7.**). It is also worth noting that a linear polymorph of **18** did not show fluorescence due to a lack of coordination of the pyridine. Although the complexes showed more difference in their excitation spectrum, they all consistently showed emission from 550-520 nm. These broad excitation and emission spectra are indicative of a charge transfer nature of the excited states. The group also looked at the rate at which an excited state decays by emitting light or the radiative rate constants and found that **17**-**20** had an enhanced rate by a factor of 2-3 as compared

to **21**. This finding highlights the importance of the cuprophilic interaction that **17**-**20** have which can lead to a higher quantum yield and TADF-like behavior.

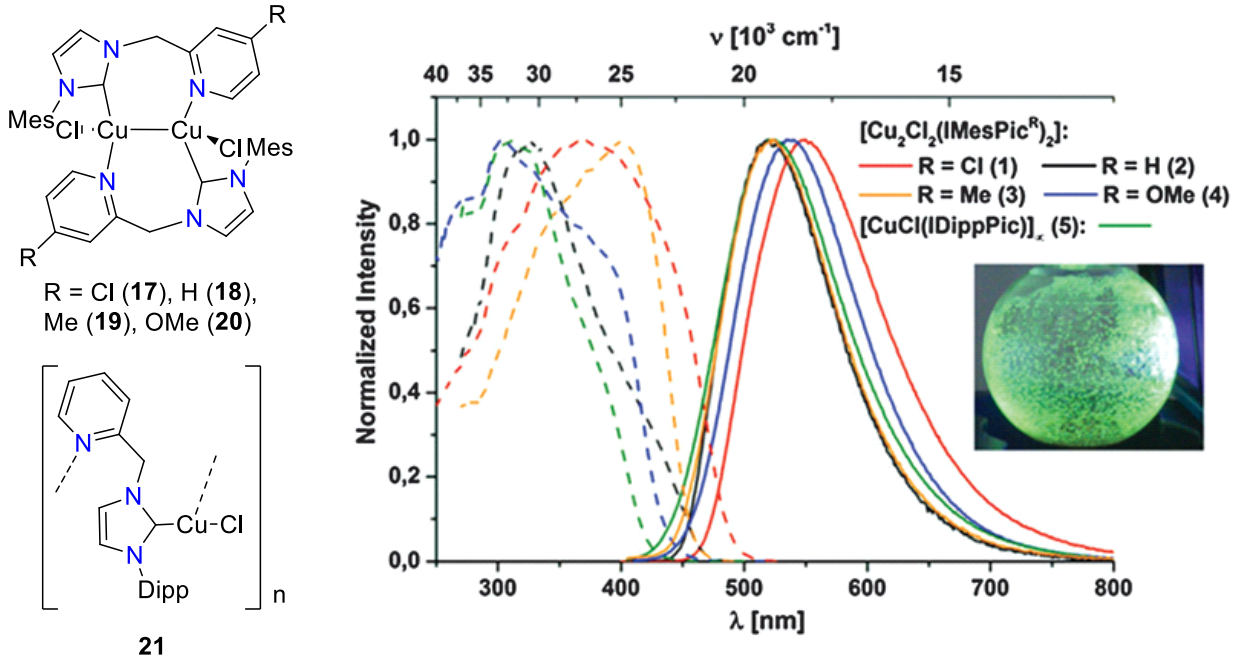

Figure 1.7. Chemical Structure of 17-21. Solid-state excitation, broken line, and emission spectra for 17-21. Picture inset is of crystalline 18 under near UV light. Adapted with permission from Nitsch, J. et al. Cuprophilic Interactions in Highly Luminescent Dicopper(i)-NHC-Picolyl Complexes-Fast Phosphorescence or TADF? Chemical Communications 2016, 52 (14), 2932–2935. Copyright 2015 Royal Society of Chemistry.

1.3. Conclusion

To summarize, luminescent complexes represent a crucial class of materials with potential for numerous applications, particularly in the fields of displays, OLEDs, and other optoelectronic devices. As the demand for more sustainable and cost-effective materials grows, there is a need and increasing interest in moving away from traditional toxic, expensive, and heavy transition metals, such as iridium and platinum, which have been widely used in these technologies. In response to this, Cu^{I} TADF-emitters have emerged as a promising class of complexes. Cu^{I} TADF-

emitters offer the advantage of high QE and tunable emission properties making them highly attractive for the next generation of optoelectronic devices and OLEDs.

An underexplored subset of Cu^{I} complexes demonstrating cuprophilic interactions has recently gained attention due to its potential to provide novel luminescent properties and new design possibilities. Cuprophilic interactions can influence the electronic structure of the complexes leading to enhanced emission properties. These interactions offer unique advantages for applications in displays and OLEDs including more efficient light emission and longer lifetimes.

Furthermore, it has been demonstrated that ligand modification plays a critical role in tailoring both the Cu^{I}-Cu^{I} interaction and the fluorescence characteristics of these complexes. By adjusting the ligand environment, it could be possible to fine-tune the luminescent properties such as emission color, quantum yield, and thermal stability. This versatility in ligand design allows for the development of Cu^{I} TADF-emitters with customizable properties for specific applications. Despite these promising developments, there is still much to explore regarding the fundamental mechanisms behind cuprophilic interactions and their impact on the photophysical properties of these complexes. Further research into the relationship between the metal-metal interaction, ligand design, and luminescent behavior could open up new pathways for optimizing these materials, leading to more efficient, sustainable, and cost-effective emitters for use in displays, OLEDS or other optoelectronics.

Chapter 2 - Phosphorescent and Fluorescent Properties of a Thiophene-Containing SNN Ligand and its Corresponding Dinuclear Cu and Ag Complexes

2.1 Abstract

Fluorescent molecules are potentially useful in a vast range of applications such as in organic light-emitting diodes (OLEDs) and thermally activated delayed fluorescence (TADF) emitters; however, many promising candidates lack the ability to fluoresce in the solid state which is needed in the manufacturing of these materials. Herein, the synthesis of a novel bidentate ligand, 2-methyl-*N*-((5-(2-(thiophen-2-yl)propan-2-yl)-1*H*-pyrrol-2-yl)methyl)propan-2-amine or **SNNH^{t}Bu,** and the corresponding dinuclear copper (I) and silver (I) complexes are reported with metal-metal bond lengths of 2.686 Å for **[CuSNNH^{t}Bu]$_2$** and 2.88 Å for **[AgSNNH^{t}Bu]$_2$**.

2.2. Introduction

The importance of luminescent compounds, highlighted by their wide range of applications in biosensors,[54] dyes,[55] and solid-state lighting, has driven extensive research in the field. In particular, since the first report of organic light-emitting diodes (OLEDs) by Tang and Van Slyke in 1987,[56] over the past several decades a significant amount of work by both industry and academia has gone in to improving these systems due to their use in displays.[57] One promising approach for generating more efficient OLEDs is the incorporation of transition metal complexes, which has been shown to dramatically improve quantum efficiencies.[58,59] One issue is that the complexes utilized often employ rare and expensive 5d- [58–61] and 4d- metals [62–64] to achieve high fluorescence output. This has inspired more recent research into the use of earth-abundant 3d-

metals such as Ni,[65,66] Fe,[67,68] Co,[69,70] and Cu[71–73] for use in OLEDs. Moreover, the use of thermally activated delayed fluorescence (TADF) emitters has seen a drastic spike, as these species have extremely high emission yields, and can achieve internal quantum efficiencies approaching 100%.[74,75] The key to enabling TADF is a small singlet-triplet energy difference between the lowest excited singlet state (S_1) and the lowest excited triplet state (T_1).[76] This can be facilitated through charge separation in the excited state, with larger distances between the hole and electron.[76] As such, transition metal complexes, which can exhibit ligand-to-metal charge-transfer (LMCT), or metal-to-ligand charge-transfer (MLCT) are promising candidates for TADF.

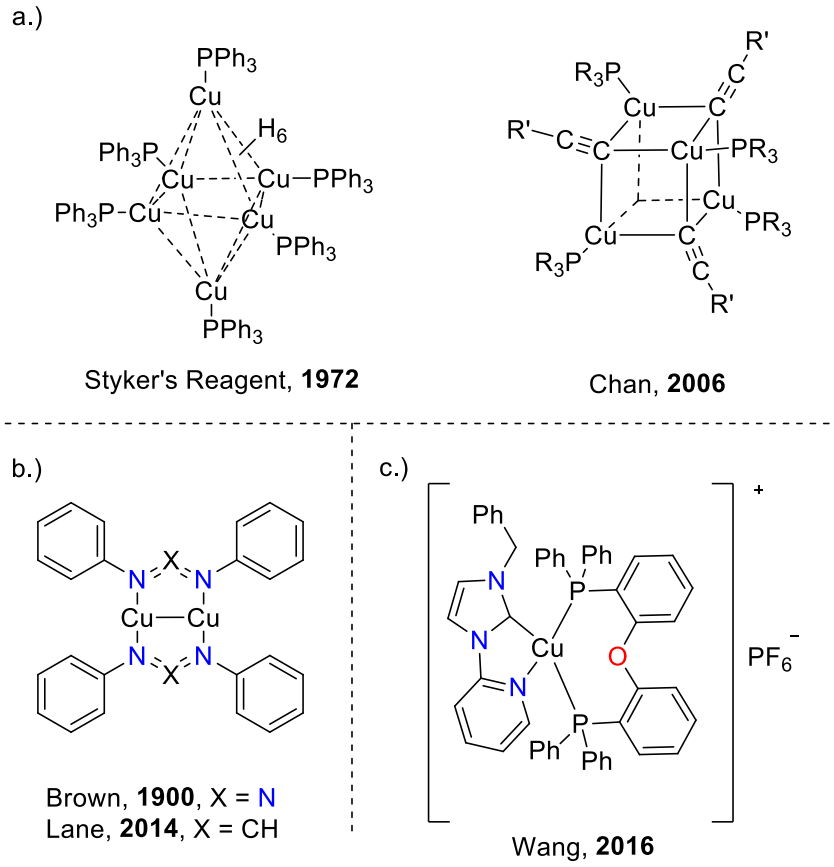

Figure 2.1. Select examples of a.) copper clusters and cubes, b.) dinuclear copper complexes, and c.) tetrahedral copper TADF.

Of particular interest are Cu^{I} luminophores because of the metal's high abundance, cheap cost, and relatively low toxicity. Additionally, due to the flexible coordination geometries adopted by Cu(I), multiple configurations are possible, such as clusters,[77–79] cubes,[80,81] polymers,[82,83] and other multimetallic assemblies (**Figure 2.1.a.**).[41] This allows Cu^{I} luminophores to show a diverse array of photophysical properties. Another unique property of copper is its ability to form cuprophilic interactions, where the distance between interacting copper centers is less than that of the van der Waals radii (< 2.80 Å).[84,85] This is reflected in the aforementioned luminescent Cu^{I} species, which often contained dinuclear, tetranuclear, or even larger copper cores. Regardless of the number of copper atoms, however, the majority of these systems adopted tetrahedral or tetrahedral-like geometries about the metal centers, typically with bridging halides, alkyls, or other ligands.

This is a major issue, as tetrahedral Cu^{I} complexes are susceptible to weak emission due to geometric excited-state distortions accelerating non-radiative decay.[86] While there is an example of a tetrahedral Cu^{I} complex that displayed TADF properties (Figure 1),[87] recent studies have shown that four-coordinate Cu^{I} luminophores are outperformed by two- and three-coordinate Cu^{I} species.[88] As far as three-coordinate Cu^{I} complexes are concerned, they typically display trigonal planar or pseudo-trigonal planar geometries with L-type ligands and various counter-ions.[89–93] The first trigonal Cu^{I} species containing a Cu-Cu bond, diazoaminobenzenecopper(I), was initially synthesized in 1900, and since then, it has been characterized via single crystal X-ray diffractometry in 1960,[94] and its fluorescence properties were examined in 1995.[95] After this seminal discovery, there have been several reports of similar diazoamino Cu^{I} species with Cu-Cu bonds in the 2.42-2.44 Å range. It is important to note, however, that their fluorescent properties remain unexplored.[96,97] Analogous Cu^{I} amidinate complexes were also synthesized by Lane *et al.*,

which displayed slightly longer Cu-Cu bond lengths of 2.45-2.55 Å and fluorescence in solution (**Figure 2.1.b.**).[98]

Unfortunately, a major problem with transition metal complexes is that they will often fluoresce in solution, but not in the solid state. This is critical obstacle for implementation as TADF emitters in OLEDs, which consist of solid films.[56,99–101] This phenomenon is typically referred to as "aggregation-caused quenching" or ACQ, and was originally reported by Förster in 1954.[102] Since then, there has been a large amount of research regarding ACQ, which has been thoroughly discussed in Birks' book "Photophysics of Aromatic Molecules".[103] It should be noted, however, that ACQ is most often seen in highly aromatic fluorophores where π-π stacking can be a major contributor to non-radiative decay. This is in contrast to "aggregation-induced emission" or AIE, recently coined in 2001, which is the polar opposite of ACQ.[104] For AIE, highly concentrated solutions induce fluoresce, whereas more dilute ones do not. Regardless of ACQ or AIE, these are solution state phenomena, and as mentioned above, most fluorophores show significantly inferior luminescent properties, if any at all, in the solid state. Therefore, it is clear that more work is needed to develop multinuclear Cu^{I} complexes that fluoresce when not dissolved in solution.

Herein, we describe the synthesis and characterization of pyrrole ligand containing A thiophene moiety, 2-methyl-N-((5-(2-(thiophen-2-yl)propan-2-yl)-1H-pyrrol-2-yl)methyl)propan-2-amine or **SNNH^{t}Bu**, as well as its corresponding coinage-metal Cu(I) and Ag(I) complexes, **[CuSNNH^{t}Bu]$_2$** and **[AgSNNH^{t}Bu]$_2$**, respectively. Upon coordination, dimeric species containing T-like coordination geometries about the metal centers formed with cuprophilic and argentophilic interactions. Moreover, the solution and solid state photophysical properties of the ligand, as well as the two bimetallic complexes were investigated both experimentally and computationally.

2.3. Results and Discussion

2.3.1. Synthesis and Characterization

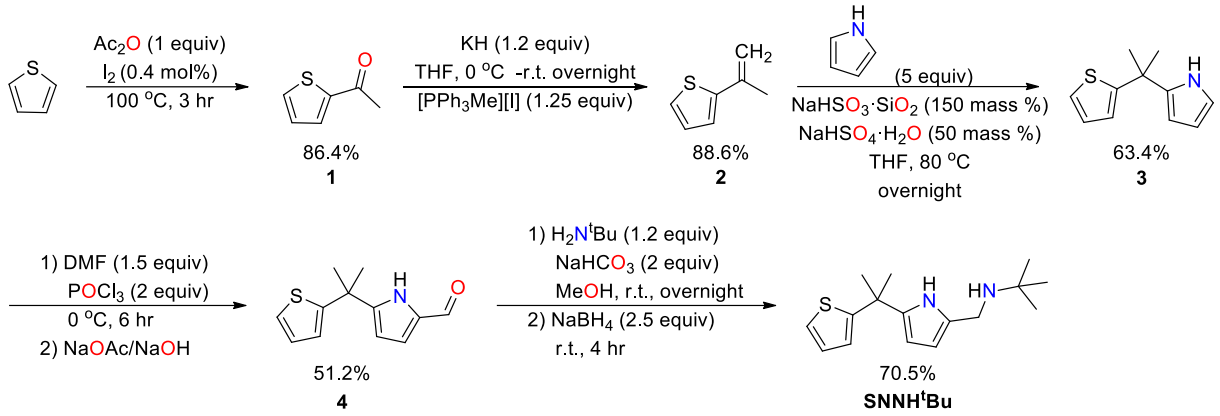

Scheme 2.1. Synthesis of the **SNNH^{t}Bu** Ligand.

The synthetic approach utilized to access the targeted thiophene-containing ligand, **SNNH^{t}Bu**, is outlined in Scheme 1. Starting with thiophene, acetylation to form **1**,[105] followed by a Wittig reaction to generate the geminal alkene, **2**,[106] were carried out using modified literature procedures. With **2** in hand, a hydroarylation of the olefin was performed using a sodium bisulfate/silica gel catalyst following a protocol developed by Kannasani *et al.*[107] to give **3** in modest yields as a red-brown oil. ^{1}H NMR spectroscopy confirmed the formation of the desired product with the disappearance of the olefin peaks around 5.39 and 4.96 ppm, the appearance of a new characteristic N-H peak at 7.84 ppm, as well as desymmetrization of pyrrole producing peaks at 6.65, 6.14, and 6.10 ppm, which integrated 1:1 with the corresponding thiophene peaks. Subsequently, a Vilsmeier-Haack reaction was conducted to install an aldehyde functionality on the more nucleophilic pyrrole moiety to give **4** in modest yields as an orange solid. The disappearance of the pyrrole-2-H peak at 6.10 ppm and the formation of an aldehyde peak at 9.39 ppm in the ^{1}H NMR spectrum of **4** were indicative that the desired product had been isolated. Moreover, further confirmation of the structure of **4** was achieved through single crystal X-ray

diffraction (see Supporting Information for further discussion). Lastly, with the aldehyde in hand, a hydroamination reaction using *tert*-butylamine was carried out to generate **SNNH^{t}Bu** as a yellow microcrystalline solid in good yields. ^{1}H NMR spectroscopy supported the formation of the desired product, with the loss of the aldehyde peak, as well as the appearance of characteristic methylene and *tert*-butyl peaks at 3.69 and 1.10 ppm, respectively.

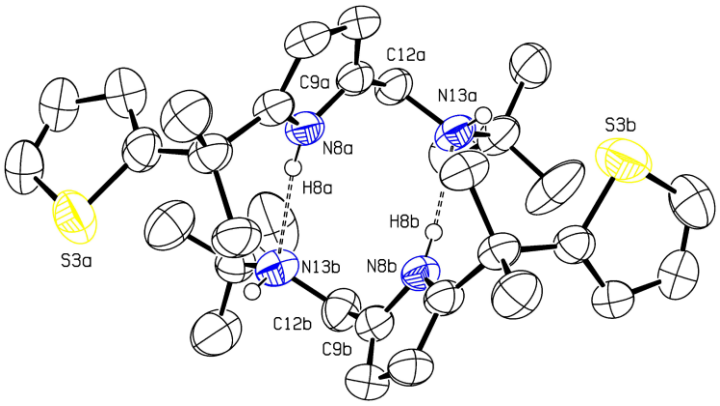

Figure 2.2. ORTEP3 representation (thermal ellipsoids at 50% probability) and atom numbering for **SNNH^{t}Bu**, most of the hydrogens have been omitted for clarity.

In addition to NMR spectroscopy, **SNNH^{t}Bu** was characterized by single crystal X-ray diffraction (**Figure 2.2.**). In the solid state, intertwined dimers formed with hydrogen bonding between the pyrrole hydrogens and the amine nitrogens; N(13b)--H(8a) and N(13a)--(H8b) distances of 2.311 and 2.259 Å, respectively, and N(13b)-N(8a) and N(13a)-N(8b) distances of 3.187 and 3.134 Å, respectively. These results were somewhat similar to the crystal structures obtained from related calixpyrrole ligands, which also formed intertwined dimers held together by hydrogen bonding in the solid state.[108] Additionally, the thiophene moieties were disordered across two positions, which is typical for these types of functionalities.[109] For notable bond lengths and angles for **SNNH^{t}Bu** see **Table 2.1.**

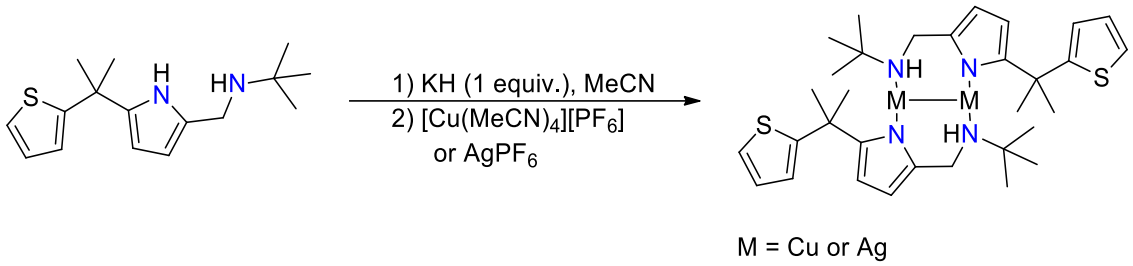

Scheme 2.2. Synthesis of the **[CuSNNH^{t}Bu]$_2$** and **[AgSNNH^{t}Bu]$_2$** Complexes.

In order to investigate the binding mode of **SNNH^{t}Bu**, the thiophene-containing ligand was coordinated to the coinage metals Cu^I and Ag^I. To generate the targeted complexes, the pyrrole functionality was first deprotonated using potassium hydride in acetonitrile. Once the formation of hydrogen gas had ceased, the deprotonated ligand was added to a solution of $[Cu(I)(MeCN)_4][PF_6]$ or $AgPF_6$ in acetonitrile (the silver synthesis was carried out in the dark). Almost immediately, a red precipitate formed and was collected by filtration. Undesired KPF_6 salts were removed by dissolving the solid product in chloroform and then filtering through Celite. Subsequent evaporation of the solvent under reduced pressure yielded complexes **[CuSNNH^{t}Bu]$_2$** and **[AgSNNH^{t}Bu]$_2$** in 67.1% and 8.4% yield, respectively.

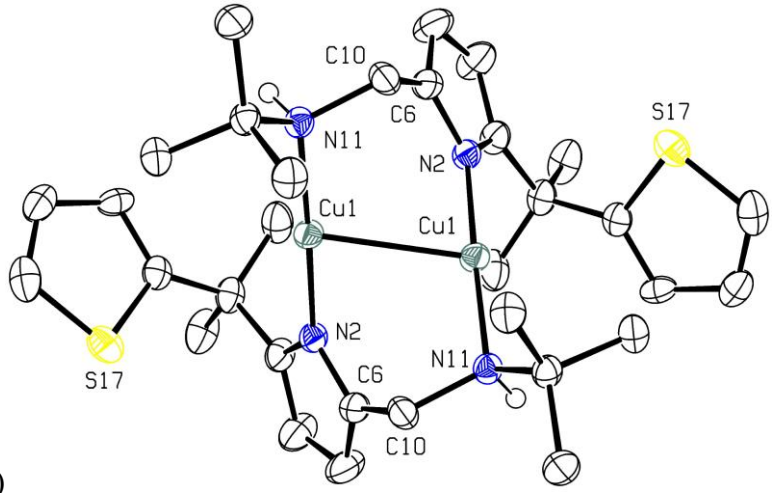

a)

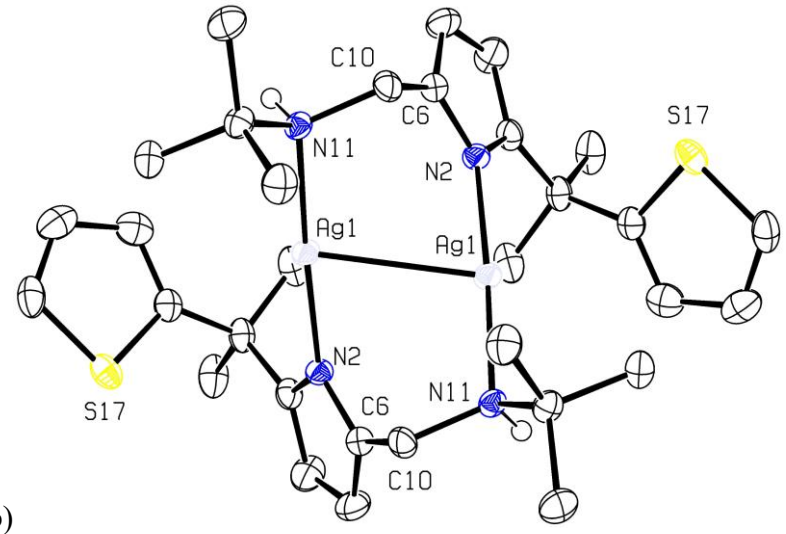

b)

Scheme 2.3. ORTEP3 representation (thermal ellipsoids at 50% probability) and atom numbering for: a) **[CuSNNH^{t}Bu]$_2$**, most of the hydrogens have been omitted for clarity; and b) **[AgSNNH^{t}Bu]$_2$**, most of the hydrogens have been omitted for clarity.

The complexes were first characterized by ^{1}H NMR in $CDCl_3$, and one of the initial confirmations that coordination had occurred was a lack of a pyrrole N-H peak. Further support that the targeted **[CuSNNH^{t}Bu]$_2$** and **[AgSNNH^{t}Bu]$_2$** complexes had formed came from the methyl groups in between the pyrrole and the thiophene moieties, which split and became chemically distinct. Lastly, a desymmetrization of the methylene protons occurred upon coordination, with two distinct signals at 3.78 ppm and 3.63 ppm for **[CuSNNH^{t}Bu]$_2$** and 3.93 and 3.39 ppm for **[AgSNNH^{t}Bu]$_2$**. While NMR spectroscopy indicated metal coordination, the definitive structures of **[CuSNNH^{t}Bu]$_2$** and **[AgSNNH^{t}Bu]$_2$** were elucidated via single crystal X-Ray diffraction. Both crystal structures showed a dimeric structure with two metal centers, two antiparallel bridging **SNNH^{t}Bu** ligands, and disorder in the orientation of the thiophene ring. A T-like geometry was seen about each metal center where the Cu^I or Ag^I atoms were connected to each other, as well as the pyrrolide donor of one ligand and the amine donor of another (*trans* to each other). The N(11)-M(1)-N(2) bond angles for **[CuSNNH^{t}Bu]$_2$** and **[AgSNNH^{t}Bu]$_2$** were

almost linear and very close to the ideal 180°; 178.2° and 175.4°, respectively. The N(2)-M(1)-M(1) and N(11)-M(1)-M(1) bond angles, on the other hand, deviated significantly from the ideal 90° with values of 80.4° and 101.4° for **[CuSNNH^{t}Bu]$_2$**, respectively, and 78.5° and 98.2° for **[AgSNNH^{t}Bu]$_2$**, respectively. Notably, the bond angles involving the amine donor were expanded above 90°, whereas the bond angles involving the pyrrolide group were compressed. This could be a function of the shorter M(1)-N(2) bond in comparison to the M(1)-N(11) bond (1.860 Å vs. 1.937 Å for **[CuSNNH^{t}Bu]$_2$** and 2.073 Å vs. 2.154 Å for **[AgSNNH^{t}Bu]$_2$**). In addition, the M(1)-M(1) distances were found to be 2.686 Å for the Cu(I) species and 2.879 Å for the Ag(I) species. These values fell well within the range of van der Walls radii of < 2.80 Å for Cu and < 3.44 Å for Ag indicating the presence of a metallic bond.[84] For **[CuSNNH^{t}Bu]$_2$**, while not the shortest Cu-Cu interaction reported in the literature, 2.316 Å in an organocopper cluster by Vogt and coworkers,[110] 2.686 Å was in line with known structures.[41] As for **[AgSNNH^{t}Bu]$_2$**, although it was not the shortest reported distance either, 2.705 Å in a dinuclear Ag(I) N,N'-di-p-toylformamidinato complex from Cotton *et al.*,[111] 2.879 Å was still on the shorter side for known argentophilic interactions.[112] Interestingly, the ligand backbone angles remained mostly unchanged upon Cu^I and Ag^I coordination, likely because the dimeric structure and hydrogen bonding interactions evident for **SNNH^{t}Bu** in the solid state (**Figure 2.2.**) arranged the ligands in a similar fashion as **[CuSNNH^{t}Bu]$_2$** and **[AgSNNH^{t}Bu]$_2$**. For notable bond lengths and angles see **Table 2.1.**

Table 2.1. Selected Bond Lengths (Å), Bond Angles (deg), and Torsion Angles (deg) for SNNHtBu, **[CuSNNHtBu]$_2$**, and **[AgSNNHtBu]$_2$**. [a] H(8b)-N(13a)-C(12a) and H(8a)-N(13b)-C(12b). [b] N(13a)-C(12a)-C(9a) and N(13b)-C(12b)-C(9b). [c] C(12a)-C(9a)-N(8a) and C(12b)-C(9b)-N(8b). [d] C(9a)-N(8a)-H(8a) and C(9b)-N(8b)-H(8b)

	SNNH^{t}Bu	**[CuSNNH^{t}Bu]$_2$**	**[AgSNNH^{t}Bu]$_2$**
		Bond Lengths (Å)	
M(1)-M(1)	N/A	2.686(2)	2.879(1)
M(1)-N(2)	N/A	1.860(5)	2.073(4)
M(1)-N(11)	N/A	1.937(4)	2.154(4)
		Bond Angles (deg)	
N(11)-M(1)-N(2)	N/A	178.2(2)	175.4 (2)
N(2)-M(1)-M(1)	N/A	80.4(2)	78.5(1)
N(11)-M(1)-M(1)	N/A	101.4(2)	98.2(1)
H(8)-N(13)-C(12)/M(1)-N(11)-C(10)	112.04 and 111.01[a]	111.5(3)	111.2(3)
N(13)-C(12)-C(9)/N(11)-C(10)-C(6)	111.3(6) and 111.1(9)[b]	112.3(4)	112.9(5)
C(12)-C(9)-N(8)/C(10)-C(6)-N(2)	122.5(9) and 122.0(9)[c]	121.6(5)	121.9(5)
C(9)-N(8)-H(8)/C(6)-N(2)-M(1)	124.9 and 125.1[d]	127.5(4)	127.8(4)
	Torsion Angles (deg)		
N(2)-M(1)-M(1)-N(11)	N/A	52.6	49.2
N(11)-M(1)-M(1)-N(11)	N/A	128.0	127.5
N(2)-M(1)-M(1)-N(2)	N/A	126.8	134.0

2.3.2. Optical Properties

It was initially observed that **SNNH^{t}Bu**, **[CuSNNH^{t}Bu]$_2$**, and **[AgSNNH^{t}Bu]$_2$** had interesting optical properties when the solid products were subjected to UV-light from a standard lamp used to visualize compounds for thin layer chromatography. For **SNNH^{t}Bu**, the pale-yellow solid exhibited a blue glow that was observed briefly after irradiation, for colorless **[CuSNNH^{t}Bu]$_2$**, a blue-green glow was observed during irradiation, and for brown/red **[AgSNNH^{t}Bu]$_2$**, a yellow-green glow was apparent during irradiation (Figure 4). Attempts at observing fluorescence in solution surprisingly gave no results, which led to multiple attempts to induce either ACQ or ACE. In these experiments, **SNNH^{t}Bu**, **[CuSNNH^{t}Bu]$_2$**, and **[AgSNNH^{t}Bu]$_2$** were dissolved in varying amounts of chloroform (as the solvent) and acetonitrile (as the counter solvent in which the compounds were not soluble) 100% chloroform to 0% chloroform in 10% increments. Once again, we were surprised to find that no fluorescence could be observed when these solution were subjected to UV-light (using the same source described above). These observations prompted more in-depth investigations into the optical properties of **SNNH^{t}Bu**, **[CuSNNH^{t}Bu]$_2$**, and **[AgSNNH^{t}Bu]$_2$**.

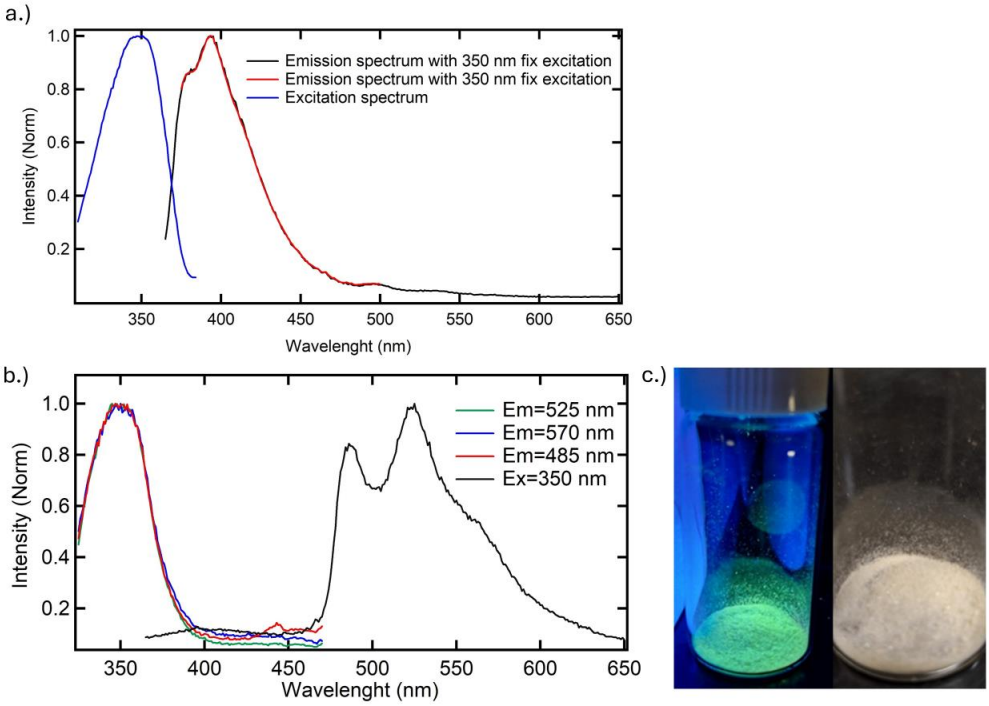

Figure 2.3. a.) Emission and excitation spectrum of **SNNH^{t}Bu**, b.) Emission and excitation spectrum of **[CuSNNH^{t}Bu]$_2$**, and c.) **[CuSNNH^{t}Bu]$_2$** under UV light (left) and incandescent light (right).

To further investigate the fluorescent properties, the solid-state emission, excitation and absorbance of each compound were looked at. All compounds in the solid-state UV-vis absorbance showed an absorbance near 225 nm while **[AgSNNtBu]$_2$** also showed a small bump at 550 nm. **SNNtBu** showed a peak excitation around 350 nm and gave a near UV-emission of 393 nm and had a UV-Vis absorbance of 225 nm. **[CuSNNtBu]$_2$** showed a slightly blue-shifted excitation at 350 nm while it had two emission peaks within the blue and blue/green region of the visible spectrum: 525 and 486 nmn, respectively. Despite observation of fluoresce under a UV-lamp, attempts at recording the excitation and emission spectrum of **[AgSNNtBu]$_2$** proved unfruitful either in solid-state or in solution.

2.4. Conclusion

To summarize, a novel bidentate ligand, **SNNtBu**, was synthesized. This ligand demonstrated a dimerization with hydrogen bonding between the pyrrole N-H and the tbutylamine pentant group. The ligand also demonstrated fluorescent behavior. Coordination to two coinage metals, Cu and Ag, led to a dinuclear metal complex that demonstrated metal-metal interactions within that of the van der Waals radii and fluorescent properties. These two complexes, **[CuSNNtBu]$_2$** and **[AgSNNtBu]$_2$**, had metal-metal distances of 2.686 Å and 2.88 Å, respectfully. Although it was not possible to obtain a fluorescence spectrum of **[AgSNNtBu]$_2$**, the solid-state fluorescence spectrum of **[CuSNNtBu]$_2$** showed two major peaks in the blue region. Using DFT, it was found that these two distinct peaks arise from contributions of the two isomers in the solid-state. These isomers are due to the disorder that is commonly found in thiophene rings. These results suggest that these findings may lead to new fluorescent materials or potential applications in solid-state OLEDs or TADF emitters.

2.5. Supporting Information

2.5.1. General Considerations

All procedures and manipulations were performed under an argon or nitrogen atmosphere using standard Schlenk-line and glove box techniques unless stated otherwise. Solvents were dried and deoxygenated under argon using a LC Technology Solutions Inc. SP-1 stand-alone solvent purification system, unless stated otherwise. Deuterated solvents were purchased from Cambridge Isotope Laboratories, Sigma Aldrich, Acros Organics, or Alfa Aesar, degassed, and dried over activated molecular sieves prior to use. Triphenylmethylphosphnium iodide[113] and $NaHSO_4 \cdot SiO_2$[114] were synthesized according to literature procedures (spectroscopic characterization matched reported data where applicable). All other reagents were purchased from

commercial sources and utilized without further purification unless stated otherwise. NMR spectra were recorded at ambient temperature and pressure using a Bruker 400 MHz spectrometer (600 MHz or 400 MHz for ^{1}H, and 151 MHz or 100 MHz for ^{13}C). The ^{1}H and ^{13}C NMR spectra were measured relative to partially deuterated solvent peaks but are reported relative to tetramethylsilane (TMS). Fluorescent measurements were recorded on a Fluoromax-2. High-resolution mass spectrometry (HRMS) was performed at the University of Illinois Mass Spectrometry Laboratory, and electrospray ionization (ESI) spectra were collected on a Waters Synapt G2-Si spectrometer. Single crystal X-ray data were collected using a Rigaku XtaLAB Synergy-S diffractometer equipped with a HyPix-6000HE Hybrid Photon Counting (HPC) detector and dual Mo and Cu microfocus sealed X-ray source (Cu Kα λ = 1.54184 Å). The data collection strategy was calculated using CrysAlisPro to ensure desired data redundancy and percent completeness. Unit cell determination, initial indexing, data collection, frame integration, Lorentz-polarization corrections and final cell parameter calculations were carried out using CrysAlisPro. An absorption correction was performed using the SCALE3 ABSPACK scaling algorithm embedded within CrysAlisPro. The structures were solved using the ShelXT structure solution program using Intrinsic Phasing and refined by Least Squares using the ShelXL program. All non-hydrogen atoms were refined anisotropically. Hydrogen atom positions were calculated geometrically and refined using the riding model. Olex2 was used for the preparation of the publication materials.

2.5.2. Synthetic Procedures for 1-4, SNNH^{t}Bu, [CuSNNH^{t}Bu]$_2$, and [AgSNNH^{t}Bu]$_2$

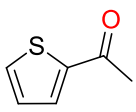

1-(thiophen-2-yl)ethenone, 1. Compound **1** was synthesized using a modified literature procedure.[115] Thiophene (16.8 g, 200 mmol) and acetic anhydride (20.4 g, 200 mmol) were loaded neat into an oven-dried 150 mL round-bottom flask. To this mixture, I_2

(101 mg, 0.8 mmol, 0.4 mol %) was added, along with a condenser. The reaction was then heated 100 °C and stirred for 4.5 hours. The reaction was then cooled to room temperature and quenched with 20 mL of deionized (DI) water. The suspension was allowed to stir for 1 h, and then the aqueous phase was extracted with 3 x 20 mL DCM. The combined organic phases were washed with 50 mL portions of saturated $NaHCO_3$ solution (until the formation of CO_2 stopped). The organic layer was then dried over Na_2SO_4, filtered, and dried under reduced pressure. The crude reaction mixture was passed through a silica plug (7.5 cm wide by 4 cm tall) eluting with 800 mL of 9:1 hexanes:ethyl acetate. The filtrate was collected and dried to afford **1** as a light yellow-orange oil. Yield: 21.8 g (86.4%). Spectroscopic characterization matched reported data. **1** was used without further purification.

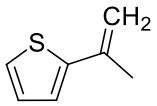

2-(prop-1-en-2-yl)thiophene, 2. Compound **2** was synthesized using a modified literature procedure.[106] A suspension of potassium hydride (7.63 g, 190 mmol, 1.2 equiv) in 450 mL THF was cooled to 0 °C. Triphenylmethylphosphonium iodide (80.09 g, 198 mmol, 1.25 equiv) was added as a solid and the formation of the phosphorous ylide was allowed to procced for 2 hours until the formation of hydrogen gas had ceased. Subsequently, **1** (20.0 g, 158 mmol) was added dropwise over the course of 15 min. The reaction was then warmed to room temperature and stirred overnight. The reaction was then filtered, and the precipitate was washed with 600 mL of hexanes. The filtrate was concentrated under reduced pressure, loaded onto a silica plug (7.5 cm wide by 4 cm tall), and eluted with 1 L of hexanes. The filtrate was dried under reduced pressure to give a pale-yellow oil. Yield: 17.5 g (88.6%). Spectroscopic characterization matched reported data. **2** was used without further purification.

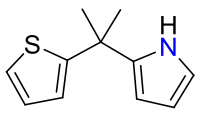

2-(2-(thiophen-2-yl)propan-2-yl)-1H-pyrrole, 3. An oven-dried 1 L round-bottom flask was charged with $NaHSO_4 \cdot SiO_2$ (25.0 g, 143% w/w to **2**) and

$NaHSO_4 \cdot H_2O$ (8.35 g, 48% w/w to **2**). Pyrrole (47.0 g, 700 mmol, 5 equiv) was then added, followed by **2** (17.4 g, 140 mmol), and 550 mL of THF. The reaction was then heated to 85 °C and refluxed overnight. The progress of the reaction was monitored by ^{1}H NMR spectroscopy (disappearance of the alkene peaks), and once completed, the solvent and excess pyrrole were removed under reduced pressure while heating at 70 °C. The crude reaction was then pushed through a silica plug (7.5 cm wide by 4 cm tall) eluting with 1 L of hexanes. The solvent was then removed under reduced pressure to give a red/brown oil. Yield 17.1 g (63.4%). ^{1}H NMR (400 MHz, $CDCl_3$) δ: 7.84 (br s, 1H, pyrrole-NH), 7.17 (d, 1H, thiophene-CH, *J* = 5.4 Hz), 6.93 (t, 1H, thiophene-CH, *J* = 4.5 Hz), 6.85-6.80 (m, 1H, thiophene-CH), 6.66 (s, 1H, pyrrole-CH), 6.16 (s, 1H, pyrrole-CH), 6.11 (s, 1H, pyrrole-CH), and 1.77 (s, 6H, CH_3) ppm. ^{13}C NMR (101 MHz, $CDCl_3$) δ 154.93 (aromatic-C), 139.83 (aromatic-C), 126.63 (thiophene-CH), 123.80 (thiophene-CH), 123.10 (thiophene-CH), 116.89 (pyrrole-CH), 107.98 (pyrrole-CH), 103.78 (pyrrole-CH), 38.00 ($\underline{C}$-$(CH_3)_2$), and 31.48 (C-($\underline{C}H_3)_2$) ppm. HRMS (ESI) *m/z*$^+$: $[M+H]^+$ Calcd for $[C_{11}H_{14}NS]^+$: 192.0847; Found: 192.0844.

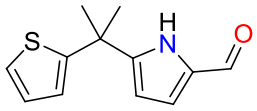

5-(2-(thiophen-2-yl)propan-2-yl)-1H-pyrrole-2-carbaldehyde, 4. An oven-dried 150 mL 3-neck round bottom flask was charged with **3** (12.2 g, 63.9 mmol) and DMF (19.6 g, 128 mmol, 2 equiv), and then cooled to 0 °C. Subsequently, $POCl_3$ (7.00 g, 95.8 mmol, 1.5 equiv) was added dropwise over 10 minutes, and the reaction was stirred for 3 hours at 0 °C. After this time, the reaction was quenched with 85 mL of DI water, and solid NaOH was then added in portions until the reaction mixture was highly basic with a pH >12 (all at 0 °C). The reaction was then stirred overnight, filtered, and the precipitate was washed with approximately 500 mL of DI water. The solid product was then dissolved in 300 mL of DCM, filtered, dried over $MgSO_4$, filtered once again, and concentrated under reduced pressure. The

crude mixture was then pushed through a silica plug (7.5 cm tall by 4 cm wide) eluting with 2.4 L of 6:1 hexanes:ethyl acetate. The solvent was removed under reduced pressure, and the solid product was recrystallized from 400 mL of 10:1 hexanes:ethyl acetate to give a light orange solid. Yield: 7.18 g (51.2%). Crystals suitable for single crystal X-Ray diffraction were grown by layering pentane on top of a DCM solution of **4**. ^{1}H NMR (600 MHz, $CDCl_3$) δ: 9.39 (s, 1H, aldehyde-CH), 8.87 (s, 1H, pyrrole-NH), 7.20 (dd, 1H, thiophene-CH, *J* = 5.1, 1.2 Hz), 6.94 (dd, 1H, thiophene-CH, *J* = 5.1, 3.5 Hz), 6.89 (dd, 1H, pyrrole-CH, *J* = 3.9, 2.5 Hz), 6.86 (dd, 1H, thiophene-CH, *J* = 3.6, 1.2 Hz), 6.22 (dd, 1H, pyrrole-CH, *J* = 3.9, 2.6 Hz), and 1.78 (s, 6H, CH_3) ppm. ^{13}C NMR (101 MHz, $CDCl_3$) δ: 178.76 (O=CH), 152.34 (aromatic-C), 148.95 (aromatic-C), 132.16 (aromatic-C), 126.91 (thiophene-CH), 124.42 (thiophene-CH), 123.74 (thiophene-CH), 121.76 (pyrrole-CH), 107.85 (pyrrole-CH), 38.34 ($\underline{C}$-$(CH_3)_2$), and 31.00 (C-($\underline{C}H_3)_2$) ppm. HRMS (ESI) *m/z*$^{+}$: $[M+H]^+$ Calcd for $[C_{12}H_{14}NOS]^+$: 220.0796; Found: 220.0799.

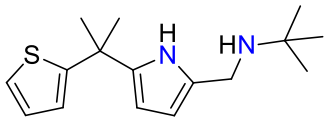

2-methyl-N-((5-(2-(thiophen-2-yl)propan-2-yl)-1H-pyrrol-2-yl)methyl)propan-2-amine, SNNH^{t}Bu. In air, a 50mL round bottom flask was charged with **4** (1.00 g, 4.56 mmol), $NaHCO_3$ (1.26 g, 9.12 mmol, 2 equiv), and 20 mL of MeOH. The reaction was stirred for 5 minutes, and then *tert*-butylamine (400 mg, 5.47 mmol, 1.2 equiv) was added. The reaction was capped, stirred overnight, and monitored via ^{1}H NMR spectroscopy (disappearance of the aldehyde peak and formation of the imine peak). Upon completion, $NaBH_4$ (732 mg, 11.4 mmol, 2.5 equiv) was added and the reaction was allowed to stir open to air for 5 hours. The solvent was subsequently removed under reduced pressure, and the crude product was dissolved in 60 mL of DCM. After stirring for 2 h, the reaction was filtered through a Celite plug, which washed with a further 20 mL of DCM. The solvent was removed under reduced pressure and the resulting solid was dissolved in boiling hexanes. The resulting

solution was stored overnight in a freezer (-30 °C) to give the product as pale-yellow crystals. Yield: 0.889 g (70.5%). Crystals suitable for single crystal X-Ray diffraction were grown by slow evaporation of a solution of **SNNH^{t}Bu** in DCM. ^{1}H NMR (400 MHz, $CDCl_3$) δ: 8.28 (s, 1H, pyrrole-NH), 7.14 (dd, 1H, thiophene-CH, *J* = 5.1, 1.2 Hz), 6.90 (dd, 1H, thiophene-CH, *J* = 5.1, 3.5 Hz), 6.80 (dd, 1H, thiophene-CH, *J* = 3.6, 1.2 Hz), 5.95 (t, 1H, pyrrole-CH, *J* = 3.1 Hz), 5.92 – 5.87 (m, 1H, pyrrole-CH), 3.69 (s, 2H, CH_2), 1.74 (s, 6H, CH_3), and 1.10 (s, 9H, $C(CH_3)_3$) ppm. ^{13}C NMR (101 MHz, $CDCl_3$) δ: 155.47 (aromatic-C), 138.96 (aromatic-C), 131.02 (aromatic-C), 126.53 (thiophene-CH), 123.55 (thiophene-CH), 122.94 (thiophene-CH), 104.87 (pyrrole-CH), 103.74 (pyrrole-CH), 50.60 ($\underline{C}$-$(CH_3)_3$), 40.22 (CH_2), 38.02 ($\underline{C}$-$(CH_3)_2$), 31.46 (C-($\underline{C}H_3)_2$), and 29.12 (C-($\underline{C}H_3)_3$) ppm. HRMS (ESI) *m/z*$^+$: $[M-H]^+$ Calcd for $[C_{16}H_{23}N_2S]^+$: 275.1582; Found: 275.1577.

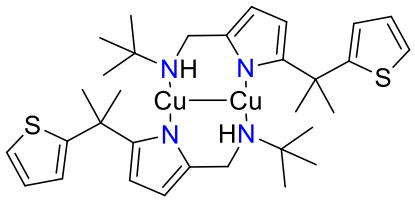

Complex [CuSNNH^{t}Bu]$_2$. A solution of **SNNH^{t}Bu** (750 mg, 2.71 mmol) in 7 mL MeCN was added to a slurry of potassium hydride (109 mg, 2.71 mmol, 1 equiv) in 1 mL MeCN. The reaction turned orange and hydrogen gas formation was observed. Once the formation of gas had ceased, the reaction was allowed to stir for an additional 15 min. After this time, the reaction mixture was added to a solution of $[Cu(MeCN)_4][PF_6]$ (1.01 g, 2.71 mmol, 1 equiv) in 7 mL MeCN. The reaction was allowed to stir for 2 hours, and the formation of a precipitate was seen. The crude solid product was isolated on a frit and washed with 5 mL MeCN. The solid was then dissolved in 10 mL $CHCl_3$ and filtered through Celite. The solvent was removed under reduced pressure and the solid residue was stirred in 5 mL MeCN. The precipitate was isolated by filtration and dried under vacuum to give the desired product as a colorless solid. Yield: 0.617 g (67.1%). Crystals suitable for single crystal X-Ray diffraction were grown by layering a **[CuSNNH^{t}Bu]$_2$**

solution in $CHCl_3$ and with MeCN and storing in a freezer (-30 °C) overnight. ^1H NMR (400 MHz, $CDCl_3$) δ: 6.98 (dd, 1H, thiophene-CH, *J* = 5.1, 1.2 Hz), 6.79 – 6.76 (m, 1H, thiophene-CH), 6.65 (dd, 1H, thiophene-CH, *J* = 5.0, 3.4 Hz), 6.09 (d, 1H, pyrrole-CH, *J* = 3.1 Hz), 6.01 (d, 1H, thiophene-CH, *J* = 3.1 Hz), 3.78 (dd, 1H, CH_2, *J* = 11.6, 2.3 Hz), 3.63 (t, 1H, CH_2, *J* = 11.8 Hz), 1.69 (s, 3H, CH_3), 1.68 (s, 3H, CH_3), and 1.21 (s, 9H, $C(CH_3)_3$) ppm. ^{13}C NMR (151 MHz, $CDCl_3$) δ: 157.32 (aromatic-C), 151.05 (aromatic-C), 131.77 (aromatic-C), 125.26 (thiophene-CH), 124.42 (thiophene-CH), 124.19 (thiophene-CH), 108.30 (pyrrole-CH), 103.73 (pyrrole-CH), 54.23 ($\underline{C}$-$(CH_3)_3$), 47.27 (CH_2), 40.38 ($\underline{C}$-$(CH_3)_2$), 34.39 (CH_3), 34.36 (CH_3), and 29.71 (C-($\underline{C}H_3)_3$) ppm.

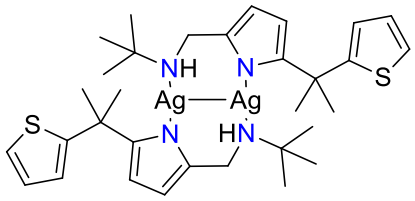

Complex [AgSNNH^{t}Bu]$_2$. This complex was synthesized in a similar manner to **[CuSNNH^{t}Bu]$_2$**. A solution of **SNNH^{t}Bu** (500 mg, 1.81 mmol) in 3 mL MeCN was added to a slurry of potassium hydride (72.5 mg, 1.81 mmol, 1 equiv) in 1 mL MeCN. The reaction turned orange and hydrogen gas formation was observed. Once the formation of gas had ceased, the reaction was allowed to stir for an additional 15 min After this time, the reaction mixture was added to a solution of $AgPF_6$ (457.3 mg, 1.81 mmol, 1 equiv) in 5 mL MeCN in the dark (a vial wrapped in tape). The reaction was allowed to stir for 2 hours and the formation of a precipitate was seen. The solid product was isolated on a frit and washed with 5 mL MeCN. The solid was then dissolved in 10 mL DCM and filtered through Celite. The solid gave the desired product as a red/brown solid. Yield: 58.3 mg (8.4%). Crystals suitable for single crystal X-Ray diffraction were grown by layering a **[AgSNNH^{t}Bu]$_2$** solution in $CHCl_3$ and with MeCN and storing in a freezer (-30 °C) overnight. ^1H NMR (600 MHz, $CDCl_3$) δ 6.95 (s, 2H, thiophene-CH), 6.72 (s, 2H, thiophene-CH), 6.61 (s, 2H, thiophene-CH), 6.17 (d, 2H, pyrrole-CH, *J* = 3.0 Hz), 6.05 (d, 2H, pyrrole-CH, *J* =

3.1 Hz), 3.93 (br, 2H,-CH_2-), 3.39 (br, 2H, -CH_2-), 1.87 (s, 1H, NH), 1.70 (s, 6H, C-$(CH_3)_2$), and 1.19 (s, 18H, C-$(CH_3)_3$).

2.5.3. ^{1}H and ^{13}C NMR for 1-4, SNNH^{t}Bu, [CuSNNH^{t}Bu]$_2$, and [AgSNNH^{t}Bu]$_2$

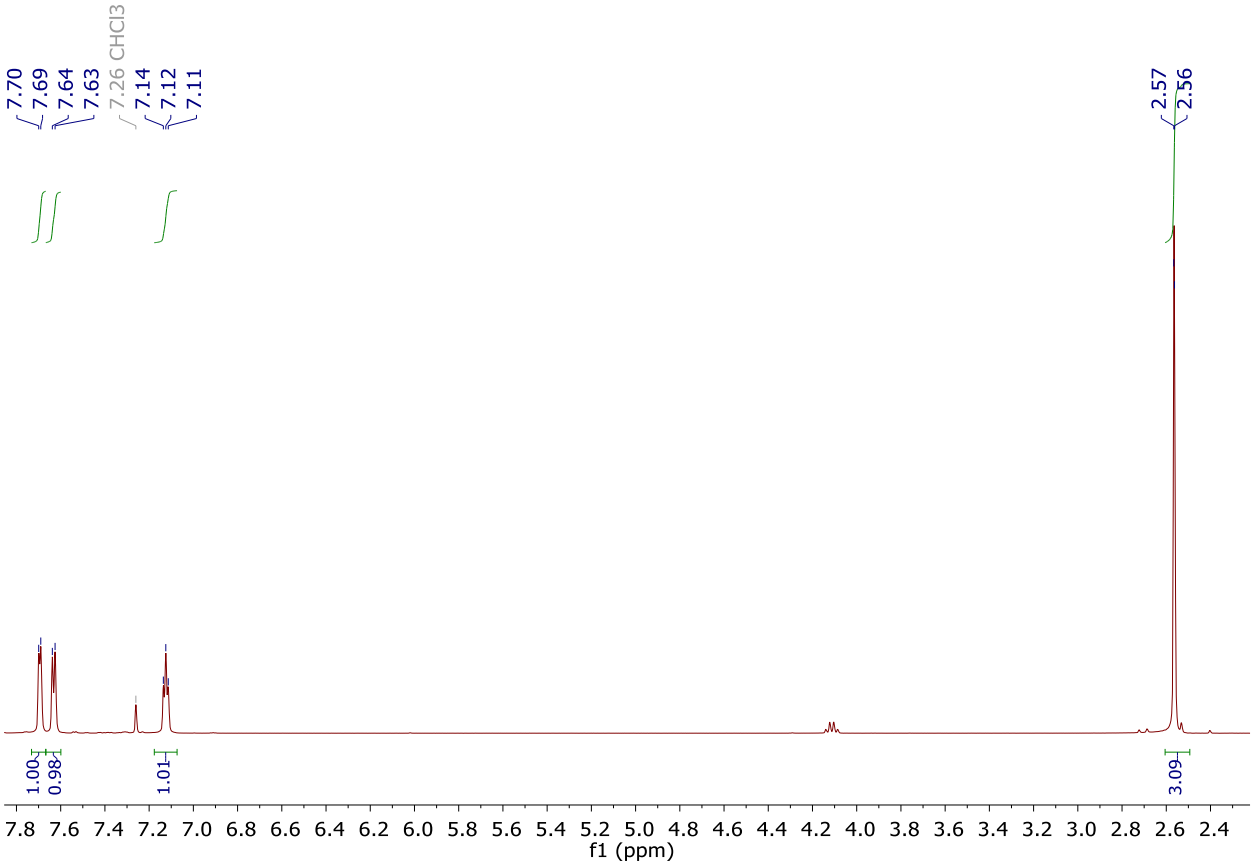

Figure 2.4. ^{1}H NMR of Compound **1**.

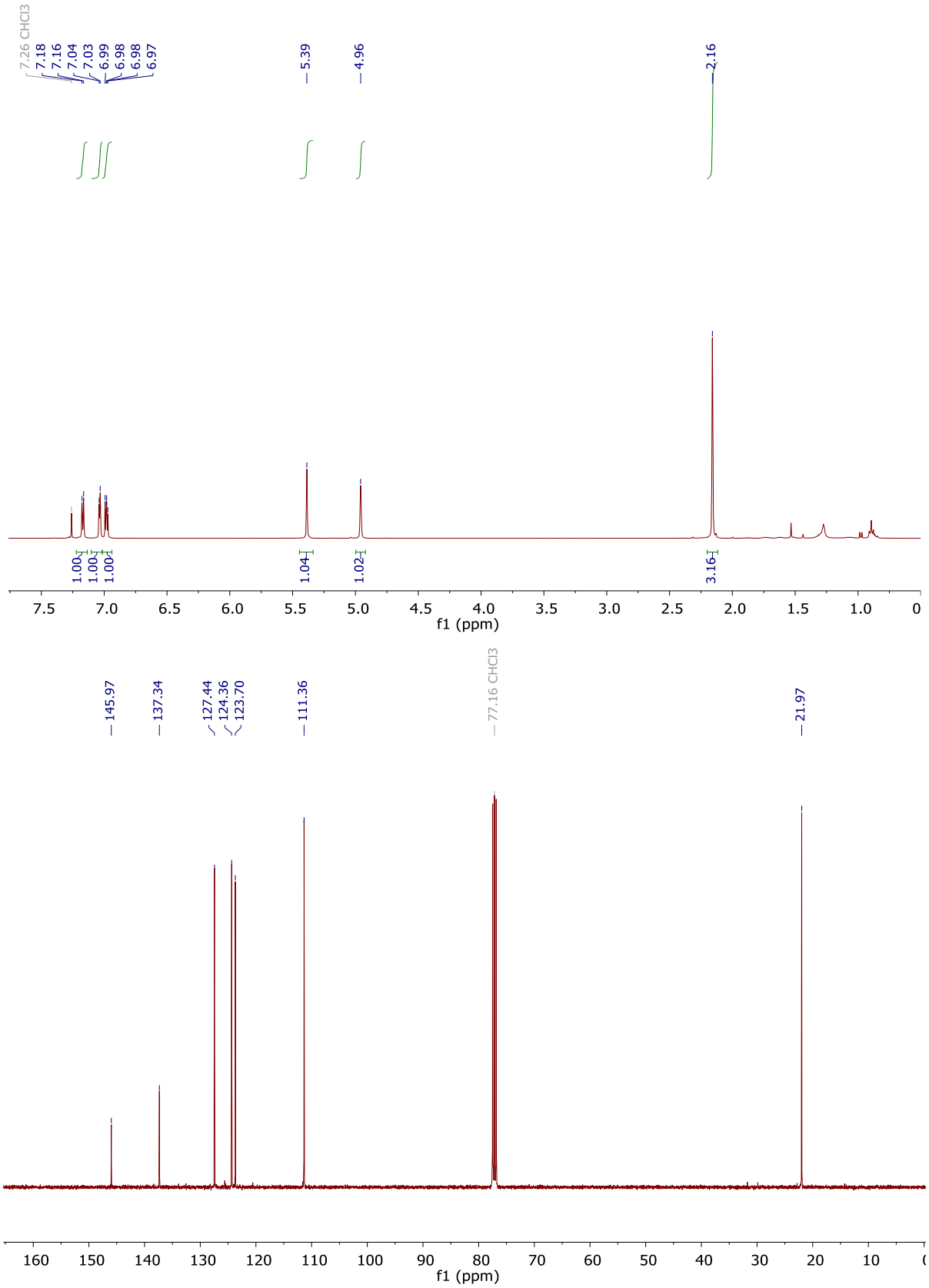

Figure 2.5. ^{1}H and ^{13}C NMR of Compound **2**.

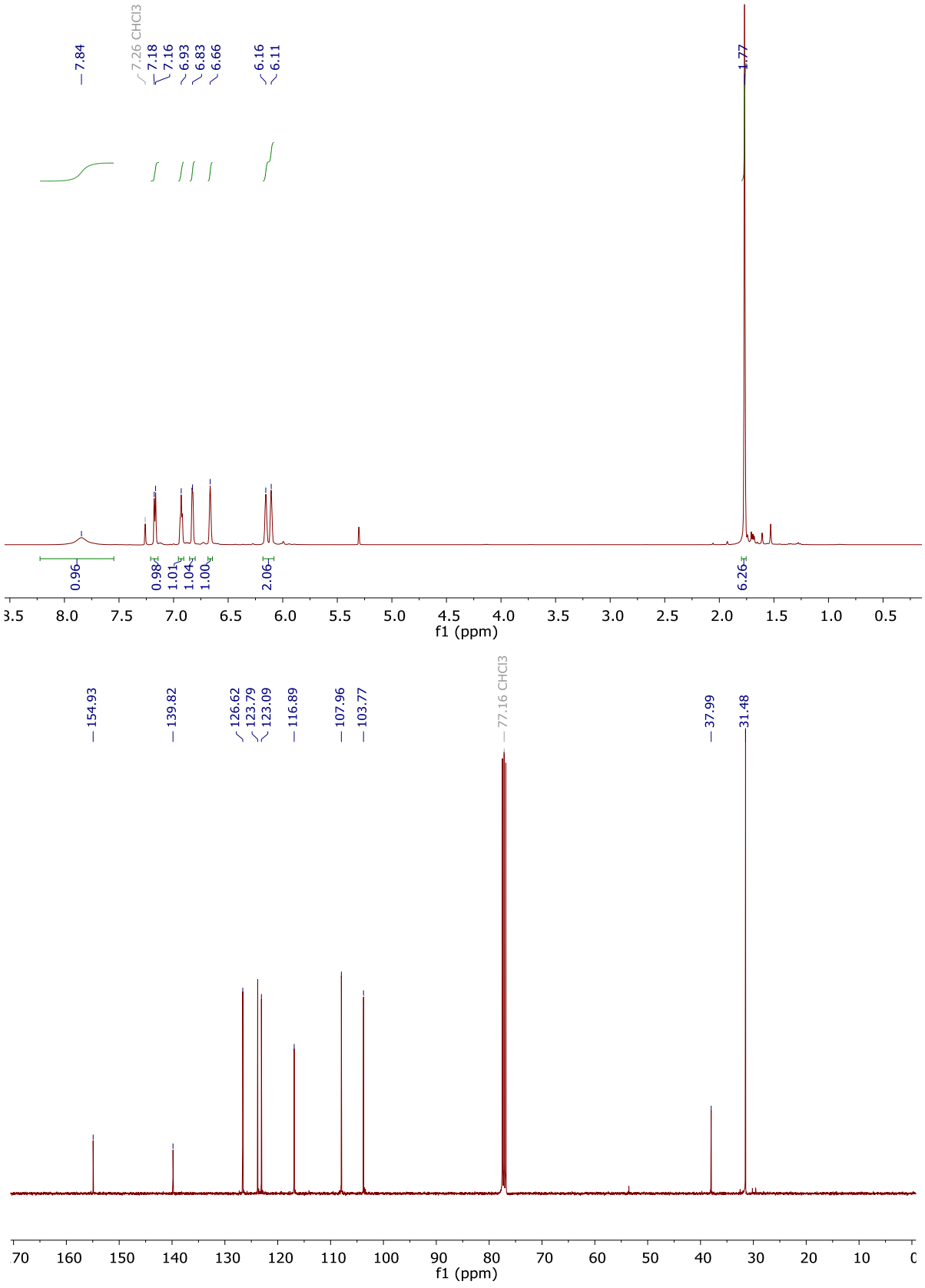

Figure 2.6. ^{1}H and ^{13}C NMR of Compound **3**.

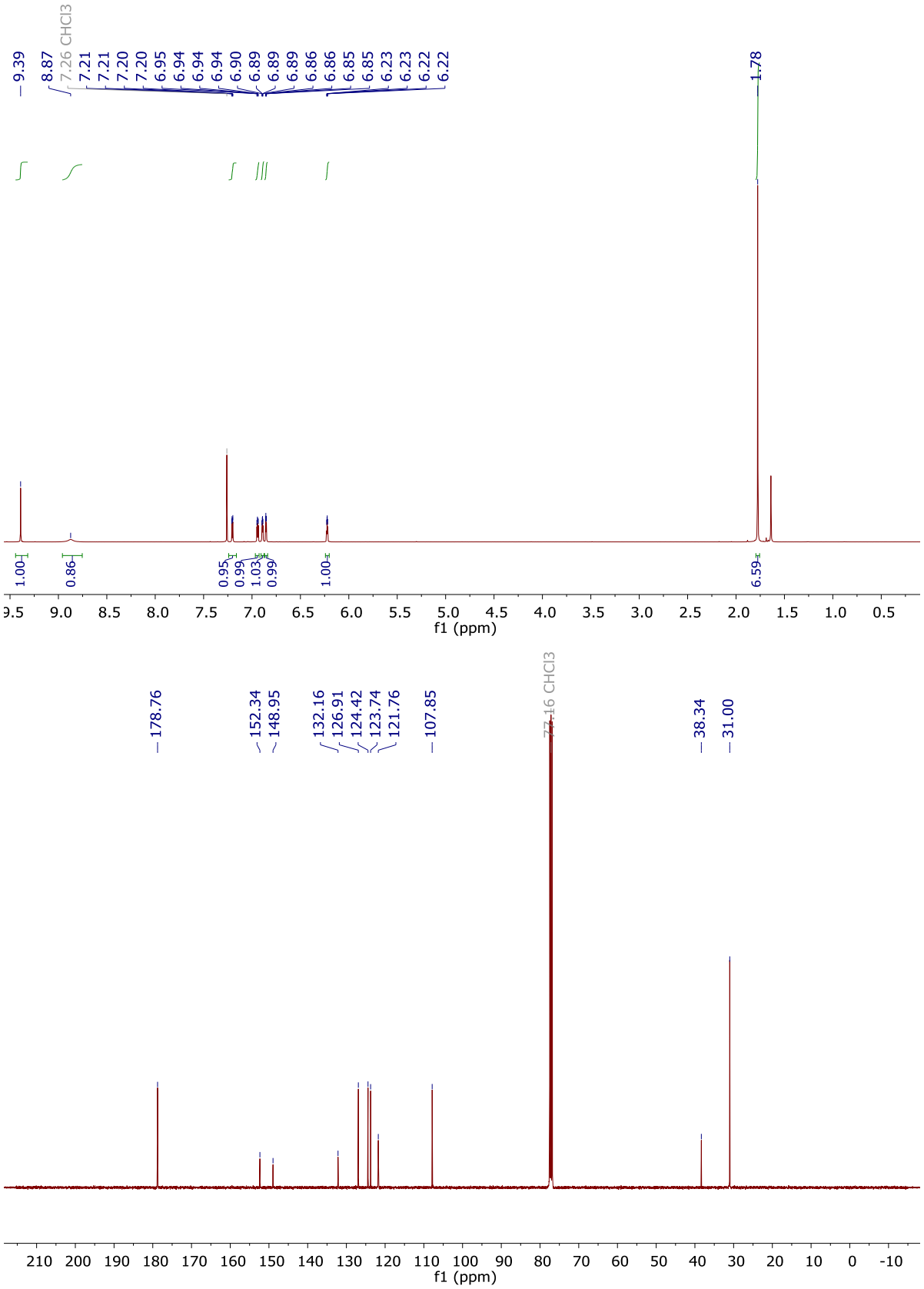

Figure 2.7. ^{1}H and ^{13}C NMR of Compound **4**.

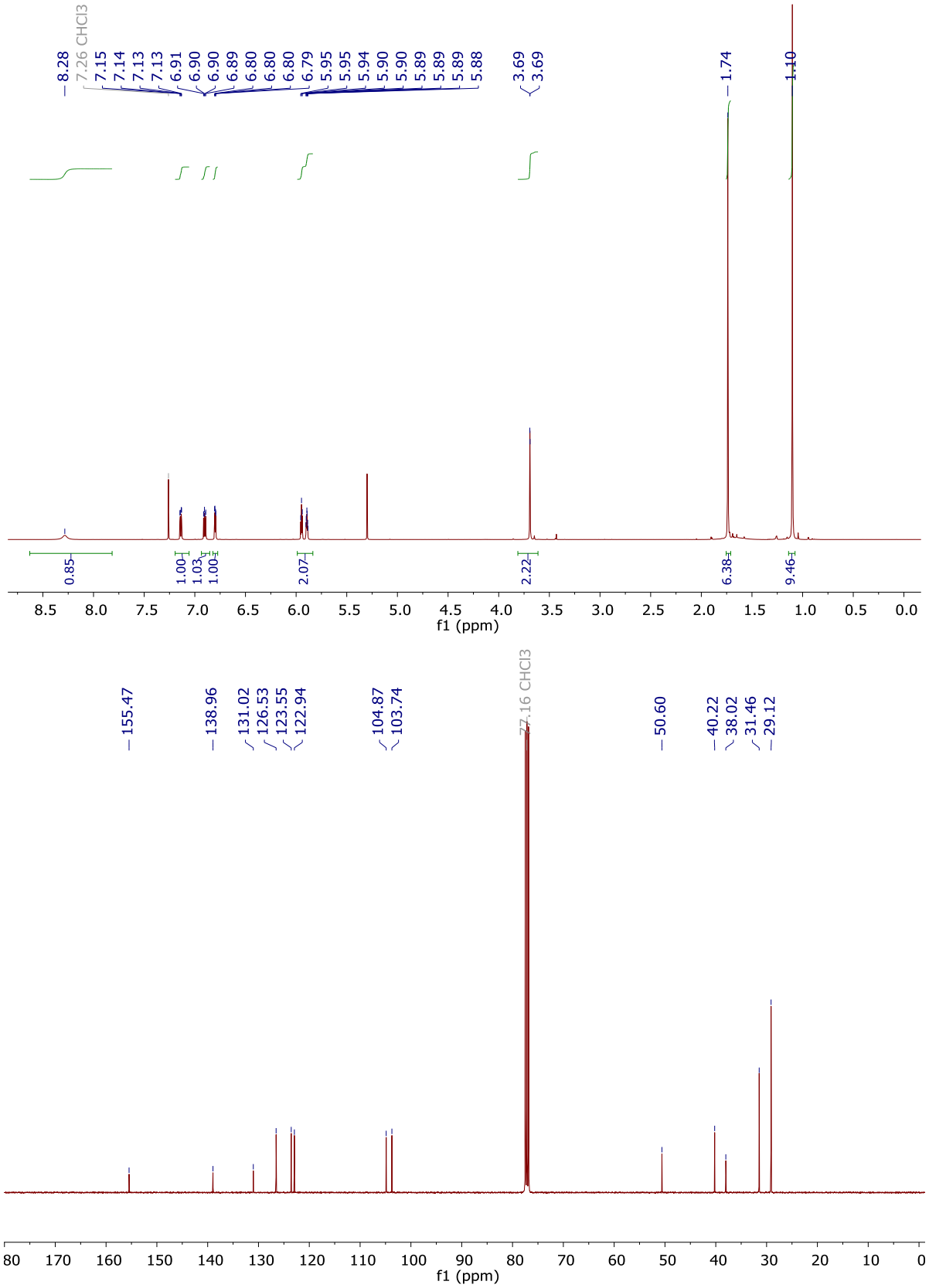

Figure 2.8. ^{1}H and ^{13}C NMR of **SNNH^{t}Bu**.

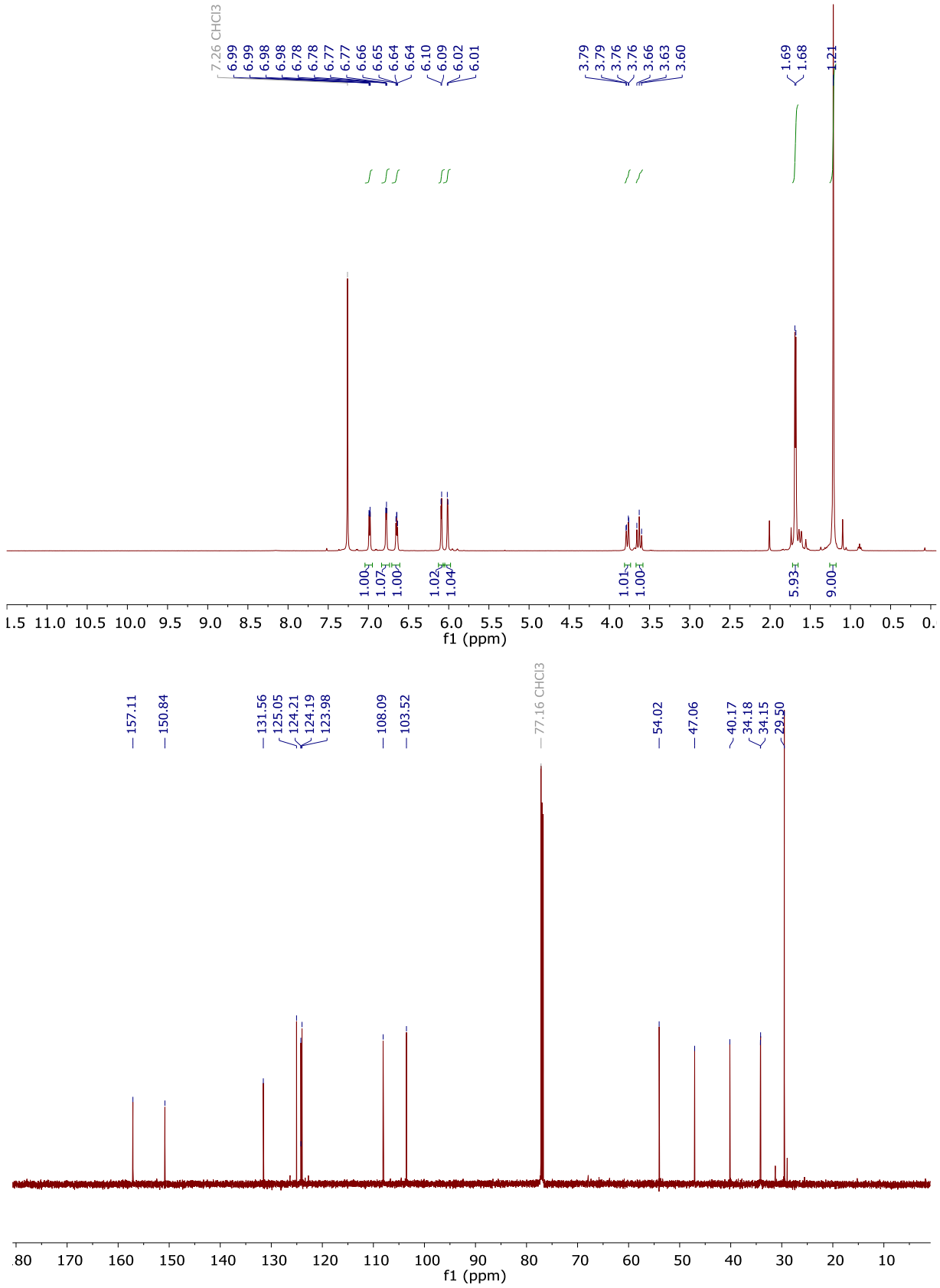

Figure 2.9. ^{1}H and ^{13}C NMR of **[CuSNNH^{t}Bu]$_2$**.

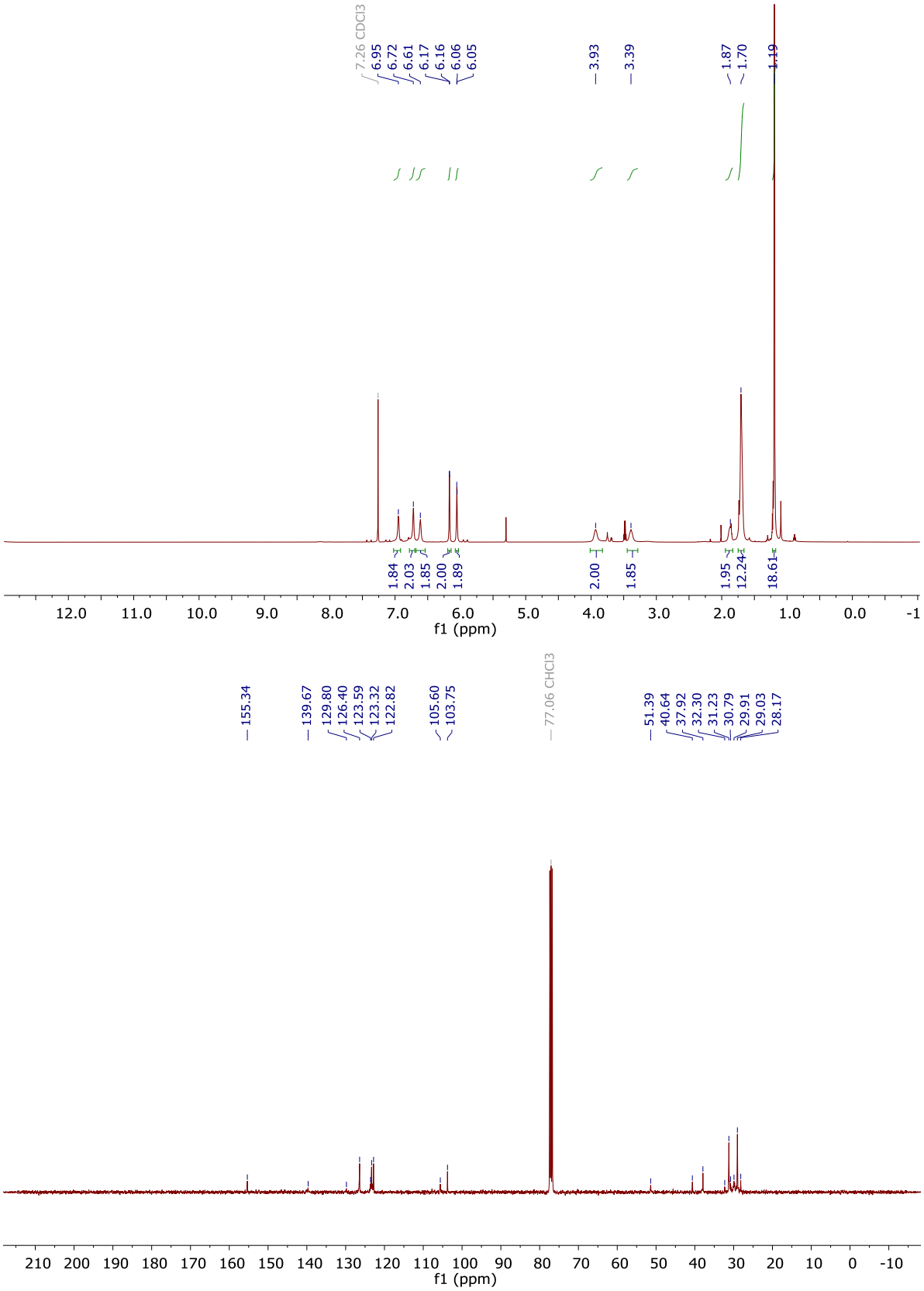

Figure 2.10. ^{1}H and ^{13}C NMR of **[AgSNNH^{t}Bu]$_2$**.

2.5.4. Solid-State UV-Vis Absorbance of SNNH^{t}Bu, [CuSNNH^{t}Bu]$_2$, and [AgSNNH^{t}Bu]$_2$

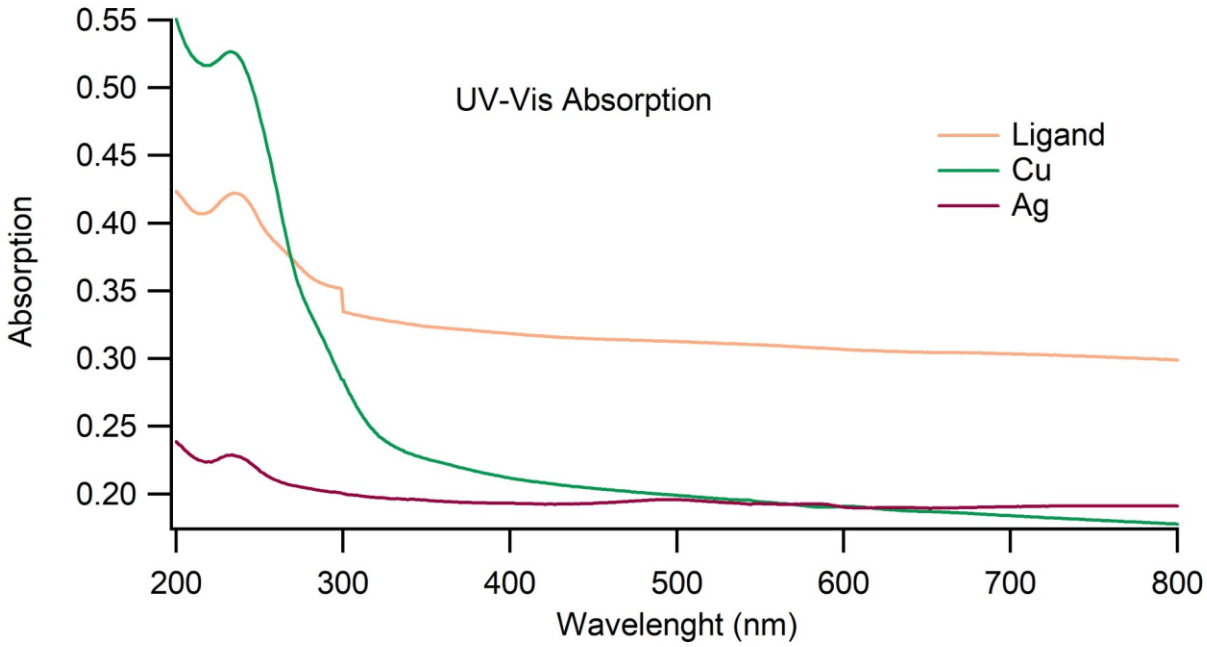

Figure 2.11. Solid-state UV-vis absorption of **SNNHtBu**, **[CuSNNHtBu]$_2$**, and **[AgSNNHtBu]$_2$**. Spectra were recorded using an Agilent Cary 5000 UV-Vis-NIR Spectrophotometer, and by placing a thin layer of the solid compound as a powder between two quartz slides.

2.5.5. ORTEP Visualization of Compound 4

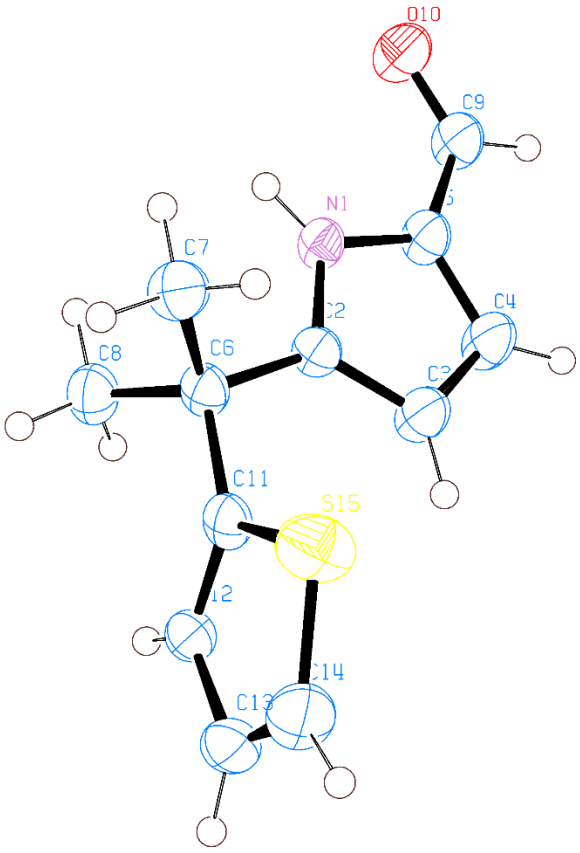

Figure 2.12. ORTEP3 representation (thermal ellipsoids at 50%) for Compound **4**.

2.5.6. Crystallographic Data for 4, SNNH^{t}Bu, [CuSNNH^{t}Bu]$_2$, and [AgSNNH^{t}Bu]$_2$

Table 2.2. Select Crystal Data, Data Collection, and Refinement Parameters for Compound **4** and **SNNH^{t}Bu**. [a]Definition of R indices: $R_1 = \Sigma(F_O - F_C)/\Sigma(F_O)$; $wR_2 = [\Sigma[w(F_O^2 - F_C^2)^2]/[\Sigma[w(F_O^2)^2]]^{1/2}$

	4	**SNNH^{t}Bu**
empirical formula	$C_{12}H_{13}NOS$	$C_{16}H_{24}N_2S$
FW	219.29	276.43
lattice type	Monoclinic	Triclinic
space group	*P2$_1$/c*	*P-1*
T, K	200.00(10)	200.00(10)
a, Å	6.29549(17)	9.7036(5)
b, Å	24.5765(6)	9.8370(6)
c, Å	7.34896(19)	18.7673(5)
α, deg	90	90.700(4)
β, deg	95.716(2)	93.064(3)
γ, deg	90	114.759(6)
V, Å^3	1131.39(5)	1623.24(15)
Z	4	4
ρ_{calc}/Mg m^{-3}	1.287	1.131
μ(Cu/Mo, Kα) mm^{-1}	2.310 (Cu)	1.54184 (Cu)
F(000)	464.0	600.0
crystal size, mm^3	0.22x0.05x0.03	0.08x0.06x0.06
range Θ collected, deg	3.597 to 79.933	2.359 to 72.128
Reflns (collected/unique)	9110/2420	21979/6325
Abs cor	Semi Empirical based upon equivalents	
max and min transmn coeff.	1.000 and 0.679	0.985 and 0.978
goodness of fit	1.080	1.090
R_1 (I>2σ(I))[a]	0.0572	0.0796
wR_2 (all data)[a]	0.1699	02648
Peak and hole, e Å^{-3}	0.488 and -0.622	0.470 and -0.632

Table 2.3. Select Crystal Data, Data Collection, and Refinement Parameters **[CuSNNH^{t}Bu]$_2$** and **[AgSNNH^{t}Bu]$_2$**. [a]Definition of R indices: $R_1 = \Sigma(F_O - F_C)/\Sigma(F_O)$; $wR_2 = [\Sigma[w(F_O^2 - F_C^2)^2]/[\Sigma[w(F_O^2)^2]]^{1/2}$

	[CuSNNH^{t}Bu]$_2$	**[AgSNNH^{t}Bu]$_2$**
empirical formula	$C_{32}H_{46}Cu_2N_4S$	$C_{32}H_{46}Ag_2N_4S$
FW	677.93	766.59
lattice type	orthorhombic	Orthorhombic
space group	*Pbcn*	*Pbcn*
T, K	200.00(10)	149.99(10)
a, Å	19.30860(10)	19.40740(10)
b, Å	14.49140(10)	14.44240(10)
c, Å	11.34470(10)	11.56380(10)
α, deg	90	90
β, deg	90	90
γ, deg	90	90
V, Å^3	3174.34(4)	3241.21(4)
Z	4	4
ρ_{calc}/Mg m^{-3}	1.419	1.571
μ(Cu/Mo, Kα) mm^{-1}	3.085 (Cu)	11.099 (Cu)
F(000)	1424.0	1568.0
crystal size, mm^3	0.17x0.13x0.06	0.13x0.08x0.04
range Θ collected, deg	3.814 to 79.791	3.815 to 79.986
Reflns (Collectd/unique)	15711/3424	18175/3524
Abs cor	Semi Empirical based upon equivalents	
max and min transmn coeff.	1.000 and 0.841	1.000 and 0.578
goodness of fit	1.032	1.074
R_1 (I>2σ(I))[a]	0.0321	0.0241
wR_2 (all data)[a]	0.0896	0.0631
Peak and hole, e Å^{-3}	0.602 and -0.477	0.328 and -0.878

Chapter 3 - Effects of Ligand Modification on the Fluorescent Properties and the Cu-Cu Interaction of a Dinuclear Cu^{I} Complex

3.1. Abstract

Organic light emitting dioides (OLEDs) and thermally activated delayed fluorescent (TADF) emitters are becoming a more common feature used in display technologies. A desire to move away from heavy and rare earth metals has made Copper (I) or Cu^{I} a desirable alternative. However, fine tuning of the excitation and emission properties of these complexes is of high importance. As such, we report the structural modification of a previously reported thiophene containing SNN dincuclear Cu^{I} complex. The synthesis, characterization, and fluorescent properties of two new ligands are investigated. Coordination of these two new ligands along with **NNH^{t}Bu** to Cu^{I} are conducted. These three new dinuclear Cu^{I} complexes are synthesized, characterized and their fluorescent and structural properties are compared and contrasted against themselves and the parent compound of **[CuSNNH^{t}Bu]$_2$**.

3.2. Introduction

Compounds capable of emitting light after entering an electronically excited state are often referred to as lumiphores. These compounds and materials have gained immense interest in many academic fields such as biology, chemistry, and material sciences for their application in diagnostic tools, fluorescent dyes, and in biological imaging giving the ability to visualize and study complex systems. [15–17] Industrial applications of lumiphores have also been applied to chemical detection,[116,117] sensing and anti-counterfeit deterrents[118–120] and textiles.[121,122] One of the most notorious applications of lumiphores are in displays such as liquid crystal displays (LCDs)[123–125] and organic light emitting diodes (OLEDs).[20,126]

OLEDs often relay on rare and expensive transition metals such as In,[19] Pd,[127] Ir,[58,59] and Pt.[30] With a strong spin-orbit coupling, these systems are allowed to harvest triplet state electrons which is something simple organic molecules cannot do.[21] However, these metals are often associated with high cost, toxicity and hazardous environmental impact. As such, recent advances in this field have shown that thermally activated delayed fluorescent (TADF) emitters, more specifically Cu TADF emitters, are a good alternative.[33–35,128] Designed to have a small energy splitting between the first singlet excited state (S_1) and the first triplet excited state (T_1), TADFs are able to have a low energy barrier for intersystem and reverse intersystem crossing.[35] At ambient temperatures, this allows for what appears to be delayed fluorescence and harvesting of excited electrons in the singlet state.[21]

When looking at Cu^I TADF emitters in the literature, they often fall into two classes either mono- or dinuclear complexes. Mononuclear complexes can further be split into three main categories; cationic tetrahedrally coordinated, neutral tetrahedrally coordinated, or trigonally coordinated complexes. From these classes, it has been shown that trigonally coordinated complexes can have external quantum efficiencies (EQEs) over 20%, outperforming tetrahedrally coordinated complexes that have EQEs in the range of 15-18%. Dinuclear complexes are overwhelmingly made up of halide- or pseudo halide-bridged Cu^I complexes in a tetrahedral coordination. These complexes have been shown to have EQEs of up to 16%. These findings highlight how trigonally coordinated complexes can outperform tetrahedrally coordinated complexes. This results from tetrahedrally coordinated complexes being able to under John-Teller Distortion resulting in nonradiative decay.

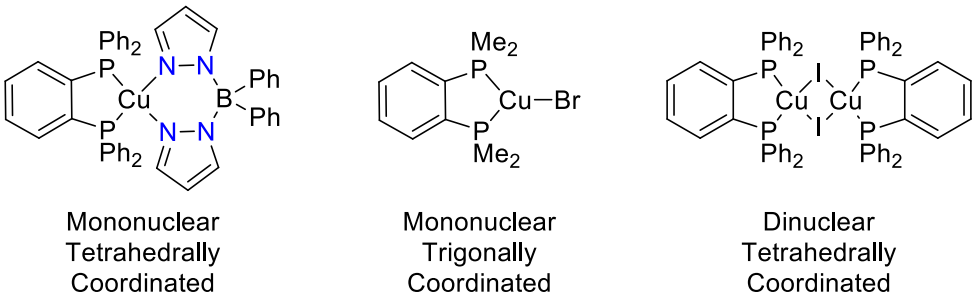

Figure 3.1. Select examples of fluorescent Cu^{I} complexes that demonstrate TADF emission.

Due to the closed d-shells of Cu^{I} species, Cu^{I} has the ability to form a variety of different conformations such as cubes, clusters, extended metal atomic chains, and more. One particular structure that has not seen any applications in the field of luminescence and TADF emitters are dinuclear trigonally coordinated complexes. This kind of coordination has been structurally known since 1961[42] when the crystal structure of diazoaminebenzene Cu^{I} (**1**) was elucidated. It wasn't until 1995[43] when its fluorescent properties were first investigated despite being synthesized as early as 1900. When comparing the fluorescence of **1** to that of an amidinate-supported dinuclear Cu^{I} (**2**),[49] a drastic change is observed. The fluorescence of **1** suggested that the emission (600 nm) was polarized parallel to the absorption (500 nm) which indicates that symmetry of the Frank-Condon active modes was the same along the spectrum.[43] Compound **2**, on the other hand, demonstrated an excitation maximum at 330 nm (λ_{ems} = 535 nm) and had a consistent emission peak at 535 nm despite being excited over a wide range demonstrating non-Frank-Condon active modes.[49] The vast change in absorption and symmetry of these complexes demonstrates how a simple, single atom change in the ligand can have consequences on the fluorescence of the molecule.

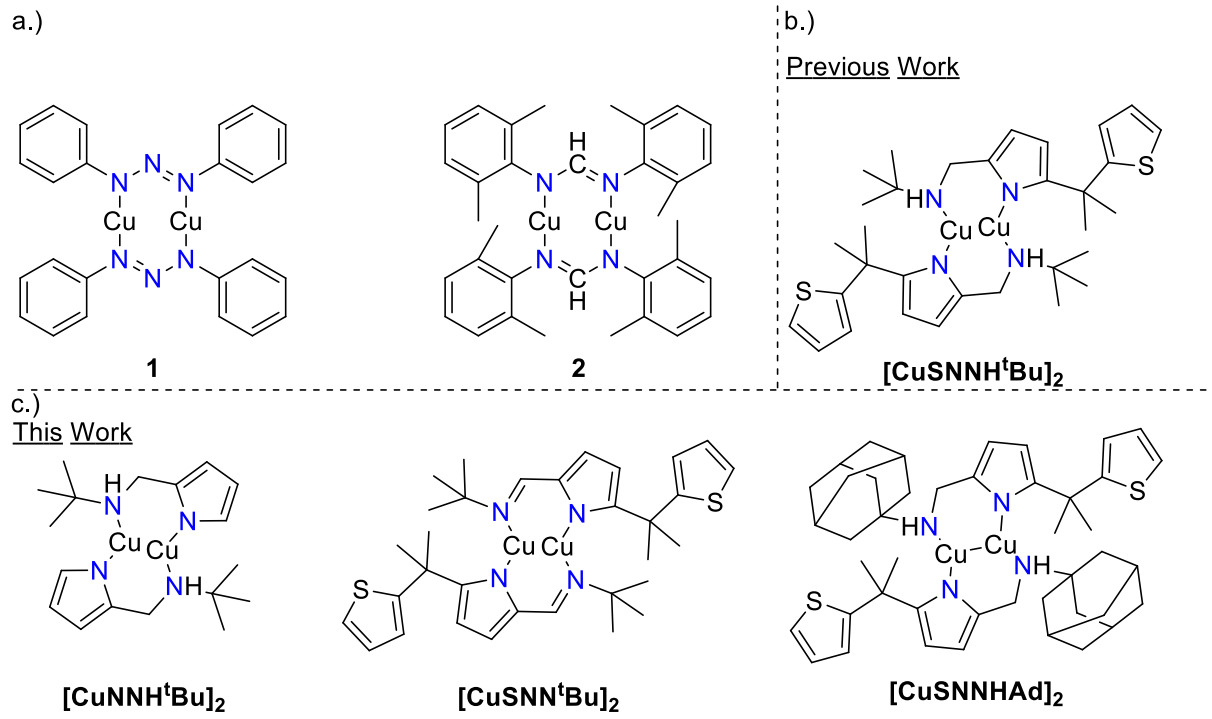

Figure 3.2. a.) Chemical structures of compounds **1** and **2**, b.) chemical structure of **[CuSNNH^{t}Bu]$_2$**, and c.) chemical structures of **[CuNNH^{t}Bu]$_2$**, **[CuSNN^{t}Bu]$_2$**, and **[CuSNNHAd]$_2$**.

With this in mind, our group had previously synthesized a dinuclear Cu^I complex, **[CuSNNH^{t}Bu]$_2$**, based upon a thiophene-containing SNN ligand, **SNNH^{t}Bu**, that demonstrated T-shape geometry around the Cu^I centers. When looking at the fluorescence spectrum of **SNNH^{t}Bu**, it was seen to have an excitation maximum at 355 nm (λ_{ems} = 398 nm) and a major emission peak at 398 nm while demonstrating Frank-Condon like active modes. Upon coordination, **[CuSNNH^{t}Bu]$_2$** demonstrated a Cu-Cu distance of 2.686 Å and had a similar excitation maximum at 350 nm which is suggestive of ground-state homogeneity (e.g., one emitting species). The emission of **[CuSNNH^{t}Bu]$_2$** showed two distinct peaks: 486 and 525 nm. These two peaks were ascribed to the two different isomers found based upon the disorder in the thiophene. This was further verified by time-dependent DFT. With these findings, we wanted to

further investigate how the ligand impacted fluorescence as well as the Cu-Cu interaction. Herein, we report the synthesis of two new ligands and three new dinuclear Cu^{I} complexes. The fluorescence of each as well as their fluorescent properties are investigated and discussed.

3.3. Results and Discussion

3.3.1. Ligand Synthesis and Characterization

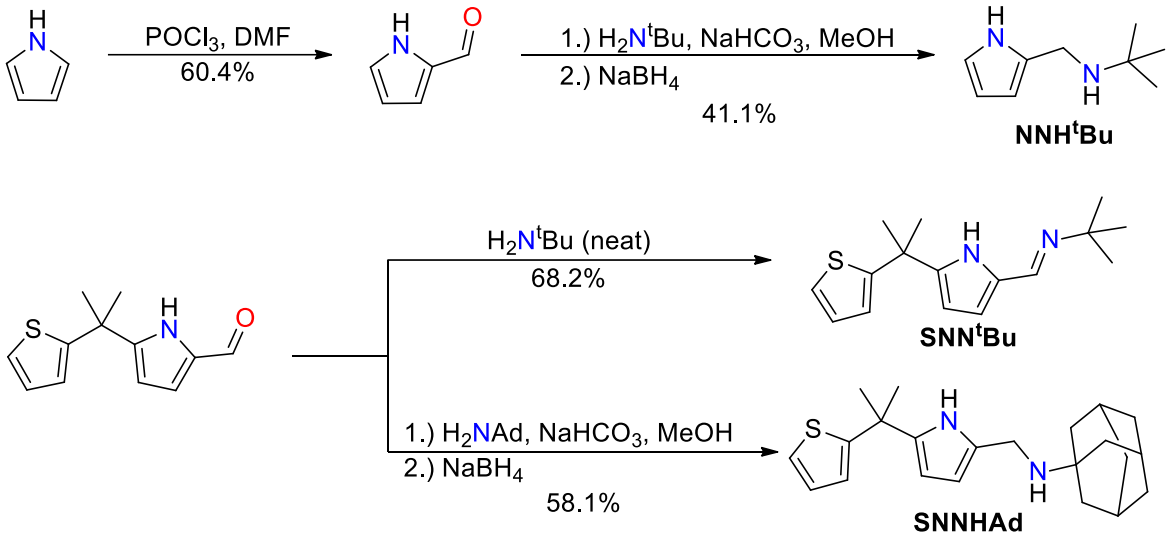

Scheme 3.1. Synthetic pathway for the synthesis of **NNH^{t}Bu**, **SNN^{t}Bu**, and **SNNHAd**.

Three different ligands were synthesized for this study. The first ligand was N-((1H-pyrrol-2-yl)methyl)-2-methylpropan-2-amine or **NNH^{t}Bu**. By first conducting a formylation under Vielsmeyer-Haack conditions to generate the 2-formyl pyrrole, a subsequent reductive amination could be carried out by monitoring via ^{1}H NMR for the disappearance of the aldehyde peak at 9.74 ppm and the formation of the imine at 7.98 ppm. The crystal structure of **NNH^{t}Bu** had been previously reported showing dimerization with hydrogen bonding between the pyrrole N-H and the pendant ^{t}butylamine.[129]

The other two ligands were synthesized from the corresponding aldehyde that had been previously reported (see **Chapter 1**). The imine or **SNN^{t}Bu** was synthesized by mixing the

aldehyde with 5 equivalents of ^{t}butylamine neat. The reaction was monitored via ^{1}H NMR by watching for the disappearance of the aldehyde at 9.39 ppm and the product imine peak at 7.97 ppm. After removal of excess ^{t}butylamine, the desired product was obtained in 68.2% yield. It is worth noting that depending on the concentration of the NMR sample, the pyrrole N-H would drastically shift. This may have to do with resonance of the pyrrole and imine as well as hydrogen bonding to water (**Figure 3.**). The product was characterized via NMR as well as single crystal X-Ray diffraction (XRD). Crystals could be grown by slow evaporation from hexanes. Unlike the saturated version, **SNNH^{t}Bu**, did not dimerize on itself, but instead formed a dimer with a single water molecule trapped inside. The water molecule formed four hydrogen bonds. Two of the bonds were between the oxygen of water and the pyrrole N-H with a distance of 2.064 Å. An additional hydrogen bond was also seen between the hydrogen of water and the nitrogen of the imine with a distance of 1.955 Å.

By performing a similar one-pot reductive amination as with **NNH^{t}Bu** and **SNNH^{t}Bu**, **SNNHAd** could be generated in 58% yield. The ligand was characterized by NMR as well as single crystal XRD. Crystals were also grown by evaporation from a solution of hexanes. Analogous to the two previously mentioned saturated ligands, **SNNHAd** also showed dimerization with hydrogen bonding between the pyrrole N-H and the adamantyl nitrogen with a distance of 2.150 Å. This bond is approximately 0.109 Å shorter compared to **SNNH^{t}Bu** which has a distance of 2.259 Å. In each of the symmetrically independent molecules, the thiophene rings are disordered. In one molecule, the occupancies are 53%, 18%, and 29% for the thiophene, while in the other it is 69% and 31%. The adamantyl-group also shows disorder with occupancies of 83% and 17% for the first molecule and 66% and 34% for the second.

It is worth noting that a 4-methoxybenzylamine derivative, **SNNHBn-4-MeO**, was also synthesized following a similar synthetic pathway to **SNNHAd** (See **3.5. Supplementary Information**). This complex showed a hydrogen bond distance of 2.159 Å between the pyrrole N-H and the benzylic amine. While being exactly 0.1 Å shorter than **SNNH^{t}Bu**, it does appear slightly longer than **SNNHAd**. While still being bulky, it does have more flexibility than adamantylamine does which could explain the slightly longer hydrogen bond as the flexibility allows for the pyrrole and amine to distance themselves. The shortening of the hydrogen bond distance of **SNNHAd** and **SNNHBn-4-MeO** is likely contributed to the bulk of the pendent amine pushing the pyrrole N-H and amine closer together.

a.)

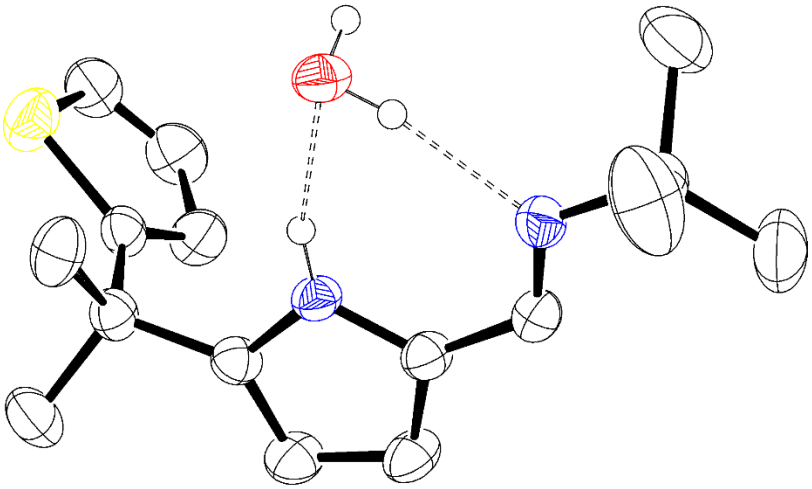

b.)

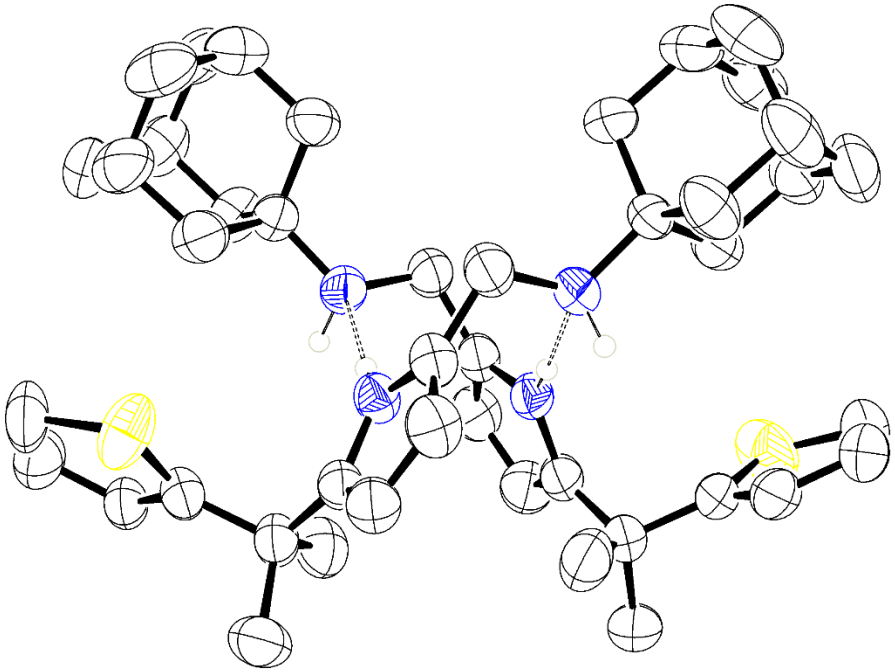

Figure 3.3. ORTEP3 representation (thermal ellipsoids at 50% probability) for a.) **SNN^{t}Bu**, most hydrogens have been omitted for clarity; and b.) **SNNHAd**, most hydrogens and disorder in the thiophene and adamantyl-groups have been omitted for clarity.

3.3.2. Ligand Fluorescence

The fluorescence of each of the new thiophene containing ligands were investigated by placing a solid sample of the powdered ligand between two quartz slides. The slides were then placed into a FluoroMax-2 in a front face illumination configuration. We began by first looking at the fluorescence of **SNN^{t}Bu**. This ligand appeared as an off yellow sample; however, crystals appeared colorless. When held under a standard UV-lamp, no fluorescence or phosphorescence was observed. When samples were run on the FluoroMax-2, **SNN^{t}Bu** was seen to have a main excitation peak at 370 nm while showing several small emission peaks at 374, 383 and 394 nm which are on the cusp of the visible region. These spectra are significantly different compared to **SNNH^{t}Bu**. The conjugation has red shifted the excitation spectrum and blue shifted the emission spectrum. This is common as conjugation can often reduce the energy gap of the HOMO and LUMO.[130]

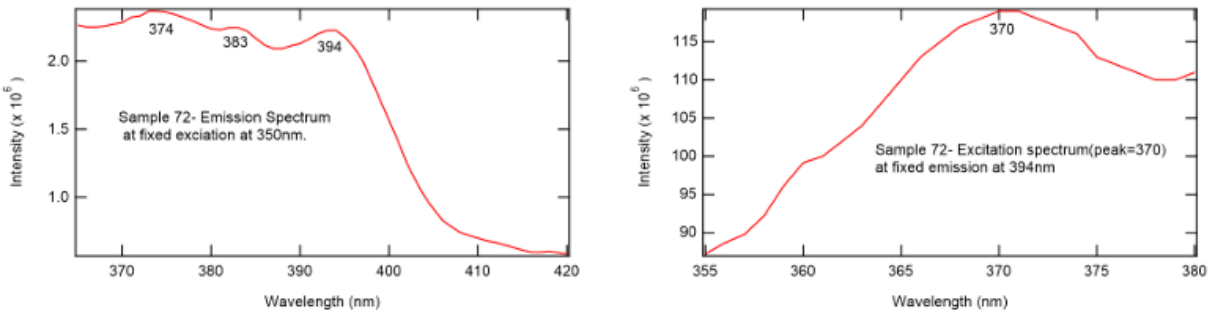

Figure 3.4. Emission (left) and excitation (right) spectrum of **SNN^{t}Bu**.

Our investigations then moved to **SNNHAd** which appeared to have a broad excitation range from 345-355 nm. The emission spectrum gave a fairly similar spectrum to that of **SNNH^{t}Bu** with a major peak at 401 nm and a small shoulder at 398 nm. These results are nearly identical to that of **SNNH^{t}Bu** which had an excitation range of 345-360 nm and showed the major excitation peak at 398 nm. These results suggest that distance bulk as well as the distance of the pyrrole to

the amine has little effect on the fluorescence. This makes sense as for **SNNH^{t}Bu** the HOMO is almost entirely on the pyrrole and the LUMO is on the thiophene.

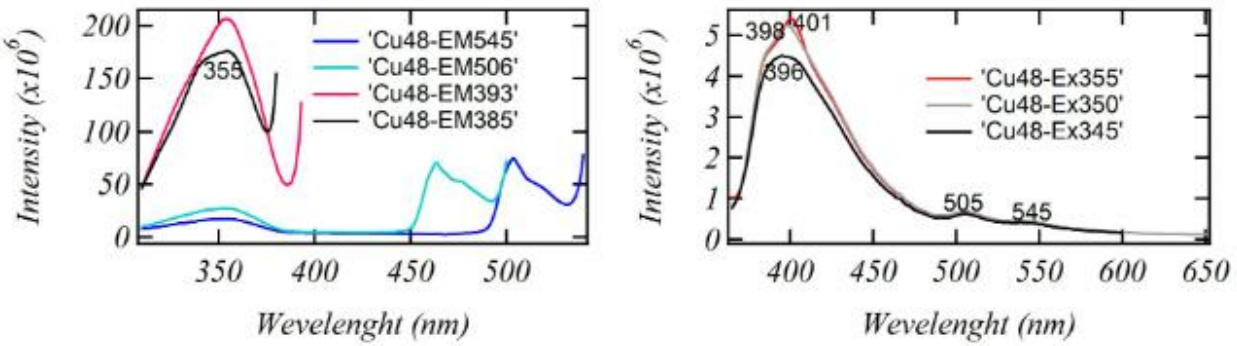

Figure 3.5. Excitation (left) and emission (right) spectrum of **SNNHAd**.

3.3.3. Synthesis and Characterization of Cu^I Complexes

The corresponding dinuclear complexes;**[CuNNH^{t}Bu]$_2$**, **[CuSNN^{t}Bu]$_2$**, and **[CuSNNAd]$_2$**, were synthesized in a similar fashion to **[CuSNNH^{t}Bu]$_2$**. **[CuNNH^{t}Bu]$_2$** was synthesized by first deprotonation of the ligand with KH in acetonitrile. After the generation of hydrogen gas had ceased, [Cu(MeCN)$_4$][PF$_6$] was added as a solution in acetonitrile and stirred for two hours, and the reaction was placed in a -35^{o}C freezer overnight. The reaction was filtered and the solid dissolved in DCM. The suspension was filtered through a celite plug to remove undesired salts, followed by removal of solvent. Undesired organic materials were removed by washing the red-brown powder with pentanes to afford the desired dinuclear complex in only 13.2% yield. Coordination was first confirmed by the disappearance of the pyrrole N-H at 8.74 ppm as well as a broadening of the methylene peak at found at 4.02 ppm in the ^{1}H NMR. The structure was further established by single crystal XRD. Crystals were grown from a saturated solution of the complex in DCM layered with acetonitrile with the structure shown in **Figure 3.6**. Select bond lengths, angles and torsion angles are summarized in **Table 3.1**. The structure showed two independent dimeric species per unit cell. The Cu-Cu interactions had distances of 2.6923 Å

and 2.6722 Å. The average of these two, 2.6917 Å, was only 0.0056 Å longer than **[CuSNNH^{t}Bu]$_2$**. These findings suggest that the thiophene ring does not contribute to or affect the Cu-Cu interaction.

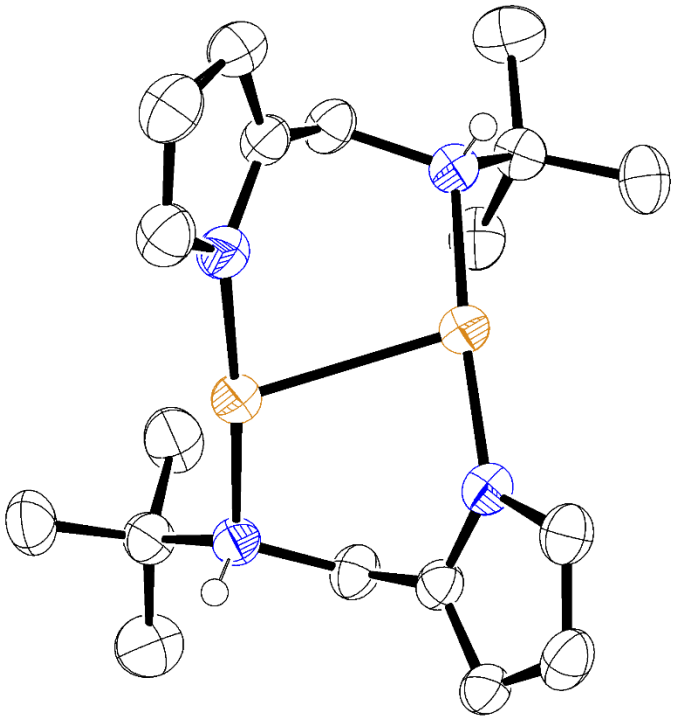

Figure 3.6. ORTEP3 representation (thermal ellipsoids at 50%) for **[CuNNH^{t}Bu]$_2$** with most hydrogens omitted for clarity.

[CuSNN^{t}Bu]$_2$ and **[CuSNNAd]$_2$** were synthesized in an identical manner to each other. A solution of the ligand in acetonitrile was added to solid KH. The reaction was allowed to continue until the formation of hydrogen gas ceased. At this point, the deprotonated ligand was added to a solution of $[Cu(MeCN)_4][PF_6]$ in acetonitrile which caused an immediate precipitate to form. The reaction was allowed to stir for an additional two hours. This precipitate was collected on a glass frit and washed with acetonitrile to remove residual KPF_6. The solid was then stirred with DCM and filtered through celite to remove any undesired salts. The solvent was removed, and the powder

was washed with pentanes to afford the corresponding dinuclear complex. Crystals of both could be grown from a solution of DCM layered with acetonitrile and stored at -30ºC.

The unsaturated complex, **[CuSNN^{t}Bu]$_2$**, was first confirmed via ^{1}H NMR by noticing the absence of the pyrrole N-H. Allow significant changes were not seen for the imine C-H, dimethyls, or ^{t}butyl functional groups, changes in the aromatic protons were seen. The thiophenic protons saw an upfield shift from 7.15, 6.91, and 6.82 ppm to 6.79, 6.68, and 6.41 ppm after coordination. The pyrrolic protons, on the other hand, saw a downfield shift from 6.36 and 6.08 ppm to 6.59 and 6.34 ppm. **[CuSNN^{t}Bu]$_2$** was characterized by NMR as well as by single XRD with the structure shown in **Figure 3.7**. From the crystal structure, it was elucidated that the complex formed a dimeric species with two metal centers and two ligands similar to **[CuSNNH^{t}Bu]$_2$**. The thiophenes of each ligand showed disorder with an occupancy of 65 and 35% for one molecule and 55 and 45% for the other. A comparable T-shape geometry was seen around each of the Cu centers where a pyrrolide donor from one ligand and the imine donor from another were *trans* to each other. The bond angle of N_{Pyr}-Cu-N_{tBu} was found to be 174.43º which is a further delineation as compared to the saturated version of 177.97º. However, looking at the other two bond angles around the Cu center showed that the complex was more T-shaped. Bond angles of 85.67º and 93.55º were seen for the N_{Pyr}-Cu-Cu and N_{tBu}-Cu-Cu angles as compared to 80.48º and 101.47º for **[CuSNNH^{t}Bu]$_2$**, respectively. This may contribute to a more equal distance of each donor nitrogen from the metal center as compared to the saturated version (see **Table 3.1.**). **[CuSNN^{t}Bu]$_2$** was found to have a Cu-Cu distance of 2.4659 Å which is much smaller than the 2.6863 Å distance seen in **[CuSNNH^{t}Bu]$_2$**. The reason for this is likely that the unsaturation and increase in conjugation limits flexibility pushing the metal centers closer.

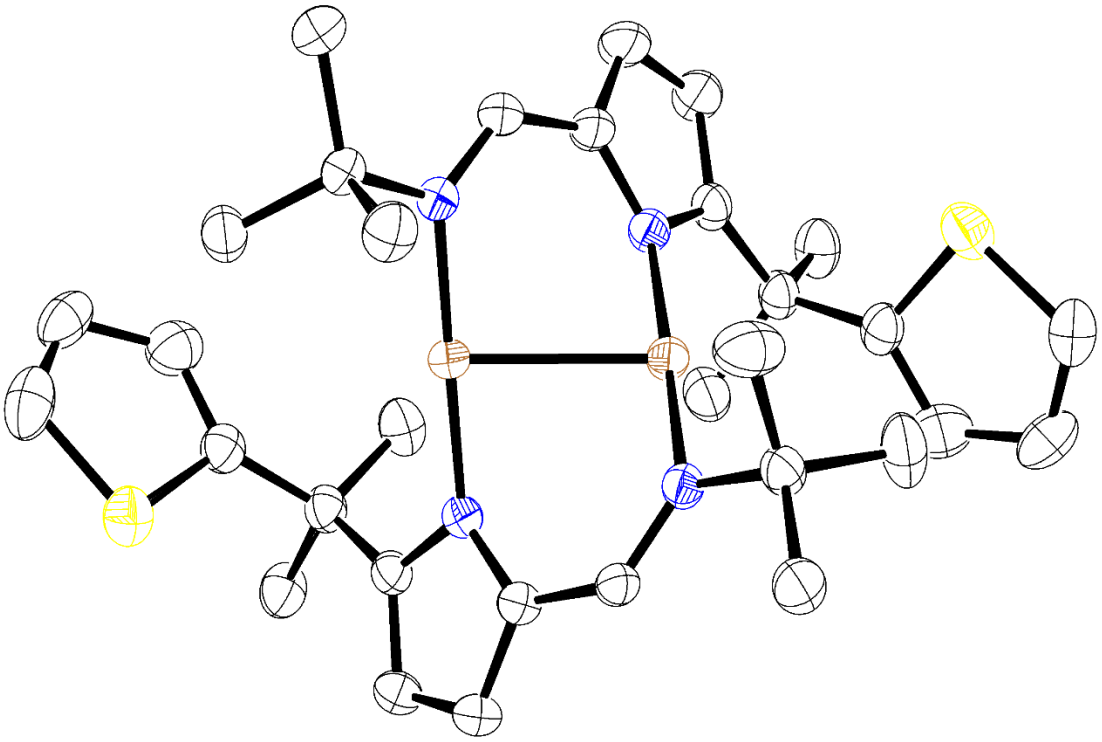

Figure 3.7. ORTEP3 representation (thermal ellipsoids at 50%) for **[CuSNN^{t}Bu]$_2$** with most hydrogens omitted for clarity representation

When looking at **[CuSNNHAd]$_2$**, the ^{1}H NMR was similar to that of **[CuSNNH^{t}Bu]$_2$**. The disappearance of the pyrrole N-H at 8.24 ppm was the first sign of coordination, while another sign was desymmetrization of the methylene protons generating a doublet at 3.85 ppm and a triplet at 3.62 ppm. Aside from characterization via NMR, single crystal XRD was also used to fully elucidate the structure as shown in **Figure 3.8**. Originally, a crystal structure containing three chloroform molecules, and two acetonitrile molecules was obtained. Although the structure was taken using a shorter experiment, they steadily decomposed even at low temperature. Another crystal was also found in the same batch. This crystal lacked any chloroform in the crystal

structure, contained two acetonitrile molecules and appeared to be more stable. As such, discussion as well as data presented in **Table 3.1.** will be the averages of each bond length, bond angle, or torsion angles over the two crystal structures.

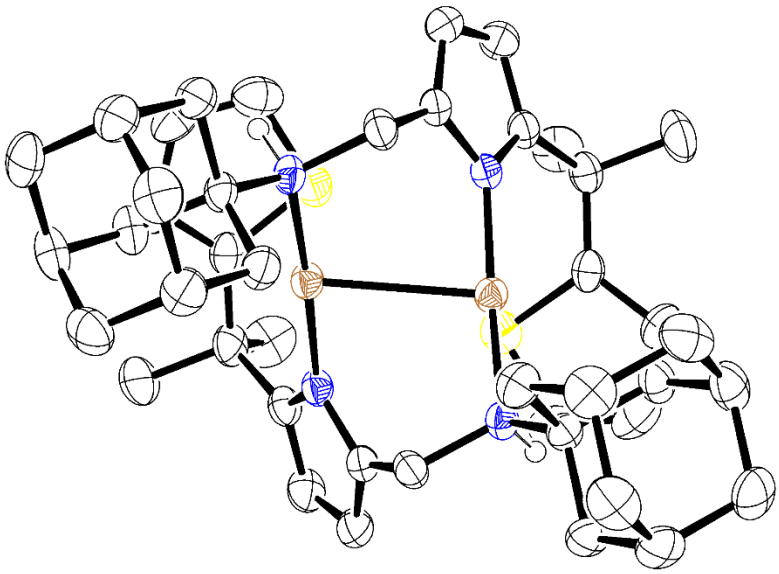

Figure 3.8. ORTEP3 representation (thermal ellipsoids at 50%) for **[CuSNNAd]$_2$** with most hydrogens omitted for clarity representation

[CuSNNHAd]$_2$ formed a dinuclear Cu^I complex with slight distortion from a true T-shaped geometry around each Cu^I center. Compared to **[CuSNNH^{t}Bu]$_2$**, **[CuSNNHAd]$_2$** showed more of a deviation from linearity with a N_{Pyr}-Cu-N_{Ad} bond angle of 172.15º. The N_{Pyr}-Cu-Cu and N_{Ad}-Cu-Cu angles, however, appeared closer to 90º with angles of 84.18º and 99.00º, respectively. **[CuSNNHAd]$_2$** also showed an elongation of the pyrrolide and adamantylamine donors from the Cu^I centers with lengths of 1.866 and 1.943 Å. This is likely due to the bulk of the adamantyls pushing the ligands further way from the Cu^I. The Cu^I-Cu^I distance was much larger than any of the previously reported structures with a distance of 2.7823 Å which is just on the verge of the Van der Waals radii for Cu^I.[131] These observed features are again likely due to the bulk of adamantylamine giving more space for the Cu^I species to sit.

As mentioned, **SNNHBn-4-MeO** was also synthesized. However, following identical synthetic conditions to **[CuSNN^{t}Bu]$_2$** and **[CuSNNHAd]$_2$**, only the dipotassium complex, **[KSNNHBn-4-MeO]$_2$**, could be crystallized (See **3.5. Supporting Information**) despite our best attempts. This complex showed similar geometry to that of its copper counterparts with a T-shaped geometry around each of the potassium centers. The N_{Pyr}-K-N_{Bn} showed a bond angle of 175.07^o with the N_{Pyr}-K-K and N_{Bn}-K-K having bond angles of 82.28^o and 101.66^o, respectively. The N_{Pyr}-K and N_{Bn}-K distances were 1.826 and 1.712 Å, respectively. The K-K distance was 2.761 Å which is well outside the van der Waals distance for potassium.

Table 3.1. Select Bond Lengths, Angles, and Torsion Angles for **[CuNNH^{t}Bu]$_2$**, **[CuSNNHAd]$_2$**, **[CuSNN^{t}Bu]$_2$**, and **[CuSNNH^{t}Bu]$_2$**. [a]Averages of the two different dimeric species in the unit-cell. [b]Averages over both crystal structures obtained (with and without chloroform).

	[CuNNH^{t}Bu]$_2$[a]	**[CuSNNHAd]$_2$[b]**	**[CuSNN^{t}Bu]$_2$**	**[CuSNNH^{t}Bu]$_2$**
		Bond Lengths		
Cu-Cu	2.6917(1) Å	2.7823(4) Å	2.4659(3) Å	2.6863(5) Å
Cu-N_{Pyr}	1.855 Å	1.866 Å	1.876 Å	1.860(5) Å
Cu-N_R	1.897 Å	1.943 Å	1.892 Å	1.937(4) Å
		Bond Angle		
N_{Pyr}-Cu-N_R	173.79º	172.15(6)º	174.43º	177.97(6)º
N_{Pyr} -Cu-Cu	81.12º	84.18(5)º	85.67º	80.48(4)º
N_R -Cu-Cu	103.84º	99.00(3)º	93.55º	101.47(4)º
		Torsion Angles		
N_{Pyr}-Cu-Cu-N_R	45.58º	51.27º	57.83º	52.89º
N_{pyr}-Cu-Cu-N_{Pyr}	138.16º	136.37º	126.87º	127.55º
N_R-Cu-Cu-N_R	130.69º	121.45º	116.87º	126.68º
		Fluorescence		
Excitation (λ_{nm})	532 nm	360 nm	389 nm	350 nm
Emission (λ_{nm})	575 nm	508 and 538 nm	491 and 522 nm	486 and 525 nm

3.3.4. Complex Fluorescence

After the characterization of the complexes, their fluorescent properties were then examined. By first looking at **[CuNNH^{t}Bu]$_2$**, it was apparent that the thiophene was extremely important for fluorescence. When the reddish-brown powder was held under a UV-lamp it was observed that no fluorescence was seen. To further confirm this, the powder of the complex was

placed between two quartz slides and fluorescence was recorded using a FluoroMax-2. **[CuNNH^{t}Bu]$_2$** showed an excitation at 532 nm and an emission at 575 nm with the spectrum shown in **Figure 3.9**. These are similar to Frank-Condon active modes as the two spectrum appear to be near mirror images together.

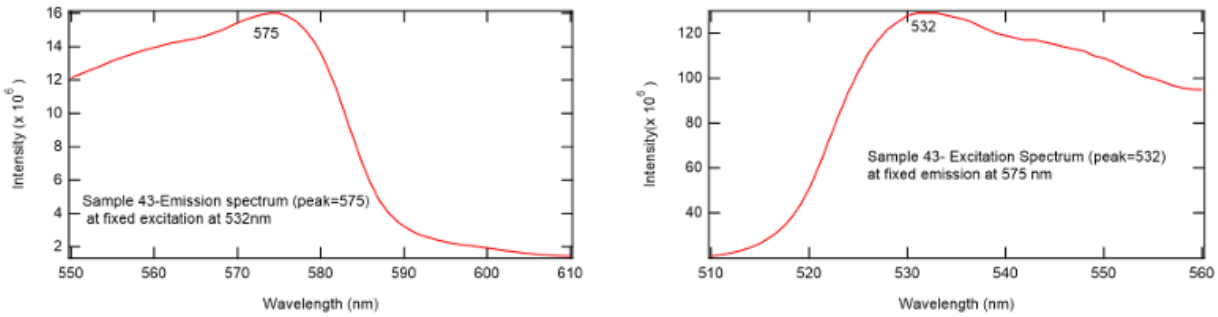

Figure 3.9. Emission (left) and excitation (right) spectrum of **[CuNNH^{t}Bu]$_2$**.

Next, the fluorescence of **[CuSNN^{t}Bu]$_2$** was investigated with the excitation and emission spectrum shown in **Figure 3.10**. **[CuSNN^{t}Bu]$_2$** showed a main excitation at 389 nm which is red shifted by approximately 40 nm compared to **[CuSNNH^{t}Bu]$_2$**. This red shift can likely be contributed to the increase in conjugation of the addition of the imine. Conjugation is known to lower the energy gap between the ground and excited states. The emissions of **[CuSNN^{t}Bu]$_2$** showed two main peaks at 491 and 522 nm. These two peaks are likely due to the two different isomers found within the crystal structure due to the disorder of the thiophene ring. Compared to **[CuSNNH^{t}Bu]$_2$**, the lower wavelength emission appears slightly red shifted from 486 nm while the longer wavelength emission is slightly blue shifted from 525 nm.

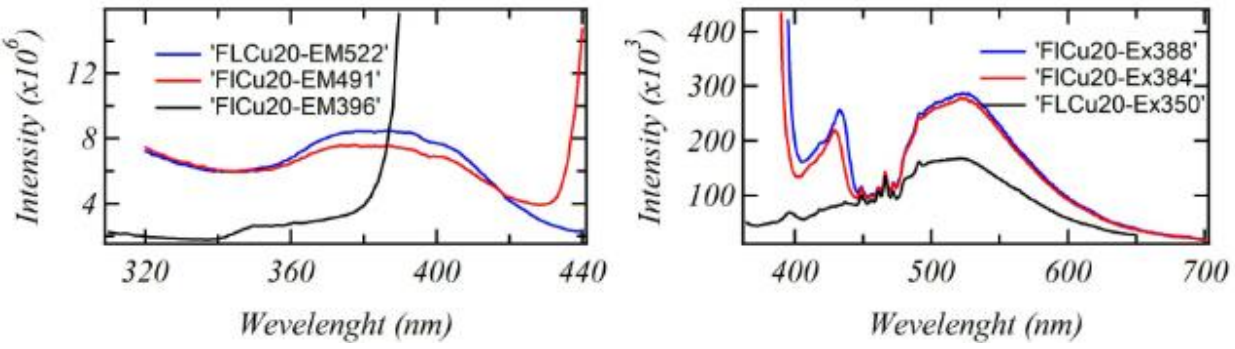

Figure 3.10. Excitation (left) and emission (right) spectrum of **[CuSNN^{t}Bu]$_2$**.

Finally, the fluorescence of **[CuSNNHAd]$_2$** was investigated. **[CuSNNHAd]$_2$** showed only a slight red shift in its excitation wavelength of 360 nm as compared to **[CuSNNH^{t}Bu]$_2$** excitation at 350 nm. The emission of **[CuSNNHAd]$_2$** showed two major peaks: one at 508 nm and another at 538 nm. These two peaks red shifted compared to the two peaks seen for **[CuSNNH^{t}Bu]$_2$** by about 15-20 nm each. The reasons for the two peaks is likely due to the different isomers seen due to the disorder in the thiophene ring, similar to **[CuSNNH^{t}Bu]$_2$**.

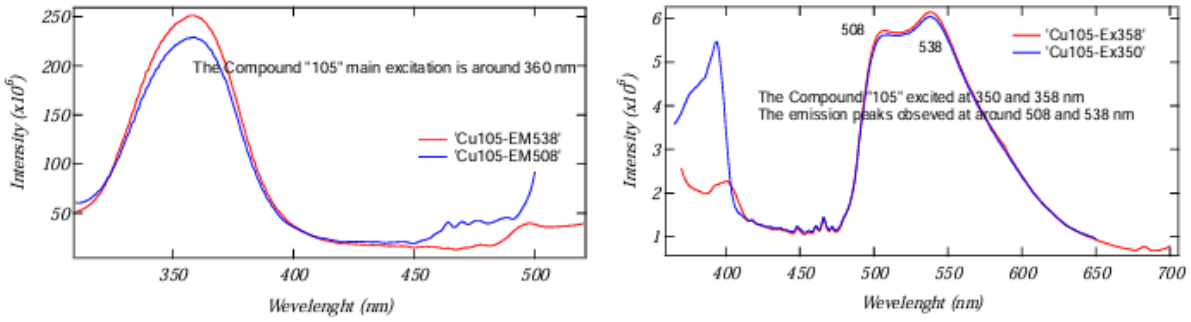

Figure 3.11. Excitation (left) and emission (right) spectrum of **[CuSNNHAd]$_2$**.

3.4. Conclusion

In conclusion, a look into structural modifications of a thiophene containing SNN ligand were investigated. Two new ligands, **SNN^{t}Bu** and **SNNHAd**, were synthesized along with three new dinuclear Cu^I complexes were also synthesized. Investigations into how these modifications affect the fluorescence of the ligand and the complexes as well as the Cu^I-Cu^I interaction were

discussed. It was found that the thiophene was crucial for fluorescence but had little impact on the Cu^{I}-Cu^{I} interaction as shown by little change in the Cu^{I}-Cu^{I} distance. Desaturation of **SNNH^{t}Bu** to **SNN^{t}Bu** showed a quenching of the fluorescence of the ligand likely due to binding to a single water molecule instead of dimerizing with itself. Upon coordination however, a red shift was seen for both the emission and excitation likely due to the increase in conjugation lowering the HOMO-LUMO gap. It was also noticed that a significant shortening of the Cu^{I}-Cu^{I} from 2.6863 Å for **[CuSNNH^{t}Bu]$_2$** to 2.4659 Å for **[CuSNN^{t}Bu]$_2$** was seen in the crystal structure likely resulting from the high ring-strain and lack of flexibility. Finally, when changing the bulk of the pendent amine from ^{t}butyl to adamantyl, a slight red shift in emission was seen but no significant change in excitation was observed. A lengthening in the Cu^{I}-Cu^{I} interaction was also observed increasing to 2.7823 Å.

3.5. Supporting Information

3.5.1. General Considerations

All procedures and manipulations were performed under an argon or nitrogen atmosphere using standard Schlenk-line and glove box techniques unless stated otherwise. Solvents were dried and deoxygenated under argon using a LC Technology Solutions Inc. SP-1 stand-alone solvent purification system, unless stated otherwise. Deuterated solvents were purchased from Cambridge Isotope Laboratories, Sigma Aldrich, Acros Organics, or Alfa Aesar, degassed, and dried over activated molecular sieves prior to use. All other reagents were purchased from commercial sources and utilized without further purification unless stated otherwise. NMR spectra were recorded at ambient temperature and pressure using a Bruker 400 MHz spectrometer (600 MHz or 400 MHz for ^{1}H, and 151 MHz or 100 MHz for ^{13}C). The ^{1}H and ^{13}C NMR spectra were measured relative to partially deuterated solvent peaks but are reported relative to tetramethylsilane (TMS).

Fluorescent measurements were recorded on a Fluoromax-2. High-resolution mass spectrometry (HRMS) was performed at the University of Illinois Mass Spectrometry Laboratory, and electrospray ionization (ESI) spectra were collected on a Waters Synapt G2-Si spectrometer. Single crystal X-ray data were collected using a Rigaku XtaLAB Synergy-S diffractometer equipped with a HyPix-6000HE Hybrid Photon Counting (HPC) detector and dual Mo and Cu microfocus sealed X-ray source (Cu Kα λ = 1.54184 Å). The data collection strategy was calculated using CrysAlisPro to ensure desired data redundancy and percent completeness. Unit cell determination, initial indexing, data collection, frame integration, Lorentz-polarization corrections and final cell parameter calculations were carried out using CrysAlisPro. An absorption correction was performed using the SCALE3 ABSPACK scaling algorithm embedded within CrysAlisPro. The structures were solved using the ShelXT structure solution program using Intrinsic Phasing and refined by Least Squares using the ShelXL program. All non-hydrogen atoms were refined anisotropically. Hydrogen atom positions were calculated geometrically and refined using the riding model. Olex2 was used for the preparation of the publication materials.

3.5.2. Synthetic Procedures for 1H-pyrrole-2-carbaldehyde, NNH^{t}Bu, [CuNNH^{t}Bu]$_2$, SNN^{t}Bu, [CuSNN^{t}Bu]$_2$, SNNHAd, [CuSNNHAd]$_2$, SNNHBn-4-MeO, and [KSNNHBn-4-MeO]$_2$

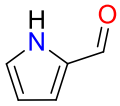

1H-pyrrole-2-carbaldehyde. An oven-dried, two-neck flask attached to a Schlenk-line was equipped with a septum and a stir bar and then put under vacuum and back-filled with nitrogen. DMF (23 mL, 2.0 equiv.) that had been stored overnight on activated sieves was injected into the reaction vessel and placed in an ice-bath. $POCl_3$ (34.0 g, 21 mL, 1.5 equiv.) was then added dropwise over the course of 30 minutes using a syringe. Once complete, the reaction was allowed to stir for an additional 30 minutes on ice and then 2 hours at room

temperature. After this time, the reaction vessel was put back into an ice-bath and pyrrole (10.0 g, 149 mmol) was added dropwise. The vessel was then allowed to continue stirring in the ice-bath and warm back up to room temperature gradually then stirred overnight. In the following morning, the reaction was again placed back into an ice-bath and quenched via a saturated K_2CO_3 solution until a pH of 7-8 had been optioned. The reaction was extracted with 100 mL of ether followed by ethyl acetate (4 x 25 mL). The organic phases were combined, washed with brine, dried over $MgSO_4$ and concentrated. The product was purified by first running a column eluting with 15:1 to 4:1 Hex:EA. The desired fractions were combined, and the product was further purified by recrystallization from boiling hexanes and cooled to 6^oC to afford extremely fine white needle crystals. Yield 8.56 g (60.4%). Spectroscopic characterization matched reported data. ^1H NMR (600 MHz, $CDCl_3$) δ 9.74 (b, 1H, pyrrole N-H), 9.53 (s,1H, aldehyde C-H), 7.15 (s, 1H, pyrrole C-H), 7.00 (s, 1H, pyrrole C-H), and 6.36 (m, 1H, pyrrole C-H).

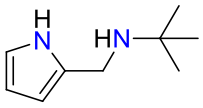

N-((1H-pyrrol-2-yl)methyl)-2-methylpropan-2-amine, NNH^{t}Bu. 1H-pyrrole-2-carbaldehyde (1.00 g, 10.5 mmol) and Na_2CO_3 (2.91 g, 2.0 equiv.) were loaded into a 250 mL round-bottom flask equipped with a stir bar. 40 mL of methanol was then added followed by tert-butylamine (1.3 mL, 1.2 equiv.) in one portion. The reaction vessel was capped with a septa and stirred overnight which upon returning had gone from colorless to yellow. After checking for the disappearance of the aldehyde peak (9.42 ppm) to go to complete imine formation (7.98 ppm) via ^1H NMR, $NaBH_4$ (994 mg, 2.5 equiv.) was added in a single portion and a vented septa was put on. The reaction was then allowed to stir for 24 hours. After that time, the solvent and excess tert-butylamine was removed via vacuum. The following colorless crude solid was then stirred in 40 mL of DCM. The reaction was filtered, washed with DCM, and concentrated. The product was then purified by recrystallization from boiling hexanes

and storing at -8°C to afford colorless prism-like crystals. Yield 658 mg (41.1%). Spectroscopic characterization matched reported data. ^{1}H NMR (400 MHz, $CDCl_3$) δ 8.74 (b, 1H, pyrrole N-H), 6.71(s, 1H, pyrrole C-H), 6.12 (s, 1H, pyrrole C-H), 6.00 (s, 1H, pyrrole C-H), 3.76 (s, 2H, CH_2), and 1.14 (s, 9H, CH_3).

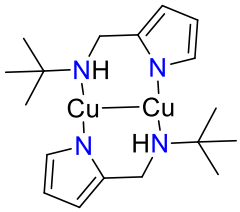

Complex [CuNNH^{t}Bu]$_2$. In a nitrogen glovebox, **NNH^{t}Bu** (250 mg, 1.62 mmol) was dissolved in 2.5 mL of dry acetonitrile. This solution was transferred to a 20 mL vial equipped with a stir bar containing KH (65 mg, 1.62 mmol, 1 equiv.) and then rinsed with 2 mL of acetonitrile. The solution bubbled and turned yellow. After 15 minutes, the reaction was poured into another 20 mL vial containing $[Cu(MeCN)_4][PF_6]$ (604 mg, 1.62 mmol, 1 equiv.) dissolved in 5 mL of acetonitrile. The reaction turned a reddish brown and was allowed to stir for 2 hours and then placed in the freezer overnight. The reaction was filtered and the brown and crystalline red solid were collected on a glass frit and dried. The solid was taken into DCM and then filtered again through celite. Removal of the solvent yielded a red-brown solid. Yield 45.7 mg (13.2%). ^{1}H NMR (400 MHz, $CDCl_3$) δ 6.75 (s, 1H, pyrrole-CH), 6.16 (m, 2H, pyrrole-CH), 4.02 (s, 2H, -CH_2-), 2.57 (s, 1H, NH), and 1.48 (s, 9H, C-$(CH_3)_3$). ^{13}C NMR (101 MHz, $CDCl_3$) δ 133.77 (aromatic-C), 129.71 (pyrrole-CH), 107.56 (pyrrole-CH), 107.35 (pyrrole-CH), 55.33 (<u>C</u>-$(CH_3)_3$), 46.55 (-CH_2-), and 29.44 (C-(<u>C</u>$H_3)_3$).

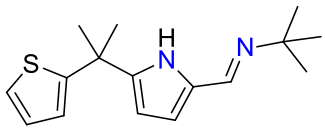

(E)-2-methyl-N-((5-(2-(thiophen-2-yl)propan-2-yl)-1H-pyrrol-2-yl)methylene)propan-2-amine, SNN^{t}Bu.

5-(2-(thiophen-2-yl)propan-2-yl)-1H-pyrrole-2-carbaldehyde (250 mg, 1.14 mmol) was loaded into a 20 mL vial equipped with a stir bar. Tert-butylamine (1 mL, 17.2 equiv.) was added, the vial capped, and the reaction stirred overnight. The following morning the reaction was monitored for the disappearance of the aldehyde peak and the formation of the imine peak. Excess tert-

butylamine was removed under vacuum followed by additional drying under high vacuum overnight. This yielded an orange-yellow solid that appeared pure via NMR. Yield 213 mg (68.2%). Crystals suitable for single crystal X-Ray diffraction could be grown by slow evaporation from hexanes. ^{1}H NMR (400 MHz, $CDCl_3$) δ: 7.97 (s, 1H, imine-CH), 7.15 (d, 1H, thiophene-CH, *J* = 5.1 Hz), 6.91 (t, thiophene-CH, *J* = 4.3 Hz), 6.82 (s, 1H, thiophene-CH), 6.36 (s, 1H, pyrrole-CH), 6.08 (d, 1H, pyrrole-CH, *J* = 3.6 Hz), 5.26 (s, 2H, pyrrole-NH)[a], 1.78 (s, 6H, C-$(CH_3)_2$), 1.21 (s, 9H, C-$(CH_3)_3$) ppm. ^{13}C NMR (101 MHz, $CDCl_3$) δ: 154.49 (aromatic-C), 146.29 (aromatic-C), 143.68 (N=CH), 130.38 (aromatic-C), 126.60 (thiophene-CH), 123.69 (thiophene-CH), 123.22 (thiophene-CH), 113.99 (pyrrole-CH), 106.14 (pyrrole-CH), 56.58 (<u>*C*</u>-$(CH_3)_3$), 38.19(<u>*C*</u>-$(CH_3)_2$), 31.25 (C-(<u>*C*</u>$H_3)_2$), and 29.98 (C-(<u>*C*</u>$H_3)_3$) ppm. [a]What appears to be the pyrrole N-H seems to drastically shift based upon concentration likely due to resonance between the pyrrole and imine or hydrogen bonding with water in solution (see section **3.3.1.**).

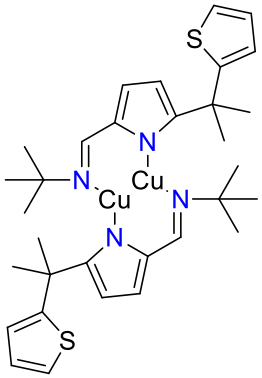

Complex [CuSNN^{t}Bu]$_2$. In a nitrogen glovebox, **SNN^{t}Bu** (140 mg, 0.51 mmol), KH (20.4 mg, 1 equiv.), and $[Cu(MeCN)_4]PF_6$ (190 mg, 1 equiv.) were weighed into separate 7 mL screw-cap vials. **SNN^{t}Bu** was dissolved in 1 mL of MeCN and transferred to KH containing a stir bar and then rinsed an additional 1 mL of MeCN. The reaction went from yellow to orange and was allowed to stir for approximately 30 minutes at which point hydrogen formation ceased. The potassium salt was then transferred to $[Cu(MeCN)_4]PF_6$ dissolved in 1 mL. The potassium salt vial again rinsed with an additional 1 mL of MeCN. The orange solution immediately turned yellow, and a colorless precipitate formed. The reaction was allowed to stir for an hour at which point the precipitate was collected on a frit and washed with excess MeCN. The solid was dissolved in DCM and filtered through a celite plug to remove excess KPF_6. Upon

concentration, the product was obtained as a slight yellow solid. Yield 168 mg (48.8%). Crystals suitable for single crystal X-Ray diffraction were grown from a solution of the complex in DCM layered in MeCN and stored at -30°C. ^{1}H NMR (400 MHz, $CDCl_3$) δ 7.93 (s, 1H, imine-CH), 6.79 (d, 1H, thiophene-CH, *J* = 5.1 Hz), 6.68 (d, 1H, thiophene-CH, *J* = 3.6 Hz), 6.59 (d, 1H, pyrrole-CH, *J* = 3.5 Hz, 1H), 6.41 (t, 1H, thiophene-CH, *J* = 4.3 Hz), 6.34 (d, 1H, pyrrole-CH, *J* = 3.6 Hz), 1.75 (d, *J* = 7.4 Hz, 6H, C-$(CH_3)_2$), and 1.20 (s, 9H, C-$(CH_3)_3$) ppm. ^{13}C NMR (101 MHz, $CDCl_3$) δ 157.64 (aromatic-C), 157.21 (aromatic-C), 155.23 (N=CH), 135.67 (aromatic-CH), 126.48 (thiophene-CH), 123.72 (thiophene-CH), 122.81 (thiophene-CH), 121.68 (pyrrole-CH), 108.44 (pyrrole-CH), 58.54 (*C*-$(CH_3)_3$), 40.13 (*C*-$(CH_3)_2$), 33.02 (C-(*C*$H_3)_2$), 32.60 (C-(*C*$H_3)_2$), and 31.46 (C-(*C*$H_3)_3$) ppm.

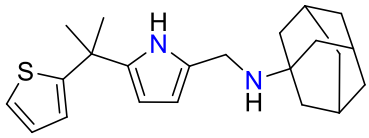

N-((5-(2-(thiophen-2-yl)propan-2-yl)-1H-pyrrol-2-yl)methyl)adamantan-1-amine, SNNHAd. 5-(2-(thiophen-2-yl)propan-2-yl)-1H-pyrrole-2-carbaldehyde (500 mg, 2.24 mmol), Na_2CO_3 (630 mg, 2.0 equiv.), and adamantylamine (414 mg, 1.2 equiv.) were loaded into a 25 mL round-bottom flask. 7.5 mL of MeOH was added, the reaction capped with a septa and allowed to stir overnight. After checking for the disappearance of the aldehyde peak to go to near-complete imine formation via ^{1}H NMR, $NaBH_4$ (216 mg, 2.5 equiv.) was added in a single portion and a vented septa was put on. The reaction was then allowed to stir for 24 hours. After that time, the solvent was removed via vacuum. The following colorless crude solid was then stirred in 20 mL of DCM. The reaction was filtered, washed with DCM, and concentrated. The product was then purified by recrystallization from boiling hexanes and storing at -8°C to afford colorless prism-like crystals. Yield 450 mg (58.1%). Crystals suitable for single crystal X-Ray diffraction were grown from a slow evaporation from a solution of hexanes. ^{1}H NMR (400 MHz, $CDCl_3$) δ 8.24 (s, 1H, pyrrole-

NH), 7.14 (dd, 1H, thiophene-CH, *J* = 5.1, 1.2 Hz), 6.90 (dd, 1H, thiophene-CH, *J* = 5.1, 3.5 Hz), 6.80 (dd, 1H, thiophene-CH, *J* = 3.5, 1.2 Hz), 5.95 (t, 1H, pyrrole-CH, *J* = 3.1 Hz), 5.87 (t, 1H, pyrrole-CH, *J* = 3.0 Hz), 3.72 (s, 2H, -NCH_2-), 2.05 (s, 3H, adamantly-CH), 1.74 (s, 6H, C-(C$\underline{H}_3$)$_2$), and 1.63 (m, 13H, adamantly-CH_2) ppm. ^{13}C NMR (101 MHz, $CDCl_3$) δ 155.48 (aromatic-C), 138.82 (aromatic-C), 131.28 (aromatic-C), 126.50 (thiophene-CH), 123.51 (thiophene-CH), 122.91 (thiophene-CH), 104.68 (pyrrole-CH), 103.71 (pyrrole-CH), 50.70 (*C*-$(CH_3)_2$), 42.84 (adamantly-CH_2), 38.12 (-N*C*H_2-) , 37.99 (adamantly-CH_2), 36.85(adamantly-CH_2), 31.42 (C-(*C*H_3)$_2$), and 29.70 (adamantly-CH) ppm.

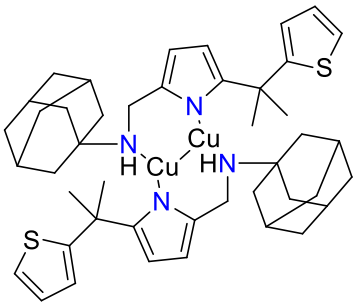

Complex [CuSNNHAd]$_2$. In a nitrogen glovebox, **SNNHAd** (250 mg, 0.705 mmol), KH (28.3 mg, 1 equiv.), and [Cu(MeCN)$_4$]PF_6 (263 mg, 1 equiv.) were weighed into separate 20 mL screw-cap vials. **SNNHAd** was dissolved in 3 mL of MeCN and transferred to KH containing a stir bar and then rinsed an additional 3 mL of MeCN. The reaction went from a slurry to a transparent solution and was allowed to stir for approximately 30 minutes at which point hydrogen formation ceased. The potassium salt was then transferred to [Cu(MeCN)$_4$]PF_6 dissolved in 3 mL. The potassium salt vial rinsed with an additional 1 mL of MeCN. A precipitate formed almost immediately and was then allowed to stir for 2 hours. The precipitate was collected on a frit and washed with excess MeCN. The solid was dissolved in chloroform and filtered through a celite plug to remove excess KPF_6. Upon concentration, the product was obtained as a light peach-colored solid. Yield 173 mg (58.7%). Crystals suitable for single crystal X-Ray diffraction were grown from a solution of the complex in chloroform layered in MeCN and stored at -30^{o}C. ^{1}H NMR (400 MHz, $CDCl_3$) δ 6.97 (d, 1H, thiophene-CH, *J* = 5.0 Hz), 6.74 (s, 1H, thiophene-CH), 6.64 (t, 1H, thiophene-CH, *J* = 4.4 Hz),

6.08 (s, 1H, pyrrole-CH), 6.00 (s, 1H, pyrrole-CH), 3.85 (d, 1H, CH_2, *J* = 11.4 Hz), 3.62 (t, 1H, CH_2, *J* = 11.7 Hz), 2.08 (s, 3H, CH_3), 1.78 – 1.53 (m, 17H). ^{13}C NMR (101 MHz, $CDCl_3$) δ 157.56, 150.97, 132.12, 125.57, 124.27, 124.19, 108.11, 103.85, 54.61, 45.11, 43.37, 40.41, 36.39, 34.49, 34.41, 29.77.

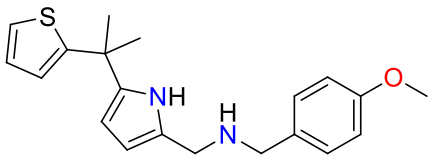

N-(4-methoxybenzyl)-1-(5-(2-(thiophen-2-yl)propan-2-yl)-1H-pyrrol-2-yl)methanamine, SNNHBn-4-MeO. 5-(2-(thiophen-2-yl)propan-2-yl)-1H-pyrrole-2-carbaldehyde (250 mg, 1.14 mmol), Na_2CO_3 (120 mg, 2.0 equiv.), and 4-methoxybenzylamine (187.6 mg, 1.2 equiv.) were loaded into a 25 mL round-bottom flask. 5 mL of MeOH was added, the reaction capped with a septa and allowed to stir overnight. After checking for the disappearance of the aldehyde peak to go to near-complete imine formation via ^{1}H NMR, $NaBH_4$ (107.8 mg, 2.5 equiv.) was added in a single portion and a vented septa was put on. The reaction was then allowed to stir for 24 hours. After that time, the solvent was removed via vacuum. The following colorless crude solid was then stirred in 20 mL of DCM. The reaction was filtered, washed with DCM, and concentrated. The resulting crude solid was then boiled in hexanes and the product was collected on a frit as a fine white powder. Yield 288.5 mg (74.4%). Crystals suitable for single X-Ray diffraction were grown by placing the boiling hexanes after filtration in a -10^{o}C freezer. ^{1}H NMR (400 MHz, $CDCl_3$) δ 8.22 (s, 2H, pyrrole-NH), 7.18 – 7.12 (m, 3H, aromatic-CH), 6.91 (d, 1H, thiophene-CH, *J* = 5.1 Hz), 6.87 – 6.80 (m, 3H, aromatic-CH), 5.97 (t, 1H, pyrrole-CH, *J* = 3.1 Hz), 5.92 (t, 1H, pyrrole-CH, *J* = 3.0 Hz), 3.80 (s, 3H, -OCH_3), 3.70 (s, 2H, -CH_2-), 3.64 (s, 2H, -CH_2-), 1.90 (s, 1H, NH), and 1.74 (s, 6H, C-$(CH_3)_2$).^{13}C NMR (101 MHz, $CDCl_3$) δ 158.72 (aromatic-C), 155.27 (aromatic-C), 139.35 (aromatic-C), 132.03 (aromatic-C), 129.51(aromatic-CH), 129.49 (aromatic-CH), 126.46 (thiophene-CH), 123.55 (aromatic-C), 122.84 (aromatic-CH),

113.86 (aromatic-CH), 105.90 (pyrrole-CH), 103.57 (pyrrole-CH), 55.31 (-O<u>C</u>H$_3$), 52.31 (-CH$_2$-), 45.73 (-CH$_2$-), 37.93 (<u>C</u>-(CH$_3$)$_2$), and 31.30 (C-(<u>C</u>H$_3$)$_2$).

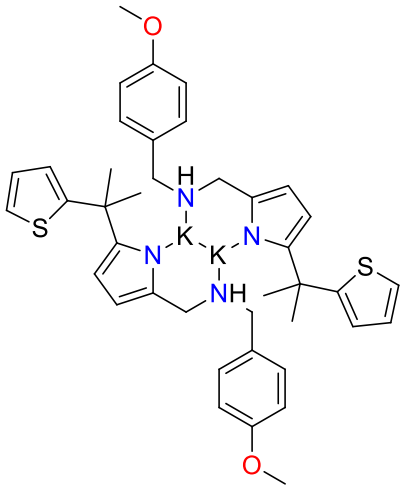

[KSNNHBn-4-MeO]$_2$: In a nitrogen glovebox, **SNNHBn-4-MeO** (250 mg, 0.735 mmol, 1 equiv.) was slurried in 5 mL of acetonitrile and transferred to a 20 mL vial containing KH (29.5 mg, 0.735 mmol, 1 equiv.) and the vial was washed twice with 1 mL of acetonitrile. The vial was stirred until gas formation ceased and then allowed to continue for 15 minutes. The solution was then transferred to another 20 mL vial containing [Cu(MeCN)$_4$][PF$_6$] (274 mg, 0.735 mmol, 1 equiv.) dissolved in 3 mL of acetonitrile. This was allowed to stir for 2 hours at which point the precipitate was collected on a frit and washed with acetonitrile. The solid was taken into DCM and filtered. The solvent was removed giving a fluffy white powder. Crystals were grown from DCM layered with acetonitrile and stored at -30^{O}C.

3.5.3. ^{1}H and ^{13}C NMR for 1H-pyrrole-2-carbaldehyde, $NNH^{t}Bu$, $[CuNNH^{t}Bu]_2$, $SNN^{t}Bu$, $[CuSNN^{t}Bu]_2$, SNNHAd, $[CuSNNHAd]_2$, and SNNHBn-4-MeO

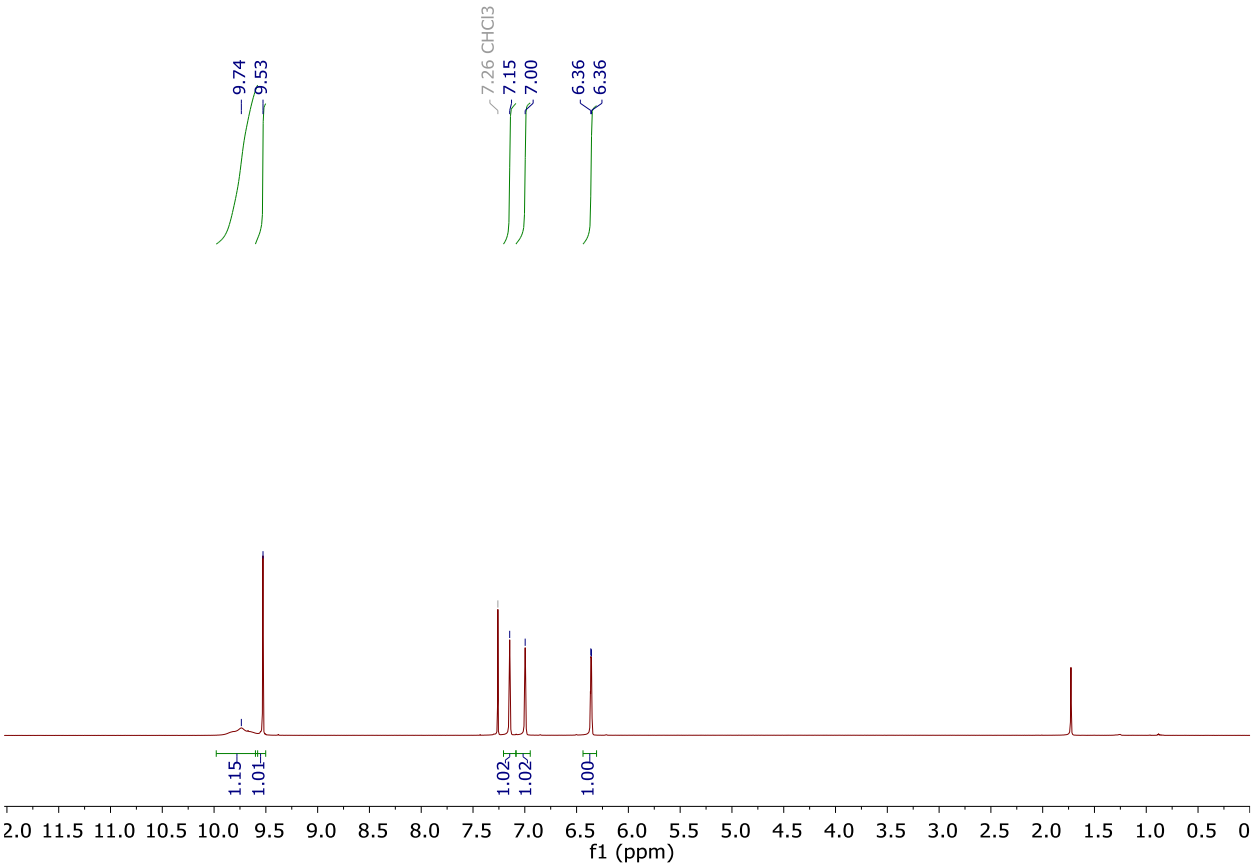

Figure 3.12. ^{1}H NMR of 2-formyl pyrrole.

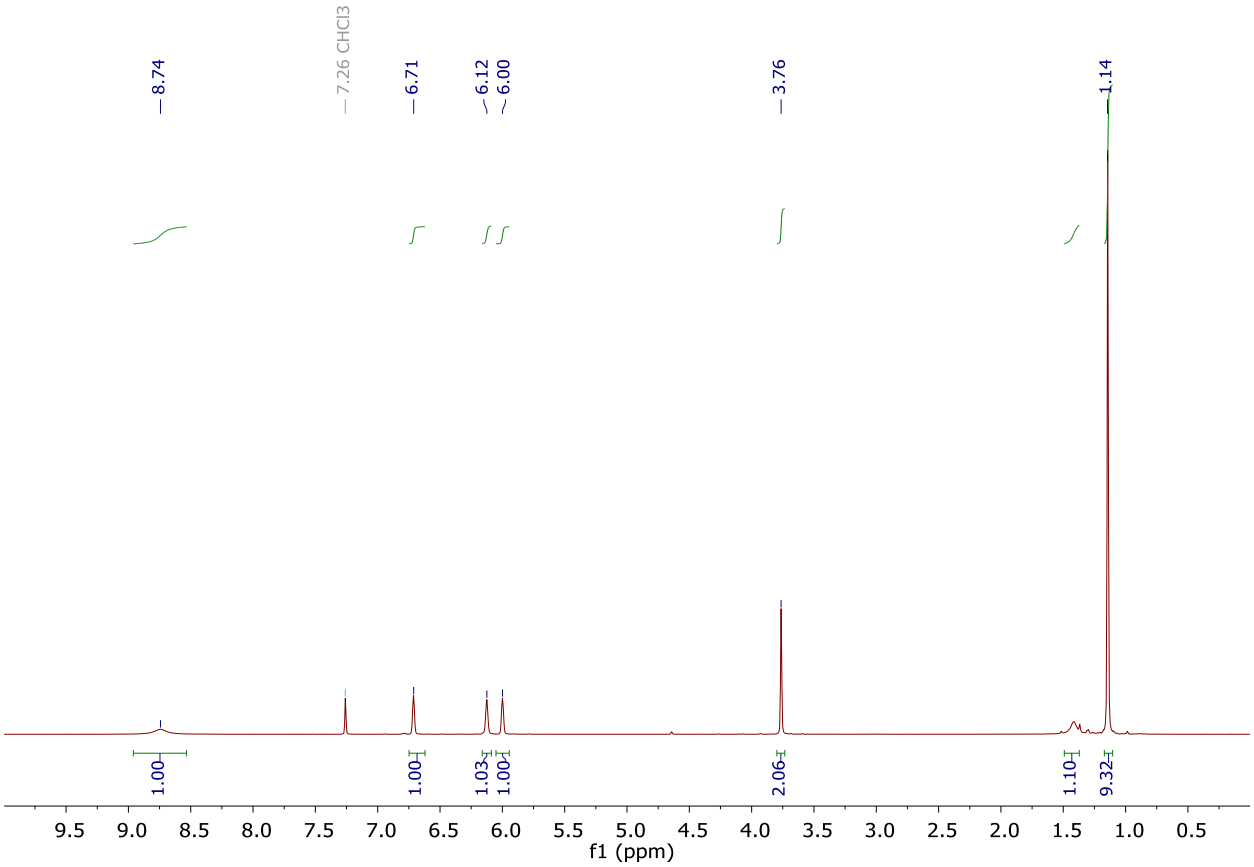

Figure 3.13. ^{1}H NMR of **NNH^{t}Bu**.

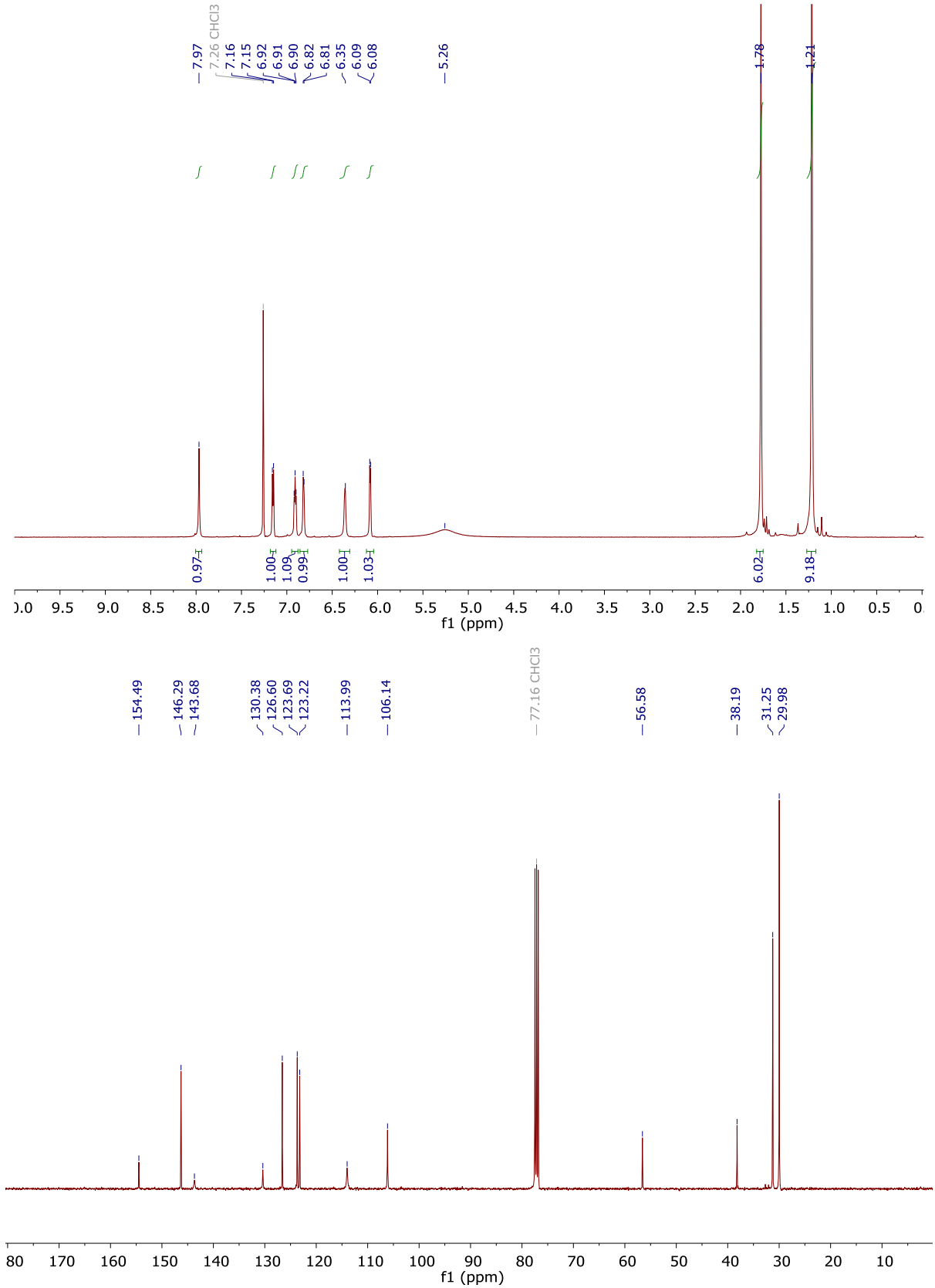

Figure 3.14. ^{1}H and ^{13}C NMR of **SNN^{t}Bu**.

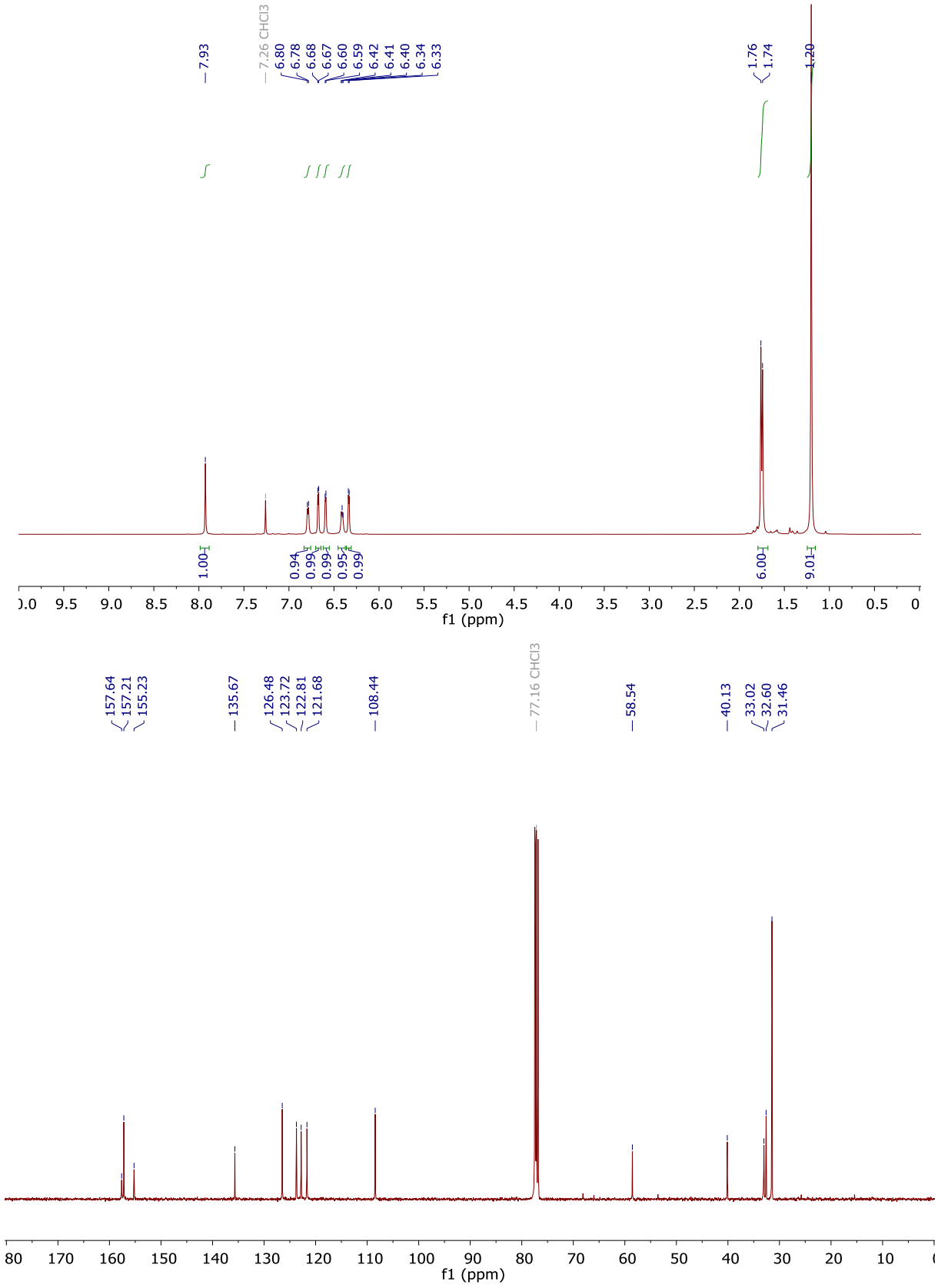

Figure 3.15. ^{1}H and ^{13}C NMR of **[CuSNN^{t}Bu]$_2$**.

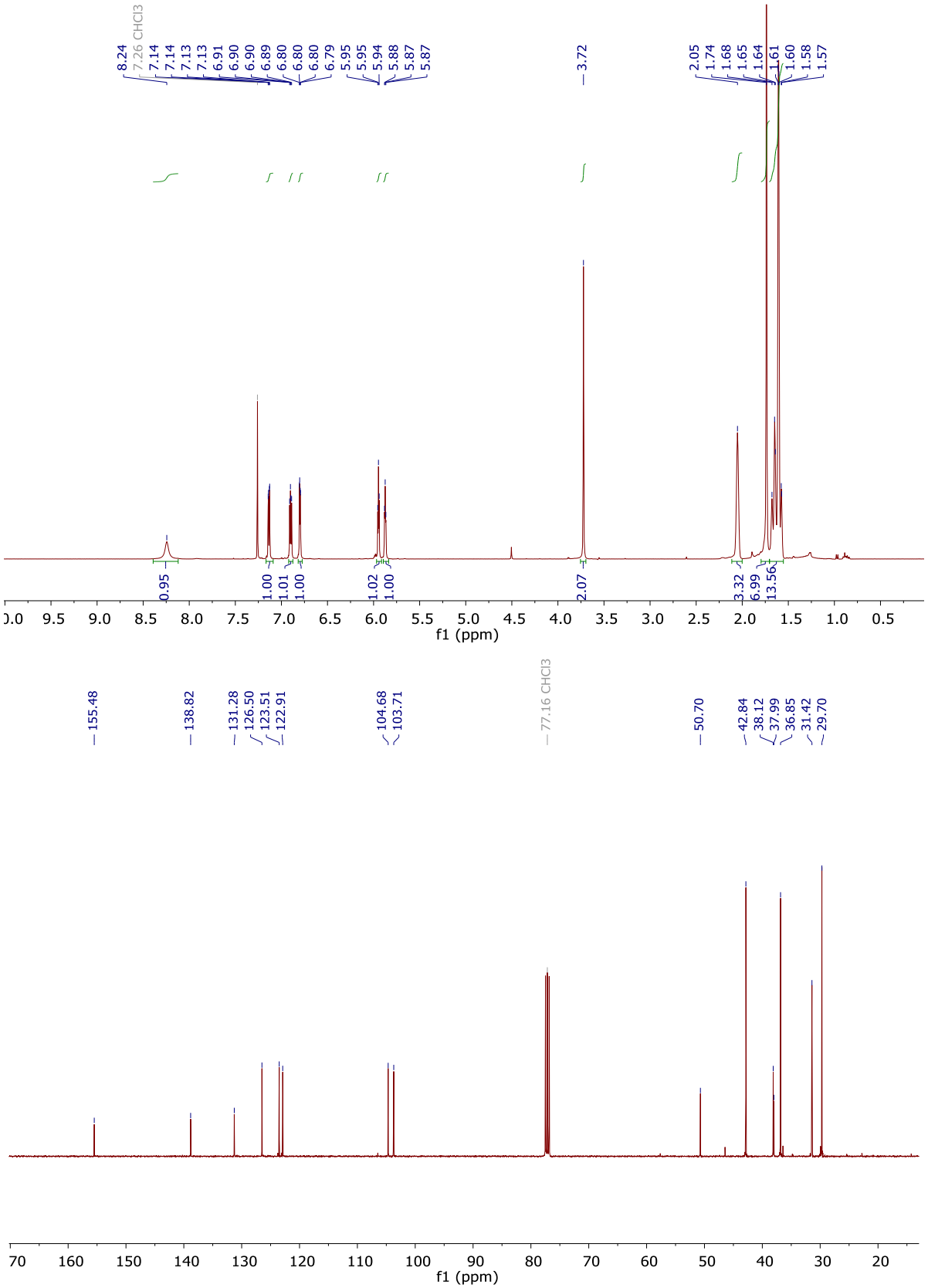

Figure 3.16. ^{1}H and ^{13}C NMR of **SNNHAd**.

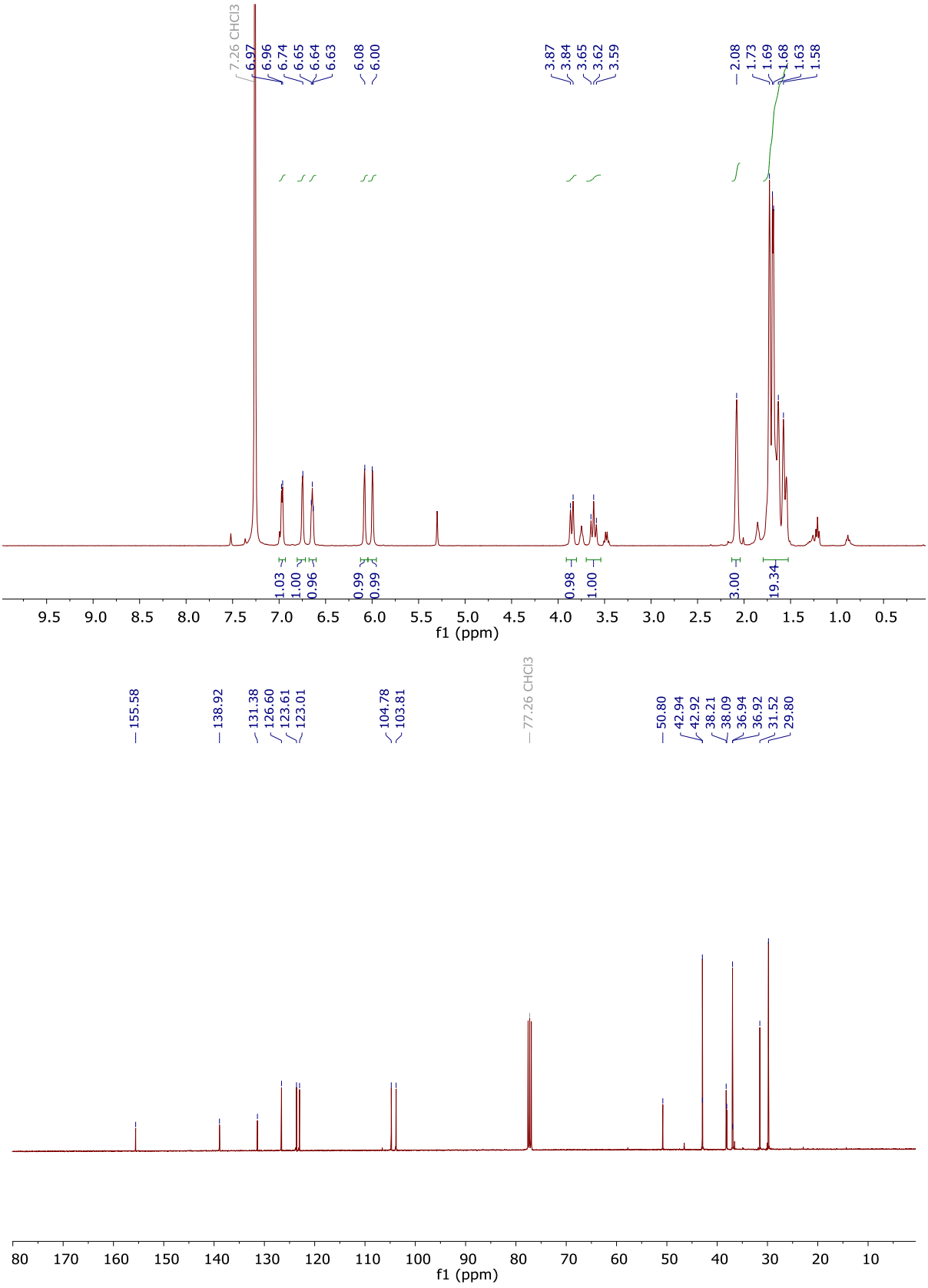

Figure 3.17. ^{1}H and ^{13}C NMR of **[CuSNNHAd]$_2$**.

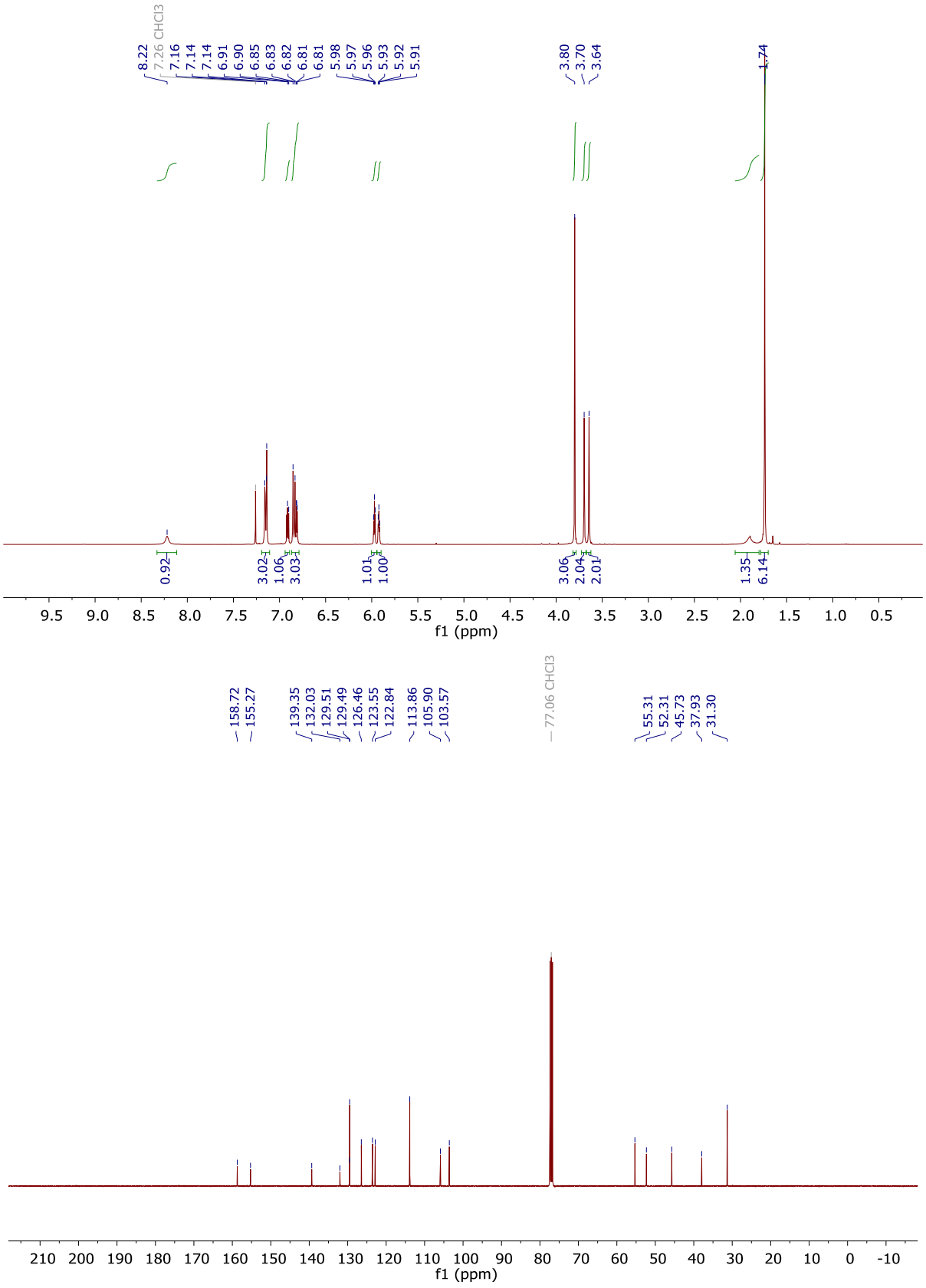

Figure 3.18. ^{1}H and ^{13}C NMR of **SNNHBn-4-MeO**.

3.5.4. ORTEP3 Representation of SNNHBn-4-MeO

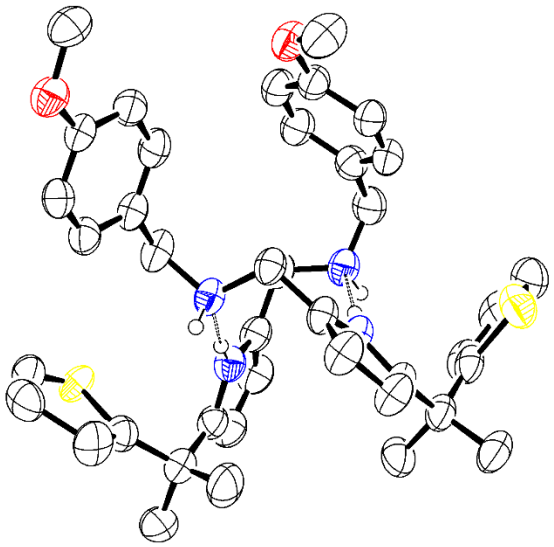

Figure 3.19. ORTEP3 representation (thermal ellipsoids at 50%) most hydrogens and disorder in thiophene are omitted for clarity for **SNNHBn-4-MeO**.

3.5.5. ORTEP3 Representation of [KSNNHBn-4-MeO]$_2$

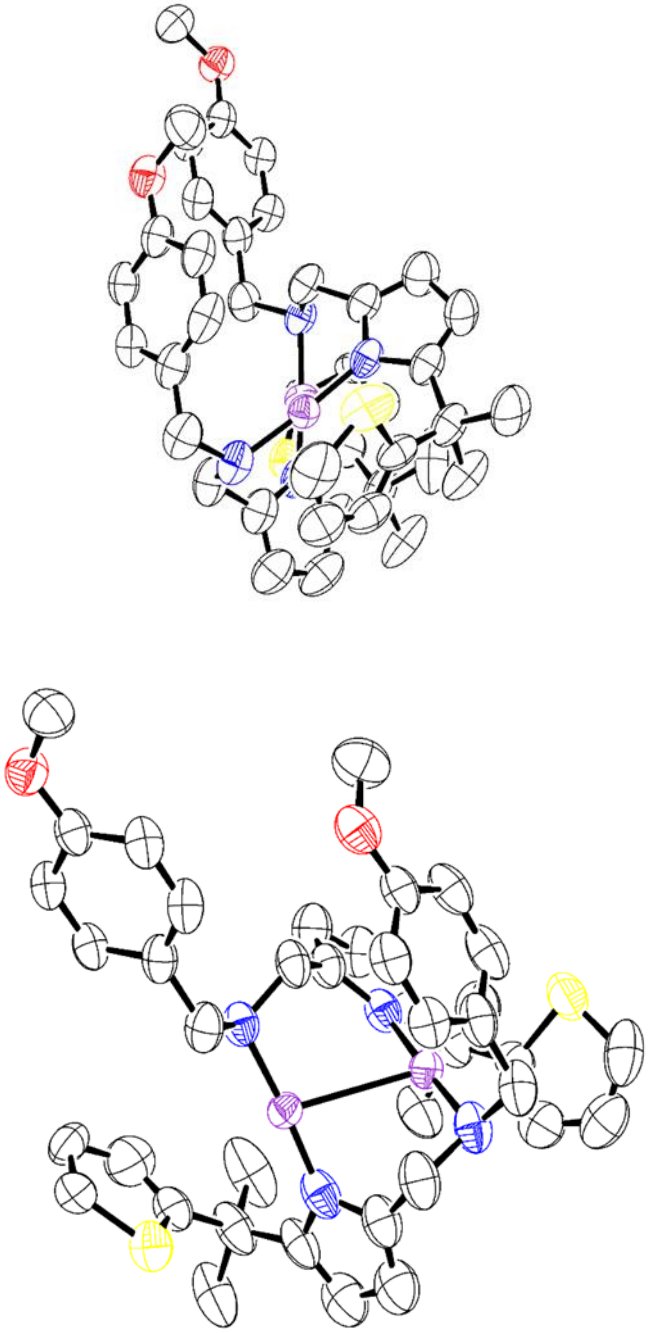

Figure 3.20. ORTEP3 representation (thermal ellipsoids at 50%) most hydrogens and disorder in thiophene are omitted for clarity for [KSNNHBn-4-MeO]$_2$. Top: viewing down the K-K interaction, and bottom: looking at the open face of the K-K interaction.

3.5.6. Crystallographic Data for $[CuNNH^tBu]_2$, SNN^tBu, $[CuSNN^tBu]_2$, SNNHAd, $[CuSNNHAd]_2$, SNNHBn-4-MeO, and $[KSNNHBn\text{-}4\text{-}MeO]_2$

Table 3.2. Select Crystal Data, Data Collection, and Refinement Parameters for **SNNHAd** and **SNN^tBu**. [a]Definition of R indices: $R_1 = \Sigma(F_O - F_C)/\Sigma(F_O)$; $wR_2 = [\Sigma[w(F_O^2 - F_C^2)^2]/[\Sigma[w(F_O^2)^2]]^{1/2}$

	SNNHAd	**SNN^tBu**
empirical formula	$C_{22}H_{30}N_2S$	$C_{16}H_{23}N_2O_{0.5}S$
FW	354.54	283.43
lattice type	monoclinic	Monoclinic
space group	*P2/c*	*I2/a*
T, K	295.17(10)	210.00(10)
a, Å	14.84291(18)	13.2196(2)
b, Å	14.52162(13)	11.85896(14)
c, Å	20.1593(2)	21.6256(3)
α, deg	90	90
β, deg	111.0049(13)	107.2017(17)
γ, deg	90	90
V, $Å^3$	4056.46(8)	3238.60(9)
Z	8	8
ρ_{calc}/Mg m^{-3}	1.161	1.163
μ(Cu/Mo, Kα) mm^{-1}	1.442 (Cu)	1.710 (Cu)
F(000)	1536.0	1224.0
crystal size, mm^3	0.21x0.17x0.13	0.14x0.04x0.02
range Θ collected, deg	3.043 to 80.002	4.280 to 79.913
Reflns (Collectd/unique)	45749/8697	14789/3500
Abs cor	Semi Empirical based upon equivalents	
max and min transmn coeff.	1.000 and 0.862	1.000 and 0.933
goodness of fit	1.080	1.085
R_1 (I>2σ(I))[a]	0.0554	0.0447
wR_2 (all data)[a]	0.1636	0.1360
Peak and hole, e $Å^{-3}$	0.370 and -0.437	0.299 sand -0.382

Table 3.3. Selected Crystal Data, Data Collection, and Refinement Parameters for **[CuNNH^{t}Bu]$_2$**, **[CuSNNHAd]$_2$** with chloroform, and **[CuSNNHAd]$_2$** without chloroform.

[a]Definition of R indices: $R_1 = \Sigma(F_O - F_C)/\Sigma(F_O)$; $wR_2 = [\Sigma[w(F_O^2 - F_C^2)^2]/[\Sigma[w(F_O^2)^2]]^{1/2}$

	[CuNNH^{t}Bu]$_2$	**[CuSNNHAd]$_2$ w/ chloroform**	**[CuSNNHAd]$_2$ w/o chloroform**
empirical formula	$C_{20}Cu_2H_{33.5}N_5O_{0.25}$	$C_{51}Cl_9Cu_2H_{67}N_6S_2$	$C_{46.67}H_{62}Cu_2N_{5.33}S_2$
FW	475.10	1274.35	888.88
lattice type	trigonal	orthorhombic	monoclinic
space group	*R*-3	Pbca	*I2/a*
T, K	200.00(10)	210.00(10)	210.00(10)
a, Å	29.7985(4)	10.04016(12)	23.76700(14)
b, Å	29.7985(4)	24.2411(3)	11.36992(7)
c, Å	27.0363(2)	48.0575(6)	48.4324(2)
α, deg	90	90	90
β, deg	90	90	92.5202(5)
γ, deg	120	90	90
V, Å^3	20790.6(6)	11696.4(2)	13075.18(13)
Z	36	8	12
ρ_{calc}/Mg m^{-3}	1.366	1.447	1.355
μ(Cu/Mo, Kα) mm^{-1}	2.372 (Cu)	5.657 (Cu)	2.390
F(000)	8064.0	4624.0	5632.0
crystal size, mm^3	0.13x0.06x0.02	0.34x0.08x0.04	0.09x0.05x0.01
range Θ collected, deg	2.367 to 79.823	7.294 to 159.766	3.654 to 80.176
Reflns (Collectd/unique)	30945/9700	53091/12431	101441/13861
Abs cor	Semi Empirical based upon equivalents		
max and min transmn coeff.	1.000 and 0.815		1.000 and 0.891
goodness of fit	1.047	1.072	1.027
R_1 (I>2σ(I))[a]	0.0266	0.0405	0.0349
wR_2 (all data)[a]	0.0799	0.1141	0.1000
Peak and hole, e Å^{-3}	0.545 and -0.421	0.67 and -0.54	0.555 and -0.653

Table 3.4. Selected Crystal Data, Data Collection, and Refinement Parameters for **[CuSNN^{t}Bu]$_2$**, **SNNHBn-4-MeO**, and **[KSNNHBn-4-MeO]$_2$**. [a]Definition of R indices: $R_1 = \Sigma(F_O - F_C)/\Sigma(F_O)$; $wR_2 = [\Sigma[w(F_O^2 - F_C^2)^2]/[\Sigma[w(F_O^2)^2]]^{1/2}$

	[CuSNN^{t}Bu]$_2$	**SNNHBn-4-MeO**	**[K SNNHBn-4-MeO]$_2$**
empirical formula	$C_{32}H_{42}Cu_2N_4S_2$	$C_{20}H_{24}N_2OS$	$C_{40}H_{44}K_2N_4O_2S_2$
FW	673.89	340.47	755.11
lattice type	monomclinic	triclinic	triclinic
space group	*P2$_1$/c*	*P*-1	*P*-1
T, K	209.99(10)	200.00(10)	210.00(10)
a, Å	12.06390(10)	9.7497(6)	9.7590(3)
b, Å	19.27340(10)	10.3662(4)	10.7299(3)
c, Å	14.77650(10)	19.4036(9)	19.3943(5)
α, deg	90	75.854(4)	75.087(3)
β, deg	112.4900(10)	77.824(5)	76.918(2)
γ, deg	90	80.600(4)	76.190(3)
V, Å^3	3174.42(4)	1845.86(17)	1876.05(10)
Z	4	4	2
ρ_{calc}/Mg m^{-3}	1.410	1.225	1.337
μ(Cu/Mo, Kα) mm^{-1}	3.084	1.611 (Cu)	3.589 (Cu)
F(000)	1408.0	728.0	796.0
crystal size, mm^3	0.15x0.12x0.07	0.13x0.06x0.02	0.19x0.07x0.04
range Θ collected, deg	3.966 to 80.018	2.387 to 69.024	2.395 to 79.974
Reflns (Collectd/unique)	48038/6906	24187/6740	23960/7709
Abs cor	Semi Empirical based upon equivalents		
max and min transmn coeff.	1.000 and 0.751	1.000 and 0.621	1.000 and 0.748
goodness of fit	1.045	1.059	1.093
R_1 (I>2σ(I))[a]	0.0343	0.0612	0.0756
wR_2 (all data)[a]	0.0943	0.1933	0.1864
Peak and hole, e Å^{-3}	0.448 and -0.422	0.365 and -0.492	0.454 and -0.632

Chapter 4 - Effects of Substitution on the Assembly of Tetranuclear Cu^{I} Complexes via a Schiff-Base Calixpyrrole Ligand System

4.1. Abstract

Copper assemblies play a vital role in biologal and synthetic processes alike. Recent advancement in extended metal chain assemblies has received significant attention due to their application in small molecule activation due to their potential application in multielectron processes and fluorescence. Schiff-base calix[2]pyrrole complexes for nickel (II) and palladium (II) have been previously reported for their use in hydrogen evolution. Herein, the utilization of symmetrical and unsymmetrical Schiff-base calix[2]pyrroles for coordination of Cu (I) to synthesize tetranuclear complexes are explored. By varying the substituents at the quaternary carbon, it was found that two different assemblies, either a distorted square-planar or a bent tetranuclear linear chain assembly were formed. Investigations also include looking into the effects of the imine on the system.

4.2. Introduction

Copper chemistry plays a crucial role in various chemical processes, both in nature[132–135] and in synthetic applications.[136–139] As a transition metal, copper exhibits a range of oxidation states, most notably as Cu^{I} and Cu^{II}. In nature, Cu^{I} enzymes, while a small class, can catalyze or serve in several highly important biological processes. These enzymes are typically broken down into three main categories based on the amount of copper in the active site and the ligation of them. Type-1[140,141] and Type-2[142,143] involve mononuclear copper enzymes while Type-3 are dinuclear copper enzymes.[144,145] Some enzymes are unique and fail to fit into these categories such nitrous-oxide reductase, N_2OR.[146] This enzyme contains two copper active sites: CuA which is a dinuclear

assembly similar to Type-3 and CuZ which contains a distinctive tetranuclear assembly with two bridging sulfide anions with the general chemical formula of $[Cu_4S_2]$.[146]

Due its closed-shell d^{10} electron count, Cu^I has the ability to form very unique metallophilic or cuprophilic interactions.[41] These interactions are typically classified when two or more copper atoms have a distance between them that is within the van der Waals radii of copper itself.[131] Because of this interaction, it has allowed for a variety of interesting synthetic arrangements of copper such as clusters,[79] cubes,[147,148] polymers,[149] and more.[41] These complexes have demonstrated their applications in catalysis, fluorescent and other unique behaviors.

One arrangement that has received notable attention over the past several decades are extended metal atomic chains or string complexes. This is because of their potential to facilitate multi-electron transfer processes, which are crucial for activation of small molecules and catalysis.[150–152] Furthermore, copper string complexes (**Figure 4.1.**) have been looked into for their unique luminescent properties as many different arrangements have shown fluorescent properties and application in various electrooptical devices such as OLEDs and as TADF-emitters.[34,49,53,128,147,149,153–159]

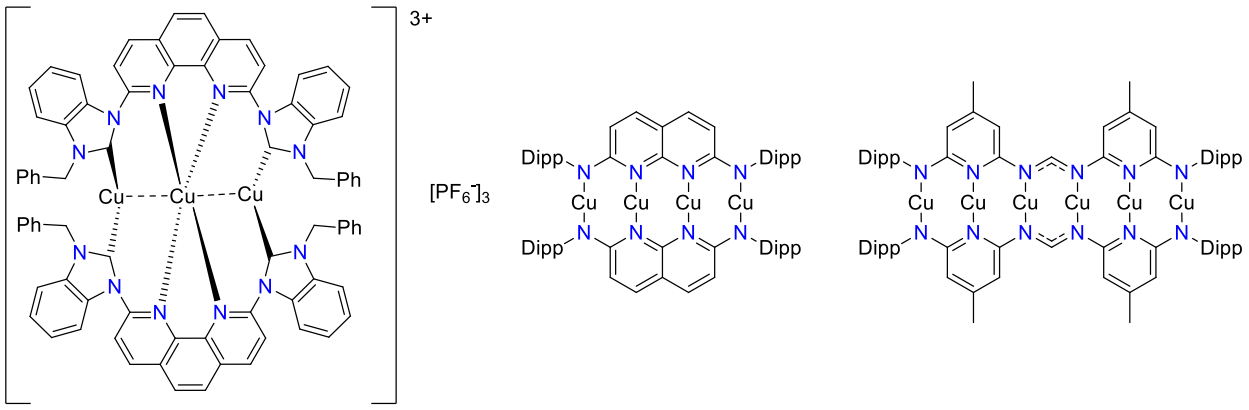

Figure 4.1. Select examples of Cu^I string complexes. Dipp = 2,6-diisopropylphenyl.

The assembly of these complexes depends heavily on the ligand scaffold. One scaffold that has received recent attention is Schiff-base calix[2]pyrrole ligands. As a dianoinic ligand, coordination to Nickel (II) and Palladium (II) have led to mononuclear complexes that have been used for hydrogen evolution (**Figure 4.2.a.**).[160,161] Modification of this ligand by the addition of a secondary binding site to form "salixpyrroles" also led a bipalladium complex for more efficient hydrogen evolution.[162] When similar calix[2]pyrrole ligands were coordinated with potassium or lithium, they led to either bimetallic or highly intricate assemblies respectively. While there are examples of calix[4]pyrroles and calix[4]pyrrole Schiff-base macrocycles being coordinated to Cu^{I} and Cu^{II} (**Figure 4.2.c.**),[163,164] calix[2]pyrroles being coordinated to Cu^{I} seems to be an unreported class of compounds and their coordination chemistry unexplored. As such, we report the synthesis and effects of the ligand on a calix[2]pyrrole system on the coordination of Cu^{I}. It was found that these complexes gave a general formula of $\mathbf{Cu_4L_2}$.

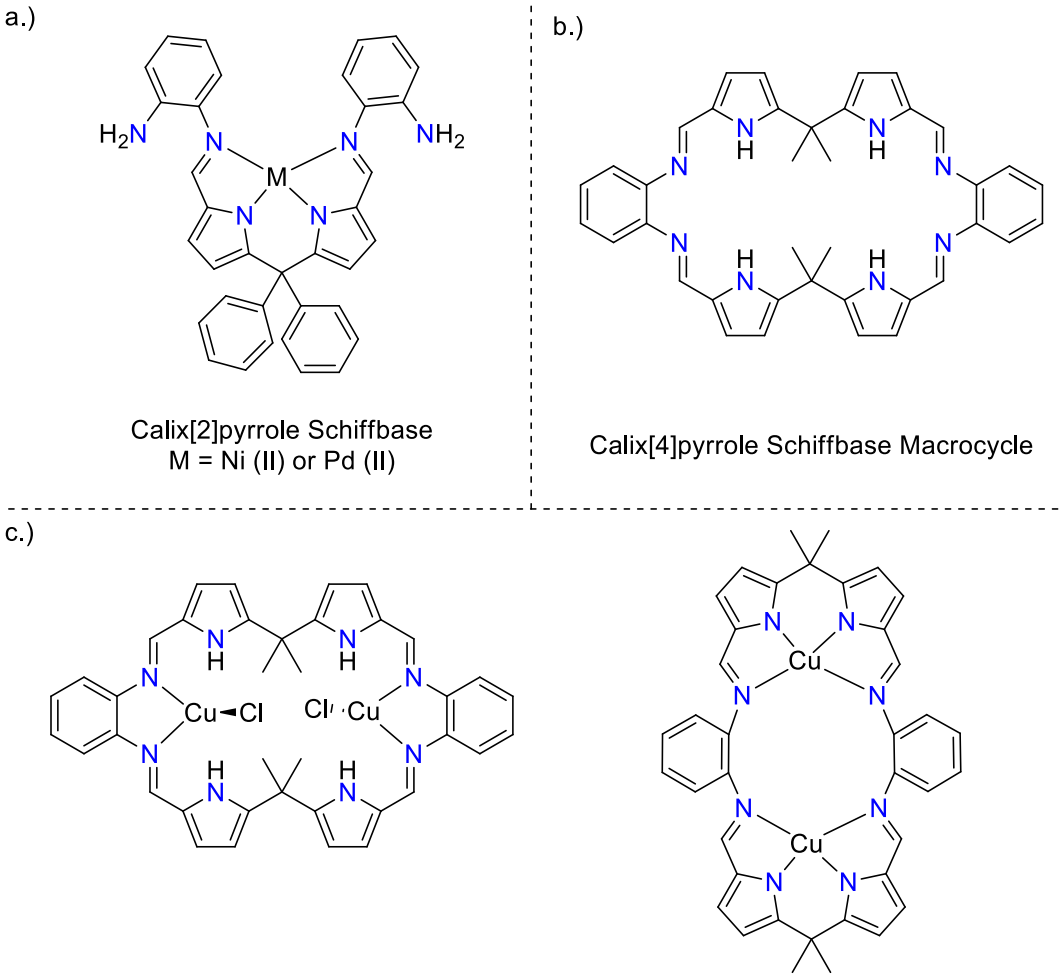

Figure 4.2. Select examples of a.) Schiff-base Calix[2]pyrrole complexes, b.) Schiff-base Calix[4]pyrrole macrocycle ligand, and c.) coordination of Cu^{I} (left) and Cu^{II} (right) to a Schiff-base Calix[4]pyrrole macrocyle.

4.3. Results and Discussion

4.3.1. Synthesis and Characterization of Ligands

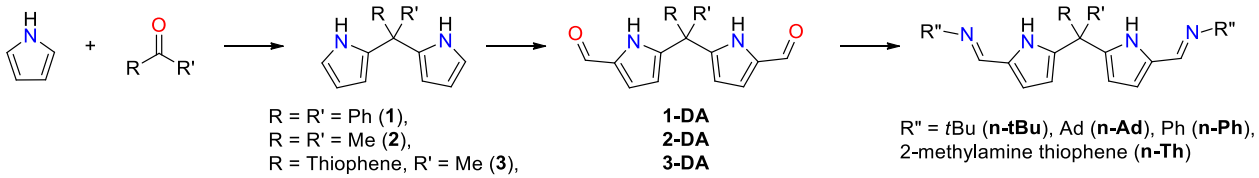

Scheme 4.1. Synthetic pathway to ligands.

The ligands were synthesized using a general procedure with slight modifications, many of which have been previously reported in the literature. The synthesis began with the condensation of pyrrole with the appropriate ketone or aldehyde under acidic conditions. Depending on the nature of the carbonyl, various acids such as trifluoroacetic acid, p-toluenesulfonic acid or methanesulfonic acid were employed. With various dipyrromethanes (**1**-**5**) in hand, the dialdehydes could be produced under Vielsmeyer-Haack conditions using $POCl_3$ and dimethylformamide in excess. Reaction progress could be monitored by observing the disappearance the starting material via TLC. Quenching the reaction with water and bases such as NaOH, $NaHCO_3$, or NaOAc would then generate the dialdehyde (**n-DA**) in varying yields shown in **Scheme 4.1**.

To generate the Schiff-base calix pyrrole ligands, the dialdehydes were mixed in methanolic conditions with a primary amine such as ^{t}butylamine (**n-tBu**), adamantylamine (**n-Ad**), or 2-methylamine thiophene (**n-Th**). The reactions could be monitored via ^{1}H NMR by watching for the disappearance of the aldehyde peaks at 9.75-9.50 ppm and the formation of the imine peaks in the 7.50-7.00 ppm region. Many of the imines would crash out of solution and after rinsing with either cold methanol or hexanes would afford the ligand in varying yields. The phenyl Schiff-base calix pyrrole ligands (**n-Ph**) proved to be more difficult to synthesize. As such, a different procedure was used. Instead, the dialdehyde and aniline were mixed in DMSO using TFA as a catalysts. After quenching with a 1% $NaHCO_3$ solution and extracting with ethyl acetate, the final ligand was isolated.

Crystals of the ligands and some intermediates were also obtained. For **3** and **3-DA**, structures were grown from DCM solutions layered in hexanes stored at -8^{o}C. **3** showed a high level of disorder in all three aromatic rings, while **3-DA** surprisingly showed no disorder in any of

the aromatic rings. (See **4.5. Supporting Information**). Crystals of **3-tBu** were grown from a slow evaporation of hexanes at -8^{o}C with the structure shown in **Figure 4.3.a**. From the structure, it was determined that the thiophene was disordered with an occupancy of 87.7 and 12.3% between two positions, and one of the tbutyl's was also disordered with two positions: 74.7 and 25.3%. It was also found that there was one water molecule per **3-tBu**. The water molecule was bridged between two **3-tBu** molecules hydrogen bonding with the pyrrole N-H (N(8)-O(1): 2.924 Å) and the imine (N(13)-O(1): 2.776 Å).

Crystals of **1-Ad** were also obtained by a slow evaporation of a solution of the ligand in DCM (**Figure 4.3.b.)**. The structure showed disorder in one of the adamantyl-groups with occupancies of 67.5 and 32.5%. It also showed one water molecule that was situated in the center of the ligand with hydrogen bonding to the two pyrrole N-H, (N(3)-O(1w): 2.932 Å and N(20)-O(1w): 2.919 Å) and the imines (N(8)-O(1w): 2.903 and N(25)-O(1w): 2.854 Å). Compared to other Schiff-base calix pyrrole, it is unique as many others form intertwined dimers with hydrogen bonding between the pyrrole hydrogens and the imine nitrogens.[160]

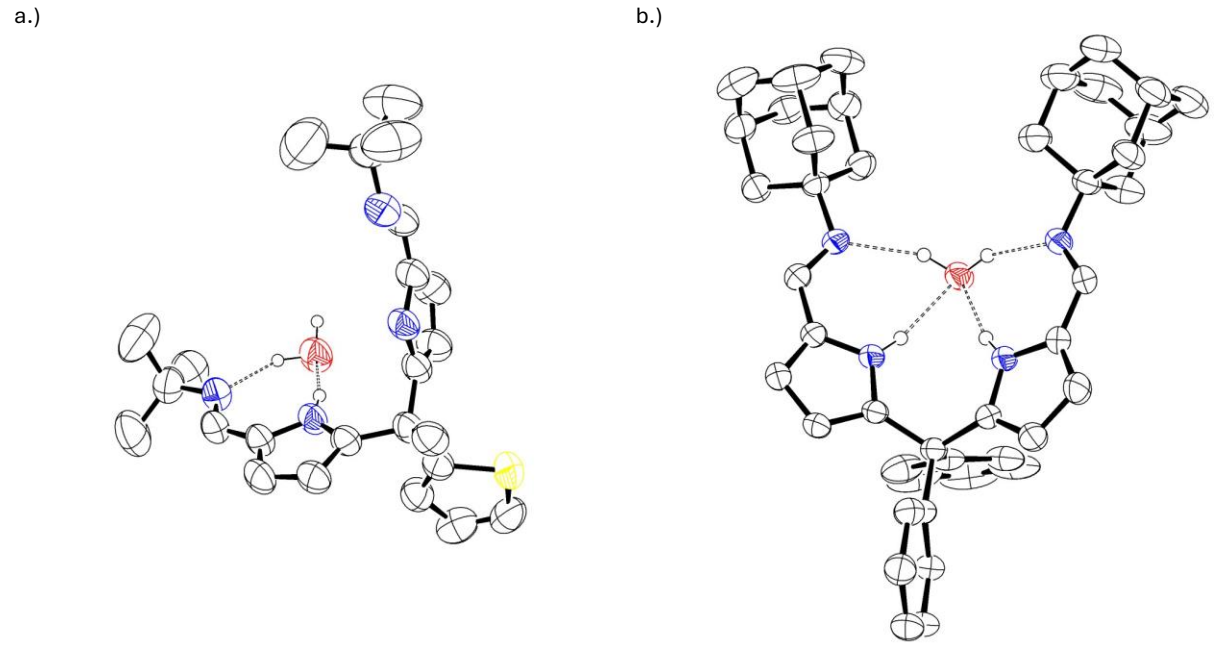

Figure 4.3. ORTEP3 representation (thermal ellipsoids at 50% probability) for a.) **3-tBu**, most hydrogens and disorder in the thiophene have been omitted for clarity, and b.) **1-Ad**, most hydrogens and disorder in the adamantyl have been omitted for clarity.

4.3.2. Synthesis of Tetranuclear Complexes

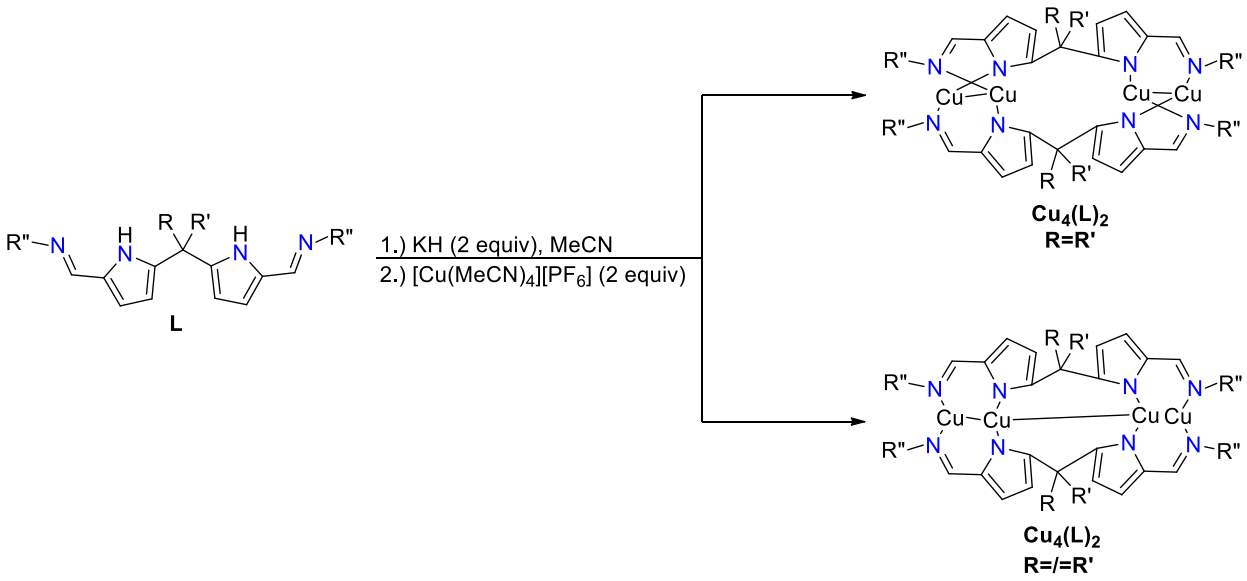

Scheme 4.2. Synthesis and general structures of tetranuclear complexes, **Cu_4L_2**.

Coordination of Cu^{I} was carried out under near identical conditions for all complexes. In a nitrogen glovebox, a solution of the ligand in acetonitrile was added to a vial containing two equivalents of KH to generate the potassium salt often giving a dark-yellow or orange solution. Once generation of hydrogen gas had ceased, the solution was transferred to another vial containing two equivalents of $[Cu(MeCN)_4][PF_6]$ pre-dissolved in acetonitrile. This would result in a precipitate forming almost immediately followed by continuous stirring. The precipitate was then collected on a frit, washed with excess acetonitrile to remove undesired KPF_6. The crude powder was then dissolved in DCM and pushed through a celite plug. The solvent was then removed, and the powder was washed with hexanes to afford the corresponding Cu^{I} complexes typically as yellow or orange or red solids in varying yields. Success of coordination was first suggested by noting a color change as many of the ligands were beige or yellow. Further confirmation of coordination was done via ^{1}H NMR as the pyrrole N-H of the ligand (8.5-8.25 ppm) was absent in all of the complexes. The final structure of these complexes was relieved by single crystal X-ray diffraction (XRD). Single crystals of each complex could be grown by dissolving the complex in either DCM or chloroform, layer with acetonitrile, and storing in a -30^{o}C freezer.

4.3.3. Structural Properties of Symmetrical Schiff-Base Calixpyrroles Cu^{I} Complexes

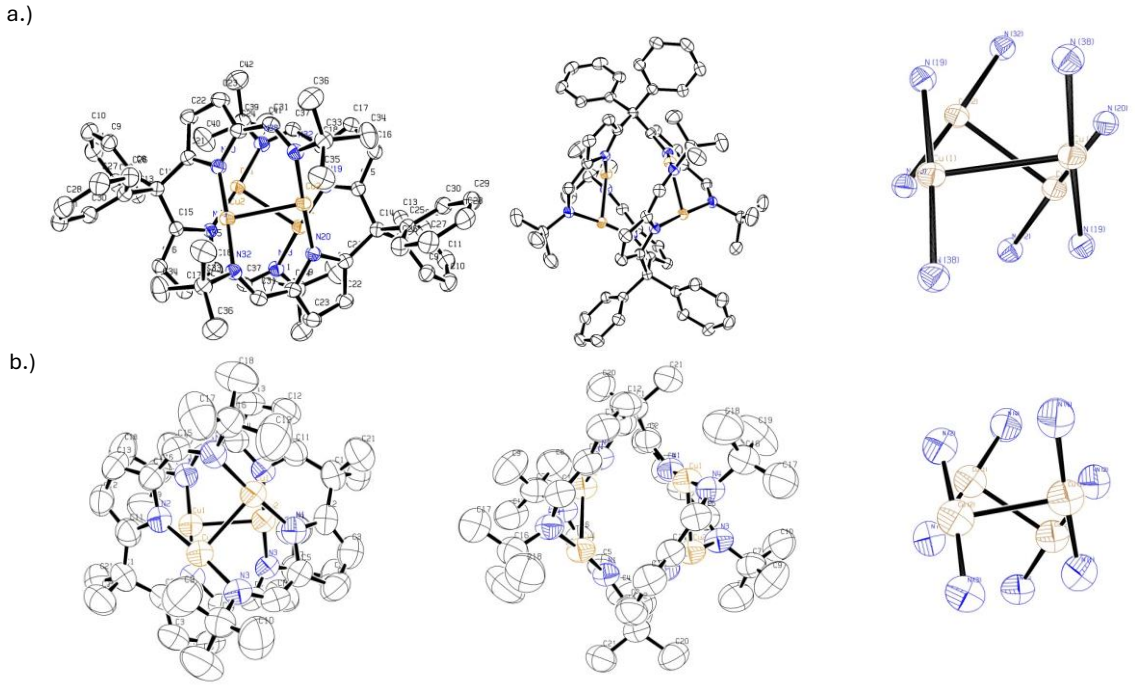

Figure 4.4. ORTEP3 representation (thermal ellipsoids at 50% probability) for a.) **Cu_4(1-tBu)$_2$**, hydrogens have been omitted for clarity, and b.) **Cu_4(2-tBu)$_2$**, hydrogens have been omitted for clarity. The left picture is from a top view, the middle is from a side view, and the right picture is excluding carbons for clarity of the metal-nitrogen assembly.

Two symmetrical Schiff-base Calixpyrroles were chosen to be investigated, diphenyl- (**1**) and dimethyldipyrromethane (**2**), to see how the bulk of the quaternary carbon affected the Cu^{I} assemblies. Using the tbutyl-functionalized ligand as a model, crystals of **Cu_4(1-tBu)$_2$** and **Cu_4(2-tBu)$_2$** showed similar structures where a cluster of four Cu^{I}'s and two ligands were seen to form the tetranuclear complex. Each of the four Cu^{I}'s were in a T-shaped geometry where the Cu was bonded to a pyrrolide of one ligand, the imine nitrogen of another ligand and then to another Cu^{I}.

The four Cu^{I}'s together formed a distorted square-like geometry. Select bond lengths, bond angles and torsion angles are shown in **Table 4.1.** for **$Cu_4(1\text{-}tBu)_2$** and **$Cu_4(2\text{-}tBu)_2$**.

Looking more closely at **$Cu_4(1\text{-}tBu)_2$** it was seen that the molecule showed a high level of symmetry with two molecules of DCM per tetranuclear complex. Each Cu^{I} center was bound to a pyrrolide of one ligand with distances of 1.8796 and 1.8829 Å for Cu(1) and Cu(2) respectively. They were also bound to the imine of the other ligand having bond distances of 1.8954 Å and 1.8971 Å for Cu(1)-N(38i) and Cu(2)-N(32i) respectively. The slightly longer imine distance is likely due to the L-type nature of the imine as compared to the X-type ligand characteristics of the pyrrolide. Each Cu^{I} interacted with the same Cu^{I} of the other ligand having similar Cu^{I}-Cu^{I} distances of 2.5263 and 2.5255 Å for Cu(1)-Cu(1i) and Cu(2)-Cu(2i) respectively. A distance of 3.828 Å was seen between Cu(1) and Cu(2) and an angle of 84.59^{o} between the two Cu^{I} pairs.

Bond angles found within the molecule were also looked into. As previously mentioned, each Cu^{I} center was in a T-shaped geometry with the two nitrogen donors found in a near linear fashion around the Cu^{I} center with exact angles of 175.85^{O} for N(19)-Cu(1)-N(38i) and 176.38^{o} for N(20)-Cu(2)-N(32i). The pyrrolide-Cu-Cu angle was near a true 90^{o} with an average of the two pairs found to be 89.425^{o} while the imine-Cu-Cu angle was slightly larger than 90^{o} with an average of 93.5^{o}.

When the diphenyls were substituted to the less sterically demanding dimethyls **$Cu_4(2\text{-}tBu)_2$** also showed a similar geometry; however, no solvent was seen in the crystal structure. The symmetry of this molecule was also high, and it was found that the Cu(1) of one half of the molecule was now bound to Cu(2i) of the other half instead of Cu(1i) as seen with the diphenyl version. The pyrrolide-Cu distance was found to be 1.865 and 1.862 Å for Cu(1)-N(1) and Cu(2)-

N(2) respectively. These are slightly shorter than the diphenyl version and is likely contributed to the smaller bulk at the quaternary carbon. Similar to the **Cu_4(1-tBu)$_2$**, the Cu-imine distance was elongated with distances of 1.914 and 1.889 Å for Cu(1)-N(4i) and Cu(2)-N(3i) respectively. Comparing the averages of the two imines for **Cu_4(1-tBu)$_2$** and **Cu_4(2-tBu)$_2$**, 1.8962 and 1.9015 Å, it can be seen that they are fairly similar. This is likely due to both having the same tbutylimine at this position as this interaction isolated away from the quaternary carbon. When looking at the Cu^I-Cu^I interaction, it was found that both pairs of Cu^I had the same interaction distance of 2.4997 Å. This is shorter than what was found for either Cu^I pairs in **Cu_4(1-tBu)$_2$** and is likely due to the lack of bulk at the quaternary carbon allowing the two ligands to get closer together in return pushing the Cu^I-Cu^I closer together.

The bond angles around the Cu^I centers were similar to that found in **Cu_4(1-tBu)$_2$** with a T-shaped geometry around the metal center. The pyrrolide-Cu-imine bond angles for N(1)-Cu(1)-N(4i) and Cu(2)-N(3i) were 174.9^o and 173.7^o respectively. These angles are farther away than the ideal 180^o for a true T-shape geometry molecule. Similarly, the pyrrolide-Cu-Cu bond angles were both elongated from a true 90^o and from that of **Cu_4(1-tBu)$_2$** with angles of 91.33^o and 92.11^o for N(1)-Cu(1)-Cu(2i) and N(2)-Cu(2)-N(1i) respectively. The imine-Cu-Cu were found to be 91.55^o and 92.36^o for N(4i)-Cu(1)-Cu(2i) and N(3i)-Cu(2)-Cu(1i) respectively. The rational for the shift away from a true T-shape geometry is that the dimethyls allow for more twisting in the ligand back bone as compared to the bulky diphenyls.

Table 4.1. Select Bond Lengths, Bond Angles, and Torsioin Angles for **Cu(1-tBu)$_2$**, **Cu$_4$(2-tBu)$_2$**, and **Cu$_4$(3-tBu)$_2$**.

	Cu$_4$(1-tBu)$_2$	**Cu$_4$(2-tBu)$_2$**	**Cu$_4$(3-tBu)$_2$**
	Bond Lengths		
Cu-Cu	Cu(1)-Cu(1i) 2.5263(6) Cu(2)-Cu(2i) 2.5255(6)	Cu(1)-Cu(2i) 2.4997(12)	Cu(1)-Cu(2) 2.4922(7)
	Cu(1)-Cu(2) 3.828	Cu(1)-Cu(2) 3.784	Cu(1)-Cu(1) 2.9110(9)
Cu-N$_{Pyr}$	Cu(1)-N(19) 1.8796(16) Cu(2)-N(20) 1.8829(17)	Cu(1)-N(1) 1.865(5) Cu(2)-N(2) 1.862(5)	Cu(1)-N(1) 1.885(3) Cu(1)-N(18i) 1.891(3)
Cu-N$_{tBu}$	Cu(1)-N(38i) 1.8954(17) Cu(2)-N(32i) 1.8971(17)	Cu(1)-N(4i) 1.914(5) Cu(2)-N(3i) 1.889(5)	Cu(2)-N(7) 1.897(3) Cu(2)-N(24i) 1.900(3)
	Bond Angles		
N$_{Pyr}$-Cu-N$_{tBu}$ Or N-Cu-N (**Cu$_4$(3-tBu)$_2$**)	N(19)-Cu(1)-N(38i) 175.85(7) N(20)-Cu(2)-N(32i) 176.38(8)	N(1)-Cu(1)-N(4i) 174.9(2) N(2)-Cu(2)-N(3i) 173.7(2)	N(1)-Cu(1)-N(18) 174.36 N(7)-Cu(2)-N(24) 170.36
N$_{Pyr}$-Cu-Cu	N(19)-Cu(1)-Cu(1i) 89.14(5) N(20)-Cu(2)-Cu(2i) 89.71(5)	N(1)-Cu(1)-Cu(2i) 91.33(14) N(2)-Cu(2)-N(1i) 92.11(14)	N(1)-Cu(1)-Cu(2) 86.06 N(18)-Cu(1)-Cu(2) 88.40
N$_{tBu}$-Cu-Cu	N(38i)-Cu(1)-Cu(1i) 94.12(6) N(32i)-Cu(2)-Cu(2i) 92.88(5)	N(4i)-Cu(1)-Cu(2i) 91.55(14) N(3i)-Cu(2)-Cu(1i) 92.36(15)	N(7)-Cu(2)-Cu(1) 96.18 N(24)-Cu(2)-Cu(1) 88.40
Cu-Cu-Cu	Cu(1)-Cu(2)-Cu(2i) 84.59 Cu(2)-Cu(1)-Cu(1i) 84.59	Cu(1)-Cu(2)-Cu(1i) 83.09 Cu(2)-Cu(1)-Cu(2i) 86.15	Cu(2)-Cu(1)-Cu(1i) 148.05
	Torsion Angles		
N$_{Pyr}$-Cu-Cu-N$_{Pyr}$		134.43	
N$_{Pyr}$-Cu-Cu-N$_{tBu}$		125.89 49.75	
N$_{tBu}$-Cu-Cu-N$_{tBu}$		125.89	
Cu-Cu-Cu-Cu			0.82

4.3.4. Effects of the Imine on Symmetrical Schiff-Base Calixpyrrole Cu^{I} Complexes

After looking at the effect of quaternary carbon, we wanted to investigate the effects of the imine. To do this, the diphenyldipyrromethane (**1**) was used as our model substrate. Three additional imine substituents; adamantyl (**1-Ad**), phenyl (**1-Ph**), and 2-methylaminethiophene (**1-Th**), were investigated to afford the tetranuclear complexes. All three of the tetranuclear Cu^{I} complexes showed similar assembly to that of the tbutyl parent complex. Crystals of each were additionally grown from a solution of the complex in either DCM or chloroform layered with acetonitrile and stored at -30^{o}C. A table of select bond lengths and angles for **Cu_4(1-tBu)$_2$**, **Cu_4(1-Ad)$_2$**, **Cu_4(1-Ph)$_2$**, and **Cu_4(1-Th)$_2$** are shown in **Table 4.2.** where each value is an average over all similar bonds in the molecular structure for easier presentation and discussion of the effects of the imine.

To see how larger bulk affected the Cu^{I} assemblies, the adamantyl versions, **1-Ad** and **Cu_4(1Ad)$_2$,** were synthesized. Crystals that were suitable for single-crystal XRD were twinning and showed a similar level of symmetry to **Cu_4(2-tBu)$_2$** in that Cu(1) was paired with Cu(2i). Both the pyrrolide-Cu and the imine-Cu average bond distances were lengthed to 1.8915 Å and 1.9034 Å as compared to **Cu_4(1-tBu)$_2$**. Despite this observation, the Cu^{I}-Cu^{I} interaction distance was smaller than **Cu_4(1-tBu)$_2$** at 2.5029 Å as well as the distance between the two metal pairs with a distance of 3.551 Å. This indicates that the metal cluster is smaller and is likely due to the steric repulsion of the ligands to each other induced by the adamantyl amine. The bond angles around the metal centers were fairly similar to **Cu_4(1-tBu)$_2$** with a N_{Pyr}-Cu-N_R angle slightly smaller at 175.08^{O}, a N_{Pyr}-Cu-Cu angle elongated to 91.51^{O} and a N_R-Cu-Cu bond angle that had shrank to 91.55^{O}. These changes, again, are likely due to the steric bulk of the adamantyl group as it pushes the imine in, shrinking the angle, it also elongates the pyrrolide angle.

Next, **$Cu_4(1\text{-}Ph)_2$** was investigated. When crystals were grown two different crystals were found in the vial: orange and red crystals. The orange crystals had P-1 symmetry with four independent tetranuclear molecules. Due to the low symmetry, these crystals took over a week to run and gave an incomplete experiment. The red crystals had a P21/n symmetry with two independent tetranuclear molecules. Although weak and bad quality they did give an R1 value >10% and will be used for the following discussion. The pyrrolide-Cu distance of 1.8741 Å was shorter than both **$Cu_4(1\text{-}tBu)_2$** and **$Cu_4(1\text{-}Ad)_2$** but is longer than **$Cu_4(1\text{-}Th)_2$** which is discussed below. The imine-Cu bond was found to be 1.8939 Å which is similar to **$Cu_4(1\text{-}tBu)_2$** and only slightly shorter than **$Cu_4(1\text{-}Ad)_2$**. As for the Cu^I-Cu^I pairs, **$Cu_4(1\text{-}Ph)_2$** was found to have the shortest average distance at 2.4921 Å but had a distance of 3.757 Å between pairs of the same molecule. The reason for many of these observations is likely due to the flatness of the phenyl ring. Although the phenyl substituent is more sterically demanding than a methyl, its flatness can provide more room compared to tbutyl or adamantyl. Another reason for these observations may be due to the electron-withdrawing nature of the phenyl group. As for the bond angles and geometry around each metal center, they were found to be nearly identical to that of **$Cu_4(1\text{-}tBu)_2$**. This observation also suggests that the steric from the phenyl are more similar to the tbutyl and the bond angles are likely due to the previous mentioned reasons as compared to steric arguments.

Finally, **$Cu_4(1\text{-}Th)_2$** when grown provided fragile, thin plates. Due to this the crystals were poor quality and of unpublishable quality; however, use of them should suffice for discussion herein. Here, it was seen that each metal center was unique, and the molecule did not possess the high level of symmetry as seen with the other molecules. It was also observed that one of the thiophenes was disordered over two positions having occupancies of 47 and 53%. Although the reliability of the bond lengths and angles are questionable, it should be noted that a similar

geometry is seen to those previously discussed. The most notable feature is the shortened Cu pair distance.

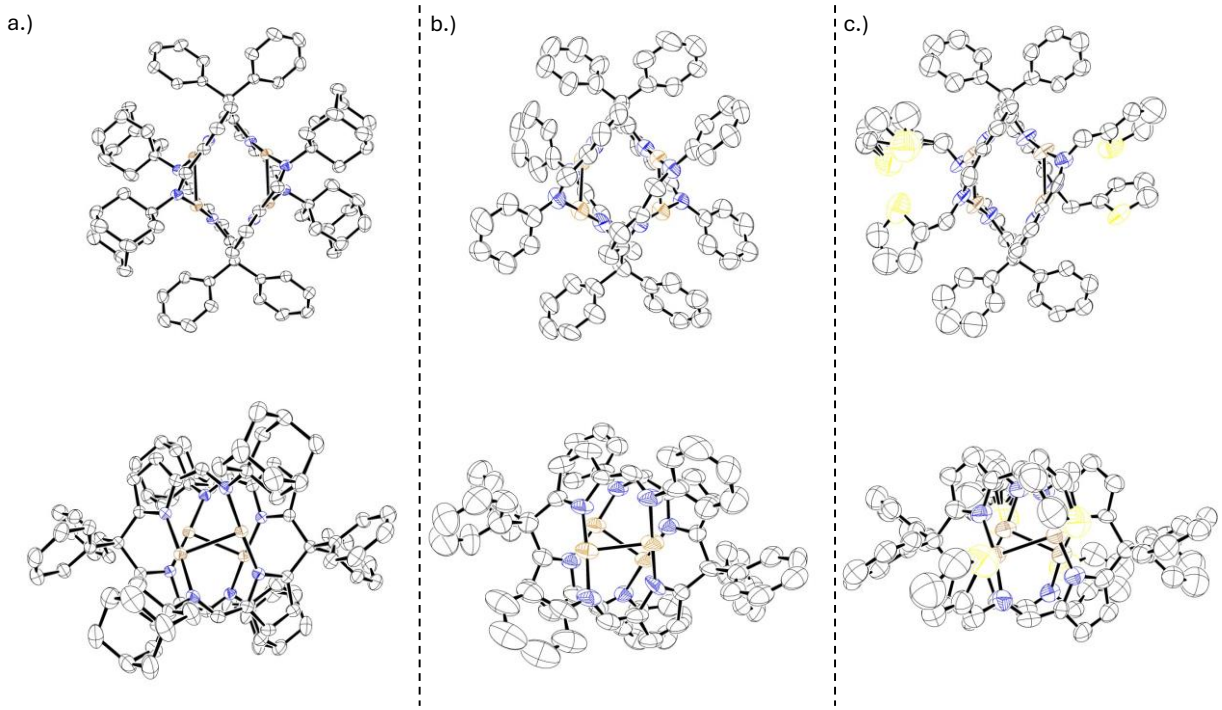

Figure 4.5. ORTEP3 representation (thermal ellipsoids at 50% probability) for a.) **Cu_4(1-Ad)$_2$**, hydrogens have been omitted for clarity, b.) **Cu_4(2-Ph)$_2$**, hydrogens and one independent molecule have been omitted for clarity, and c.), **Cu_4(1-Th)$_2$** hydrogens have been omitted for clarity. The top picture is from a sideview while the bottom picture is from a top view.

Table 4.2. Select Bond Lengths and Bond Angles of **Cu_4(1-tBu)$_2$**, **Cu_4(1-Ad)$_2$**, **Cu_4(1-Ph)$_2$**, and **Cu_4(1-Th)$_2$**. [a]Average of similar Bond Lengths and Bond Angles. [b]Averages over the two independent molecules.

	Cu_4(1-tBu)$_2$	**Cu_4(1-Ad)$_2$**	**Cu_4(1-Ph)$_2$[b]**	**Cu_4(1-Th)$_2$**
		Bond Lengths[a]		
Cu-Cu intrapair distance	Cu(1)-Cu(1i) 2.5259	Cu(1)-Cu(2i) 2.5029(4)	2.4921	Cu(1/3)-Cu(2/4) 2.5195

Cu pair distance	Cu(1)-Cu(2)	Cu(1)-Cu(2)		Cu(1/2)-Cu(3/4)
	3.828	3.551	3.757	3.481
Cu-N_{Pyr}	1.8812	1.8915	1.8741	1.8580
Cu-N_R	1.8962	1.9034	1.8939	1.8470
Bond Angles[a]				
N_{Pyr}-Cu-N_R	176.12	175.08	176.68	172.4
N_{Pyr}-Cu-Cu	89.42	91.51	89.77	91.82
N_R-Cu-Cu	93.50	91.55	93.13	95.55
Cu-Cu-Cu	84.59	84.45	85.25	84.5

4.3.5. Unsymmetrical Schiff-Base Calixpyrrole Cu^I Complexes

To look at the effects of unsymmetrical quaternary carbons on the tetranuclear assemblies, acetothiophene was chosen to be used. Coordination of Cu^I to **3-tBu** led to the isolation and structural determination of **Cu_4(3-tBu)$_2$**. Crystals of the complex were grown in a similar manner as those previously discussed by layer a solution of the complex in DCM with acetonitrile and storing at -30°C. To our surprise, this complex did not show a cluster like assembly of the four Cu^I atoms as was seen with **Cu_4(1-tBu)$_2$** and **Cu_4(2-tBu)$_2$**, but instead, it showed a linear chain like assembly. The crystal also showed a high level of symmetry. Select bond lengths, bond angles, and torsion angles are found in **Table 1**. Although each Cu^I had a similar T-shaped geometry, it was found that the exterior metal center, Cu(2), was bound to two imines, N(7) and N(24), with bond lengths of 1.897 Å and 1.900 Å, respectively, while the more center metal center, Cu(1) was bound to two pyrrolides, N(1) and N(18), with lengths of 1.885 Å and 1.891 Å. Looking from a side-view, the metals appear to be in a U- or horseshoe-shape, while if looking from the top, the metal centers appear to be in a straight line. Cu(1)-Cu(2) had an interaction distance of 2.4922 Å

while the interior distance of Cu(1)-Cu(1i) was found to be 2.9110 Å. This data suggests that there is a cuprophilic interaction between Cu(1) and Cu(2), but not Cu(1) and Cu(1i) as it falls short of the van der Waals distance for copper.[131]

As mentioned, the geometry around each Cu^{I} center was T-shaped. Each metal center showed a near linear relationship between the two nitrogen donors as N(1)-Cu(1)-N(18) had a bond angle of 174.36^{O} and N(7)-Cu(2)-N(24) had a bond angle of 170.36^{O}. The reason for Cu(2)'s deviation away from linearity is that it lacks as much bulk on the exterior and the tbutyl groups are allowed to get closer together as compared to the pyrrolides of Cu(1). The pyrrolide-Cu(1)-Cu(2) had bond angles of 88.40^{O} and 86.06^{O} for N(18) and N(1) respectively, while the imine-Cu(2)-Cu(1) had bond angles of 96.18^{O} and 93.45^{O} for N(7) and N(24) respectively. The reason for this deviations from 90^{o} is likely due to the bulk around Cu(1) pushing the nitrogen donors further into the Cu-Cu interaction and the lack of bulk around Cu(2) allowing for the imines to stretch out. The

four coppers show a torsion angle of 0.82° highlighting the near linear and eclipsed geometry of them.

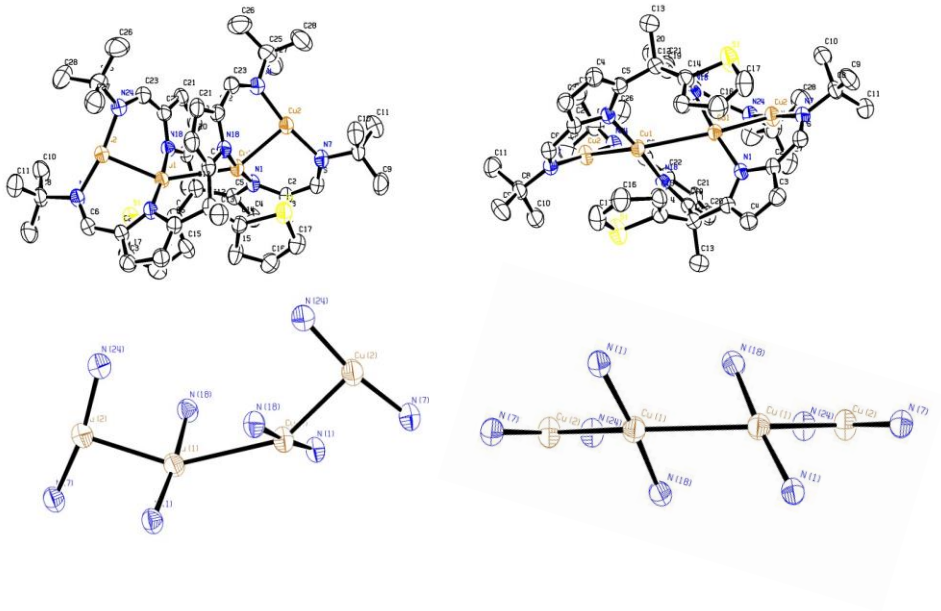

Figure 4.6. ORTEP3 representation (thermal ellipsoids at 50% probability) for **Cu_4(3-tBu)$_2$** Hydrogens have been omitted for clarity. Top left: side view with carbons and sulfur. Top right: top view with carbons and sulfur. Bottom left: side view only including copper and nitrogen. Bottom right: top view only includes copper and nitrogen.

4.4. Conclusion

In conclusion, symmetrical and unsymmetrical Schiff-base Calix pyrrole ligands were synthesized and coordinated to Cu^I to provide unique tetranuclear complexes. Based upon the substituents around the quaternary carbon, two structurally different tetranuclear assemblies were realized. If the initial ketone was symmetrical (benzophenone or acetone), then a distorted square-like assembly was seen where each Cu^I was bound to a pyrrolide of one ligand and one imine of another ligand. The effect of steric bulk at the quaternary position seemed to affect the

tightness of the metal assembly as the dimethyl tetranuclear complex, **Cu_4(2-tBu)$_2$**, displaced shorter Cu^I-Cu^I distance as well as a shortened pair distance compared to the diphenyl, **Cu_4(1-tBu)$_2$**, complex. On the other hand, if the ketone was unsymmetrical (acetothiophene) then an atomic linear chain complex was seen as shown by **Cu_4(1-tBu)$_2$**. Investigations to see how the bulk of the imine effected the assemblies three additional ligands and complexes were synthesized. While the imine seemed to have little effect on the geometry around each metal center, it did play a role, again, in the packing of the tetranuclear metal center.

4.5. Supporting Information

4.5.1. General Considerations

All procedures and manipulations were performed under an argon or nitrogen atmosphere using standard Schlenk-line and glove box techniques unless stated otherwise. Solvents were dried and deoxygenated under argon using a LC Technology Solutions Inc. SP-1 stand-alone solvent purification system, unless stated otherwise. Deuterated solvents were purchased from Cambridge Isotope Laboratories, Sigma Aldrich, Acros Organics, or Alfa Aesar, degassed, and dried over activated molecular sieves prior to use. Compounds **1**, **2**, **1-DA**, and **2-DA** were synthesized according to previous literature procedures.[165] All other reagents were purchased from commercial sources and utilized without further purification unless stated otherwise. NMR spectra were recorded at ambient temperature and pressure using a Bruker 400 MHz spectrometer (600 MHz or 400 MHz for ^{1}H, and 151 MHz or 100 MHz for ^{13}C). The ^{1}H and ^{13}C NMR spectra were measured relative to partially deuterated solvent peaks but are reported relative to tetramethylsilane (TMS). Single crystal X-ray data were collected using a Rigaku XtaLAB Synergy-S diffractometer equipped with a HyPix-6000HE Hybrid Photon Counting (HPC) detector and dual Mo and Cu microfocus sealed X-ray source (Cu Kα λ = 1.54184 Å).

The data collection strategy was calculated using CrysAlisPro to ensure desired data redundancy and percent completeness. Unit cell determination, initial indexing, data collection, frame integration, Lorentz-polarization corrections and final cell parameter calculations were carried out using CrysAlisPro. An absorption correction was performed using the SCALE3 ABSPACK scaling algorithm embedded within CrysAlisPro. The structures were solved using the ShelXT structure solution program using Intrinsic Phasing and refined by Least Squares using the ShelXL program. All non-hydrogen atoms were refined anisotropically. Hydrogen atom positions were calculated geometrically and refined using the riding model. Olex2 was used for the preparation of the publication materials.

4.5.2. Synthetic Procedures for Schiff-base Calixpyrrole Ligands and Tetranuclear Cu^{I} Complexes

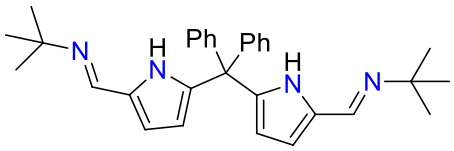

<u>1-tBu</u>: On a benchtop, **1-DA** (250 mg, 0.705 mmol, 1 equiv.) was weighed into a 20 mL screwcap vial equipped with a stir bar. 10 mL of methanol was added followed by approximately 0.75 mL of tbutylamine (10 equiv.). After 10 minutes, everything went into solution and the solution became yellow in color. The reaction was allowed to stir overnight. In the morning, the solvent and excess tbutylamine was removed on a rotovap followed by drying on a high vacuum. This produced an orange oil. Excess tbutylamine was removed by the addition of DCM and subsequently removing it on high vacuum. Finally, a yellowish solid was obtained that was used in the following step without further purification. Yield 267.8 mg (81.7%). NMR matched those reported in the literature.[166] ^{1}H NMR (400 MHz, $CDCl_3$) δ 8.12(br, pyrrole-NH), 7.95 (s, 2H, imine-CH), 7.28 (m, 6H, phenyl-CH), 7.08 (m, 4H, phenyl-CH), 6.42 (s, 2H, pyrrole-CH), 5.90 (s, 2H, pyrrole-CH), and 1.23 (s, 18H, C-$(CH_3)_3$).

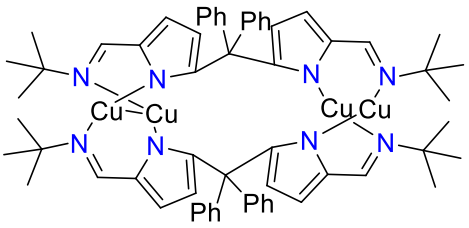

<u>Cu$_4$(1-tBu)$_2$</u>: In a nitrogen glovebox, **1-tBu** (100 mg, 0.215 mmol, 1 equiv.) was weighed into a 7 mL vial. This was dissolved in 1.5 mL of acetonitrile and transferred to another 7 mL vial containing KH (17.3 mg, 0.430 mmol, 2 equiv.) and a stir bar followed by rinsing the vial with an additional 1.5 mL of acetonitrile. The reaction was stirred for 15 minutes until formation of hydrogen gas ceased. This was then transferred to a third vial containing [Cu(MeCN)$_4$][PF$_6$] (135.4 mg, 0.430 mmol, 2 equiv.) dissolved in 1 mL of acetonitrile. The second vial was rinsed with 1 mL of acetonitrile. This was allowed to stir for 1 hour. After this time, the reaction was filtered, and the precipitate was collected on a glass frit and rinsed with cold acetonitrile. The solid was dissolved in minimal DCM and filtered through a short celite plug. The solvent was removed and the solid was washed with hexanes to afford the complex as a yellow powder. Yield 62.9 mg (49.5%). Crystals suitable for single X-ray diffraction were grown from a solution of DCM layered with MeCN and stored in a -30^{o}C fridge. (JG-03-120)

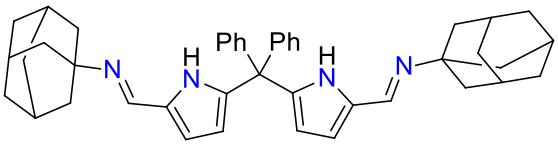

<u>1-Ad</u>: On a benchtop, **1-DA** (250 mg, 0.705 mmol, 1 equiv.) was weighed into a 20 mL screw-cap vial equipped with a stir bar. To this was added 10 mL of methanol followed by the addition of adamantylamine (427 mg, 2.8 mmol, 4 equiv.). The reaction was capped and stirred for 24 hours. The resulting precipitate was collected on a glass frit and subsequently washed with excess hexanes. The product was then dried on a vacuum line resulting in a pale-yellow powder. Yield 397 mg (90.6%). ^{1}H NMR (400 MHz, $CDCl_3$) δ 8.02 (br, 2H, pyrrole-NH), 7.90 (s, 2H, imine-CH), 7.36-7.19 (m, 6H, phenyl-CH), 7.11 – 7.00 (m, 4H, phenyl-CH), 6.44 (d, 2H-pyrrole-CH, J = 3.6 Hz), 5.86 (d, 2H, pyrrole-CH, J = 3.6 Hz), and 2.22

– 1.59 (m, 30H, adamantyl-CHs). ^{13}C NMR (101 MHz, $CDCl_3$) δ 145.57 (imine-CH), 145.42 (aromatic-C), 143.42 (aromatic-C), 131.29 (aromatic-C), 129.70 (phenyl-CH), 128.13 (phenyl-CH), 127.78 (phenyl-CH), 126.89 (phenyl-CH), 115.54 (pyrrole-CH), 112.86 (pyrrole-CH), 56.79 (quaternary-C), 56.37 (quaternary-C), 43.25 (adamantyl-CH), 36.54 (adamantyl-CH_2), and 29.63 (adamantyl-CH).

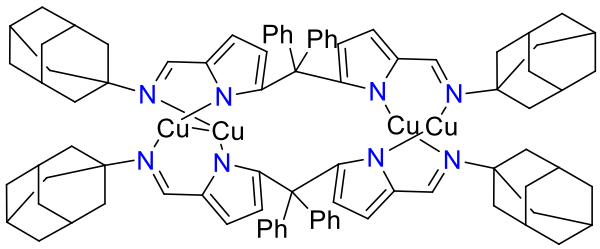

Cu$_4$(1-Ad)$_2$: In a nitrogen glovebox, **1-Ad** (250 mg, 0.403 mmol, 1 equiv.) was slurried in 4 mL of MeCN. This was then transferred to a 7 mL vial containing KH (32.3 mg, 0.805 mmol, 2 equiv.) and rinsed with an additional 1 mL of MeCN. The reaction was stirred until gas formation ceased and then continued for 15 minutes. The resulting orange solution was then transferred to a 20 mL vial containing $[Cu(MeCN)_4]PF_6$ (253 mg, 0.805 mmol, 2 equiv.) dissolved in 4 mL of MeCN. The slurry became yellow and was allowed to stir overnight. The following morning the precipitate was collected on a glass frit, washed with MeCN and then dissolved in DCM. The solution of DCM was filtered again, concentrated, and then washed with hexanes to provide a vibrant yellow powder. Yield 174.4 mg (58.1%). Crystals suitable for single X-ray diffraction were grown from a solution of DCM layered with MeCN and stored in a -30^{o}C fridge. ^{1}H NMR (400 MHz, $CDCl_3$) δ 7.89 (s, 2H, imine-CH), 7.13 – 6.94 (m, 5H, phenyl-CH), 6.54 (d, 2H, pyrrole-CH, J = 3.6 Hz), 6.33 (d, 2H, pyrrole-CH, J = 3.6 Hz), 1.91 – 1.17 (m, 30H, adamantyl-CHs). ^{13}C NMR (101 MHz, $CDCl_3$) δ 156.09 (imine-CH), 151.38 (aromatic-C), 150.82 (aromatic-C), 138.87 (aromatic-C), 126.64 (phenyl-CH), 125.54 (phenyl-CH), 119.93 (pyrrole-CH), 117.02 (pyrrole-CH), 61.31 (quaternary-C), 58.56 (quaternary-C), 44.42 (adamantyl-CH_2)f, 36.16 (adamantyl-CH_2), and 29.83 (adamantyl-CH).

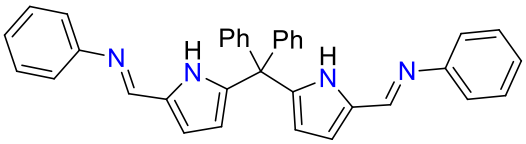

1-Ph: On a benchtop, **1-DA** (500 mg, 1.41 mmol, 1 equiv.) was weighed into a 20 mL vial equipped with a stir bar followed by dissolving in approximately 4 mL of DMSO. The reaction vessel was stirred and aniline (637 mg, 650 uL, 6.84 mmol, 4.85 equiv.) was added followed by a single drop of trifluoroacetic acid. The reaction was capped and allowed to stir for 3 hours. After this time, the reaction was quenched with 20 mL of 1% Na_2CO_3. The reaction was then extracted using diethyl ether (3 x 5 mL). The organic layers were combined, washed with 1% Na_2CO_3 (5 x 10 mL), dried over Na_2CO_3, and then concentrated to afford the desired product. Yield 421 mg (59.2%). ^{1}H NMR (600 MHz, $CDCl_3$) δ 8.19 (s, 2H, imine-CH), 7.43 – 7.28 (m, 11H),7.22 – 7.08 (m, 9H), 6.64 (s, 2H, pyrrole-CH), and 6.11 (s, 2H, pyrrole-CH). ^{13}C NMR (151 MHz, $CDCl_3$) δ 149.49 (imine-CH), 143.99 (aromatic-C), 130.86 (aromatic-C), 129.46 (aromatic-C), 129.30 (aromatic-C), 129.20 (phenyl-CH), 128.51 (phenyl-CH), 128.31 (phenyl-CH), 127.51 (phenyl-CH), 125.46 (phenyl-CH), 120.85 (phenyl-CH), 116.66 (pyrrole-CH), 112.63 (pyrrole-CH), and 56.57 (quaternary-C).

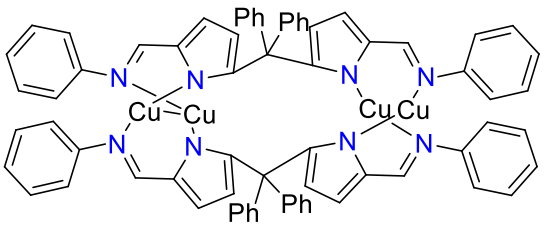

Cu_4(1-Ph)$_2$: In a nitrogen glovebox, **1-Ph** (150 mg, 0.297 mmol, 1 equiv.) was dissolved in 2 mL of MeCN. This was transferred to a 7 mL screw-cap vial equipped with a stir bar containing KH (23.8 mg, 0.594 mmol, 2 equiv.). The vial containing the ligand was rinsed twice with 1 mL of MeCN and added to the 7 mL vial. The reaction was stirred until the formation of gas had ceased and then allowed to continue for 15 minutes. After this time, the orange solution was transferred again to a 20 mL vial containing $[Cu(MeCN)_4]PF_6$ (187 mg, 0.594 mmol, 2 equiv.) dissolved in 1 mL of MeCN. A orange precipitate immediately formed upon addition and the reaction was allowed to

stir for an additional hour. The precipitate was collected on a glass frit, washed with MeCN and then dissolved in DCM. The solution of DCM was filtered again, concentrated and then washed with hexanes to provide an orange-red powder. Yield 94.5 mg (50.5%). Crystals suitable for single X-ray diffraction were grown from a solution of DCM layered with MeCN and stored in a -30°C fridge. ^{1}H NMR (400 MHz, $CDCl_3$) δ 7.93 (s, 2H, imine-CH), 7.26 – 7.19 (m, 6H, phenyl-CH), 6.94 – 6.82 (m, 10H, phenyl-CH), 6.73 (d, 2H, pyrrole-CH, *J* = 3.8 Hz), 6.63 (dd, 4H, phenyl-CH, *J* = 8.3, 1.3 Hz), and 6.29 (d, 2H, pyrrole-CH, *J* = 3.8 Hz). ^{13}C NMR (101 MHz, $CDCl_3$) δ 156.56 (imine-CH), 154.81 (aromatic-C), 150.35 (aromatic-C), 149.23 (aromatic-C), 137.98 (aromatic-C), 130.66 (phenyl-CH), 128.54 (phenyl-CH), 127.41 (phenyl-CH), 126.41 (phenyl-CH), 125.95 (pyrrole-CH), 124.70 (phenyl-CH), 122.88 (phenyl-CH), 117.87 (pyrrole-CH), and 61.95 (quaternary-C).

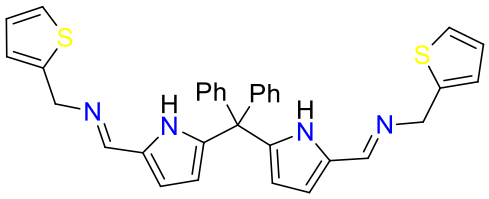

1-Th: On a benchtop, **1-DA** (250 mg, 0.705 mmol, 1 equiv.) was weighed into a 20 mL screw-cap vial equipped with a stir bar. To this was added 8 mL of methanol followed by the addition of 2-thiophenylmethylamine (192 mg, 1.69 mmol, 2.4 equiv.). After approximately 15 minutes, everything went into solution. The reaction was capped and stirred overnight. The following morning the resulting precipitate was collected on a glass frit and subsequently washed with excess cold methanol. The product was then dried on a vacuum line resulting in a pale yellow powder. Yield 294 mg (77.6%). ^{1}H NMR (600 MHz, $CDCl_3$) δ 9.03 (br, 2H, pyrrole-NH), 7.97 (s, 2H, imine-CH), 7.31 – 7.22 (m, 6H, phenyl-CH), 7.19 (d, 2H, thiophene-CH, *J* = 4.9 Hz), 7.06 (d, 4H, phenyl-CH, *J* = 6.5 Hz), 6.94 (t, 2H, thiophene-CH), 6.88 (s, 2H, thiophene-CH), 6.45 (d, 2H, pyrrole-CH, *J* = 3.8 Hz), 6.02 (d, 2H, pyrrole-CH, *J* = 3.7 Hz), and 4.70 (s, 4H, -CH_2-). ^{13}C NMR (151 MHz, $CDCl_3$) δ 161.83 (aromatic-C), 152.33 (imine-CH),

144.56 (aromatic-C), 130.01 (aromatic-C), 129.40 (phenyl-CH), 128.10 (phenyl-CH), 128.09 (phenyl-CH), 127.24 (aromatic-C), 126.86 (thiophene-CH), 125.09 (thiophene-CH), 124.69 (thiophene-CH), 114.89 (pyrrole-CH), 111.96 (pyrrole-CH), 58.26 (-CH_2-), and 56.36 (quaternary-C).

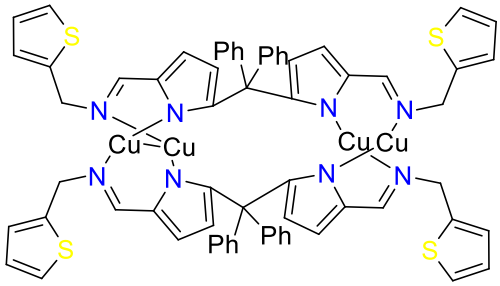

<u>Cu$_4$(1-Th)$_2$</u>: In a nitrogen glovebox, **1-Th**(150 mg, 0.275 mmol, 1 equiv.) was dissolved in 6mL of MeCN. This was transferred to a 7 mL screw-cap vial equipped with a stir bar containing KH (22.1 mg, 0.551 mmol, 2 equiv.). The vial containing the ligand was rinsed once with 1 mL of MeCN and added to the 7 mL vial. The reaction was stirred until the formation of gas had ceased and then allowed to continue for 15 minutes. After this time, the orange solution was transferred again to a 20 mL vial containing [Cu(MeCN)$_4$]PF_6 (173.2 mg, 0.551 mmol, 2 equiv.) dissolved in 3 mL of MeCN. A yellow precipitate immediately formed upon addition and the reaction was allowed to stir for an additional hour. The precipitate was collected on a glass frit, washed with MeCN and then dissolved in DCM. The solution of DCM was filtered again, concentrated and then washed with hexanes to provide an yellow powder. Yield 104 mg (56.2%). Crystals suitable for single X-ray diffraction were grown from a solution of DCM layered with MeCN and stored in a -30^{o}C fridge. ^{1}H NMR (400 MHz, Chloroform-*d*) δ 7.53 (s, 2H, imine-CH), 7.16 – 6.96 (m, 12H, aromatic-CH), 6.85 (m, 2H, thiophene-CH), 6.67 (d, 2H, thiophene-CH, J = 3.0 Hz), 6.59 (d, 2H, pyrrole-CH, J = 3.7 Hz), 6.09 (d, 2H, pyrrole-CH, J = 3.7 Hz), and 3.95 (q, 4H, -CH_2- J = 10.3 Hz). ^{13}C NMR (101 MHz, $CDCl_3$) δ 158.42 (imine-CH), 152.43 (aromatic-C), 147.92 (aromatic-C), 141.25 (aromatic-C), 133.87 (aromatic-C), 128.88 (aromatic-CH), 126.27 (aromatic-CH), 125.56 (aromatic-CH), 125.07

(aromatic-CH), 123.56 (aromatic-CH), 123.44 (aromatic-C), 122.12 (pyrrole-CH), 114.74 (pyrrole-CH), 60.45 (quaternary-C), and 59.79 (-CH_2-).

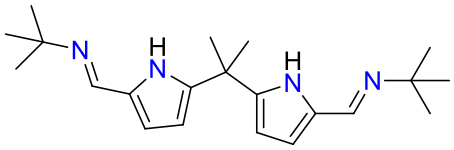

2-tBu: On a benchtop, **2-DA** (250 mg, 1.08 mmol, 1 equiv.) was weighed into a 20 mL screwcap vial equipped with a stir bar. 5 mL of MeOH was added to the compound followed by approximately 1.2 mL of tbutylamine (10 equiv.). This was allowed to stir overnight. The solvent and excess tbutylamine was removed the following morning. The remaining solid had hexanes added and was filtered and dried on the vacuum line to give a brown solid. Yield 114.7 mg (31.0%). NMR matched literature reports.[166165] ^{1}H NMR (600 MHz, $CDCl_3$) δ 8.02 (br, 2H, pyrrole-NH), 7.95 (s, 2H, imine-CH), 6.34 (d, 2H, pyrrole-CH, *J* = 3.6 Hz), 6.03 (d, 2H, pyrrole-CH, *J* = 3.6 Hz), 1.72 (s, 6H, C-$(CH_3)_2$), and 1.24 (s, 18H, C-$(CH_3)_3$).

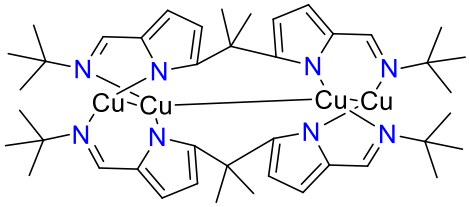

Cu$_4$(2-tBu)$_2$: In a nitrogen glovebox, **2-tBu** (100 mg, 0.294 mmol, 1 equiv.) was weighed into a 7 mL vial. This was dissolved in 1.5 mL of acetonitrile and transferred to another 7 mL vial containing KH (23.5 mg, 0.587 mmol, 2 equiv.) and a stir bar followed by rinsing the vial with an additional 1.5 mL of acetonitrile. The reaction was stirred for 15 minutes until formation of hydrogen gas ceased. This was then transferred to a third vial containing $[Cu(MeCN)_4][PF_6]$ (184.7 mg, 0.587 mmol, 2 equiv.) dissolved in 1 mL of acetonitrile. The second vial was rinsed with 1 mL of acetonitrile. This was allowed to stir for 1 hour. After this time, the reaction was filtered, and the precipitate was collected on a glass frit and rinsed with cold acetonitrile. The solid was dissolved in minimal DCM and filtered through a short celite plug. The solvent was removed and the solid was washed with hexanes to afford the complex as a orange-yellow powder. Yield 84.3 mg (84.3%). Crystals suitable for single X-ray diffraction were grown

from a solution of DCM layered with MeCN and stored in a -30ºC fridge. ^{1}H NMR (400 MHz, $CDCl_3$) δ 7.83 (s, 2H, imine-CH), 6.52 (d, 2H, pyrrole-CH, *J* = 3.5 Hz), 6.25 (d, 2H, pyrrole-CH, *J* = 3.5 Hz), 1.68 (s, 6H, C-$(CH_3)_2$), and 1.29 (s, 18H, C-$(CH_3)_3$).^{13}C NMR (101 MHz, $CDCl_3$) δ 157.85 (imine-CH), 157.66 (aromatic-C), 137.53 (aromatic-C), 121.27 (pyrrole-CH, 110.53 (pyrrole-CH), 58.23 (quaternary-C), 41.02 (quaternary-C), 31.64 (CH_3), and 31.61 (CH_3).

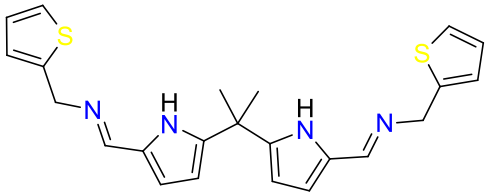

2-Th: On a benchtop, a solution of **2-DA** (250 mg, 1.086 mmol, 1 equiv.) in 8 mL of methanol was added 2-methylaminethiophene (295 mg, 2.606 mmol, 2.4 equiv.). The reaction was allowed to stir overnight. The following morning, the reaction was brown precipitate was collected via filtration and washed with cold hexanes. Yield 323.8 mg (70.9%). ^{1}H NMR (400 MHz, $CDCl_3$) δ 8.02 (s, 2H, imine-CH), 7.22 (dd, 2H, thiophene-CH, *J* = 5.0, 1.3 Hz), 7.00 – 6.92 (m, 4H, thiophene-CH), 6.42 (d, 2H, pyrrole-CH, *J* = 3.6 Hz), 6.07 (d, pyrrole-CH, *J* = 3.6 Hz), 4.82 (s, 4H, -CH_2-), and 1.67 (s, 6H, C-$(CH_3)_2$). ^{13}C NMR (101 MHz, CDCl3) δ 152.38 (imine-CH), 143.15 (aromatic-C), 142.28 (aromatic-C), 129.43 (aromatic-C), 126.95 (thiophene-CH), 125.24 (thiophene-CH), 124.83 (thiophene-CH), 115.50 (pyrrole-CH), 106.58 (pyrrole-CH), 58.39 (-CH_2-), 35.90 (*C*-$(CH_3)_2$), and 28.90 (C-(*C*$H_3)_2$).

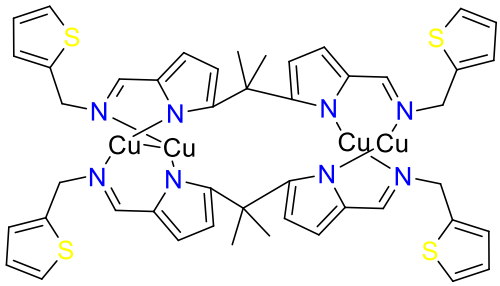

Cu$_4$(2-Th)$_2$: In a nitrogen glovebox, **2-Th** (150 mg, 0.328 mmol, 1 equiv.) was dissolved in 5 mL of acetonitrile and transferred to a 20 mL vial containing KH (26.4 mg, 0.657 mmol, 2 equiv.) followed by rinsing with 1 mL of acetonitrile. The reaction was stirred for 20 minutes, until gas formation had ceased, and the solution was a deep red color. The contents of this vial were then transferred to another 20 mL vial containing [Cu(MeCN)$_4$][PF$_6$] (206.7 mg, 0.657 mmol, 2 equiv.) dissolved in 3 mL of

acetonitrile. The reaction was allowed to stir for about 4 hours. At this time the precipitate was collected on a frit, washed with acetonitrile, and then dissolved in minimal DCM. The solution was then passed through a celite plug, and the solvent was removed. The yellow solid was washed with hexanes and dried on the vacuum line. Yield 85.7 mg (47.8%).^{1}H NMR (400 MHz, $CDCl_3$) δ 7.53 (s, 2H, imine-CH), 7.06 (dd, 2H, thiophene-CH, J = 5.1, 1.2 Hz), 6.83 – 6.75 (m, 4H, thiophene-CH), 6.63 (d, 2H, pyrrole-CH, J = 3.6 Hz), 6.40 (d, 2H, pyrrole-CH, J = 3.6 Hz), 4.54 (dd, 4H, (-CH_2-), J = 236.8, 14.6 Hz), and 1.69 (s, 6H, C-(CH_3)$_2$).^{13}C NMR (101 MHz, $CDCl_3$) δ 159.19 (imine-CH), 158.68 (aromatic-C), 142.12 (aromatic-C), 134.41 (aromatic-C), 126.74 (thiophene-CH), 124.85 (thiophene-CH), 124.68 (thiophene-CH), 123.28 (pyrrole-CH), 109.43 (pyrrole-CH), 60.92 (-CH_2-), 41.86 ($\underline{C}$-(CH_3)$_2$), and 32.34 (C-($\underline{C}H_3$)$_2$).

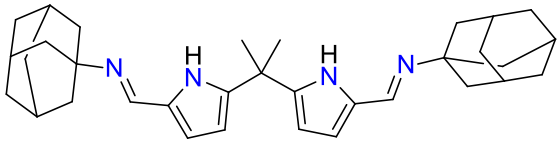

<u>2-Ad</u>: On a benchtop, **2-DA** (250 mg, 1.086 mmol, 1 equiv.) was weighed into a 20 mL vial equipped with a stir bar. 10 mL of methanol was added followed by adamantylamine (657 mg, 4.34 mmol, 4 equiv.). The vial was capped and stirred overnight. In the morning, the precipitate was collected on a frit and washed with cold methanol to afford a beige-tan powder. Yield 423 mg (78.5%). ^{1}H NMR (400 MHz, $CDCl_3$) δ 7.96 (s, 2H, imine-CH), 6.35 (d, 2H, pyrrole-CH, *J* = 3.6 Hz), 6.04 (d, 2H, pyrrole-CH, *J* = 3.6 Hz), 2.13 (s, 6H, C-(CH_3)$_2$), and 1.70 (m, 30H, adamantyl-CH). ^{13}C NMR (101 MHz, $CDCl_3$) δ 146.10 (imine-CH), 142.87(aromatic-C), 130.46 (aromatic-CH), 114.39 (pyrrole-CH), 105.91 (pyrrole-CH), 56.65 ($\underline{C}$-(CH_3)$_2$), 43.35 (adamantyl-CH_2), 36.61 (adamantyl-CH_2), 35.83 (adamantyl-C), 29.67 (C-($\underline{C}H_3$)$_2$), and 28.82 (adamantyl-CH).

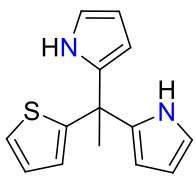

<u>2,2'-(1-(thiophen-2-yl)ethane-1,1-diyl)bis(1H-pyrrole)</u> or **<u>(3)</u>**: On the benchtop, a mixture of pyrrole (30.3 mL, 13.3 equiv.) and 2-acetylthiophene

(4.15 g, 32.9 mmol, 1 equiv.) in an ice bath was added trifluoroacetic acid (2.5 mL, 1 equiv.) dropwise. After complete addition of trifluoroacetic acid, the reaction was allowed to stir 8.5 hours. The reaction was quenched by the addition of sat. $NaHCO_3$ until basic. The crude mixture was extracted with 50 mL of DCM. The DCM layer was washed with sat. $NaHCO_3$ followed by water and then dried over Na_2SO_4. The solvent was removed and the product purified on a silica gel column eluting with 5:1 Hexane:Ethyl Acetate. The product was further purified by recrystallizing from boiling hexanes and storing at -8°C. This afforded yellow prism-like crystals. Yield 3.05 g (38.2%). Crystals suitable for single X-ray diffraction were grown from a solution of the compound dissolved in boiling hexanes and stored at -8°C. ^{1}H NMR (600 MHz, $CDCl_3$) δ 7.88 (s, 2H, pyrrole-NH), 7.22 (dd, 1H, thiophene-CH, *J* = 5.1, 1.2 Hz), 6.95 (dd, 1H, thiophene-CH, *J* = 5.1, 3.5 Hz), 6.79 (dd, 1H, thiophene-CH, *J* = 3.6, 1.2 Hz), 6.67 (q, 2H, pyrrole-CH, *J* = 2.3 Hz), 6.19 (q, 2H, pyrrole-CH, *J* = 2.9 Hz), 6.08 (dt, 2H, pyrrole-CH, *J* = 3.0, 1.7 Hz), and 2.13 (s, 3H, CH_3).

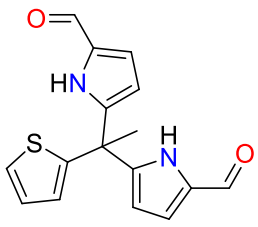

3-DA: An oven-dried 2-neck round-bottom flask was loaded with a stirbar and 2,2'-(1-(thiophen-2-yl)ethane-1,1-diyl)bis(1H-pyrrole) or **3** (5.00 g, 20.6 mmol, 1 equiv.). The reaction vessel was then capped with a septa and cycled onto a Schlenk-line under nitrogen. DMF (15 mL) that had been dried over sieves was then injected into the vessel and then allowed to cool in an ice-bath. Once chilled, $POCl_3$ (4.32 mL, 7.11 g, 46.4 mmol, 2.25 equiv.) was then added dropwise over the course of 6 minutes. After complete addition of $POCl_3$, the reaction was removed from the ice-bath and allowed to stir for 6.5 hours. The reaction was quenched first with 10 mL of DI water followed by basification with 1M NaOH until a pH of approximately 8-9. A precipitate formed and was collected on a glass frit. The precipitate was washed with a copious amount of water until the

filtrate was a neutral pH. The precipitate was then dissolved in DCM, dried over Na_2SO_4, and concentrated. The crude was purified via flash column chromatography eluting with 3:1 Hexane:Ethyl Acetate. Crystals suitable for single X-ray diffraction were grown from a solution of the compound dissolved in boiling hexanes and stored at -8°C. ^{1}H NMR (400 MHz, $CDCl_3$) δ 10.61 (s, 2H, pyrrole-NH), 9.14 (s, 2H, aldehyde-CH), 7.21 (dd, 1H, thiophene-CH, *J* = 5.1, 1.3 Hz), 6.96 – 6.90 (m, 2H, thiophene-CH), 6.84 (dd, 2H, pyrrole-CH, *J* = 4.0, 2.4 Hz), 6.14 (dd, 2H, pyrrole-CH, *J* = 4.0, 2.5 Hz), and 2.20 (s, 3H, CH_3). ^{13}C NMR (101 MHz, $CDCl_3$) δ 179.30 (aldehyde-CH), 148.90 (aromatic-C), 146.13 (aromatic-C), 132.66 (aromatic-C), 127.17 (thiophene-CH), 126.18 (thiophene-CH), 124.99 (thiophene-CH), 121.95 (pyrrole-CH), 110.50 (pyrrole-CH), 43.33 (*C*(CH_3)), and 29.88 (*C*H_3).

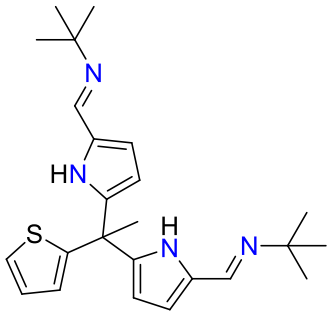

3-tBu: On the benchtop, **3-DA** (200 mg, 0.670 mmol, 1 equiv.) was weighed into a 20 mL vial equipped with a stir bar. 1 mL of neat tbutylamine was added and the reaction stirred overnight. The following morning the reaction was filtered and dried on the vacuum line to yield a light brown powder. Yield 100 mg (36.5%). ^{1}H NMR (400 MHz, $CDCl_3$) δ 7.97 (s, 2H, imine-CH), 7.34 (br, 2H, pyrrole-NH), 7.18 (dd, 1H, thiophene-CH, *J* = 5.2, 1.3 Hz), 6.90 (dd, 1H, thiophene-CH, *J* = 5.1, 3.5 Hz), 6.73 (d, 1H, thiophene-CH, *J* = 3.6 Hz), 6.39 (d, 2H, pyrrole-CH, *J* = 3.5 Hz, 1H), 6.12 (d, 2H, pyrrole-CH, *J* = 3.6 Hz), 2.16 (s, 3H, C-(CH_3)), and 1.23 (s, 18H, C-(CH_3)$_3$). ^{13}C NMR (101 MHz, $CDCl_3$) δ 152.14 (aromatic-C), 146.92 (imine-CH), 140.80 (aromatic-C), 130.93 (aromatic-C), 126.76 (thiophene-CH), 125.40 (thiophene-CH), 124.83 (thiophene-CH), 114.29 (pyrrole-CH), 107.59 (pyrrole-CH), 56.85 (quaternary-C), 42.82 (quaternary-C), 30.01 (CH_3), and 29.51 (CH_3).

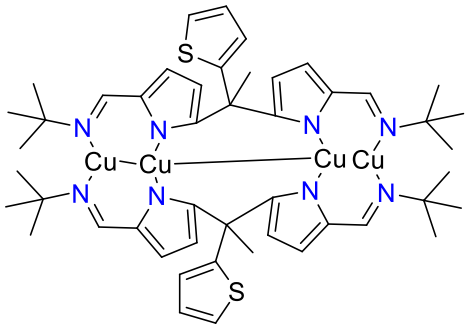

<u>Cu$_4$(3-tBu)$_2$</u>. In a nitrogen glovebox, **3-tBu** (83.7 mg, 0.205 mmol, 1 equiv.) was weighed into a 7 mL vial and dissolved in 1 mL of MeCN. This was transferred to another 7 mL vial containing KH (16.4 mg, 0.410 mmol, 2 equiv.). The reaction was stirred until gas formation ceased and then an additional 15 minutes. After this time, the reaction mixture was transferred to a 7 mL vial with [Cu(MeCN)$_4$][PF$_6$] (152.7 mg, 0.410 mmol, 2 equiv.) dissolved in 1 mL of acetonitrile. The reaction immediately formed a yellow precipitate. The reaction was allowed to stir for 1 hour and the precipitate was collected on a frit. The solid was washed with additional acetonitrile, dissolved in DCM, and filtered. The solvent removed and the corresponding yellow powder was collected and washed with hexanes. Yield 54.7 mg (50.1%). Crystals suitable for single X-ray diffraction were grown from a solution of the compound dissolved in DCM layered with acetonitrile and stored at -30^{O}C.

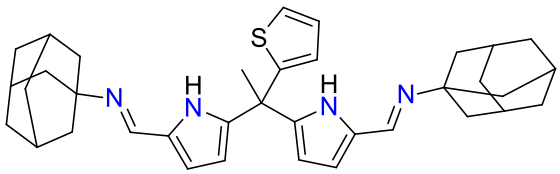

<u>3-Ad</u>: On a benchtop, **3-DA** (250 mg, 0.838 mmol, 1 equiv.) was weighed into a 20 mL vial with a stir bar and adamantylamine (253 mg, 1.676 mmol, 2.2. equiv.). 10 mL of methanol was added, and the reaction was stirred overnight. In the morning, the precipitate was collected and washed with hexanes yielding a off white solid. Yield 61.4 mg (12.9%). ^{1}H NMR (400 MHz, CDCl$_3$) δ 8.71 (s, 2H, pyrrole-NH), 7.99 (s, 2H, imine-CH), 7.20 (d, 1H, thiophene-CH, *J* = 5.1 Hz), 6.92 (dd, 1H, thiophene-CH, *J* = 5.1, 3.6 Hz, 1H), 6.78 (d, 1H, thiophene-CH, *J* = 3.5 Hz), 6.36 (d, 2H, pyrrole-CH, *J* = 3.6 Hz), 6.03 (d, 2H, pyrrole-CH,*J* = 3.7), 2.43 – 1.41 (m, 33H, aliphatic-Hs). ^{13}C NMR (101 MHz, CDCl$_3$) δ 151.51 (aromatic-C), 145.54 (imine-CH), 140.34 (aromatic-C), 131.14 (aromatic-C)f, 126.54 (thiophene-CH), 125.35

(thiophene-CH), 124.61 (thiophene-CH), 113.55 (pyrrole-CH), 108.16 (pyrrole-CH), 56.71 (quaternary-C), 43.32 (adamantyl-CH_2), 42.80 (quaternary-C), 36.62 (adamantyl-CH_2), 29.81(aliphatic-CH), and 29.67 (aliphatic-CH).

4.5.3. ^{1}H and ^{13}C NMR for Schiff-base Calixpyrrole Ligands and Tetranuclear Cu^{I} Complexes

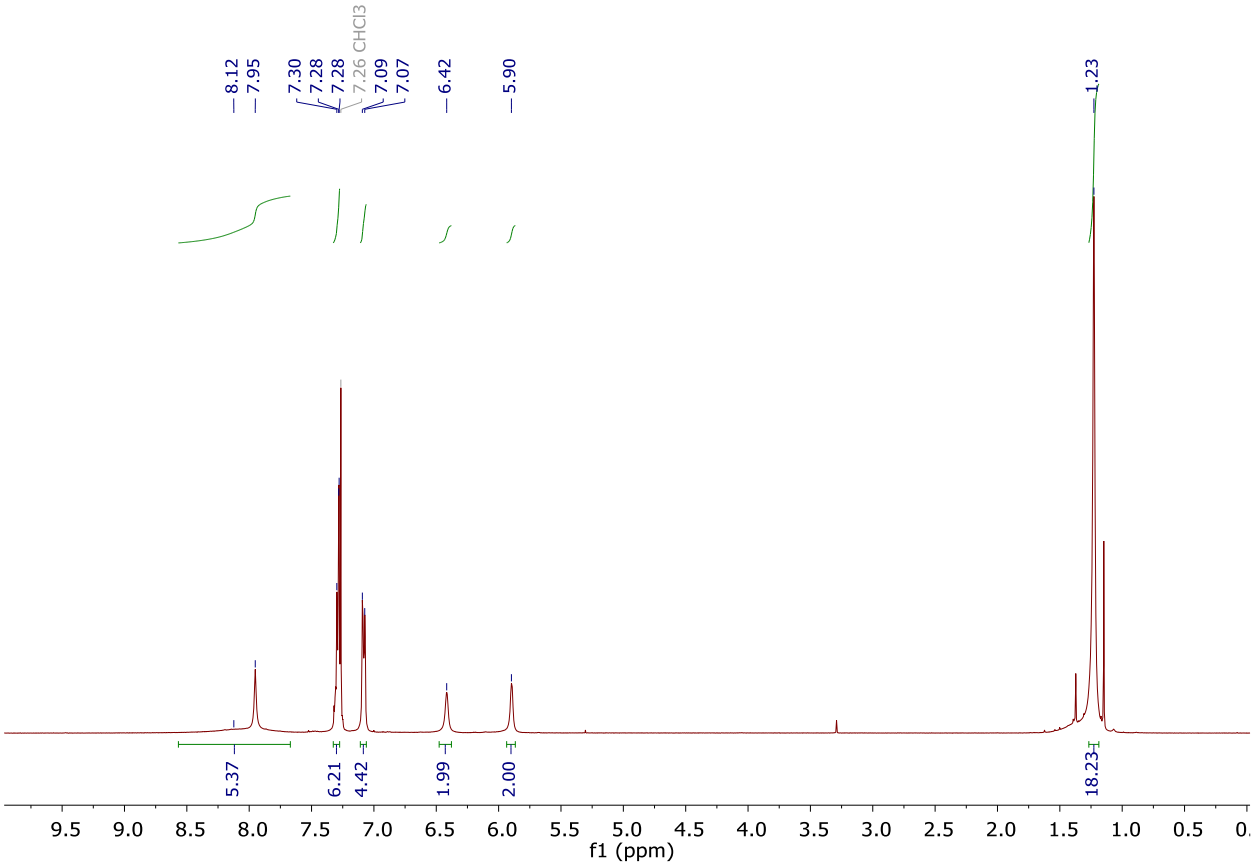

Figure 4.7. ^{1}H NMR of **1-tBu**.

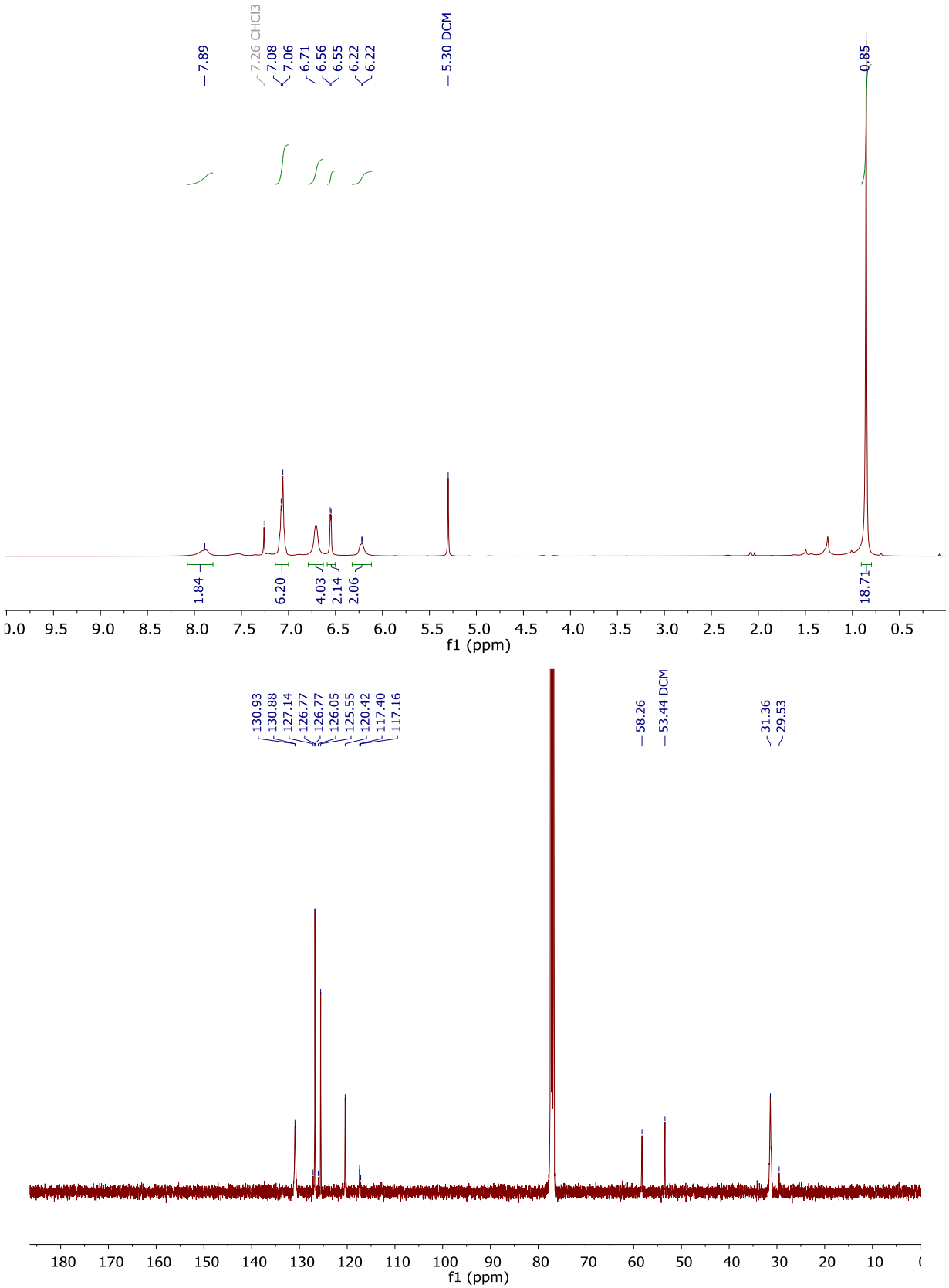

Figure 4.8. ^{1}H and ^{13}C NMR of **Cu_4(1-tBu)$_2$**.

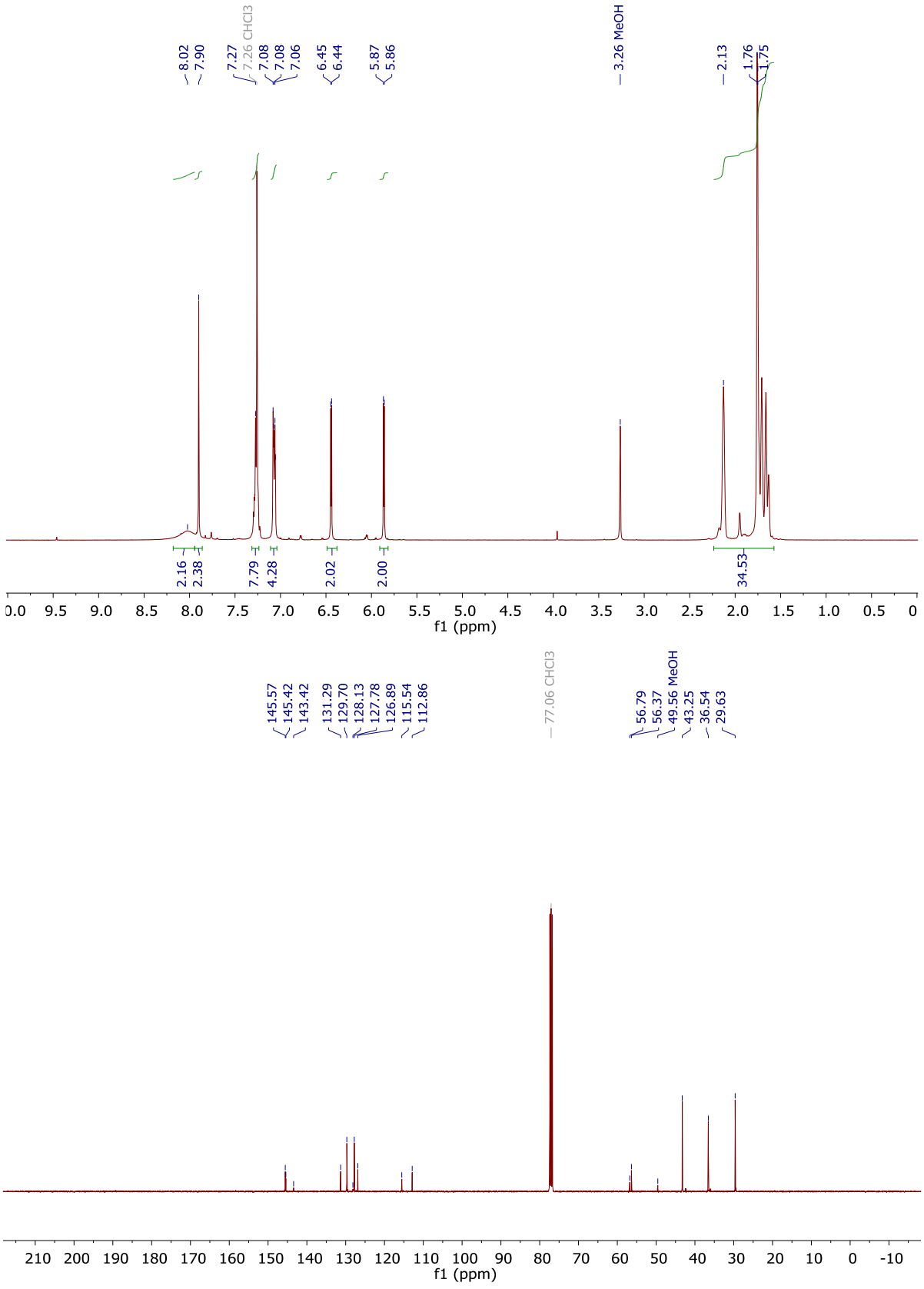

Figure 4.9. ^{1}H and ^{13}C NMR of **1-Ad**.

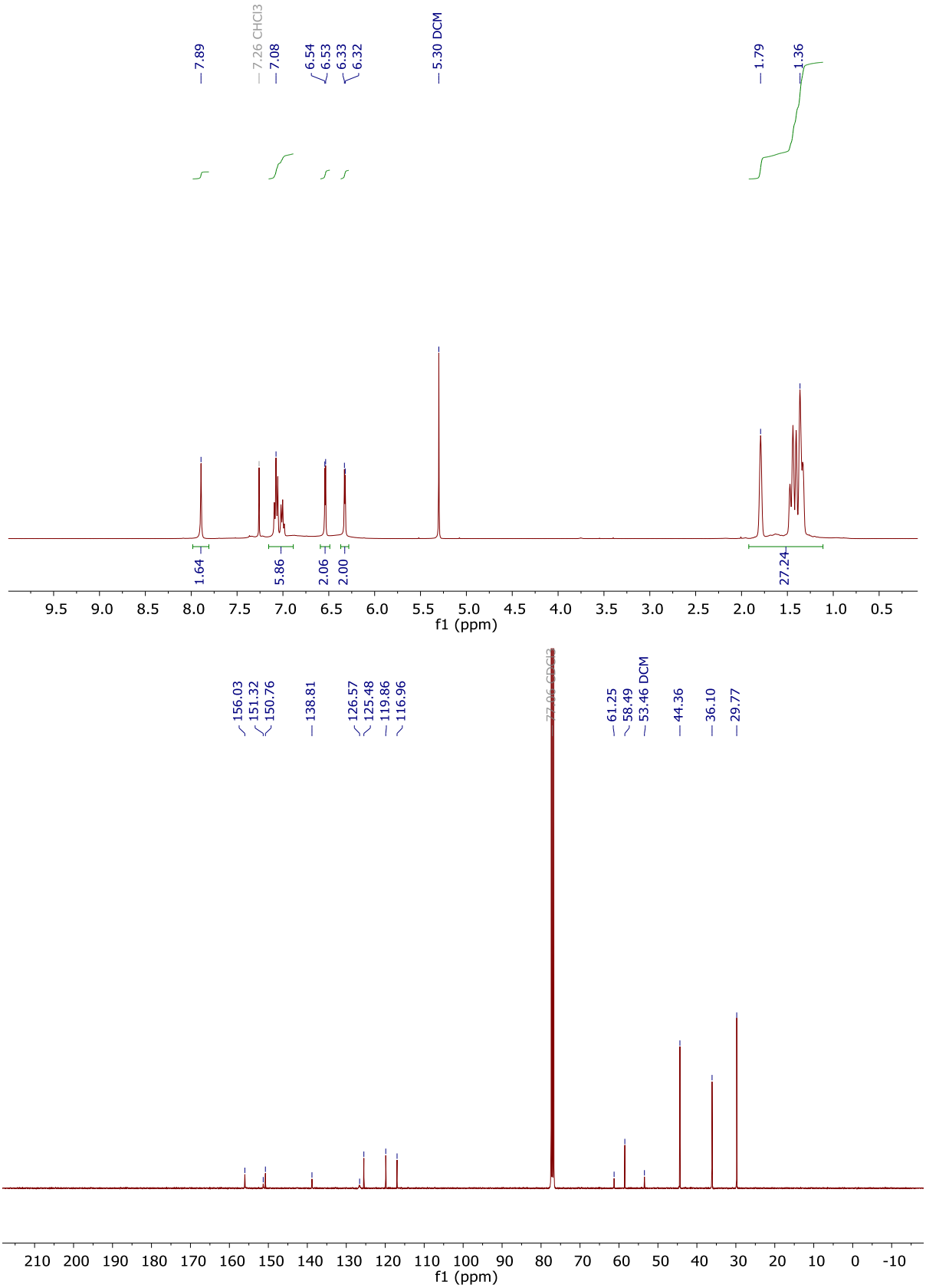

Figure 4.10. ^{1}H and ^{13}C NMR of **Cu_4(1-Ad)$_2$**.

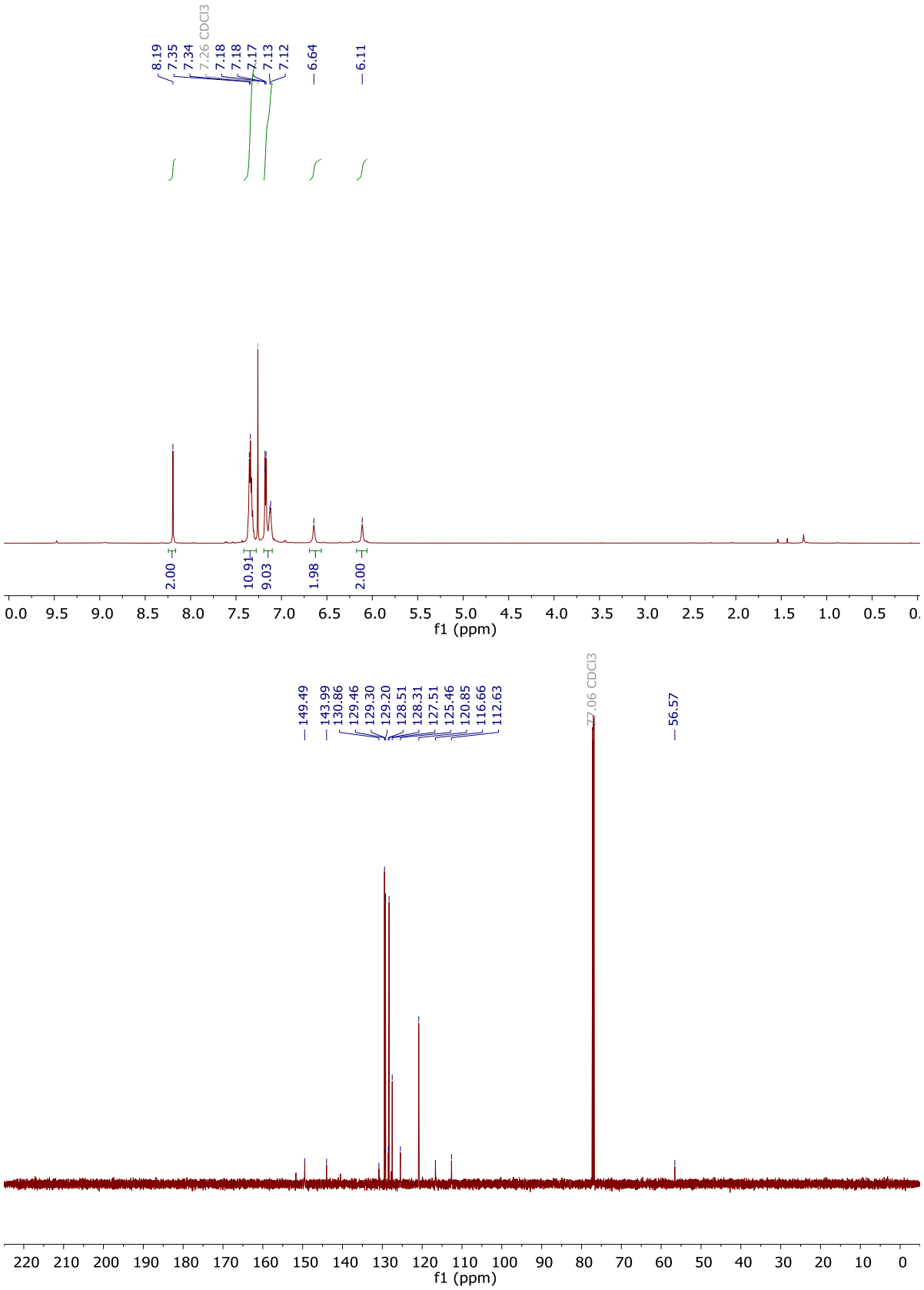

Figure 4.11. ^{1}H and ^{13}C NMR of **1-Ph**.

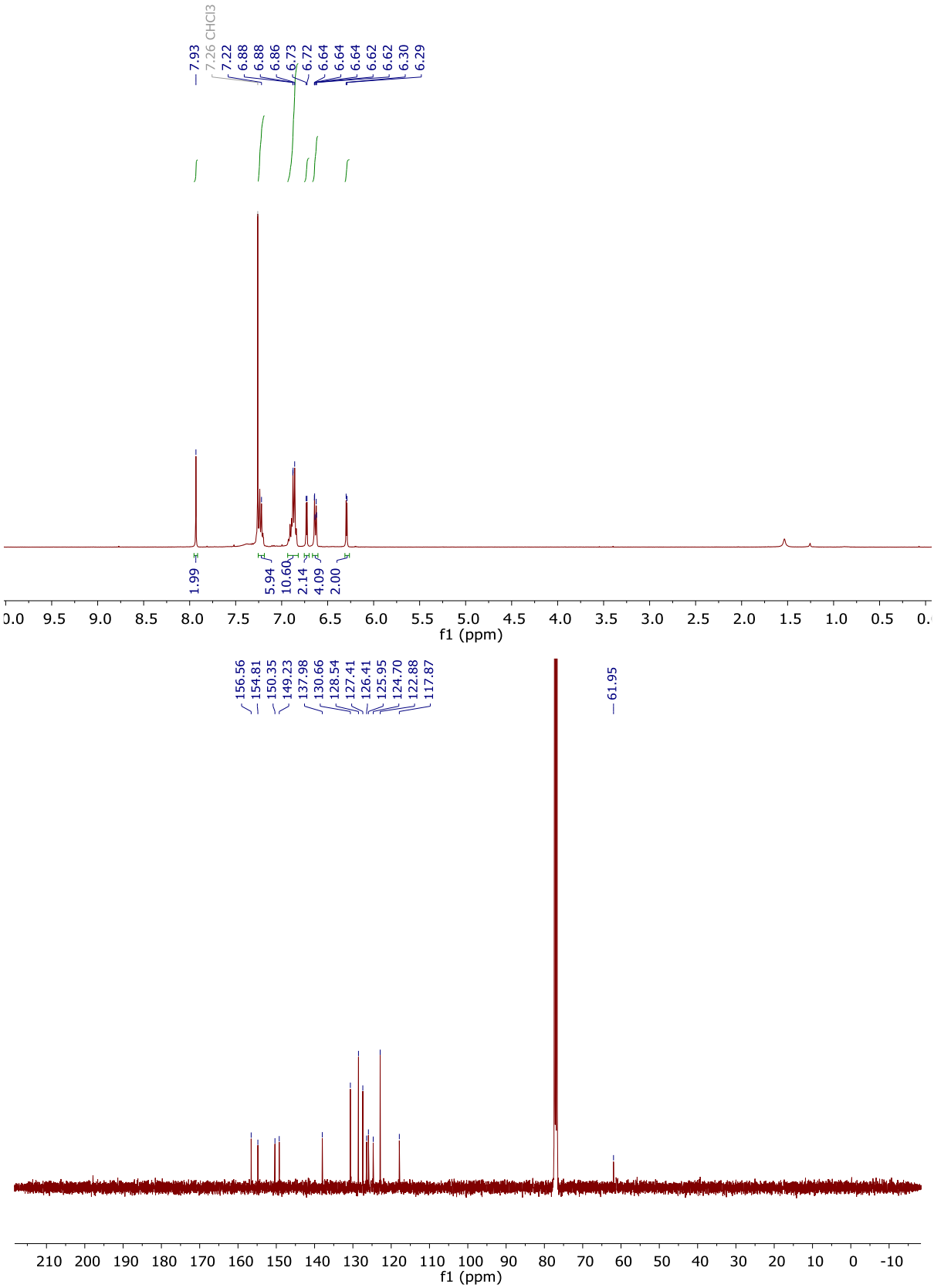

Figure 4.12. ^{1}H and ^{13}C NMR of **Cu_4(1-Ph)$_2$**.

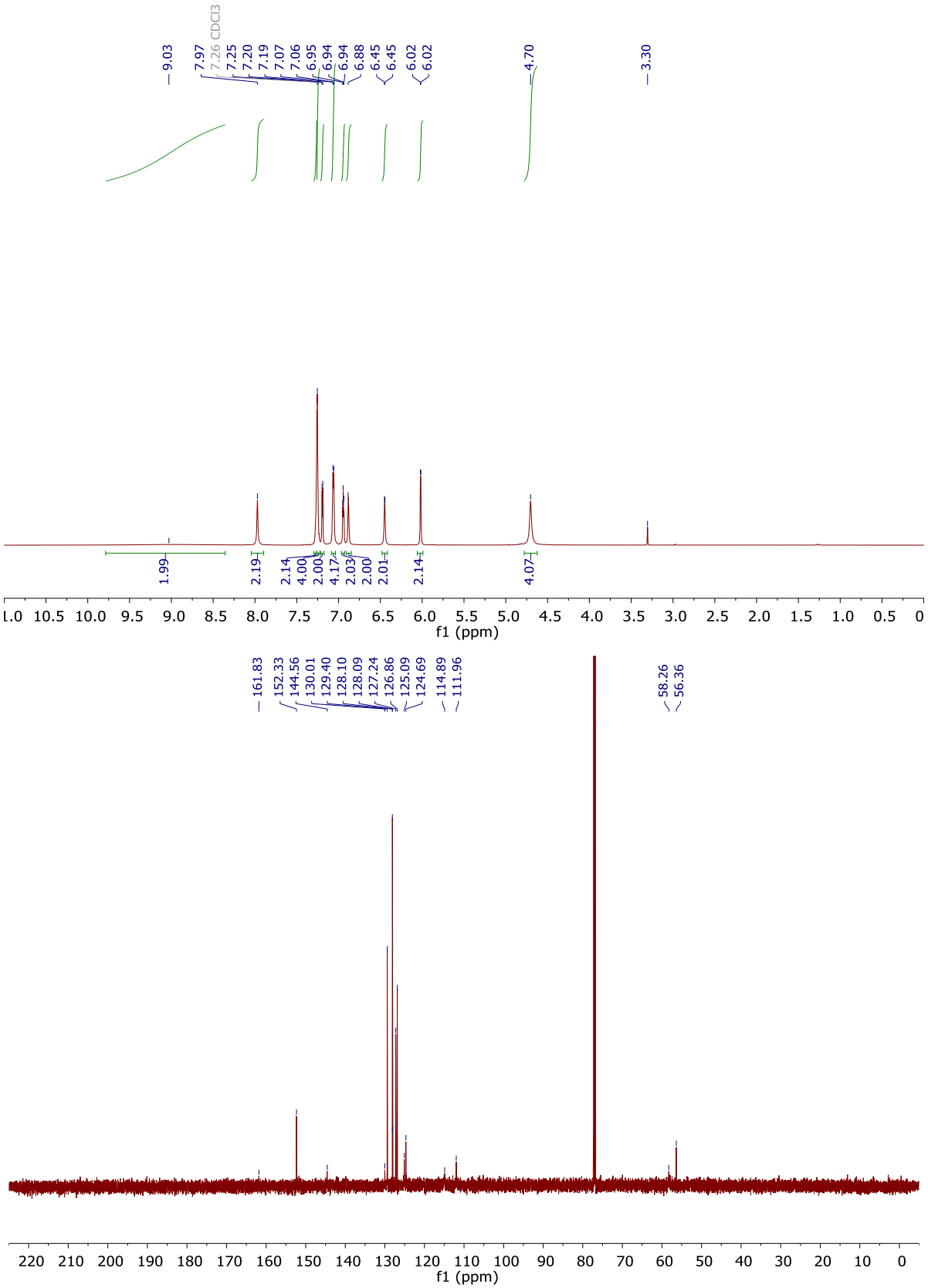

Figure 4.13. ^{1}H and ^{13}C NMR of **1-Th**.

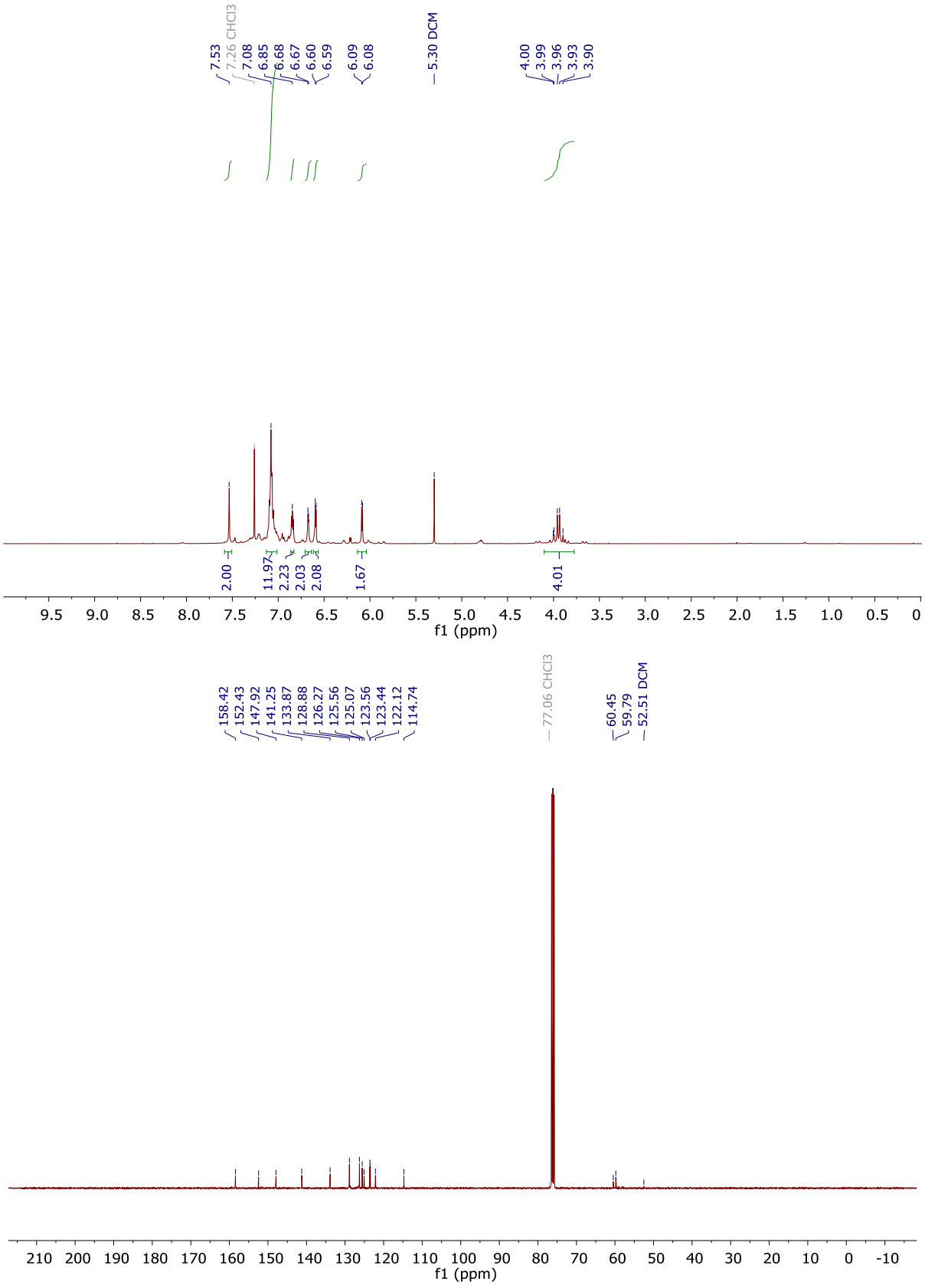

Figure 4.14. ^{1}H and ^{13}C NMR of **Cu_4(1-Th)$_2$**.

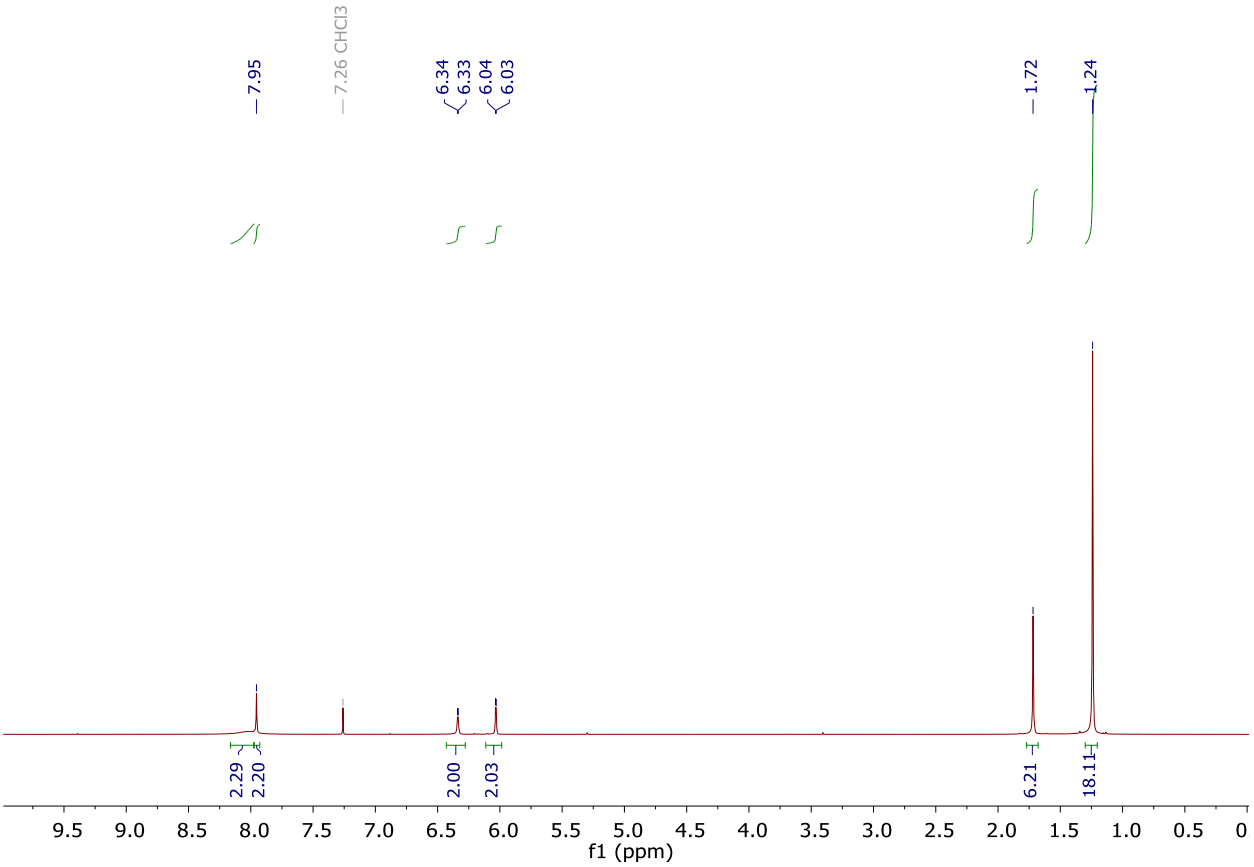

Figure 4.15. ^{1}H and ^{13}C NMR of **2-tBu**.

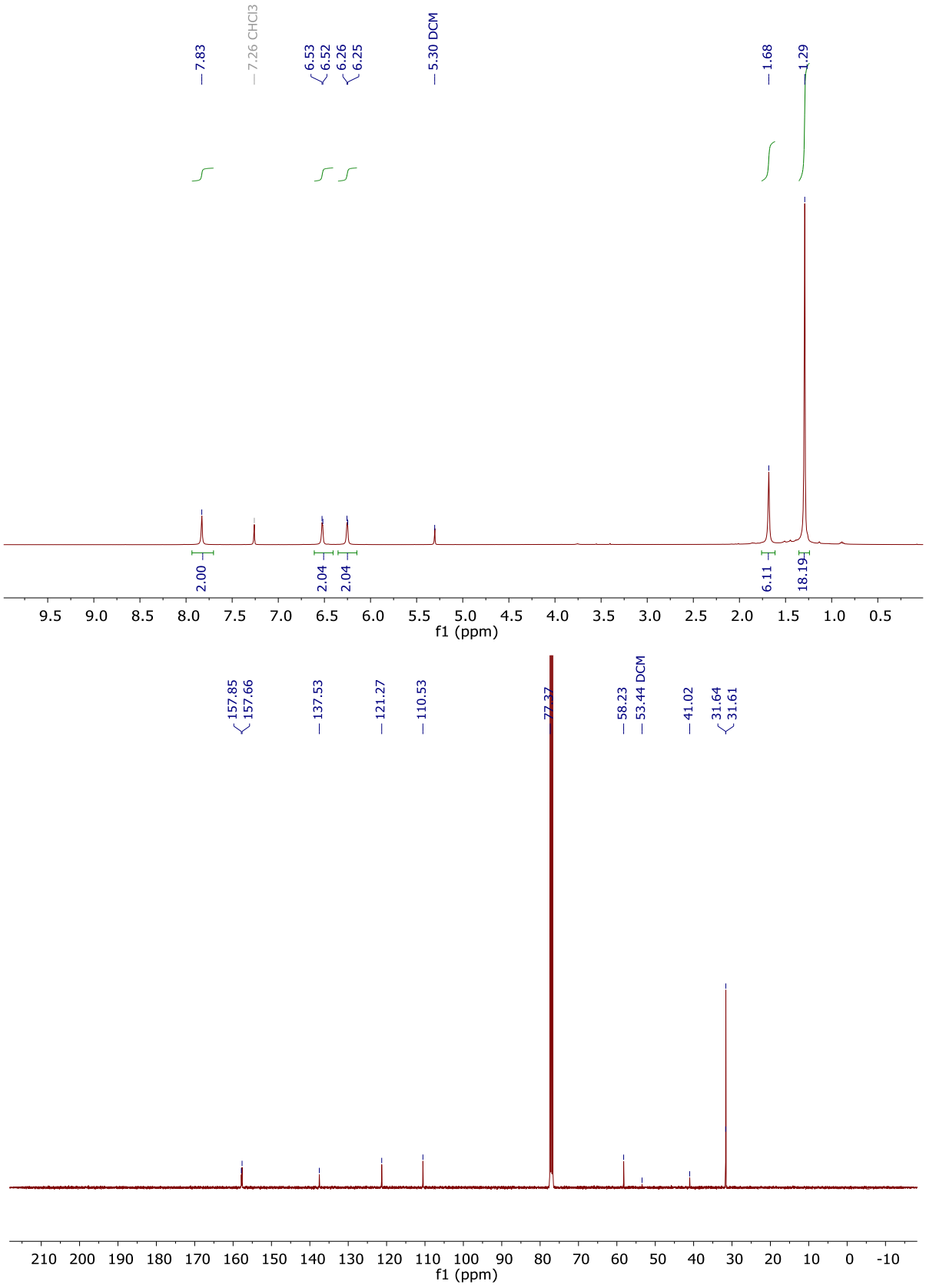

Figure 4.16. ^{1}H and ^{13}C NMR of **Cu_4(2-tBu)$_2$**.

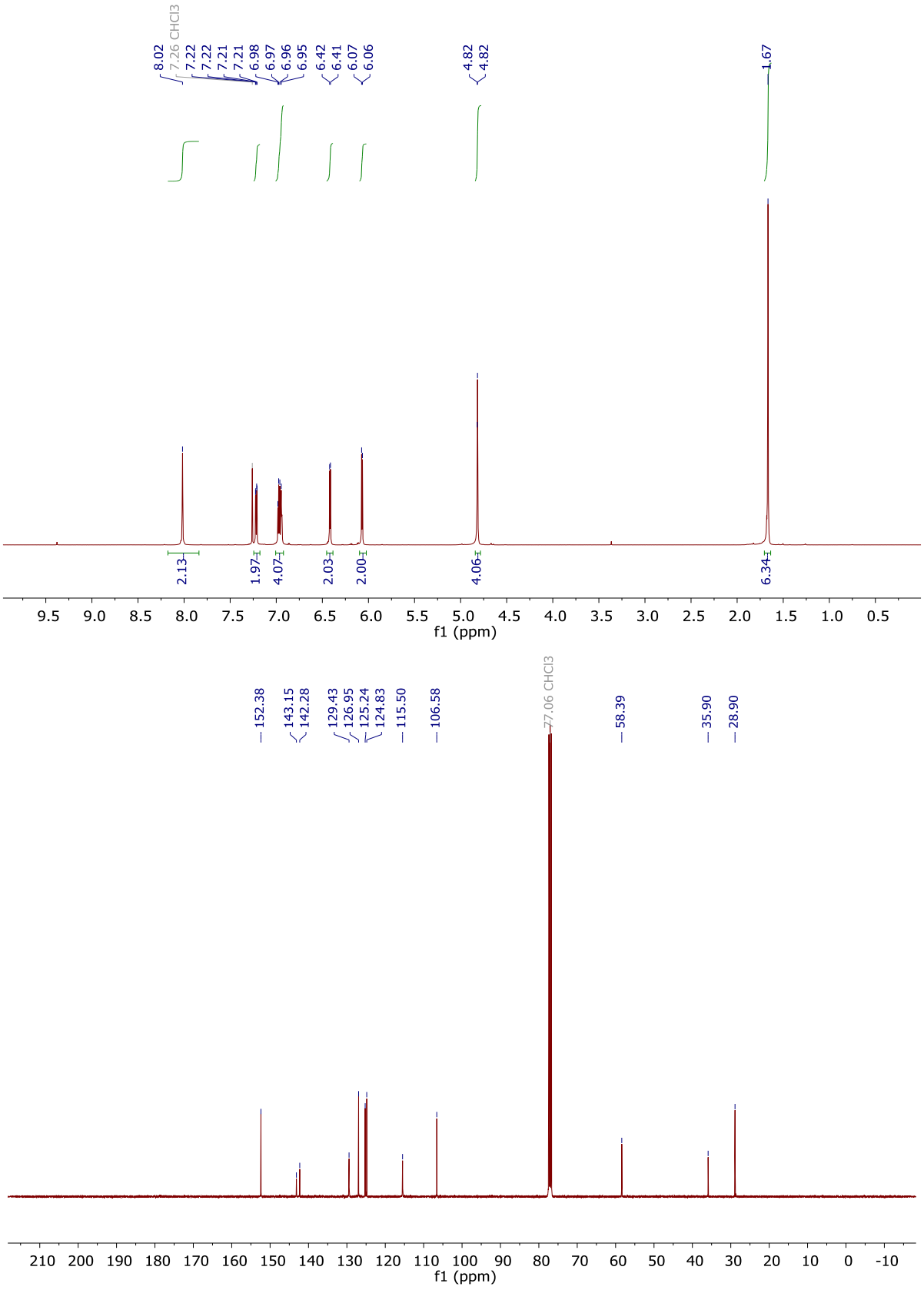

Figure 4.17. ^{1}H and ^{13}C NMR of **2-Th**.

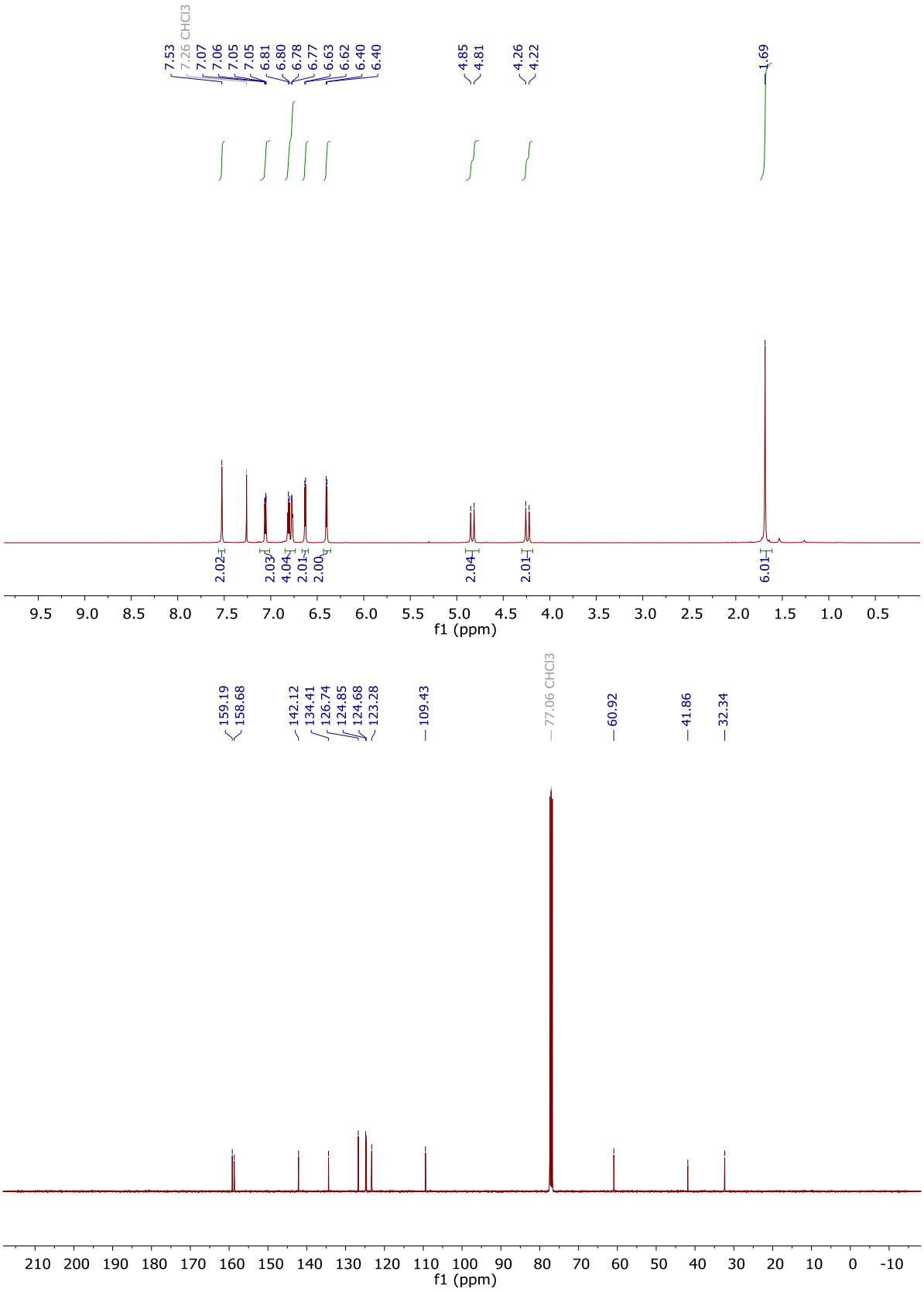

Figure 4.18. ^{1}H and ^{13}C NMR of **Cu_4(2-Th)$_2$**.

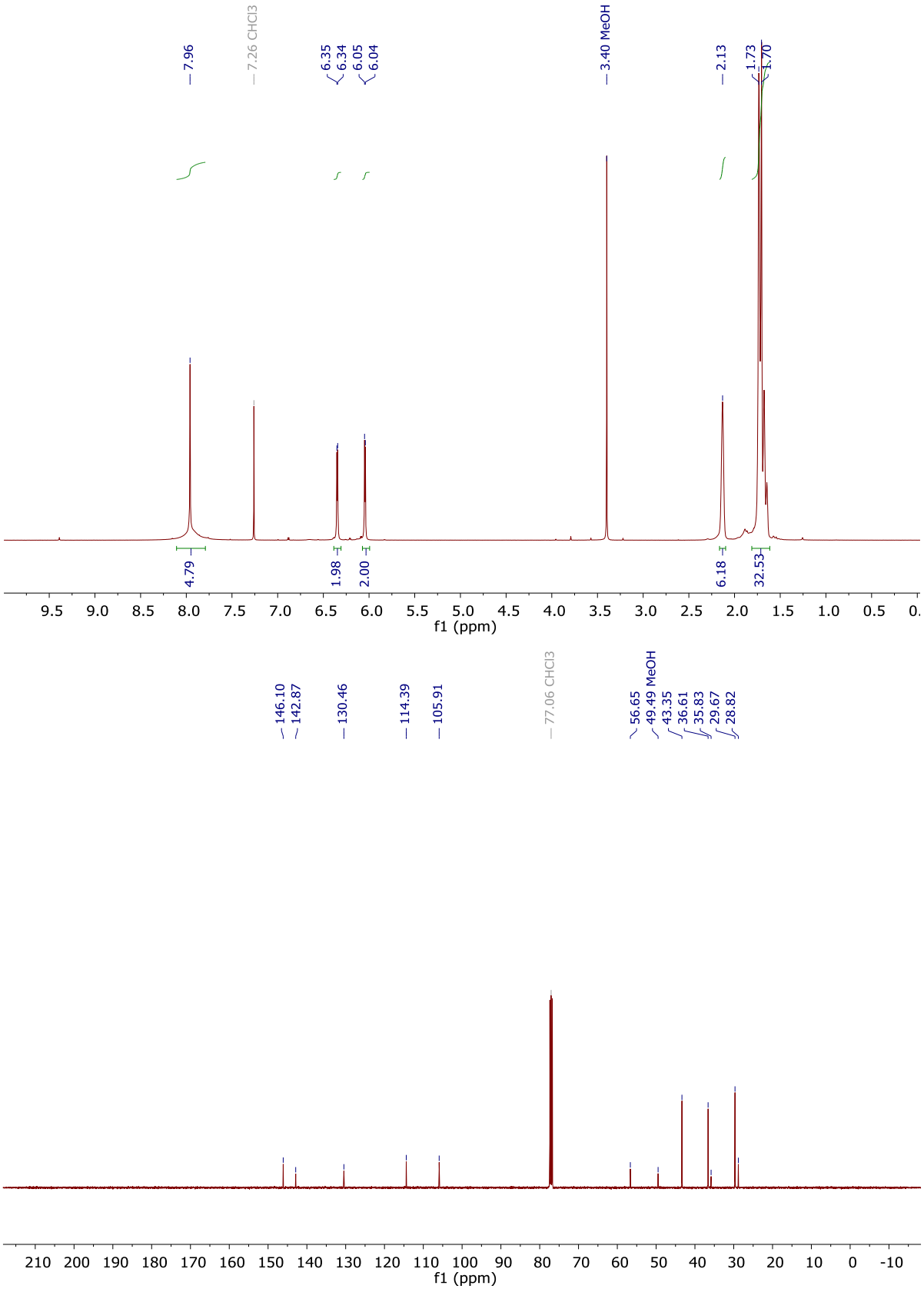

Figure 4.19. ^{1}H and ^{13}C NMR of **2-Ad**.

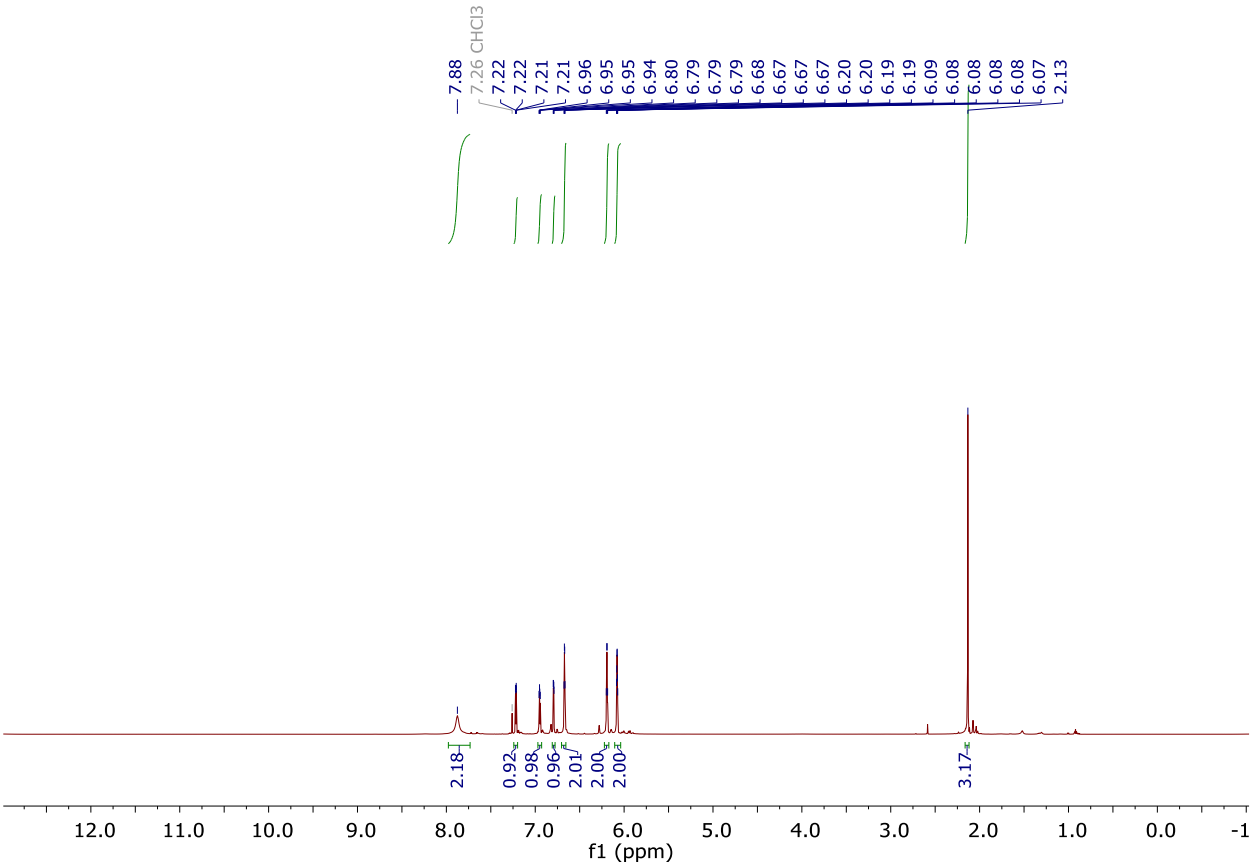

Figure 4.20. ^{1}H and ^{13}C NMR of **3**.

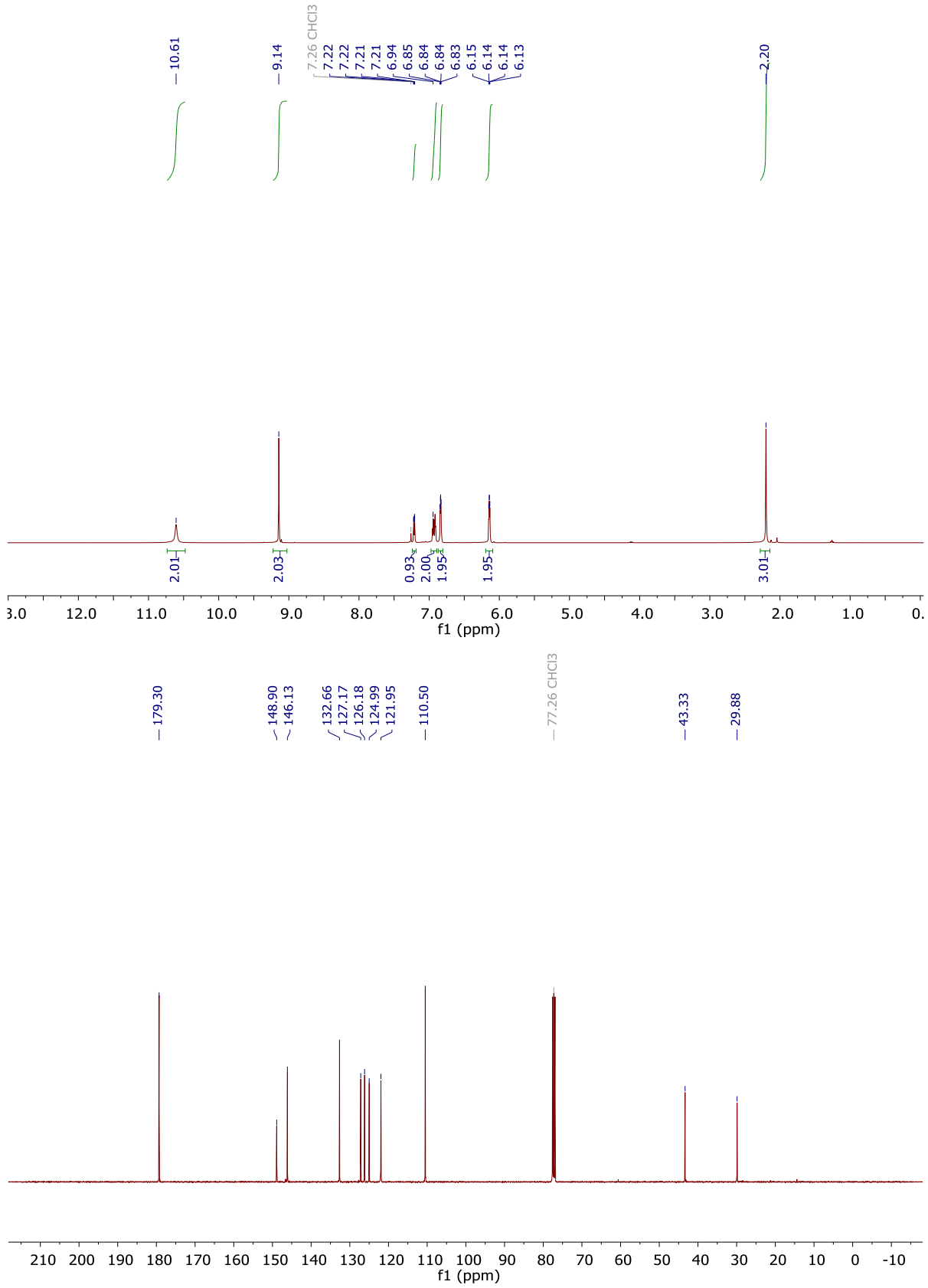

Figure 4.21. ^{1}H and ^{13}C NMR of **3-DA**.

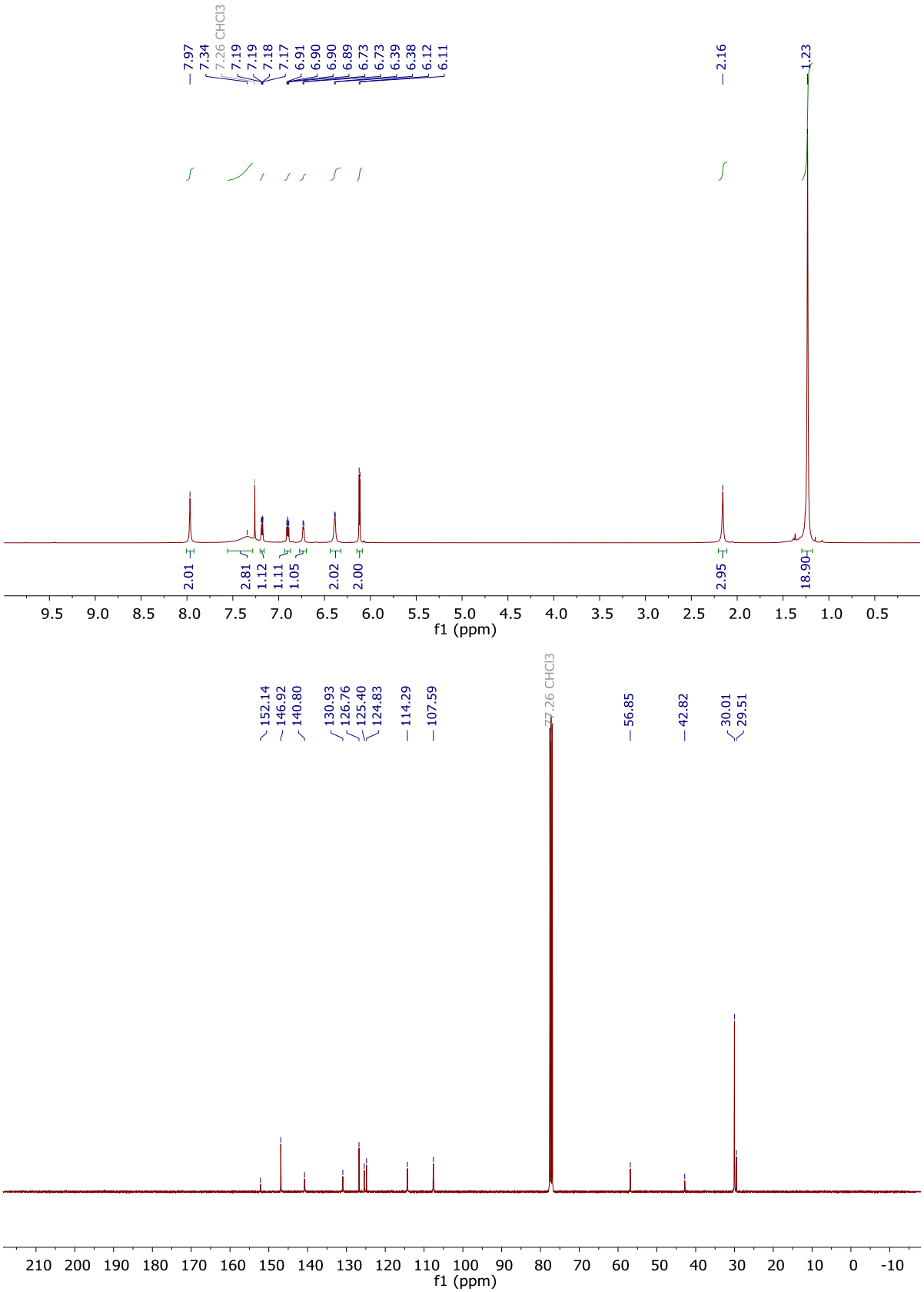

Figure 4.22. ^{1}H and ^{13}C NMR of **3-tBu**.

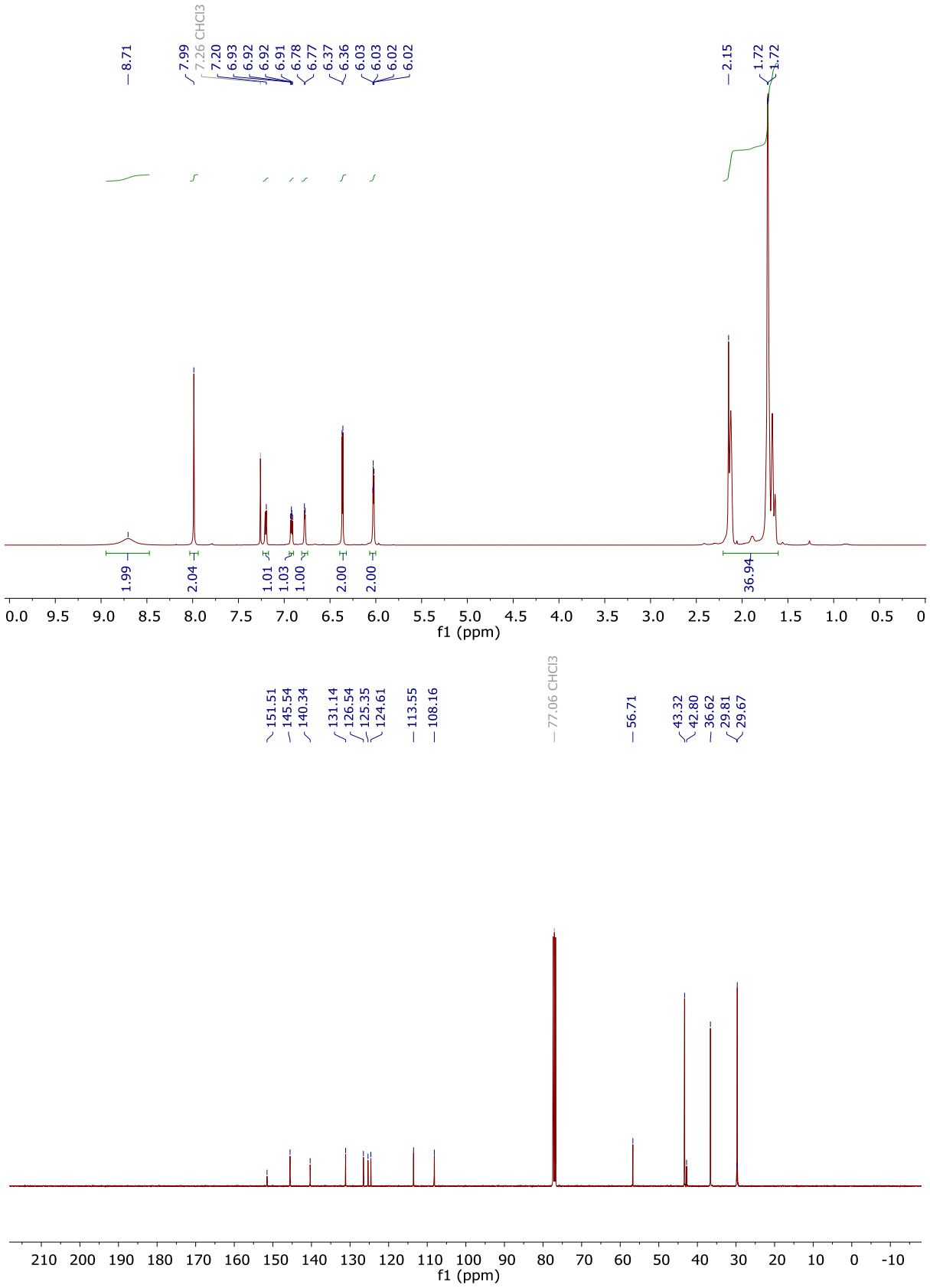

Figure 4.23. ^{1}H and ^{13}C NMR of **3-Ad**.

4.5.4. ORTEP3 Representation of 3 and 3-DA

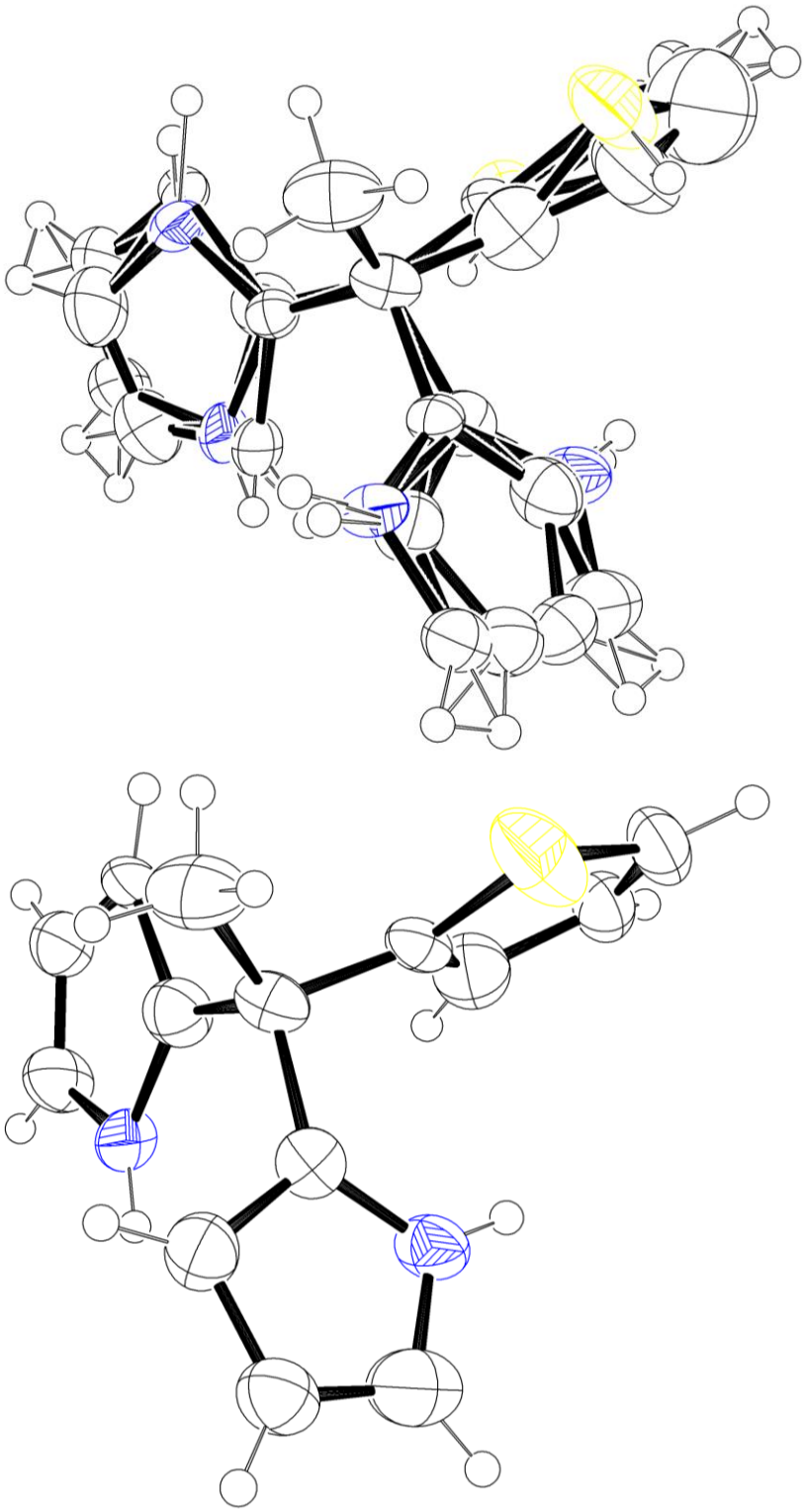

Figure 4.24. ORTEP3 representation (thermal ellipsoids at 50% probability) of **3**. Top: with disorder in rings. Bottom: without disorder in rings.

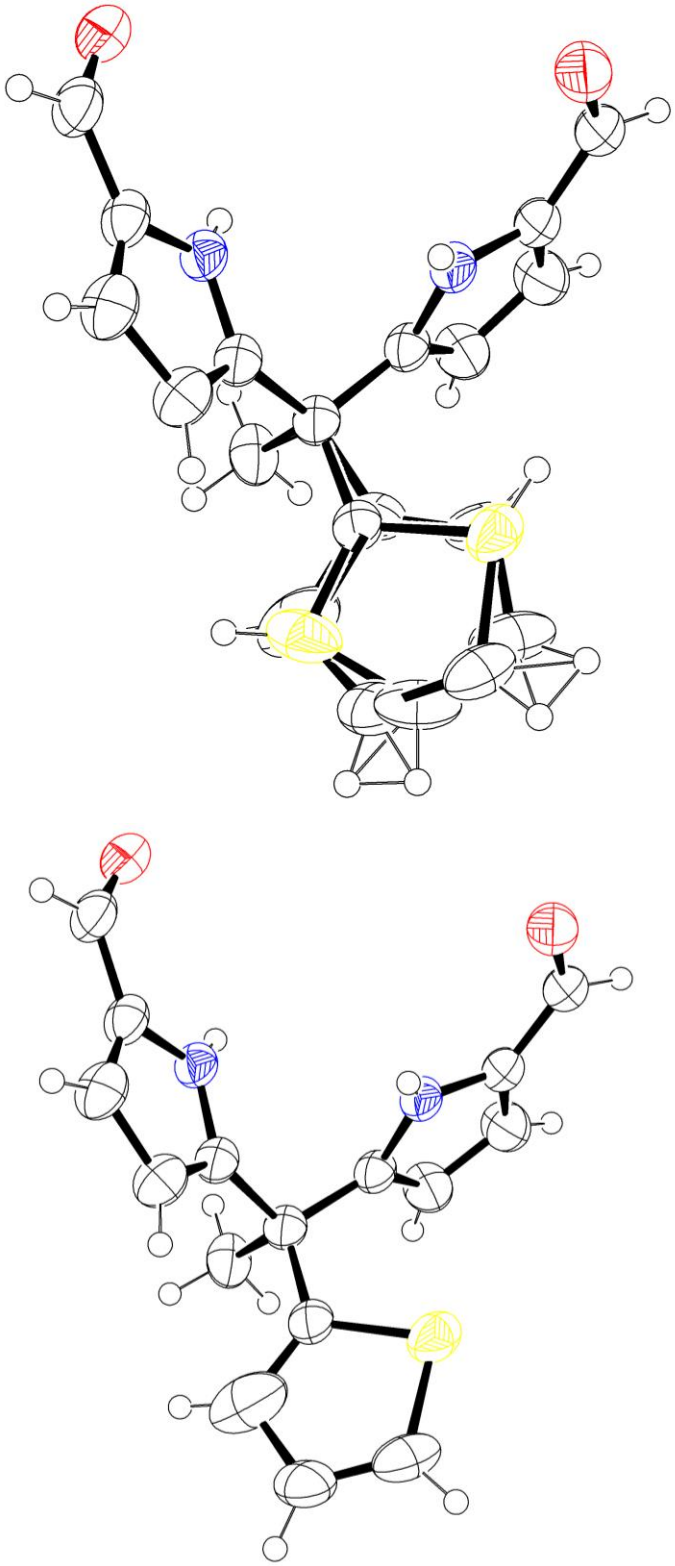

Figure 4.25. ORTEP3 representation (thermal ellipsoids at 50% probability) of **3-DA**. Top: with disorder. Bottom: without disorder.

4.5.5. Crystallographic Data

Table 4.3. Select Crystal Data, Data Collection, and Refinement Parameters for **3** and **3-DA**. [a]Definition of R indices: $R_1 = \Sigma(F_O - F_C)/\Sigma(F_O)$; $wR_2 = [\Sigma[w(F_O^2 - F_C^2)^2]/[\Sigma[w(F_O^2)^2]]]^{1/2}$

	3	**3-DA**
empirical formula	$C_{14}H_{14}N_2S$	$C_{16}H_{14}N_2O_2S$
FW	242.33	298.35
lattice type	Orthorhombic	Monoclinic
space group	$Pna2_1$	C2/c
T, K	210.00	210.00
a, Å	6.48128(3)	13.03601(13)
b, Å	27.58076(12)	13.60621(13)
c, Å	7.04759(3)	16.82383(18)
α, deg	90	90
β, deg	90	100.3267(10)
γ, deg	90	90
V, $Å^3$	1259.818(10)	2935.72(5)
Z	4	8
ρ_{calc}/Mg m^{-3}	1.278	1.350
μ(Cu/Mo, Kα) mm^{-1}	2.090	2.009
F(000)	512.0	1248.0
crystal size, mm^3	0.17x0.13x0.09	0.15x0.12x0.08
range Θ collected, deg	3.205 to 79.966	4.738 to 79.801
Reflns (Collectd/unique)	446392/2740	20135/3196
Abs cor	Semi Empirical based upon equivalents	
max and min transmn coeff.	1.000 and 0.881	1.000 and 0.795
goodness of fit	1.095	1.071
R_1 (I>2σ(I))[a]	0.0641	0.0378
wR_2 (all data)[a]	0.2051	0.1079
Peak and hole, e $Å^{-3}$	0.452 and -0.499	0.312 and -0.218

Table 4.4. Selected Crystal Data, Data Collection, and Refinement Parameters for **3-tBu, 1-Ad**, and **Cu_4(1-tBu)$_2$**. [a]Definition of R indices: $R_1 = \Sigma(F_O - F_C)/\Sigma(F_O)$; $wR_2 = [\Sigma[w(F_O^2 - F_C^2)^2]/[\Sigma[w(F_O^2)^2]]^{1/2}$

	3-tBu	**1-Ad**	**Cu_4(1-tBu)$_2$**
empirical formula	$C_{24}H_{34}N_4OS$	$C_{43}H_{50}N_4O$	$C_{65}H_{74}Cl_6Cu_4N_8$
FW	426.61	638.87	1434.18
lattice type	Triclinic	Monoclinic	Monoclinic
space group	P-1	C2/c	C2/c
T, K	270.00(10)	210.00	210.00
a, Å	6.8713(4)	30.6403(4)	12.03820(10)
b, Å	9.6637(4)	14.06613(12)	23.57000(10)
c, Å	19.4370(9)	17.2890(2)	23.83100(10)
α, deg	81.934(4)	90	90
β, deg	86.781(5)	104.8637(13)	103.1270(10)
γ, deg	89.049(4)	90	90
V, $Å^3$	1275.83(12)	7218.97(15)	6585.12(7)
Z	2	8	4
ρ_{calc}/Mg m^{-3}	1.110	1.176	1.447
μ(Cu/Mo, Kα) mm^{-1}	1.277	0.542	4.045
F(000)	460.0	2752.0	2952.0
crystal size, mm^3	0.11x0.09x0.07	0.10x0.07x0.04	0.29x0.17x0.14
range Θ collected, deg	2.299 to 78.008	2.984 to 79.886	3.751 to 79.998
Reflns (Collectd/unique)	16203/5167	30291/7698	46962/7121
Abs cor	Semi Empirical based upon equivalents		
max and min transmn coeff.	1.000 and 0.830	1.000 and 0.955	1.000 and 0.294
goodness of fit	1.037	1.027	1.035
R_1 (I>2σ(I))[a]	0.0652	0.0474	0.0410
wR_2 (all data)[a]	0.2025	0.1212	0.1088
Peak and hole, e $Å^{-3}$	0.344 and -0.236	0.193 and -0.215	0.977 and -0.823

Table 4.5. Selected Crystal Data, Data Collection, and Refinement Parameters for **Cu_4(1-Ad)$_2$**, **Cu_4(1-Ph)$_2$**, and **Cu_4(1-Th)$_2$**.

	Cu_4(1-Ad)$_2$	**Cu_4(1-Ph)$_2$**	**Cu_4(1-Th)$_2$**
empirical formula	$C_{86}H_{92}Cu_4N_8$	$C_{94}H_{100}Cu_4N_8O_6$	$C_{66}H_{52}Cu_4N_8S_4$
FW	1491.83	1691.97	1339.55
lattice type	Monoclinic	Monoclinic	Monoclinic
space group	I2/a	$P2_1/n$	$P2_1/c$
T, K	210.00	210.00	210.00
a, Å	24.8942(5)	19.9636(3)	17.1612(17)
b, Å	10.96420(10)	36.2023(6)	26.0387(13)
c, Å	29.2704(6)	22.9413(5)	13.9197(9)
α, deg	90	90	90
β, deg	116.083(3)	109.663(2)	93.289(8)
γ, deg	90	90	90
V, Å^3	7175.6(3)	15613.5(5)	6209.8(8)
Z	4	8	4
ρ_{calc}/Mg m^{-3}	1.381	1.440	1.433
μ(Cu/Mo, Kα) mm^{-1}	1.731	1.722	3.163
F(000)	3120.0	5152.0	2736.0
crystal size, mm^3	0.14x0.09x0.07	0.32x0.07x0.02	0.11x0.08x0.01
range Θ collected, deg	3.362 to 80.533	2.382 to 67.078	2.579 to 41.122
Reflns (Collectd/unique)	14686/14686	101919/27561	20111/3891
Abs cor	Semi Empirical based upon equivalents		
max and min transmn coeff.	0.848 and 0.723	1.000 and 0.688	1.000 and 0.674
goodness of fit	1.054	1.076	1.357
R_1 (I>2σ(I))[a]	0.0367	0.0948	0.1107
wR_2 (all data)[a]	0.1085	0.2988	0.3409
Peak and hole, e Å^{-3}	0.566 and -0.366	1.179 and -0.836	1.101 and -0.560

Table 4.6. Selected Crystal Data, Data Collection, and Refinement Parameters for **$Cu_4(2\text{-}tBu)_2$** and **$Cu_4(3\text{-}tBu)_2$**. [a]Definition of R indices: $R_1 = \Sigma(F_O - F_C)/\Sigma(F_O)$; $wR_2 = [\Sigma[w(F_O^2 - F_C^2)^2]/[\Sigma[w(F_O^2)^2]]^{1/2}$

	$Cu_4(2\text{-}tBu)_2$	**$Cu_4(3\text{-}tBu)_2$**
empirical formula	$C_{42}H_{60}Cu_4N_8$	$C_{51.2}H_{64.4}Cl_{2.4}Cu_4N_{9.2}$
FW	931.14	1212.08
lattice type	Monoclinic	Orthorhombic
space group	C2/c	Pnna
T, K	292.6(9)	210.00
a, Å	21.2048(14)	23.6284(3)
b, Å	10.7623(4)	12.2069(2)
c, Å	20.9610(15)	18.5184(2)
α, deg	90	90
β, deg	116.353(8)	90
γ, deg	90	90
V, Å^3	4286.4(5)	5341.25(12)
Z	4	4
ρ_{calc}/Mg m^{-3}	1.443	1.507
μ(Cu/Mo, Kα) mm^{-1}	2.527	3.972
F(000)	1936.0	2208.0
crystal size, mm^3	0.03x0.02x0.02	0.17x0.02x0.02
range Θ collected, deg	4.654 to 68.826	3.032 to 80.091
Reflns (Collectd/unique)	16955/3917	23222/5681
Abs cor	Semi Empirical based upon equivalents	
max and min transmn coeff.	0.979 and 0.961	1.000 and 0.809
goodness of fit	1.016	1.076
R_1 (I>2σ(I))[a]	0.0710	0.0505
wR_2 (all data)[a]	0.2419	0.1573
Peak and hole, e Å^{-3}	0.986 and -0.592	0.567 and -0.803

Chapter 5 - Conclusion

Fluorescent materials have a variety of applications.[15,18,117,167] One application that has impact to both industry and academia is lighting such as displays, OLEDs and other optoelectronic devices.[20] However, many of current fluorescent materials used in these suffer from poor quantum efficiency or require toxic and expensive rare-earth metals.[21,29,30,127,168,169] Recent developments in Copper (I) or Cu^{I} fluorescent complexes and materials have played a significant role in the advancement in this field by offering higher quantum yields and being a less toxic, cheaper alternative.[126,170–172]

Herein, we discussed the synthesis of a unique fluorescent, bidentate ligand, **SNNH^{t}Bu**. The synthesis of this ligand began from thiophene to generate 2-acetylthiophene. From here, a Wittig reaction was carried out to generate the geminal olefin. Using a $NaHSO_4 \cdot H_2O$ catalyst, a hydroarylation of the olefin was done to provide a biaryl compound. Utilization of the more nucleophilic pyrrole, a selective Vielsmeyer-Haack reaction was carried out to afford a formylation on the pyrrole. In a one-pot reductive amination using ^{t}butylamine and $NaBH_4$, **SNNH^{t}Bu** was produced. This molecule showed delayed fluorescence under a conventional UV lamp. Coordination of the ligand to different coinage metals resulted in dinuclear complexes that also displayed non-Frank Cordon fluorescence. These complexes showed a metal-metal distance of 2.686 and 2.879 for **[CuSNNH^{t}Bu]$_2$** and **[AgSNNH^{t}Bu]$_2$**, respectively. Using density functional theory, it was found that the HOMO resided predominantly on the Cu-pyrollide, while the LUMO was on the thiophene ring.

With these initial observations and results, an investigation into how the ligand affected the metal-metal interaction as well as the fluorescence was carried out. Three main features of the **SNNH^{t}Bu** ligand framework were considered: the thiophene, bite-angle and conjugation, and the

size of the pendent amine. Removal of the thiophene to generate the ligand **NNH^{t}Bu** confirmed that the thiophene was essential to fluorescence showing that neither the ligand nor the complex displayed any fluorescence. The thiophene also had little effect on the Cu-Cu interaction as **[CuNNH^{t}Bu]$_2$** had a Cu-Cu distance of 2.692 Å which is only slightly elongated from that of the parent complex. To investigate the bite-angle and conjugation, the imine version of the ligand, **SNN^{t}Bu**, was synthesized. This ligand showed similar fluorescent properties to the reduced version. Upon coordination to Cu^I, a significant shortening of the Cu-Cu interaction was seen as **[CuSNN^{t}Bu]$_2$** had a distance of 2.466 Å. The fluorescence of the complex also was affected with a red shift in the excitation spectrum. Finally, the steric bulk of amine was looked into by substituting the ^{t}butylamine for adamantylamine. This change showed a lengthening of the Cu-Cu distance for **[CuSNNHAd]$_2$** with a distance of 2.783 Å. The fluorescence of the ligand did not appear to have any significant changes compared to **SNNH^{t}Bu**; however, the complex showed a slight red shift in its emissions.

Our group had previously investigated nickel (II) and palladium (II) schiff-based calix pyrrole ligand systems for hydrogen evolution.[160,162] It was initially hypothesized that incorporation of Cu^I and thiophene may create tetranuclear fluorescent complexes. The synthesis of symmetrical and unsymmetrical, at the quaternary carbon, Schiff-base calix pyrrole ligands were discussed. Upon coordination of Cu^I, it was observed that two distinct Cu^I assemblies were formed. If the quaternary carbon was symmetrical, then a distorted square-like arrangement of the Cu^I was seen where an imine of one ligand and the pyrrolide of the other ligand were bound to each Cu^I; however, if the quaternary carbon was unsymmetrical, then a near linear Cu^I configuration was observed with a Cu^I either being bound to two imines or two pyrrolides. Their

spectroscopic and structure characteristics were also discussed. Unfortunately, no fluorescence was seen from any of these complexes.

5.1. Future Work

5.1.1 Fluorescence: Ligand Modification

Based upon the results and data gathered from these studies, several different avenues for continuing the fluorescent work of these complexes are possible. One route to go down would be further ligand modification. For the dinuclear complexes, it was shown via DFT and experimentally that the thiophene was key to fluorescence. Due to the LUMO residing predominantly on the thiophene, it is hypothesized that incorporation of other fluorescent emitters such as furan, selenophene, benzothiophene, napthylene, anthracene, ect. (**Figure 5.1.**) could allow for control and tunability of emission of these complexes.

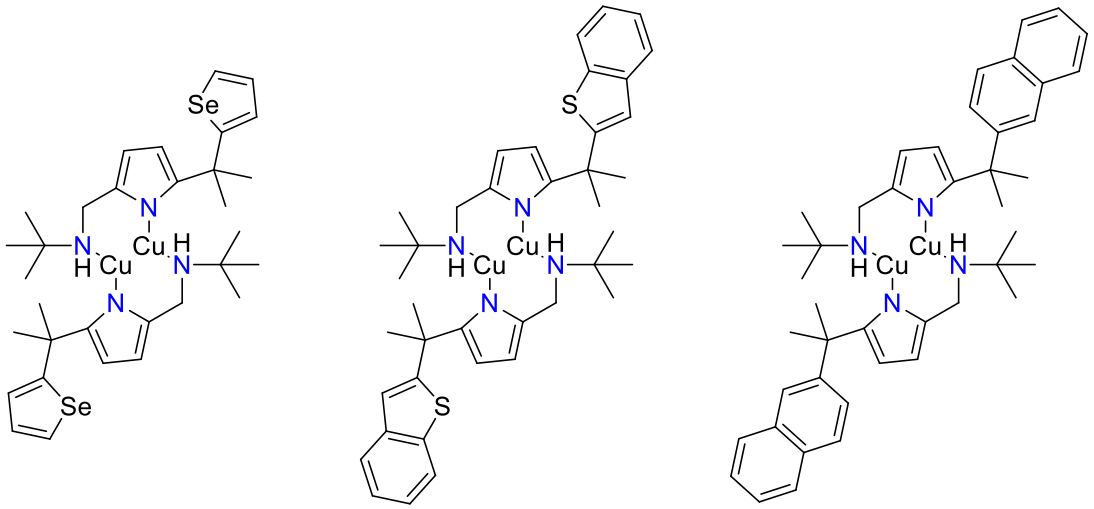

Figure 5.1. Potential fluorescent targets for dinuclear Cu^{I} complexes.

Although the tetranuclear Cu^{I} complexes did not display any fluorescence, it may be possible to generate fluorescent complexes. Often fluorescence molecules contain high levels of conjugation. The same can be said about Cu^{I} complexes as well. One complex that draws inspiration was synthesized by the Stollenz group in 2016.[173] This complex shows a near linear

arrangement of the four Cu^{I} atoms similar to the unsymmetrical quaternary carbon Schiff-base Calix pyrrole ligands previously mentioned. One key difference between the two is the substituent at the quaternary-carbon position of the imine. Two synthetic pathways can be proposed to synthesize substituted Schiff-base Calix pyrroles (**Scheme 5.1.**). The first involves using the nucleophilicity of the pyrrole ring to do carry out an electrophilic aromatic substitution of various aromatic anhydrides of acid chlorides to generate the ketone. Another method to generate the substituted ketone would be to start with aldehyde. From here, the corresponding nitrile can be synthesized via an oxidative amination utilizing Cu^{0} and oxygen. Once the nitrile is obtained, different aromatic nucleophiles such as Grignard's, organozinc, or organolithium species can be added. After acidic work-up, the substituted ketone would be formed. Either method allows for different functional groups to be incorporated into the ligand framework. After the ketone is formed, acid conditions or others could be used to generate the respective substituted Schiff-base Calix pyrrole.

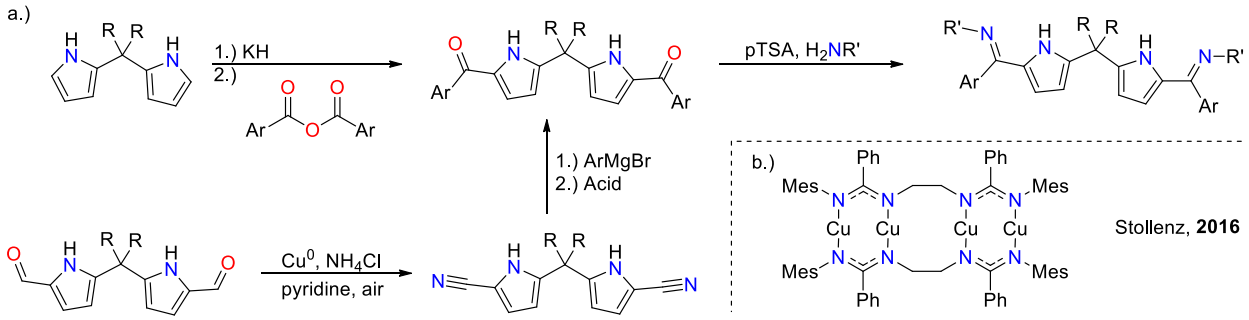

Scheme 5.1. a.) Potential routes to substituted Schiff-Base Calixpyrroles and b.) structure of a fluorescent and linear tetranuclear Cu^{I} complex.

5.1.2. Fluorescent Dinuclear Bridged Complexes

While discussion and research has predominantly been on di- and tetranuclear Cu^{I} complexes with metal-metal interactions, multinuclear Cu^{I} species containing bridging halides or other anions seem to be more prevalent in the field of Cu^{I}-based fluorescent complexes and

materials.[153,174–176] These complexes are typically tetrahedral bound to two L-type donor ligands and to two bridging halides. One complex, in particular, involves a bis(iminothienyl)methene as a radical ligand to coordinate CuI (**Scheme 5.2.a.**).[177] This complex was investigated by the Love group to see how the donating properties of the redox-active thiophene impacted the chemistry and reactivity of transition-metal complexes. While they characterized this complex via XRD, EPR, CV, and UV/vis, they did not mention any efforts towards investigating their fluorescent properties.

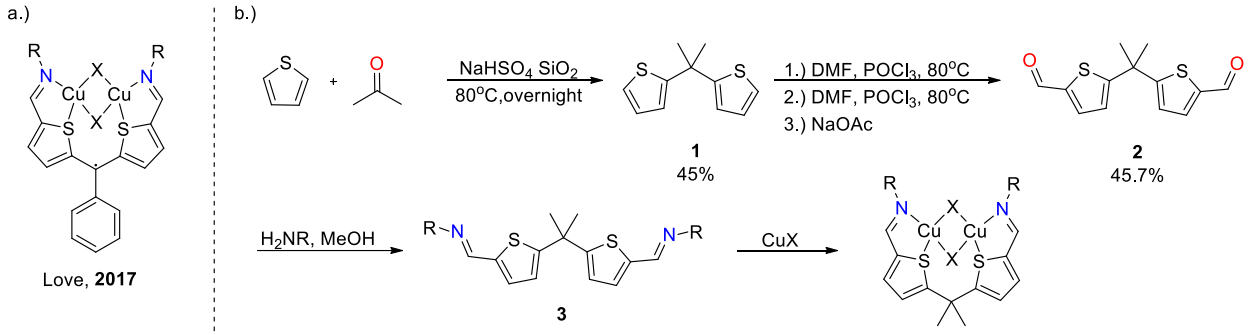

Scheme 5.2. a.) Structure of a dinuclear Cu^{I} complex bridged by halides and b.) synthetic pathway to various Schiff-base Calixthiophenes.

With the results gained from the previous studies, we hypothesized that similar complexes to Love's may display fluorescence. As such, a series of Schiff-base Calix thiophene ligands were synthesized. This was done by carrying out a condensation reaction between thiophene and acetone using a $NaHSO_4 \cdot SiO_2$ as a catalyst to afford the dithiophene methane **1** in modest yields. To generate the dialdehyde **2**, Vielsmeyer-Haack conditions were employed to afford the desired product in modest yield. The crystal structure of **2** (**Figure 4**) showed a unique unit-cell which contained eight independent molecules. Each molecule was twisted about the quaternary carbon. That is to say that one thiophene and aldehyde pointed forward while the other thiophene and aldehyde pointed backwards. This feature alternated down the eight molecules in the cell.

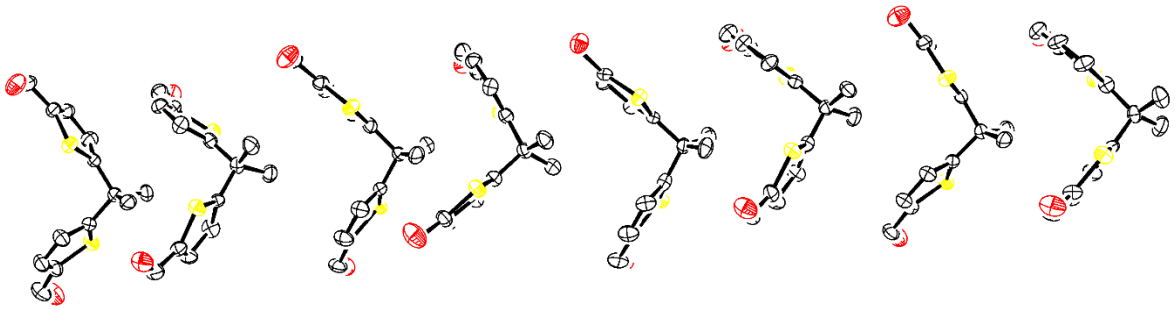

Figure 5.2. ORTEP3 representation (thermal ellipsoids at 50% probability) hydrogens are omitted for clarity for **2**.

From here, a variety of different imines (**3**) could be generated by mixing the dialdehyde with the amine of choice in methanol. This reaction could be monitored by watching for the disappearance of the aldehyde C-H at 9.35 ppm, and the formation of the imine C-H generally found in the 8.25 ppm region. Crystals of these various imines were typically grown from a solution of DCM layered with hexanes and stored at -8°C (See **5.3. Supporting Information**). Currently, efforts towards coordinating various Cu^{I} halides are underway.

5.1.3. Unique Reactivity: Cu^{III}

It is also worth mentioning, before formally concluding, some of the unique reactivity that was observed with several of these complexes. Of particular interest was the reactivity of **[CuNNH^{t}Bu]$_2$** towards oxygen. When crystals grown under a nitrogen atmosphere from a solution of **[CuNNH^{t}Bu]$_2$** in chloroform layered with acetonitrile were exposed to oxygen surrounded by solvent, they generated a new complex. This new complex showed a single Cu atom bound to two pyrrolides and two amines. However, the two pyrrolides were bonded together by an oxygen atom to form a dipyrrole ether ligand. In the crystal structure, there was also a PF_6 anion associated with the complex. This gives a formal charge to the Cu atom as a Cu^{III}. The PF_6 anion likely comes from trace amounts of KPF_6 remaining in the powder that crystals were grown from.

Structurally, the Cu^{III} shows a distorted square-planar geometry and is symmetrical around the metal center. The pyrrolide N(1)-Cu bond distance is 1.894 Å while the ^{t}butylamine N(7)-Cu distance is 2.061 with a N(1)-Cu-N(7) bond angle of 82.08º forming a 5-member ring. The N(1)-Cu-N(1') bond angle is 88.37º forming a 6-member ring while the N(7)-Cu-N(7') bond angle is much larger than the ideal 90º at 110.05º.

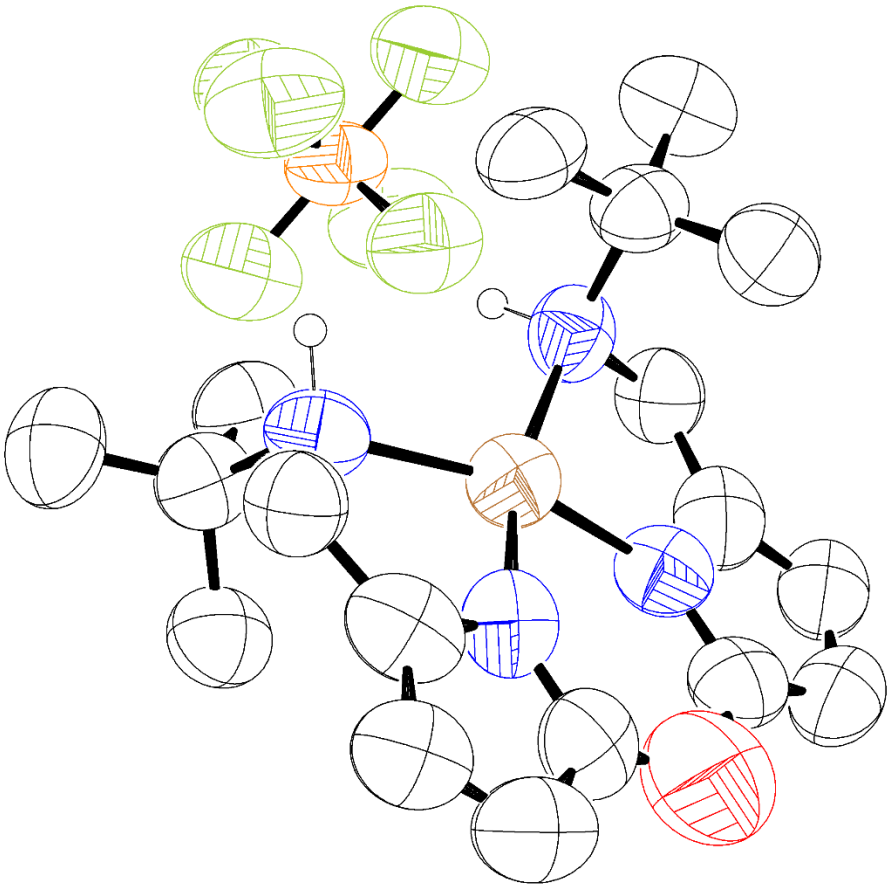

Figure 5.3. ORTEP3 representation (thermal ellipsoids at 50% probability) with most hydrogens omitted for clarity for **[CuNNH^{t}Bu]$_2$** after being exposed to oxygen.

5.2. Conclusion

In conclusion, fluorescence and Cu^{I} complexes are both equally important classes of compounds, complexes and materials. When combined they display promising properties that are

desirable for applications in OLEDs, TADF-emitters and have the potential to be used as well-defined catalysts. The advancement of this field will likely revolve around the ability to synthesize unique ligands and discover complexes reactivity towards various functional groups or small molecules while determining mechanistic and kinetic properties of said reactions.

5.3. Supporting Information

5.3.1. General Considerations

All procedures and manipulations were performed under an argon or nitrogen atmosphere using standard Schlenk-line and glove box techniques unless stated otherwise. Solvents were dried and deoxygenated under argon using a LC Technology Solutions Inc. SP-1 stand-alone solvent purification system, unless stated otherwise. Deuterated solvents were purchased from Cambridge Isotope Laboratories, Sigma Aldrich, Acros Organics, or Alfa Aesar, degassed, and dried over activated molecular sieves prior to use. All other reagents were purchased from commercial sources and utilized without further purification unless stated otherwise. NMR spectra were recorded at ambient temperature and pressure using a Bruker 400 MHz spectrometer (600 MHz or 400 MHz for ^{1}H, and 151 MHz or 100 MHz for ^{13}C). The ^{1}H and ^{13}C NMR spectra were measured relative to partially deuterated solvent peaks but are reported relative to tetramethylsilane (TMS). Single crystal X-ray data were collected using a Rigaku XtaLAB Synergy-S diffractometer equipped with a HyPix-6000HE Hybrid Photon Counting (HPC) detector and dual Mo and Cu microfocus sealed X-ray source (Cu Kα λ = 1.54184 Å). The data collection strategy was calculated using CrysAlisPro to ensure desired data redundancy and percent completeness. Unit cell determination, initial indexing, data collection, frame integration, Lorentz-polarization corrections and final cell parameter calculations were carried out using CrysAlisPro. An absorption correction was performed using the SCALE3 ABSPACK

scaling algorithm embedded within CrysAlisPro. The structures were solved using the ShelXT structure solution program using Intrinsic Phasing and refined by Least Squares using the ShelXL program. All non-hydrogen atoms were refined anisotropically. Hydrogen atom positions were calculated geometrically and refined using the riding model. Olex2 was used for the preparation of the publication materials.

5.3.2. Synthetic Procedures for 1, 2, 3-^{t}Bu, 3-Ad, 3-Ph, 3-CH_2Th, and 3-NAcPh

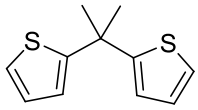

2,2'-(propane-2,2-diyl)dithiophene (1): Thiophene (140 mL) and acetone (1.16 g, 1.48 mL, 20 mmol) was loaded into a 250 mL round-bottom flask. A mixture of $NaHSO_4 \cdot SiO_2$ (4 g) was then added. The reaction vessel was equipped with a stir bar and a condenser. The reaction was heated in an oil bath set to 80°C and stirred overnight (18.5 hrs). Excess thiophene was then removed on a rotovap with the water bath set to 80°C. The SiO_2 was then loaded onto a column and eluted with pure hexanes. The product fractions were collected to give a clear oil that would freeze at -8°C. Yield 1.90 g (45%). ^{1}H NMR (400 MHz, $CDCl_3$) δ 7.16 (d, 2H, thiophene-CH, J = 5.1 Hz), 6.92 (t, 2H, thiophene-CH, J = 3.4 Hz), 6.87 (s, 2H, thiophene-CH), and 1.87 (s, 6H, C-$(CH_3)_2$). ^{13}C NMR (101 MHz, $CDCl_3$) δ 155.53 (aromatic), 126.36 (thiophene-CH), 123.51 (thiophene-CH), 123.07 (thiophene-CH), 40.21 (*C*-$(CH_3)_2$), and 33.20 (C-(CH$_3$)$_2$).

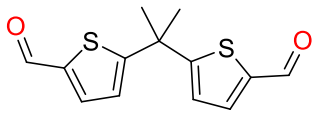

5,5'-(propane-2,2-diyl)bis(thiophene-2-carbaldehyde) (2): 2,2'-(propane-2,2-diyl)dithiophene (6.50g, 31.2 mmol, 1 equiv.) was weighed into a two-neck round-bottom flask equipped with a stir bar, septa and a condenser. The reaction was cycled onto a Schlenk-line under nitrogen. Dry DMF (3.63 mL, 39 mmol, 1.25 equiv.) was injected into the vessel, and the reaction was placed in an ice-bath. This was followed by the slow addition of $POCl_3$ (3.03 mL, 39.3 mmol, 1.26 equiv.) dropwise over ten minutes. After the

complete addition of $POCl_3$, the reaction was heated in an oil bath set to 80°C for three hours. The reaction was then cooled back to room temperature and additional dry DMF (1.25 equiv.) was injected. The vessel was then re-cooled in an ice-bath and $POCl_3$ (1.26 equiv.) was added dropwise. The reaction was allowed to slowly warm to room temperature. After an hour, the vessel was placed in an oil bath set to 80°C and stirred for an additional three hours. The reaction was then cooled to room temperature followed by placing in an ice-bath. DI water (20 mL) was then injected dropwise to quench the reaction followed by the addition of sat. NaOAc (10 mL). The reaction formed a precipitate and was then allowed to stir overnight. The following moring the reaction was diluted with DI water (15 mL) and then basified with solid NaOH until highly basic (pH 12-14). The precipitate was collected and washed with water. To remove excess water, the solid was dissolved in DCM, dried over $MgSO_4$, filtered and concentrated. The following crude product was further purified by dissolving in boiling 100 mL of THF:Hexanes (1:1) and placed in a -8°C freezer to afford a pale tan solid. Yield 2.42 g (29.4%). Another batch of product could be obtained concentrating the THF:Hexane solution and repeating the recrystallization with minimal THF:hexanes. Yielded an additional 1.35 g (45.7%). Crystals suitable for single-crystal XRD were grown by layering a solution of compound in THF with hexanes. ^{1}H NMR (400 MHz, $CHCl_3$) δ 9.85 (s, 2H, aldehyde-CH), 7.61 (d, 2H, thiophene-CH, *J* = 3.5 Hz,), 7.00 (d, 2H, thiophene-CH, *J* = 3.6 Hz), and 1.90 (s, 9H, C-$(CH_3)_2$). ^{13}C NMR (101 MHz, $CDCl_3$) δ 182.93 (aldehyde-CH), 164.33 (aromatic-C), 142.24 (aromatic-C) 136.35 (thiophene-CH), 125.18 (thiophene-CH), 41.64 (<u>*C*</u>-$(CH_3)_2$), and 32.29 (C-(<u>*C*</u>$H_3)_2$).

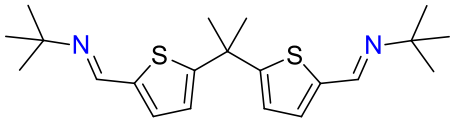

<u>3-^{t}Bu</u>: 5,5'-(propane-2,2-diyl)bis(thiophene-2-carbaldehyde) (100 mg, 0.378 mmol, 1 equiv.) was weighed into a 20 mL screw cap vial equipped with a stir bar. 5 mL of methanol followed by ^{t}butylamine

(0.16 mL, 1.51 mmol, 4 equiv.) was added and the reaction stirred overnight. The solvent and excess ^{t}butylamine was removed under vacuum. Yield 83.9 mg (59.2%). ^{1}H NMR (400 MHz, $CDCl_3$) δ 8.26 (s, 2H, imine-CH), 7.07 (d, 2H, thiophene-CH, *J* = 3.7 Hz), 6.83 (d, thiophene-CH, 2H, *J* = 3.8 Hz), 1.83 (s, 6H, C-$(CH_3)_2$), and 1.25 (s, 18H, C-$(CH_3)_3$). ^{13}C NMR (101 MHz, $CDCl_3$) δ 157.74 (aromatic-C), 149.07 (imine-CH), 142.03 (aromatic-C), 129.41 (thiophene-CH), 123.56 (thiophene-CH), 57.20 (<u>C</u>-$(CH_3)_3$), 40.88 (<u>C</u>-$(CH_3)_2$), 32.49 (C-(<u>C</u>$H_3)_2$), and 29.75 (C-(<u>C</u>$H_3)_3$).

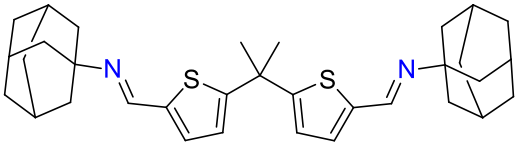

<u>3-Ad</u>: 5,5'-(propane-2,2-diyl)bis(thiophene-2-carbaldehyde) (100 mg, 0.378 mmol, 1 equiv.) was weighed into a 20 mL screw cap vial equipped with a stir bar. 5 mL of methanol followed by adamantlyamine (229 mg, 1.51 mmol, 4 equiv.) was added and the reaction stirred overnight. A precipitate formed and was collected on a glass frit. The solid was washed with cold MeOH and gave a white solid. Yield 168 mg (83.9%). Crystals suitable for single-crystal XRD were grown by slow evaporation from DCM. ^{1}H NMR (400 MHz, Chloroform-*d*) δ 8.26 (s, 2H, imine-CH), 7.06 (d, thiophene, 2H, *J* = 3.8 Hz), 6.82 (d, 2H, thiophene-CH, *J* = 3.7 Hz), 2.13 (s, 6H, C-$(CH_3)_2$), and 1.97 – 1.50 (m, 30H, adamantyl-CHs). ^{13}C NMR (101 MHz, $CDCl_3$) δ 157.63 (aromatic-C), 148.76 (imine-CH), 142.25 (aromatic-C), 129.39 (thiophene-CH), 123.57 (thiophene-CH), 57.46 (adamantyl-C), 43.10(adamantyl-CH_2), 40.86 (<u>C</u>-$(CH_3)_2$), 36.55 (adamantyl-CH_2), 32.47 (adamantyl-CH), and 29.60 (C-(<u>C</u>$H_3)_2$).

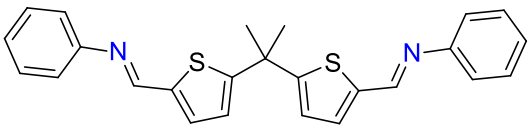

<u>3-Ph</u>: 5,5'-(propane-2,2-diyl)bis(thiophene-2-carbaldehyde) (100 mg, 0.378 mmol, 1 equiv.) was weighed into a 20 mL screw cap vial equipped with a stir bar. 5 mL of methanol followed by aniline (0.14 mL, 1.51 mmol, 4 equiv.) was added and the reaction stirred overnight. A precipitate formed and was collected on a glass frit. The solid was washed with cold hexanes which gave an

off-white, yellow solid. Yield 135 mg (85.8%). Crystals suitable for single-crystal XRD were grown by layer of the compound in DCM with hexanes and storing at -8°C. ^{1}H NMR (400 MHz, $CDCl_3$) δ 8.48 (s, 1H, imine-CH), 7.37 (dd, 4H, phenyl-CH, *J* = 8.3, 7.3 Hz), 7.31 (d, 2H, thiophene-CH, *J* = 3.8 Hz), 7.24 – 7.17 (m, 6H, phenyl-CH), 6.95 (d, 2H, thiophene-CH, *J* = 3.8 Hz), and 1.92 (s, 6H, C-$(CH_3)_2$). ^{13}C NMR (101 MHz, $CDCl_3$) δ 159.91(aromatic-C), 153.09 (imine-CH), 151.38 (aromatic-CH), 141.02 (aromatic-C), 132.17 (thiophene-CH), 129.15 (phenyl-CH), 125.99 (phenyl-CH), 124.30 (thiophene-CH), 121.02 (phenyl-CH), 41.23 (<u>*C*</u>-$(CH_3)_2$), and 32.36 (C-(<u>*C*</u>$H_3)_2$).

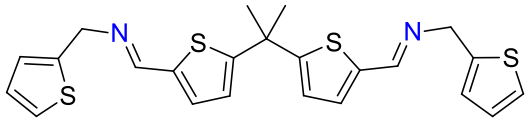

<u>3-CH_2Th</u>: 5,5'-(propane-2,2-diyl)bis(thiophene-2-carbaldehyde) (100 mg, 0.378 mmol, 1 equiv.) was weighed into a 20 mL screw cap vial equipped with a stir bar. 5 mL of methanol followed by 2-methylamine thiophene (171 mg, 1.51 mmol, 4 equiv.) was added and the reaction stirred overnight. A precipitate formed and was collected on a glass frit. The solid was washed with cold hexanes which gave an off-white, yellow solid. Yield 130 mg (75.3%). Crystals suitable for single-crystal XRD were grown by layer of the compound in DCM with hexanes and storing at -8°C. ^{1}H NMR (400 MHz, $CDCl_3$) δ 8.31 (s, 2H, imine-CH), 7.22 (dd, 2H, *J* = 5.0, 1.4 Hz), 7.15 (s, 2H, thiophene-CH), 6.99 – 6.94 (m, 4H), 6.84 (d, 2H, thiophene, *J* = 3.8 Hz), 4.91 (s, 4H,-CH_2-), and 1.84 (s, 6H, C-$(CH_3)_2$). ^{13}C NMR (101 MHz, $CDCl_3$) δ 155.51(imine-CH), 141.44 (aromatic-C), 140.13 (aromatic-C), 130.87 (thiophene-CH), 126.89 (thiophene-CH), 125.40 (thiophene-CH), 124.85 (thiophene-CH), 123.88 (thiophene-CH), 58.29 (-<u>*C*</u>H_2-), 40.99 (<u>*C*</u>-$(CH_3)_2$), and 32.32 (C-(<u>*C*</u>$H_3)_2$).

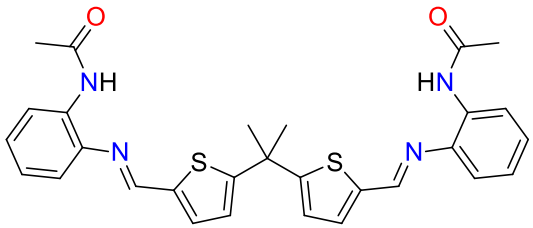

3-NAcPh: 5,5'-(propane-2,2-diyl)bis(thiophene-2-carbaldehyde) (372 mg, 1.41 mmol, 1 equiv.) was added to a 50 mL round-bottom flask equipped with a stir bar. 25 mL of MeOH was added followed by N-(2-aminophenyl)acetamide (1.14 g, 7.56 mmol, 5.4 equiv.) and pTSA·H_2O (287 mg, 1.1 equiv.). The reaction was stirred overnight and was quenched the following morning by the addition of 20 mL of sat. $NaHCO_3$ and 10 mL of DI water. The reaction was extracted with ethyl acetate (30 mL x 3). The organic layers were combined and dried over Na_2SO_4, filtered and concentrated. The crude was then loaded onto a column and eluted with 2:1 then 1:1 hexane:ethyl acetate which yielded a yellow powder. Yield 427 mg (42.7%). Attempts at growing crystals suitable for single-crystal XRD were done by layering a solution of the compound in benzene with hexanes but resulted in **3-NAcPh-Decomp** instead.

5.3.3. ^{1}H and ^{13}C NMR of 1, 2, , 3-^{t}Bu, 3-Ad, 3-Ph, 3-CH_2Th, and 3-NAcPh

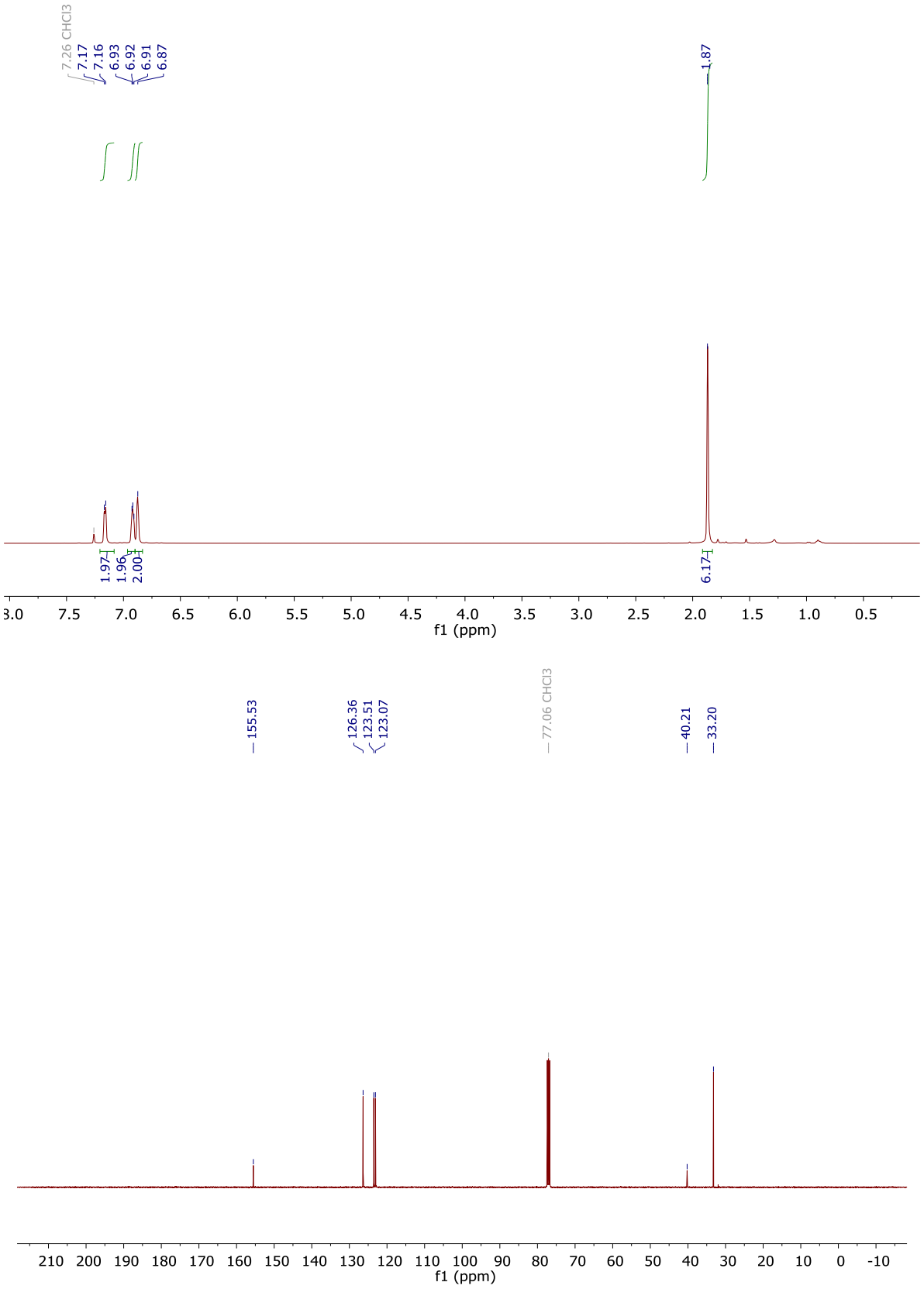

Figure 5.4. ^{1}H and ^{13}C NMR of **1**.

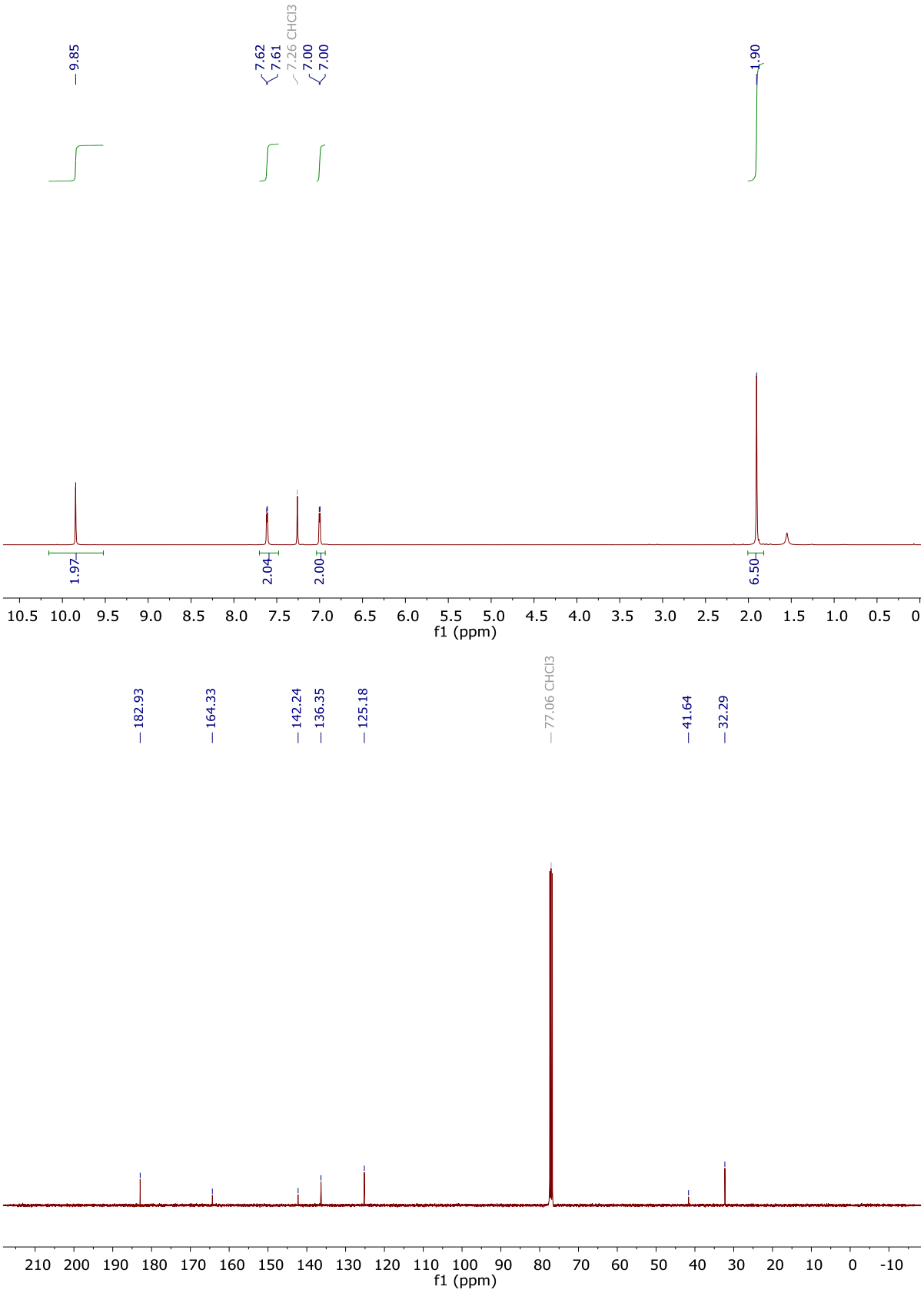

Figure 5.5. ^{1}H and ^{13}C NMR of **2**.

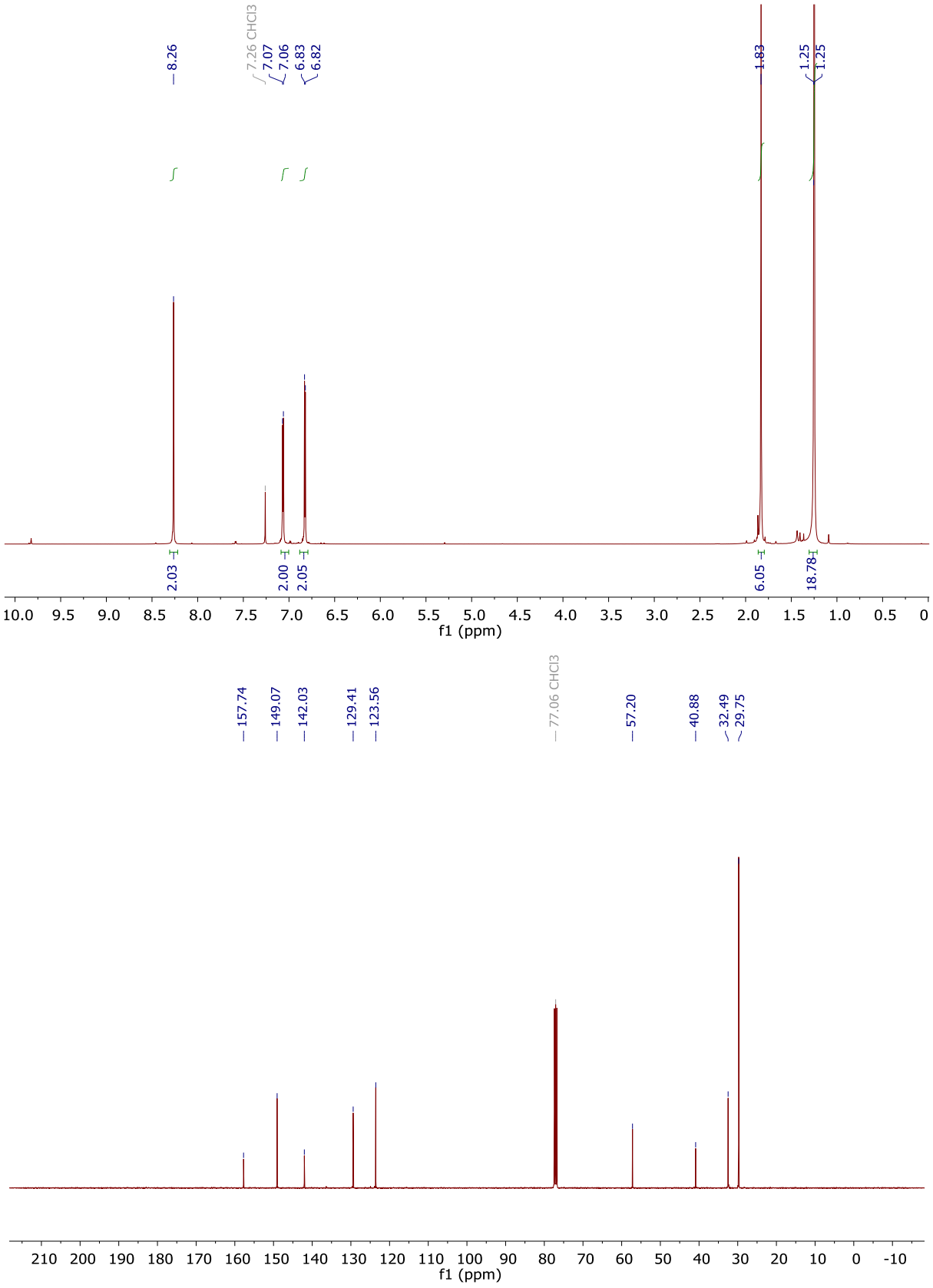

Figure 5.6. ^{1}H and ^{13}C NMR of **3-^{t}Bu**.

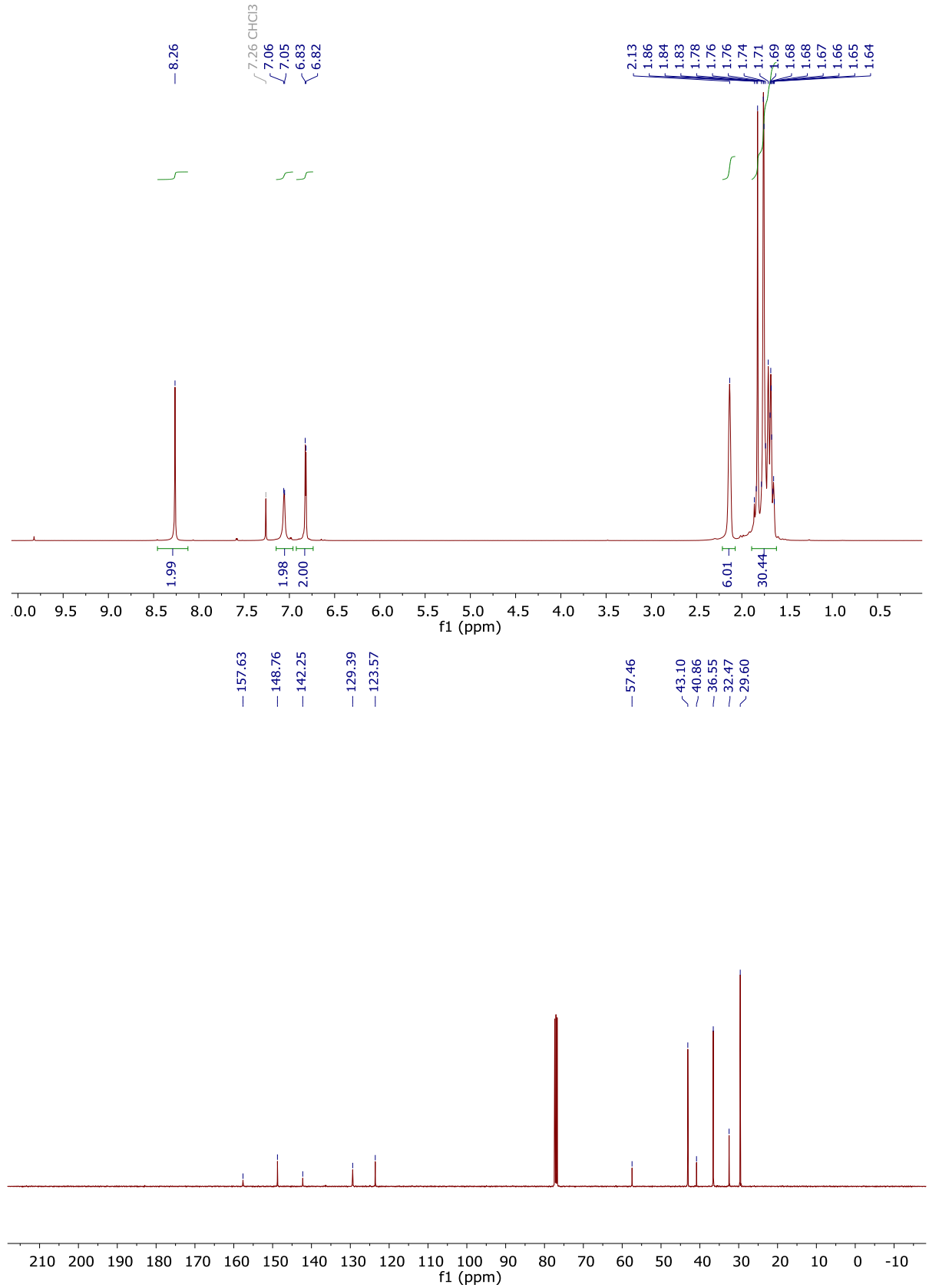

Figure 5.7. ^{1}H and ^{13}C NMR of **3-Ad**.

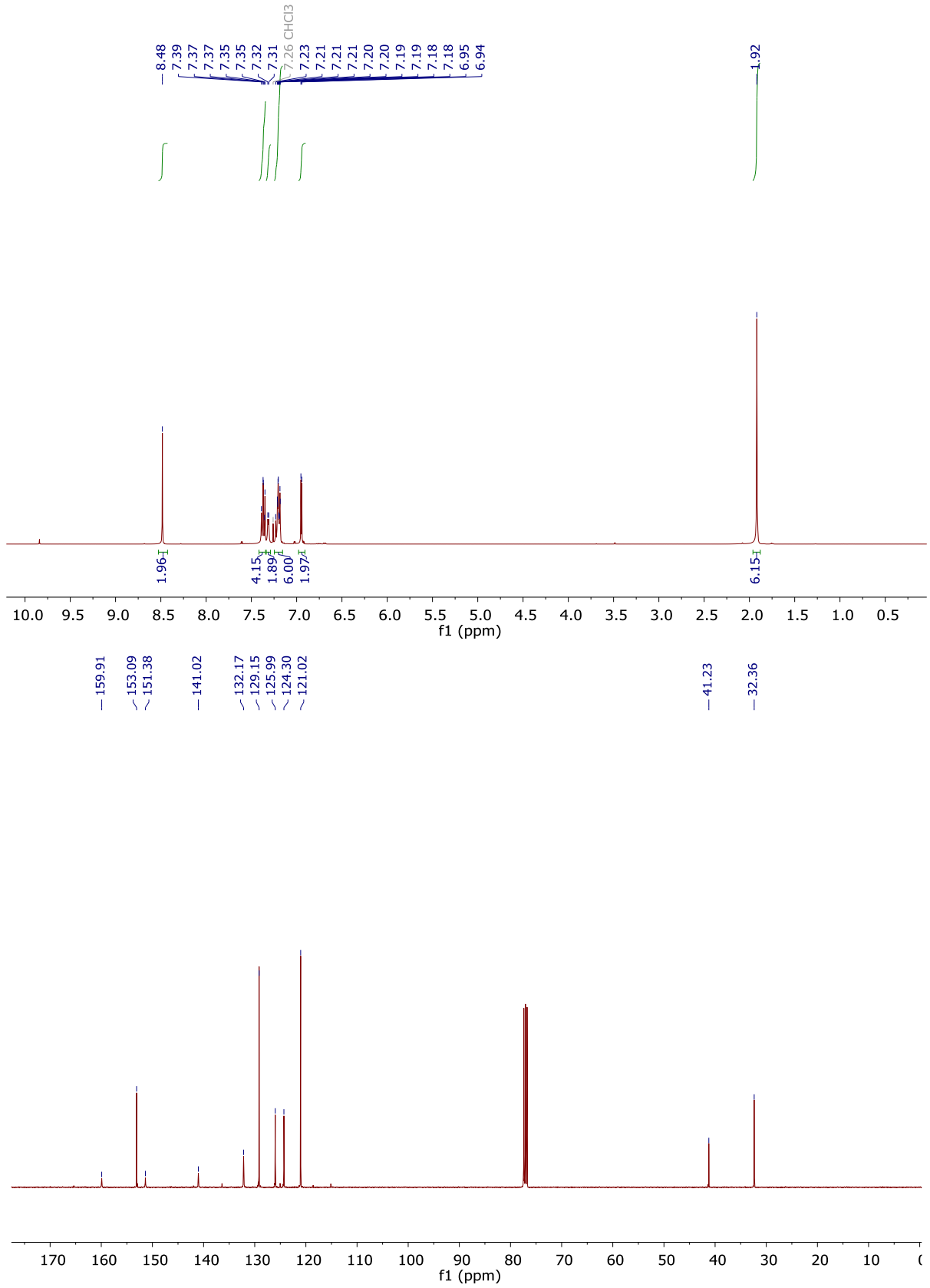

Figure 5.8. ^{1}H and ^{13}C NMR of **3-Ph**.

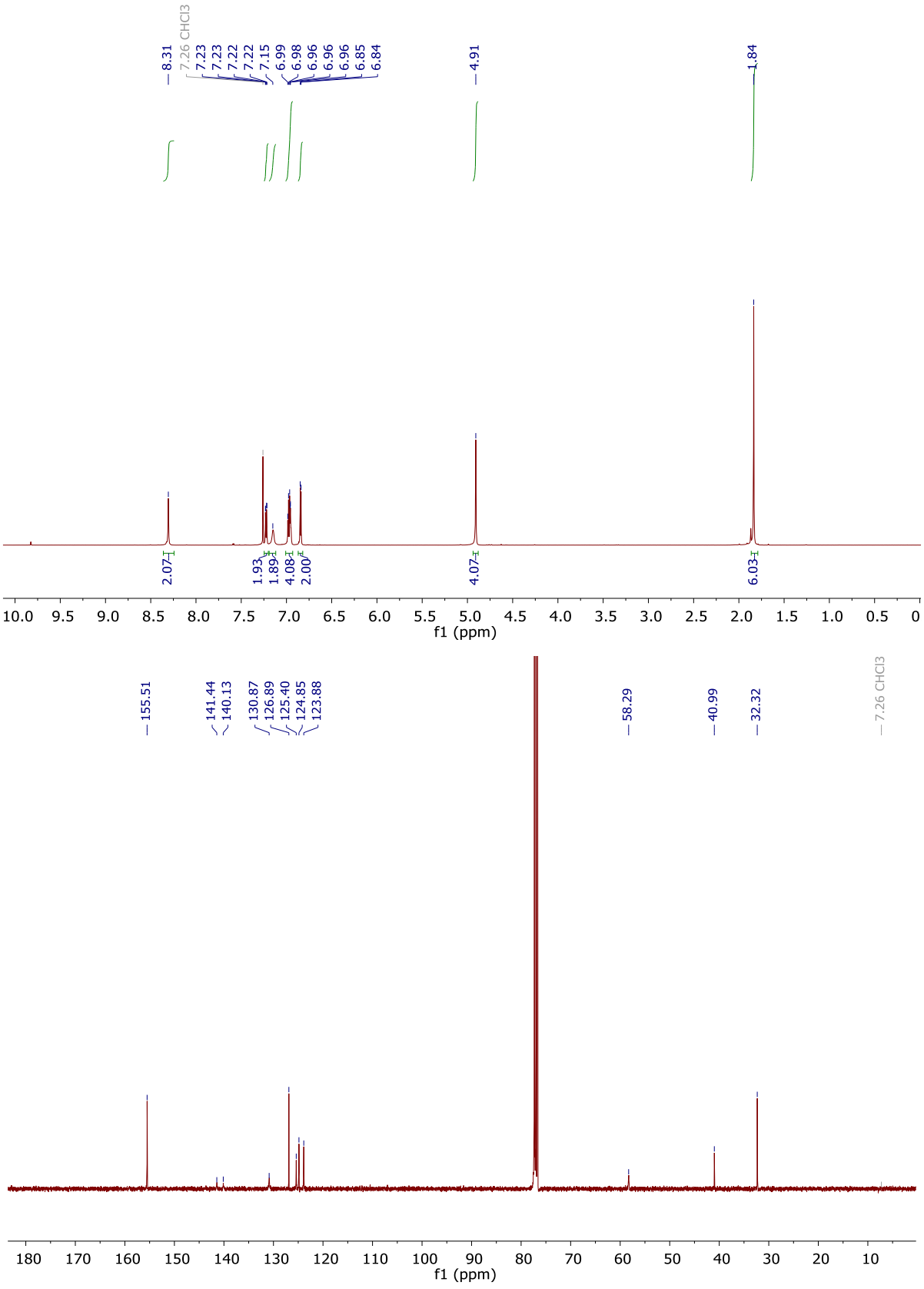

Figure 5.9. ^{1}H and ^{13}C NMR of **3-CH_2Th**.

5.3.4. ORTEP3 representation of 2, 3-^{t}Bu, 3-Ad, 3-Ph, 3-CH_2Th, 3-NAcPh, and [CuNNH^{t}Bu]$_2$ exposed to air

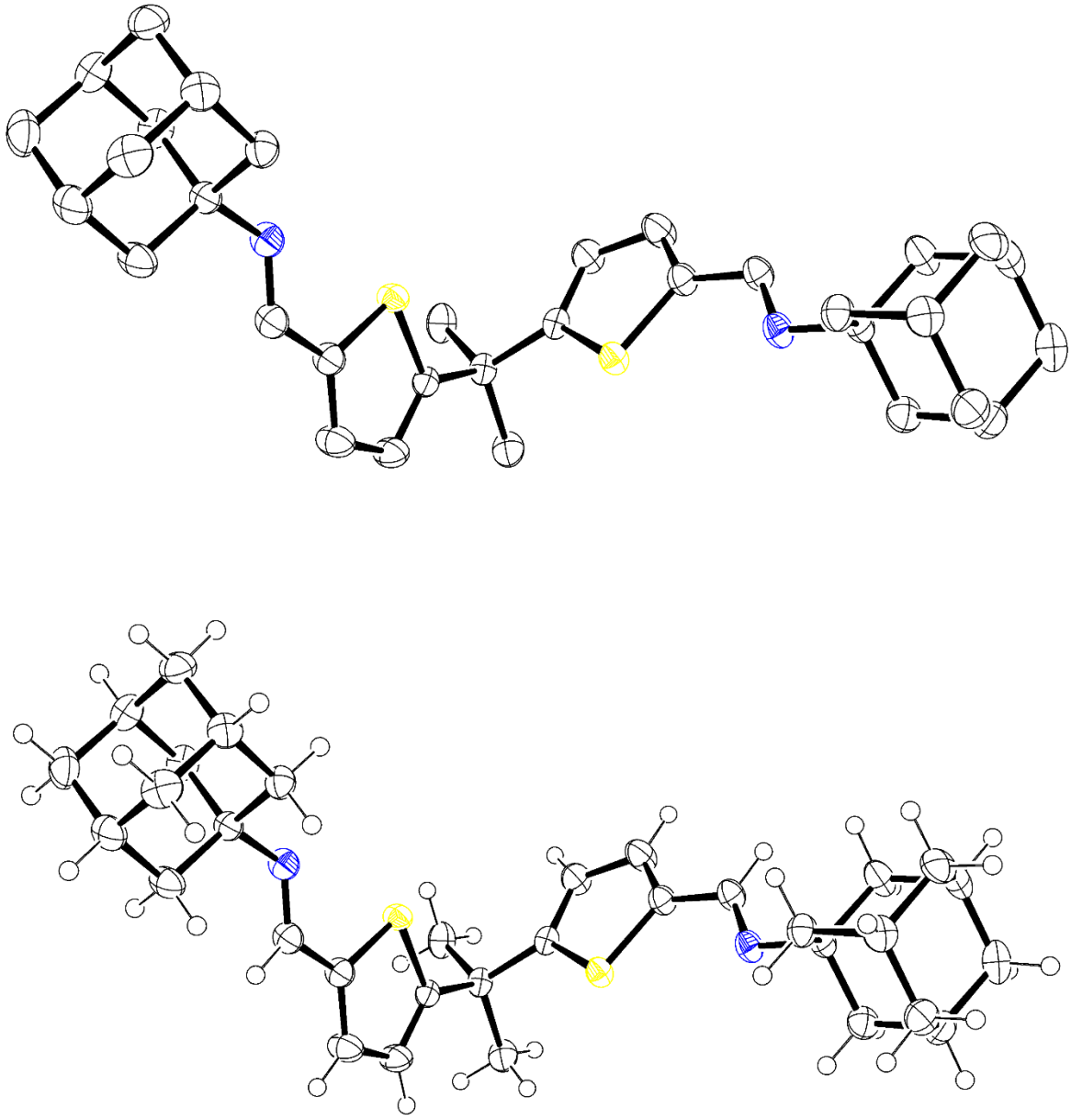

Figure 5.10. ORTEP3 representation (thermal ellipsoids at 50% probability) of **3-Ad**. Top: Hydrogens have been omitted for clarity.

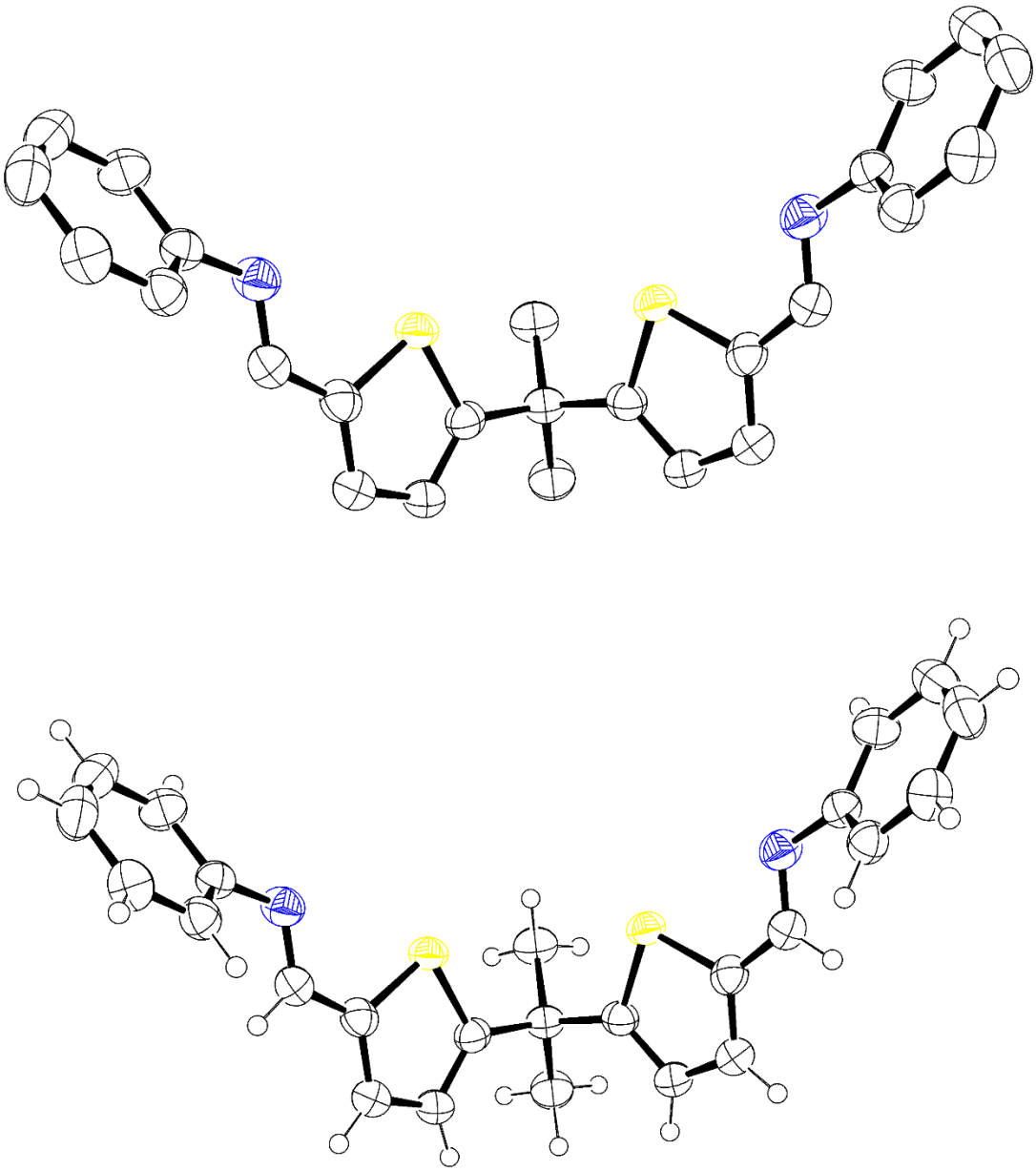

Figure 5.11. ORTEP3 representation (thermal ellipsoids at 50% probability) of **3-Ph**. Top: Hydrogens have been omitted for clarity.

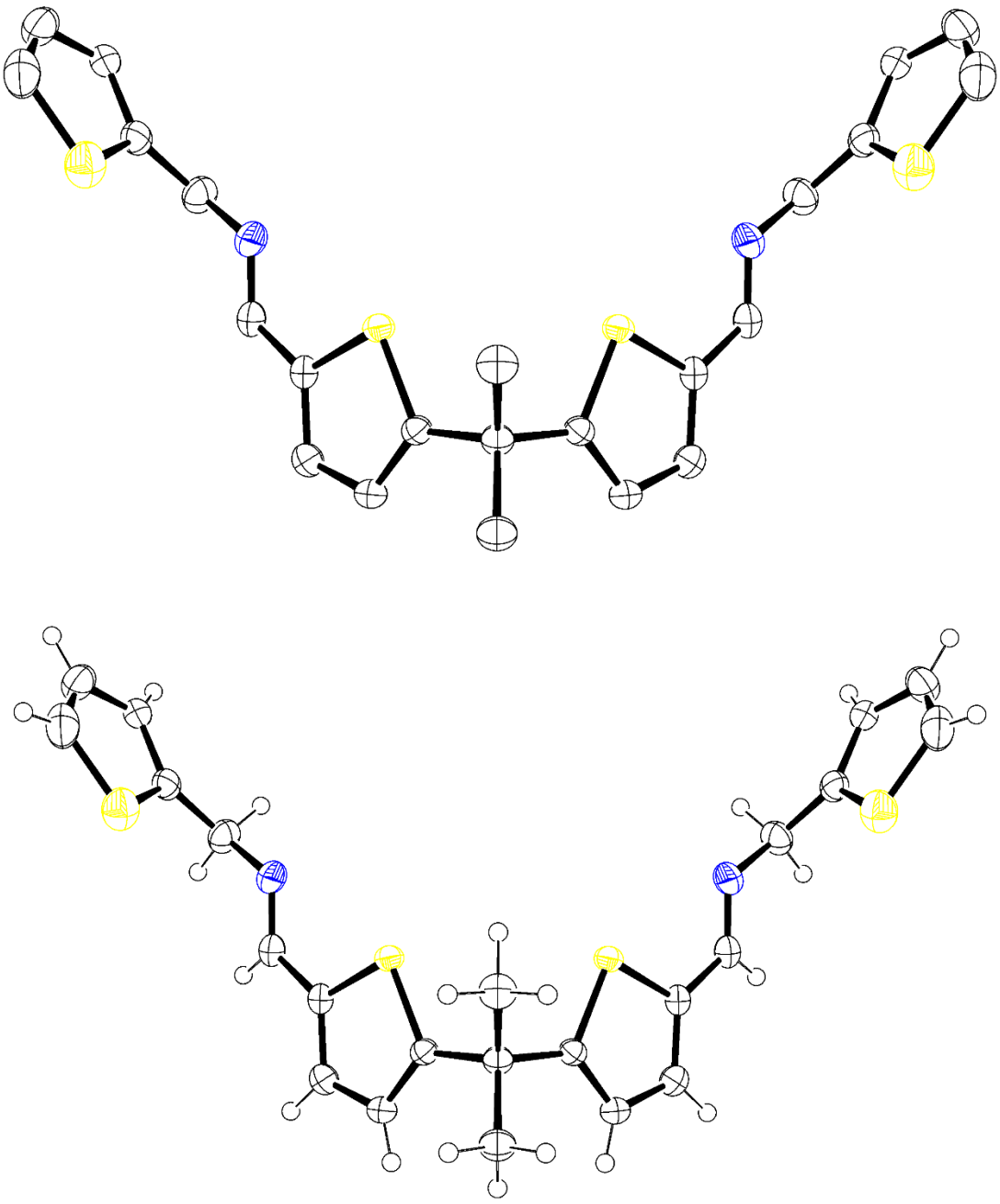

Figure 5.12. ORTEP3 representation (thermal ellipsoids at 50% probability) of **3-CH$_2$Th**. Top: Hydrogens have been omitted for clarity.

5.3.5. Select Crystal Data for 2, 3-^{t}Bu, 3-Ad, 3-Ph, 3-CH_2Th, 3-NAcPh decomp., and [CuNNH^{t}Bu]$_2$ exposed to air

Table 5.1. Select Crystal Data, Data Collection, and Refinement Parameters for **2**, **3-Ad**, and **3-Ph**. [a]Definition of R indices: $R_1 = \Sigma(F_O - F_C)/\Sigma(F_O)$; $wR_2 = [\Sigma[w(F_O^2 - F_C^2)^2]/[\Sigma[w(F_O^2)^2]]^{1/2}$

	2	**3-Ad**	**3-Ph**
empirical formula	$C_{13}H_{12}O_2S_2$	$C_{33}H_{42}N_2S_2$	$C_{23}H_{22}N_2S_2$
FW	264.35	530.80	454.66
lattice type	Orthorhombic	Monoclinic	Orthorhombic
space group	$P2_12_12_1$	C2/c	Pnma
T, K	200.00	210.00	210.00
a, Å	6.57240(10)	20.5157(2)	10.92869(13)
b, Å	17.38090(10)	6.84873(5)	33.4936(4)
c, Å	87.3946(7)	22.6144(2)	6.03115(7)
α, deg	90	90	90
β, deg	90	115.8889(13)	90
γ, deg	90	90	90
V, Å^3	9983.45(18)	2858.57(5)	2207.65(4)
Z	32	4	4
ρ_{calc}/Mg m^{-3}	1.407	1.233	1.368
μ(Cu/Mo, Kα) mm^{-1}	3.758	1.858	4.042
F(000)	4416.0	1144.0	952.0
crystal size, mm^3	0.37x0.08x0.03	0.27x0.23x0.19	0.25x0.04x0.01
range Θ collected, deg	2.592 to 80.768	4.346 to 79.902	2.638 to 80.055
Reflns (Collectd/unique)	75243/21397	16833/3127	14104/2440
Abs cor	Semi Empirical based upon equivalents		
max and min transmn coeff.	1.000 and 0.474	1.000 to 0.873	1.000 to 0.602
goodness of fit	1.048	1.063	1.074
R_1 (I>2σ(I))[a]	0.0429	0.0330	0.0439
wR_2 (all data)[a]	0.1020	0.0882	0.1263
Peak and hole, e Å^{-3}	0.256 and -0.311	0.237 and -0.280	0.769 and -0.526

Table 5.2. Select Crystal Data, Data Collection, and Refinement Parameters for **3-Th**, **3-NAcPh-Decomp.**, and **[CuNNH^{t}Bu]$_2$+O$_2$**. [a]Definition of R indices: $R_1 = \Sigma(F_O - F_C)/\Sigma(F_O)$; $wR_2 = [\Sigma[w(F_O^2 - F_C^2)^2]/[\Sigma[w(F_O^2)^2]]^{1/2}$

	3-Th	**3-NAcPh Decomp.**	**[CuNNH^{t}Bu]$_2$+O$_2$**
empirical formula	$C_{23}H_{22}N_2S_4$	$C_{30}H_{27}N_4OS_2$	$C_{18}H_{26}CuF_6N_4OP$
FW	454.66	523.67	522.94
lattice type	Orthorhombic	Orthorhombic	Monoclinic
space group	Pnma	Pbca	C2/c
T, K	210.00	293(2)	210.00
a, Å	10.92869(13)	9.3236(4)	13.524(3)
b, Å	33.4936(4)	19.7791(7)	11.778(2)
c, Å	6.03115(7)	29.1209(14)	13.829(2)
α, deg	90	90	90
β, deg	90	90	92.080(17)
γ, deg	90	90	90
V, Å^3	2207.65(4)	5370.2(4)	2201.1(7)
Z	4	8	4
ρ_{calc}/Mg m^{-3}	1.368	1.295	1.578
μ(Cu/Mo, Kα) mm^{-1}	4.042	2.034	2.720
F(000)	952.0	2200.0	1072.0
crystal size, mm^3	0.25x0.04x0.01	0.10x0.07x0.01	0.06x0.05x0.04
range Θ collected, deg	2.638 to 80.055	3.035 to 66.596	4.981 to 68.249
Reflns (Collectd/unique)	14104/2440	17673/4678	8425/1982
Abs cor	Semi Empirical based upon equivalents		
max and min transmn coeff.	1.000 and 0.602	1.000 and 0.288	1.000 and 0.369
goodness of fit	1.074	1.016	1.151
R_1 (I>2σ(I))[a]	0.0410	0.0780	0.137
wR_2 (all data)[a]	0.1263	0.2333	0.4124
Peak and hole, e Å^{-3}	0.769 and -0.526	0.667 and -0.290	0.919 and -0.518

Chapter 6 - References

(1) Lindberg, D. C.; Tachau, K. H. The Science of Light and Color, Seeing and Knowing. In *The Cambridge History of Science Volume 2: Medieval Science*; Cambridge University Press, 2012; pp 485–511. https://doi.org/10.1017/CHO9780511974007.022.

(2) Barber, J.; Tran, P. D. From Natural to Artificial Photosynthesis. *J R Soc Interface* **2013**, *10* (81). https://doi.org/10.1098/rsif.2012.0984.

(3) Stirbet, A.; Lazár, D.; Guo, Y.; Govindjee, G. Photosynthesis: Basics, History and Modelling. *Annals of Botany*. Oxford University Press September 14, 2020, pp 511–537. https://doi.org/10.1093/aob/mcz171.

(4) Blankenship, R. E. Early Evolution of Photosynthesis. *Plant Physiol* **2010**, *154* (2), 434–438. https://doi.org/10.1104/pp.110.161687.

(5) Blume, C.; Garbazza, C.; Spitschan, M. Effects of Light on Human Circadian Rhythms, Sleep and Mood. *Somnologie*. Dr. Dietrich Steinkopff Verlag GmbH and Co. KG September 1, 2019, pp 147–156. https://doi.org/10.1007/s11818-019-00215-x.

(6) Küller, R. *PHYSIOLOGICAL ANTHROPOLOGY and Applied Human Science The Influence of Light on Circarhythms in Humans*; 2002; Vol. 21. http://www.jstage.jst.go.jp/en/.

(7) Vitaterna, M. H.; Takahashi, J. S.; Turek, F. W. Overview of Circadian Rhythms. *Alcohol Res Health* **2001**, *25* (2), 85–93.

(8) Diehl, J. W.; Chiu, M. W. Effects of Ambient Sunlight and Photoprotection on Vitamin D Status. *Dermatologic Therapy*. January 2010, pp 48–60. https://doi.org/10.1111/j.1529-8019.2009.01290.x.

(9) Kimlin, M. G. Geographic Location and Vitamin D Synthesis. *Molecular Aspects of Medicine*. December 2008, pp 453–461. https://doi.org/10.1016/j.mam.2008.08.005.

(10) Webb, A. R. Who, What, Where and When-Influences on Cutaneous Vitamin D Synthesis. *Progress in Biophysics and Molecular Biology*. September 2006, pp 17–25. https://doi.org/10.1016/j.pbiomolbio.2006.02.004.

(11) Nair, R.; Maseeh, A. Vitamin D: The Sunshine Vitamin. *Journal of Pharmacology and Pharmacotherapeutics*. April 2012, pp 118–126. https://doi.org/10.4103/0976-500X.95506.

(12) Learmonth, R. P.; Kable, S. H.; Ghiggino, K. P. *Basics of Fluorescence*; 2009.

(13) Croney, J. C.; Jameson, D. M.; Learmonth, R. P. Fluorescence Spectroscopy in Biochemistry: Teaching Basic Principles with Visual Demonstrations. *Biochemistry and Molecular Biology Education* **2001**, *29* (2), 60–65. https://doi.org/10.1111/j.1539-3429.2001.tb00071.x.

(14) Diagrama, E. L.; Jablonski, D. E.; Sípoš, R. R. ˇ; Sima, J. ˇ. *JABLONSKI DIAGRAM REVISITED*; 2020; Vol. 37.

(15) Ozawa, T.; Yoshimura, H.; Kim, S. B. Advances in Fluorescence and Bioluminescence Imaging. *Analytical Chemistry*. January 15, 2013, pp 590–609. https://doi.org/10.1021/ac3031724.

(16) Yao, Z.; Zhang, B. S.; Prescher, J. A. Advances in Bioluminescence Imaging: New Probes from Old Recipes. *Current Opinion in Chemical Biology*. Elsevier Ltd August 1, 2018, pp 148–156. https://doi.org/10.1016/j.cbpa.2018.05.009.

(17) Dmitriev, R. I.; Intes, X.; Barroso, M. M. Luminescence Lifetime Imaging of Three-Dimensional Biological Objects. *Journal of Cell Science*. Company of Biologists Ltd May 1, 2021. https://doi.org/10.1242/jcs.254763.

(18) Christie, R. M. *Fluorescent Dyes*; Woodhead Publishing Limited, 2011; Vol. 1. https://doi.org/10.1533/9780857093974.2.562.

(19) Tang, C. W.; Vanslyke, S. A. Organic Electroluminescent Diodes. *Appl Phys Lett* **1987**, *51* (12), 913–915. https://doi.org/10.1063/1.98799.

(20) Hong, G.; Gan, X.; Leonhardt, C.; Zhang, Z.; Seibert, J.; Busch, J. M.; Bräse, S. A Brief History of OLEDs—Emitter Development and Industry Milestones. *Advanced Materials* **2021**, *33* (9). https://doi.org/10.1002/adma.202005630.

(21) Yersin, H.; Rausch, A. F.; Czerwieniec, R.; Hofbeck, T.; Fischer, T. The Triplet State of Organo-Transition Metal Compounds. Triplet Harvesting and Singlet Harvesting for Efficient OLEDs. *Coordination Chemistry Reviews*. November 2011, pp 2622–2652. https://doi.org/10.1016/j.ccr.2011.01.042.

(22) Goushi, K.; Kawamura, Y.; Sasabe, H.; Adachi, C. Unusual Phosphorescence Characteristics of Ir(Ppy)3 in a Solid Matrix at Low Temperatures. *Japanese Journal of Applied Physics, Part 2: Letters* **2004**, *43* (7 A). https://doi.org/10.1143/JJAP.43.L937.

(23) Sajoto, T.; Djurovich, P. I.; Tamayo, A. B.; Oxgaard, J.; Goddard, W. A.; Thompson, M. E. Temperature Dependence of Blue Phosphorescent Cyclometalated Ir(III) Complexes. *J Am Chem Soc* **2009**, *131* (28), 9813–9822. https://doi.org/10.1021/ja903317w.

(24) Hofbeck, T.; Yersin, H. The Triplet State of Fac-Ir(Ppy)3. *Inorg Chem* **2010**, *49* (20), 9290–9299. https://doi.org/10.1021/ic100872w.

(25) Adachi, C.; Baldo, M. A.; Thompson, M. E.; Forrest, S. R. Nearly 100% Internal Phosphorescence Efficiency in an Organic Light Emitting Device. *J Appl Phys* **2001**, *90* (10), 5048–5051. https://doi.org/10.1063/1.1409582.

(26) Lamansky, S.; Djurovich, P.; Murphy, D.; Abdel-Razzaq, F.; Lee, H. E.; Adachi, C.; Burrows, P. E.; Forrest, S. R.; Thompson, M. E. Highly Phosphorescent Bis-Cyclometalated Iridium Complexes: Synthesis, Photophysical Characterization, and Use in Organic Light Emitting Diodes. *J Am Chem Soc* **2001**, *123* (18), 4304–4312. https://doi.org/10.1021/ja003693s.

(27) Ding, J.; Gao, J.; Cheng, Y.; Xie, Z.; Wang, L.; Ma, D.; Jing, X.; Wang, F. Highly Efficient Green-Emitting Phosphorescent Iridium Dendrimers Based on Carbazole Dendrons. *Advanced Functional Materials*. March 3, 2006, pp 575–581. https://doi.org/10.1002/adfm.200500591.

(28) Liao, J. L.; Rajakannu, P.; Gnanasekaran, P.; Tsai, S. R.; Lin, C. H.; Liu, S. H.; Chang, C. H.; Lee, G. H.; Chou, P. T.; Chen, Z. N.; Chi, Y. Luminescent Diiridium Complexes with Bridging Pyrazolates: Characterization and Fabrication of OLEDs Using Vacuum Thermal Deposition. *Adv Opt Mater* **2018**, *6* (11). https://doi.org/10.1002/adom.201800083.

(29) Tung, Y. L.; Wu, P. C.; Liu, C. S.; Chi, Y.; Yu, J. K.; Hu, Y. H.; Chou, P. T.; Peng, S. M.; Lee, G. H.; Tao, Y.; Carty, A. J.; Shu, C. F.; Wu, F. I. Highly Efficient Red Phosphorescent Osmium(II) Complexes for OLED Applications. *Organometallics* **2004**, *23* (15), 3745–3748. https://doi.org/10.1021/om0498246.

(30) Li, G.; Zhao, X.; Fleetham, T.; Chen, Q.; Zhan, F.; Zheng, J.; Yang, Y. F.; Lou, W.; Yang, Y.; Fang, K.; Shao, Z.; Zhang, Q.; She, Y. Tetradentate Platinum(II) Complexes for Highly Efficient Phosphorescent Emitters and Sky Blue OLEDs. *Chemistry of Materials* **2020**, *32* (1), 537–548. https://doi.org/10.1021/acs.chemmater.9b04263.

(31) Chow, P. K.; Cheng, G.; Ong, G. S. M. T.; To, W. P.; Kwong, W. L.; Kowk, C. C.; Ma, C.; Che, C. M. Luminescent Pincer Platinum(II) Complexes with Emission Quantum Yields up to Almost Unity: Photophysics, Photoreductive c-c Bond Formation, and Materials Applications. *Angewandte Chemie - International Edition* **2015**, *54* (7), 2084–2089. https://doi.org/10.1002/anie.201408940.

(32) Cocchi, M.; Virgili, D.; Fattori, V.; Rochester, D. L.; Williams, J. A. G. N∧C∧N-Coordinated Platinum(II) Complexes as Phosphorescent Emitters in High-Performance Organic Light-Emitting Devices. *Adv Funct Mater* **2007**, *17* (2), 285–289. https://doi.org/10.1002/adfm.200600167.

(33) Teng, J. M.; Wang, Y. F.; Chen, C. F. Recent Progress of Narrowband TADF Emitters and Their Applications in OLEDs. *Journal of Materials Chemistry C*. Royal Society of Chemistry September 7, 2020, pp 11340–11353. https://doi.org/10.1039/d0tc02682d.

(34) Housecroft, C. E.; Constable, E. C. TADF: Enabling Luminescent Copper(i) Coordination Compounds for Light-Emitting Electrochemical Cells. *Journal of Materials Chemistry C*. Royal Society of Chemistry October 12, 2021, pp 4456–4482. https://doi.org/10.1039/d1tc04028f.

(35) Czerwieniec, R.; Leitl, M. J.; Homeier, H. H. H.; Yersin, H. Cu(I) Complexes – Thermally Activated Delayed Fluorescence. Photophysical Approach and Material Design. *Coordination Chemistry Reviews*. Elsevier October 15, 2016, pp 2–28. https://doi.org/10.1016/j.ccr.2016.06.016.

(36) Dumur, F. Recent Advances in Organic Light-Emitting Devices Comprising Copper Complexes: A Realistic Approach for Low-Cost and Highly Emissive Devices? *Organic Electronics*. Elsevier B.V. 2015, pp 27–39. https://doi.org/10.1016/j.orgel.2015.02.026.

(37) Murawski, C.; Leo, K.; Gather, M. C. Efficiency Roll-off in Organic Light-Emitting Diodes. *Advanced Materials*. December 17, 2013, pp 6801–6827. https://doi.org/10.1002/adma.201301603.

(38) Beaudelot, J.; Oger, S.; Peruško, S.; Phan, T. A.; Teunens, T.; Moucheron, C.; Evano, G. Photoactive Copper Complexes: Properties and Applications. *Chemical Reviews*. American Chemical Society November 23, 2022, pp 16365–16609. https://doi.org/10.1021/acs.chemrev.2c00033.

(39) Cyclic, T. A.; Amino, A.; Gernert, A. M.; Müller, U.; Haehnel, M.; Pflaum, J.; Steffen, A.; Gernert, M.; Müller, U.; Haehnel, M.; Steffen, A. A Cyclic Alkyl (Amino) Carbene as Two-Atom- Pi -Chromophore Leading to the First Phosphorescent Linear Cu (I) Complexes. No. I. https://doi.org/10.1002/chem.201605412.

(40) Pyykkg, P.; Li, J.; Runeberg, N. *Predicted Ligand Dependence of the Au (I). . .Au (I) Attraction in (XAuPH&*; 1994; Vol. 2.

(41) Harisomayajula, N. V. S.; Makovetskyi, S.; Tsai, Y. C. Cuprophilic Interactions in and between Molecular Entities. *Chemistry - A European Journal*. Wiley-VCH Verlag July 5, 2019, pp 8936–8954. https://doi.org/10.1002/chem.201900332.

(42) Brown, I. D.; Dunitz, J. D. The Crystal Structure of Diazoaminobenzene Copper(I). *Acta Crystallogr* **1961**, *14* (5), 480–485. https://doi.org/10.1107/s0365110x61001546.

(43) Harvey, P. D. The Cu2(C6H5NNNC6H5)2 Dimer. Theoretical and Spectroscopic Investigations of the First Example of a Fluorescent D10-D10 Complex. *Inorg Chem* **1995**, *34* (8), 2019–2024. https://doi.org/10.1021/ic00112a012.

(44) Johnson, A. L.; Willcocks, A. M.; Richards, S. P. Synthesis and Structures of Group 11 Metal Triazenide Complexes: Ligand Supported Metallophilic Interactions. *Inorg Chem* **2009**, *48* (17), 8613–8622. https://doi.org/10.1021/ic901051f.

(45) Ríos-Moreno, G.; Aguirre, G.; Parra-Hake, M.; Walsh, P. J. Synthesis, Characterization, and Structure of Dinuclear Copper(I) and Silver(I) Complexes of Ortho-Functionalized 1,3-Bis(Aryl)Triazenide Ligands. *Polyhedron* **2003**, *22* (4), 563–568. https://doi.org/10.1016/S0277-5387(02)01413-4.

(46) North, A. C. T.; Phillips, D. C.; Mathews, F. S. Experimental and Theoretical Studies of the Copper(I) and Silver(I) Dinuclear N,N'-Tolylformamidinato Complexes. *J. Am. Chem. Soc.* **1988**, *110* (4), 7077–7083.

(47) Jiang, X.; Bollinger, J. C.; Baik, M. H.; Lee, D. Copper Clusters Built on Bulky Amidinate Ligands: Spin Delocalization via Superexchange Rather than Direct Metal-Metal Bonding. *Chemical Communications* **2005**, No. 8, 1043–1045. https://doi.org/10.1039/b412152j.

(48) Jiang, X.; Bollinger, J. C.; Lee, D. How Bulky Is a Bulky Ligand: Energetic Consequences of Steric Constraint in Ligand-Directed Cluster Assembly and

Disassembly. *J Am Chem Soc* **2005**, *127* (45), 15678–15679. https://doi.org/10.1021/ja055225u.

(49) Lane, A. C.; Vollmer, M. V.; Laber, C. H.; Melgarejo, D. Y.; Chiarella, G. M.; Fackler, J. P.; Yang, X.; Baker, G. A.; Walensky, J. R. Multinuclear Copper(I) and Silver(I) Amidinate Complexes: Synthesis, Luminescence, and CS2 Insertion Reactivity. *Inorg Chem* **2014**, *53* (21), 11357–11366. https://doi.org/10.1021/ic501694d.

(50) Coyle, J. P.; Monillas, W. H.; Yap, G. P. A.; Barry, S. T. Synthesis and Thermal Chemistry of Copper (I) Guanidinates. *Inorg Chem* **2008**, *47* (2), 683–689. https://doi.org/10.1021/ic701317y.

(51) Kühnel, E.; Shishkov, I. V.; Rominger, F.; Oeser, T.; Hofmann, P. Synthesis and Structures of Copper(I) Complexes with Phosphino- Functionalized N-Heterocyclic Carbenes (NHCP) and Bis-N-Heterocyclic Carbenes (Bis-NHC). *Organometallics* **2012**, *31* (22), 8000–8011. https://doi.org/10.1021/om300701u.

(52) Liu, B.; Chen, C.; Zhang, Y.; Liu, X.; Chen, W. Dinuclear Copper(I) Complexes of Phenanthrolinyl-Functionalized NHC Ligands. *Organometallics* **2013**, *32* (19), 5451–5460. https://doi.org/10.1021/om400738c.

(53) Nitsch, J.; Lacemon, F.; Lorbach, A.; Eichhorn, A.; Cisnetti, F.; Steffen, A. Cuprophilic Interactions in Highly Luminescent Dicopper(i)-NHC-Picolyl Complexes-Fast Phosphorescence or TADF? *Chemical Communications* **2016**, *52* (14), 2932–2935. https://doi.org/10.1039/c5cc09659f.

(54) Wu, D.; Sedgwick, A.; Gunnlaugsson, T.; Akkaya, E. U.; Yoon, J.; James, T. D. Fluorescent Chrmosensors: The Past, the Present and Future. *Chem Soc Rev* **2017**, *46* (23), 7105. https://doi.org/10.1039/c7cs00240h.

(55) Christie, R. M. *Fluorescent Dyes*; Woodhead Publishing Limited, 2011; Vol. 1. https://doi.org/10.1533/9780857093974.2.562.

(56) Tang, C. W.; Vanslyke, S. A. Organic Electroluminescent Diodes. *Appl Phys Lett* **1987**, *51* (12), 913–915. https://doi.org/10.1063/1.98799.

(57) Hong, G.; Gan, X.; Leonhardt, C.; Zhang, Z.; Seibert, J.; Busch, J. M.; Bräse, S. A Brief History of OLEDs—Emitter Development and Industry Milestones. *Advanced Materials* **2021**, *33* (9). https://doi.org/10.1002/adma.202005630.

(58) Adachi, C.; Baldo, M. A.; Thompson, M. E.; Forrest, S. R. Nearly 100% Internal Phosphorescence Efficiency in an Organic Light Emitting Device. *J Appl Phys* **2001**, *90* (10), 5048–5051. https://doi.org/10.1063/1.1409582.

(59) Baldo, M. A.; Lamansky, S.; Burrows, P. E.; Thompson, M. E.; Forrest, S. R. Very High-Efficiency Green Organic Light-Emitting Devices Based on Electrophosphorescence. *Appl Phys Lett* **1999**, *75* (1), 4–6. https://doi.org/10.1063/1.124258.

(60) Baldo, M. A.; Lamansky, S.; Burrows, P. E.; Thompson, M. E.; Forrest, S. R. Very High-Efficiency Green Organic Light-Emitting Devices Based on Electrophosphorescence. *Appl Phys Lett* **1999**, *75* (1), 4–6. https://doi.org/10.1063/1.124258.

(61) Tung, Y. L.; Wu, P. C.; Liu, C. S.; Chi, Y.; Yu, J. K.; Hu, Y. H.; Chou, P. T.; Peng, S. M.; Lee, G. H.; Tao, Y.; Carty, A. J.; Shu, C. F.; Wu, F. I. Highly Efficient Red Phosphorescent Osmium(II) Complexes for OLED Applications. *Organometallics* **2004**, *23* (15), 3745–3748. https://doi.org/10.1021/om0498246.

(62) Zhu, Z. Q.; Park, C. Do; Klimes, K.; Li, J. Highly Efficient Blue OLEDs Based on Metal-Assisted Delayed Fluorescence Pd(II) Complexes. *Adv Opt Mater* **2019**, *7* (6), 1–6. https://doi.org/10.1002/adom.201801518.

(63) Shafikov, M. Z.; Suleymanova, A. F.; Czerwieniec, R.; Yersin, H. Design Strategy for Ag(I)-Based Thermally Activated Delayed Fluorescence Reaching an Efficiency Breakthrough. *Chemistry of Materials* **2017**, *29* (4), 1708–1715. https://doi.org/10.1021/acs.chemmater.6b05175.

(64) Lakshmanan, R.; Shivaprakash, N. C.; Sindhu, S. Orange Fluorescent Ru(III) Complexes Based on 4′-Aryl Substituted 2,2′:6′,2″-Terpyridine for OLEDs Application. *J Fluoresc* **2018**, *28* (1), 173–182. https://doi.org/10.1007/s10895-017-2180-5.

(65) Wong, Y. S.; Tang, M. C.; Ng, M.; Yam, V. W. W. Toward the Design of Phosphorescent Emitters of Cyclometalated Earth-Abundant Nickel(II) and Their Supramolecular Study. *J Am Chem Soc* **2020**, *142* (16), 7638–7646. https://doi.org/10.1021/jacs.0c02172.

(66) Cope, J. D.; Denny, J. A.; Lamb, R. W.; McNamara, L. E.; Hammer, N. I.; Webster, C. E.; Hollis, T. K. Synthesis, Characterization, Photophysics, and a Ligand Rearrangement of CCC-NHC Pincer Nickel Complexes: Colors, Polymorphs, Emission, and Raman Spectra. *J Organomet Chem* **2017**, *845*, 258–265. https://doi.org/10.1016/j.jorganchem.2017.05.046.

(67) Kjær, K. S.; Kaul, N.; Prakash, O.; Chábera, P.; Rosemann, N. W.; Honarfar, A.; Gordivska, O.; Fredin, L. A.; Bergquist, K. E.; Häggström, L.; Ericsson, T.; Lindh, L.; Yartsev, A.; Styring, S.; Huang, P.; Uhlig, J.; Bendix, J.; Strand, D.; Sundström, V.; Persson, P.; Lomoth, R.; Wärnmark, K. Luminescence and Reactivity of a Charge-Transfer Excited Iron Complex with Nanosecond Lifetime. *Science (1979)* **2019**, *363* (6424), 249–253. https://doi.org/10.1126/science.aau7160.

(68) Chábera, P.; Liu, Y.; Prakash, O.; Thyrhaug, E.; Nahhas, A. El; Honarfar, A.; Essén, S.; Fredin, L. A.; Harlang, T. C. B.; Kjær, K. S.; Handrup, K.; Ericson, F.; Tatsuno, H.; Morgan, K.; Schnadt, J.; Häggström, L.; Ericsson, T.; Sobkowiak, A.; Lidin, S.; Huang, P.; Styring, S.; Uhlig, J.; Bendix, J.; Lomoth, R.; Sundström, V.; Persson, P.; Wärnmark, K. A Low-Spin Fe(III) Complex with 100-Ps Ligand-to-Metal Charge Transfer Photoluminescence. *Nature* **2017**, *543* (7647), 695–699. https://doi.org/10.1038/nature21430.

(69) Kaufhold, S.; Rosemann, N. W.; Chábera, P.; Lindh, L.; Bolaño Losada, I.; Uhlig, J.; Pascher, T.; Strand, D.; Wärnmark, K.; Yartsev, A.; Persson, P. Microsecond Photoluminescence and Photoreactivity of a Metal-Centered Excited State in a Hexacarbene-Co(III) Complex. *J Am Chem Soc* **2021**, *143* (3), 1307–1312. https://doi.org/10.1021/jacs.0c12151.

(70) Conti, C.; Castelli, F.; Forster, L. S. Photophysics of Cr(CN)6 3- and Co(CN)6 3- in Polyalcohol-Water Solutions at Room Temperature. *J Phys Chem* **1979**, *83* (18), 2371–2376.

(71) Leitl, M. J.; Küchle, F. R.; Mayer, H. A.; Wesemann, L.; Yersin, H. Brightly Blue and Green Emitting Cu(I) Dimers for Singlet Harvesting in OLEDs. *Journal of Physical Chemistry A* **2013**, *117* (46), 11823–11836. https://doi.org/10.1021/jp402975d.

(72) Kandasamy, N.; Keerthi, N.; Jeyasekaran, J. Mixed Ligand Copper(I) Complexes as Emitters Enable Higher OLED Device Performance for Energy-Harvesting Applications. *ACS Appl Electron Mater* **2023**, *5* (9), 4805–4815. https://doi.org/10.1021/acsaelm.3c00604.

(73) Ying, A.; Huang, Y. H.; Lu, C. H.; Chen, Z.; Lee, W. K.; Zeng, X.; Chen, T.; Cao, X.; Wu, C. C.; Gong, S.; Yang, C. High-Efficiency Red Electroluminescence Based on a

Carbene-Cu(I)-Acridine Complex. *ACS Appl Mater Interfaces* **2021**, *13* (11), 13478–13486. https://doi.org/10.1021/acsami.0c22109.

(74) Chen, J. X.; Tao, W. W.; Chen, W. C.; Xiao, Y. F.; Wang, K.; Cao, C.; Yu, J.; Li, S.; Geng, F. X.; Adachi, C.; Lee, C. S.; Zhang, X. H. Red/Near-Infrared Thermally Activated Delayed Fluorescence OLEDs with Near 100 % Internal Quantum Efficiency. *Angewandte Chemie - International Edition* **2019**, *58* (41), 14660–14665. https://doi.org/10.1002/anie.201906575.

(75) Uoyama, H.; Goushi, K.; Shizu, K.; Nomura, H.; Adachi, C. Highly Efficient Organic Light-Emitting Diodes from Delayed Fluorescence. *Nature* **2012**, *492* (7428), 234–238. https://doi.org/10.1038/nature11687.

(76) Chen, X. K.; Kim, D.; Brédas, J. L. Thermally Activated Delayed Fluorescence (TADF) Path toward Efficient Electroluminescence in Purely Organic Materials: Molecular Level Insight. *Acc Chem Res* **2018**, *51* (9), 2215–2224. https://doi.org/10.1021/acs.accounts.8b00174.

(77) Kyle, K. R.; Palke, W. E.; Ford, P. C. The Photoluminescence Properties of the Copper(I) Clusters Cu4I4A4 (A = Aromatic Amine) in Solution. *Coord Chem Rev* **1990**, *97* (C), 35–46. https://doi.org/10.1016/0010-8545(90)80078-8.

(78) Wang, J. J.; Chen, C.; Chen, W. G.; Yao, J. S.; Yang, J. N.; Wang, K. H.; Yin, Y. C.; Yao, M. M.; Feng, L. Z.; Ma, C.; Fan, F. J.; Yao, H. Bin. Highly Luminescent Copper Iodide Cluster Based Inks with Photoluminescence Quantum Efficiency Exceeding 98%. *J Am Chem Soc* **2020**, *142* (8), 3686–3690. https://doi.org/10.1021/jacs.9b12908.

(79) Churchill, M. R.; Bezman, S. A.; Osborn, J. A.; Wormald, J. Synthesis and Molecular Geometry of Hexameric Triphenylphosphinocopper(I) Hydride and the Crystal Structure of H6Cu6(PPh3)6 HCONMe2. *Inorg Chem* **1972**, *11* (8), 1818–1825.

(80) Hardt, H. D.; Pierre, A. Fluorescence Thermochromism of Pyridine Copper Iodides and Copper Iodide. *ZAAC - Journal of Inorganic and General Chemistry* **1973**, *402* (1), 107–112. https://doi.org/10.1002/zaac.19734020113.

(81) Chan, C. L.; Cheung, K. L.; Lam, W. H.; Cheng, E. C. C.; Zhu, N.; Choi, S. W. K.; Yam, V. W. W. Luminescent Molecular Copper(I) Alkynyl Open Cubes: Synthesis, Structural Characterization, Electronic Structure, Photophysics, and Photochemistry. *Chem Asian J* **2006**, *1* (1–2), 273–286. https://doi.org/10.1002/asia.200600067.

(82) Khatri, N. M.; Pablico-lansigan, M. H.; Boncher, W. L.; Mertzman, J. E.; Labatete, A. C.; Grande, L. M.; Wunder, D.; Prushan, M. J.; Zhang, W.; Halasyamani, P. S.; Monteiro, J. H. S. K.; Bettencourt-dias, A. De; Stoll, S. L. Luminescence and Nonlinear Optical Properties in Copper(I) Halide Extended Networks. **2016**, No. I. https://doi.org/10.1021/acs.inorgchem.6b01879.

(83) Kim, T. H.; Shin, Y. W.; Jung, J. H.; Kim, J. S.; Kim, J. Crystal-to-Crystal Transformation between Three Cu I Coordination Polymers and Structural Evidence for Luminescence. **2008**, 685–688. https://doi.org/10.1002/anie.200704349.

(84) Bondi, A. Van Der Waals Volumes and Radii. *Journal of Physical Chemistry* **1964**, *68* (3), 441–451.

(85) Harisomayajula, N. V. S.; Makovetskyi, S.; Tsai, Y. C. Cuprophilic Interactions in and between Molecular Entities. *Chemistry - A European Journal* **2019**, *25* (38), 8936–8954. https://doi.org/10.1002/chem.201900332.

(86) Leitl, M. J.; Zink, D. M.; Schinabeck, A.; Baumann, T.; Volz, D.; Yersin, H. Copper(I) Complexes for Thermally Activated Delayed Fluorescence: From Photophysical to Device Properties. *Topics in Current Chemistry*. Springer Verlag June 1, 2016. https://doi.org/10.1007/s41061-016-0019-1.

(87) Wang, Z.; Zheng, C.; Wang, W.; Xu, C.; Ji, B.; Zhang, X. Synthesis, Structure, and Photophysical Properties of Two Four-Coordinate CuI-NHC Complexes with Efficient Delayed Fluorescence. *Inorg Chem* **2016**, *55* (5), 2157–2164. https://doi.org/10.1021/acs.inorgchem.5b02546.

(88) Cyclic, T. A.; Amino, A.; Gernert, A. M.; Müller, U.; Haehnel, M.; Pflaum, J.; Steffen, A.; Gernert, M.; Müller, U.; Haehnel, M.; Steffen, A. A Cyclic Alkyl (Amino) Carbene as Two-Atom- Pi -Chromophore Leading to the First Phosphorescent Linear Cu (I) Complexes. No. I. https://doi.org/10.1002/chem.201605412.

(89) Wei, W.; Lu, Y.; Chen, W.; Chen, S. One-Pot Synthesis, Photoluminescence, and Electrocatalytic Properties of Subnanometer-Sized Copper Clusters. *J Am Chem Soc* **2011**, *133* (7), 2060–2063. https://doi.org/10.1021/ja109303z.

(90) Osawa, M.; Hoshino, M.; Hashimoto, M.; Kawata, I.; Igawa, S.; Yashima, M. Application of Three-Coordinate Copper(i) Complexes with Halide Ligands in Organic Light-Emitting

Diodes That Exhibit Delayed Fluorescence. *Dalton Transactions* **2015**, *44* (18), 8369–8378. https://doi.org/10.1039/c4dt02853h.

(91) Igawa, S.; Hashimoto, M.; Kawata, I.; Yashima, M.; Hoshino, M.; Osawa, M. Highly Efficient Green Organic Light-Emitting Diodes Containing Luminescent Tetrahedral Copper(i) Complexes. *J Mater Chem C Mater* **2013**, *1* (3), 542–551. https://doi.org/10.1039/c2tc00263a.

(92) Lotito, K. J.; Peters, J. C. Efficient Luminescence from Easily Prepared Three-Coordinate Copper (I) Arylamidophosphines w. **2010**, 3690–3692. https://doi.org/10.1039/c000818d.

(93) Krylova, V. A.; Djurovich, P. I.; Whited, M. T.; Thompson, M. E. Synthesis and Characterization of Phosphorescent Three-Coordinate Cu (I)– NHC Complexes w. **2010**, 6696–6698. https://doi.org/10.1039/c0cc01864c.

(94) Brown, I. D.; Dunitz, J. D. The Crystal Structure of Diazoaminobenzene Copper(I). *Acta Crystallogr* **1961**, *14* (5), 480–485. https://doi.org/10.1107/s0365110x61001546.

(95) Harvey, P. D. The Cu2(C6H5NNNC6H5)2 Dimer. Theoretical and Spectroscopic Investigations of the First Example of a Fluorescent D10-D10 Complex. *Inorg Chem* **1995**, *34* (8), 2019–2024. https://doi.org/10.1021/ic00112a012.

(96) Johnson, A. L.; Willcocks, A. M.; Richards, S. P. Synthesis and Structures of Group 11 Metal Triazenide Complexes: Ligand Supported Metallophilic Interactions. *Inorg Chem* **2009**, *48* (17), 8613–8622. https://doi.org/10.1021/ic901051f.

(97) Ríos-Moreno, G.; Aguirre, G.; Parra-Hake, M.; Walsh, P. J. Synthesis, Characterization, and Structure of Dinuclear Copper(I) and Silver(I) Complexes of Ortho-Functionalized 1,3-Bis(Aryl)Triazenide Ligands. *Polyhedron* **2003**, *22* (4), 563–568. https://doi.org/10.1016/S0277-5387(02)01413-4.

(98) Lane, A. C.; Vollmer, M. V; Laber, C. H.; Melgarejo, D. Y.; Chiarella, G. M.; Fackler, J. P.; Yang, X.; Baker, G. A.; Walensky, J. R. Multinuclear Copper(I) and Silver(I) Amidinate Complexes: Synthesis, Luminescence, and CS 2 Insertion Reactivity. **2014**, No. I.

(99) Hong, G.; Gan, X.; Leonhardt, C.; Zhang, Z.; Seibert, J.; Busch, J. M.; Bräse, S. A Brief History of OLEDs—Emitter Development and Industry Milestones. *Advanced Materials* **2021**, *33* (9). https://doi.org/10.1002/adma.202005630.

(100) Sano, T.; Fujita, M.; Fujii, T.; Hamada, Y.; Shibata, K.; Kuroki, K. Novel Europium Complex for Electroluminescent Devices with Sharp Red Emission. *Jpn. J. Appl. Phys.* **1995**, *34*, 1883–1887.

(101) Segura, J. L. The Chemistry of Electroluminescent Organic Materials. *Acta Polymerica* **1998**, *49* (7), 319–344. https://doi.org/10.1002/(SICI)1521-4044(199807)49:7<319::AID-APOL319>3.0.CO;2-Q.

(102) Forster, Th.; Kasper, K. Elin Konzentrationsumschlag Der Fluoreszenz. *Zeitschrift fur physikalische Chemie.* **1954**, *1* (56), 275–277.

(103) Birks, J. B. *Photophysics of Aromatic Molecules*; Wiley-InterScience, Ed.; London, 1970.

(104) Luo, J.; Xie, Z.; Xie, Z.; Lam, J. W. Y.; Cheng, L.; Chen, H.; Qiu, C.; Kwok, H. S.; Zhan, X.; Liu, Y.; Zhu, D.; Tang, B. Z. Aggregation-Induced Emission of 1-Methyl-1,2,3,4,5-Pentaphenylsilole. *Chemical Communications* **2001**, *18*, 1740–1741. https://doi.org/10.1039/b105159h.

(105) Hartough, H. D.; Kosak, A. I. Acylation Studies in the Thiophene and Furan Series. I. Iodine and Hydriodic Acid Catalyts. *J Am Chem Soc* **1946**, *68* (12), 2639–2641. https://doi.org/10.1021/ja01216a064.

(106) Wan, C.; Song, R. J.; Li, J. H. Electrooxidative 1,2-Bromoesterification of Alkenes with Acids and N-Bromosuccinimide. *Org Lett* **2019**, *21* (8), 2800–2803. https://doi.org/10.1021/acs.orglett.9b00771.

(107) Kannasani, R. K.; Peruri, V. V. S.; Battula, S. R. NaHSO4-SiO2 as an Efficient and Chemoselective Catalyst, for the Synthesis of Acylal from Aldehydes under, Solvent-Free Conditions. *Chem Cent J* **2012**, *6* (1), 6–9. https://doi.org/10.1186/1752-153X-6-136.

(108) Chang-Chih, H.; Wan-Jung, C.; Yih-Chern, H.; Lee, H. M. Synthesis and Characterization of Nickel(II) Complex Containing 2-(t-Butylaminomethyl)Pyrrole. *Journal of the Chinese Chemical Society* **2009**, *56* (2), 435–442. https://doi.org/10.1002/jccs.200900065.

(109) Belo, D.; Almeida, M. Transition Metal Complexes Based on Thiophene-Dithiolene Ligands. *Coord Chem Rev* **2010**, *254* (13–14), 1479–1492. https://doi.org/10.1016/j.ccr.2009.12.011.

(110) Olaru, M.; Rychagova, E.; Ketkov, S.; Shynkarenko, Y.; Yakunin, S.; Kovalenko, M. V.; Yablonskiy, A.; Andreev, B.; Kleemiss, F.; Beckmann, J.; Vogt, M. A Small Cationic

Organo-Copper Cluster as Thermally Robust Highly Photo- And Electroluminescent Material. *J Am Chem Soc* **2020**, *142* (1), 373–381. https://doi.org/10.1021/jacs.9b10829.

(111) Cotton, F. A.; Feng, X.; Matusz, M.; Poli, R. Experimental and Theoretical Studies of the Copper (I) and Silver (I) Dinuclear N,N-Di-p-Tolylformamidinato Complexes. *Journal of American Chemical Society* **1988**, No. I, 7077–7083.

(112) Schmidbaur, H.; Schier, A. Argentophilic Interactions. *Angewandte Chemie - International Edition* **2015**, *54* (3), 746–784. https://doi.org/10.1002/anie.201405936.

(113) Van Alem, K.; Belder, G.; Lodder, G.; Zuilhof, H. Photochemical Generation of Highly Destabilized Vinyl Cations: The Effects of α- and β-Trifluoromethyl versus α- and β-Methyl Substituents. *Journal of Organic Chemistry* **2005**, *70* (1), 179–190. https://doi.org/10.1021/jo0487956.

(114) Kannasani, R. K.; Peruri, V. V. S.; Battula, S. R. NaHSO4-SiO2 as an Efficient and Chemoselective Catalyst, for the Synthesis of Acylal from Aldehydes under, Solvent-Free Conditions. *Chem Cent J* **2012**, *6* (1), 6–9. https://doi.org/10.1186/1752-153X-6-136.

(115) Hartough, H. D.; Kosak, A. I. Acylation Studies in the Thiophene and Furan Series. I. Iodine and Hydriodic Acid Catalyts. *J Am Chem Soc* **1946**, *68* (12), 2639–2641. https://doi.org/10.1021/ja01216a064.

(116) Zhao, D.; Yu, S.; Jiang, W. J.; Cai, Z. H.; Li, D. L.; Liu, Y. L.; Chen, Z. Z. Recent Progress in Metal-Organic Framework Based Fluorescent Sensors for Hazardous Materials Detection. *Molecules*. MDPI April 1, 2022. https://doi.org/10.3390/molecules27072226.

(117) Sun, X.; Wang, Y.; Lei, Y. Fluorescence Based Explosive Detection: From Mechanisms to Sensory Materials. *Chemical Society Reviews*. Royal Society of Chemistry November 21, 2015, pp 8019–8061. https://doi.org/10.1039/c5cs00496a.

(118) Hazra, A.; Mondal, U.; Mandal, S.; Banerjee, P. Advancement in Functionalized Luminescent Frameworks and Their Prospective Applications as Inkjet-Printed Sensors and Anti-Counterfeit Materials. *Dalton Transactions* **2021**, *50* (25), 8657–8670. https://doi.org/10.1039/d1dt00705j.

(119) Man, Z.; Lv, Z.; Xu, Z.; Liao, Q.; Liu, J.; Liu, Y.; Fu, L.; Liu, M.; Bai, S.; Fu, H. Highly Sensitive and Easily Recoverable Excitonic Piezochromic Fluorescent Materials for

Haptic Sensors and Anti-Counterfeiting Applications. *Adv Funct Mater* **2020**, *30* (17). https://doi.org/10.1002/adfm.202000105.

(120) Zhang, Y.; Yang, H.; Ma, H.; Bian, G.; Zang, Q.; Sun, J.; Zhang, C.; An, Z.; Wong, W. Excitation Wavelength Dependent Fluorescence of an ESIPT Triazole Derivative for Amine Sensing and Anti-Counterfeiting Applications. *Angewandte Chemie* **2019**, *131* (26), 8865–8870. https://doi.org/10.1002/ange.201902890.

(121) Cinquino, M.; Prontera, C. T.; Pugliese, M.; Giannuzzi, R.; Taurino, D.; Gigli, G.; Maiorano, V. Light-Emitting Textiles: Device Architectures, Working Principles, and Applications. *Micromachines (Basel)* **2021**, *12* (6). https://doi.org/10.3390/mi12060652.

(122) Ramlow, H.; Andrade, K. L.; Immich, A. P. S. Smart Textiles: An Overview of Recent Progress on Chromic Textiles. *Journal of the Textile Institute*. Taylor and Francis Ltd. 2021, pp 152–171. https://doi.org/10.1080/00405000.2020.1785071.

(123) Wang, Y.; Shi, J.; Chen, J.; Zhu, W.; Baranoff, E. Recent Progress in Luminescent Liquid Crystal Materials: Design, Properties and Application for Linearly Polarised Emission. *Journal of Materials Chemistry C*. Royal Society of Chemistry August 21, 2015, pp 7993–8005. https://doi.org/10.1039/c5tc01565k.

(124) Schadt, M. *LIQUID CRYSTAL MATERIALS AND LIQUID CRYSTAL DISPLAYS*; 2024; Vol. 27. www.annualreviews.org.

(125) Zhao, M.; Zhang, Q.; Xia, Z. Narrow-Band Emitters in LED Backlights for Liquid-Crystal Displays. *Materials Today*. Elsevier B.V. November 1, 2020, pp 246–265. https://doi.org/10.1016/j.mattod.2020.04.032.

(126) Teng, J. M.; Wang, Y. F.; Chen, C. F. Recent Progress of Narrowband TADF Emitters and Their Applications in OLEDs. *Journal of Materials Chemistry C*. Royal Society of Chemistry September 7, 2020, pp 11340–11353. https://doi.org/10.1039/d0tc02682d.

(127) Zhu, Z. Q.; Park, C. Do; Klimes, K.; Li, J. Highly Efficient Blue OLEDs Based on Metal-Assisted Delayed Fluorescence Pd(II) Complexes. *Adv Opt Mater* **2019**, *7* (6), 1–6. https://doi.org/10.1002/adom.201801518.

(128) Leitl, M. J.; Zink, D. M.; Schinabeck, A.; Baumann, T.; Volz, D.; Yersin, H. Copper(I) Complexes for Thermally Activated Delayed Fluorescence: From Photophysical to Device Properties. *Topics in Current Chemistry*. Springer Verlag June 1, 2016. https://doi.org/10.1007/s41061-016-0019-1.

(129) Chang-Chih, H.; Wan-Jung, C.; Yih-Chern, H.; Lee, H. M. Synthesis and Characterization of Nickel(II) Complex Containing 2-(t-Butylaminomethyl)Pyrrole. *Journal of the Chinese Chemical Society* **2009**, *56* (2), 435–442. https://doi.org/10.1002/jccs.200900065.

(130) Shimizu, A.; Ishizaki, Y.; Horiuchi, S.; Hirose, T.; Matsuda, K.; Sato, H.; Yoshida, J. I. HOMO-LUMO Energy-Gap Tuning of π-Conjugated Zwitterions Composed of Electron-Donating Anion and Electron-Accepting Cation. *Journal of Organic Chemistry* **2021**, *86* (1), 770–781. https://doi.org/10.1021/acs.joc.0c02343.

(131) Bondi, A. Van Der Waals Volumes and Radii. *Journal of Physical Chemistry* **1964**, *68* (3), 441–451.

(132) Linder, M. C.; Hazegh-Azam, M. *Copper Biochemistry and Molecular Biology"2*; 1996; Vol. 63.

(133) Frieden, E. THE BIOCHEMISTRY OF COPPER. **1968**, *218* (5), 102–115. https://doi.org/10.2307/24926232.

(134) Tsang, T.; Davis, C. I.; Brady, D. C. Copper Biology. *Current Biology* **2021**, *31* (9), R421–R427. https://doi.org/10.1016/j.cub.2021.03.054.

(135) Harris, E. D. Copper Transport: An Overview. *Proceedings of the Society for Experimental Biology and Medicine* **1991**, *196* (2), 130–140. https://doi.org/10.3181/00379727-196-43171B.

(136) Ley, S. V.; Thomas, A. W. Modern Synthetic Methods for Copper-Mediated C(Aryl)-O, C(Aryl)-N, and C(Aryl)-S Bond Formation. *Angewandte Chemie - International Edition*. November 17, 2003, pp 5400–5449. https://doi.org/10.1002/anie.200300594.

(137) Evano, G.; Blanchard, N.; Toumi, M. Copper-Mediated Coupling Reactions and Their Applications in Natural Products and Designed Biomolecules Synthesis. *Chemical Reviews*. American Chemical Society 2008, pp 3054–3131. https://doi.org/10.1021/cr8002505.

(138) Shiri, P.; Cui, H.; Zhang, K.; Liu, W.; Zhang, L. Asymmetric Synthesis by Artificial Copper Biocatalysts. *Coordination Chemistry Reviews*. Elsevier B.V. August 1, 2024. https://doi.org/10.1016/j.ccr.2024.215898.

(139) Hemming, D.; Fritzemeier, R.; Westcott, S. A.; Santos, W. L.; Steel, P. G. Copper-Boryl Mediated Organic Synthesis. *Chemical Society reviews*. NLM (Medline) October 1, 2018, pp 7477–7494. https://doi.org/10.1039/c7cs00816c.

(140) Messerschmidt, A. *Metal Sites in Small Blue Copper Proteins, Blue Copper Oxidases and Vanadium-Containing Enzymes 1.2.4*; 1998.

(141) Canters, G. W.; Gilardi, G. *Engineering Type 1 Copper Sites in Proteins*; European Biochemical Societies, 1993; Vol. 325.

(142) McGuirl, M. A.; Dooley, D. M. Copper Proteins with Type 2 Sites. In *Encyclopedia of Inorganic Chemistry*; Wiley, 2005. https://doi.org/10.1002/0470862106.ia294.

(143) MacPherson, I. S.; Murphy, M. E. P. Type-2 Copper-Containing Enzymes. *Cellular and Molecular Life Sciences*. November 2007, pp 2887–2899. https://doi.org/10.1007/s00018-007-7310-9.

(144) Itoh, S.; Fukuzumi, S. Monooxygenase Activity of Type 3 Copper Proteins. In *Accounts of Chemical Research*; 2007; Vol. 40, pp 592–600. https://doi.org/10.1021/ar6000395.

(145) Kaintz, C.; Mauracher, S. G.; Rompel, A. Type-3 Copper Proteins: Recent Advances on Polyphenol Oxidases. In *Advances in Protein Chemistry and Structural Biology*; Academic Press Inc., 2014; Vol. 97, pp 1–35. https://doi.org/10.1016/bs.apcsb.2014.07.001.

(146) Pauleta, S. R.; Dell'Acqua, S.; Moura, I. Nitrous Oxide Reductase. *Coordination Chemistry Reviews*. January 5, 2013, pp 332–349. https://doi.org/10.1016/j.ccr.2012.05.026.

(147) Hardt, H. D.; Pierre, A. Fluorescence Thermochromism of Pyridine Copper Iodides and Copper Iodide. *ZAAC - Journal of Inorganic and General Chemistry* **1973**, *402* (1), 107–112. https://doi.org/10.1002/zaac.19734020113.

(148) Chan, C. L.; Cheung, K. L.; Lam, W. H.; Cheng, E. C. C.; Zhu, N.; Choi, S. W. K.; Yam, V. W. W. Luminescent Molecular Copper(I) Alkynyl Open Cubes: Synthesis, Structural Characterization, Electronic Structure, Photophysics, and Photochemistry. *Chem Asian J* **2006**, *1* (1–2), 273–286. https://doi.org/10.1002/asia.200600067.

(149) Khatri, N. M.; Pablico-lansigan, M. H.; Boncher, W. L.; Mertzman, J. E.; Labatete, A. C.; Grande, L. M.; Wunder, D.; Prushan, M. J.; Zhang, W.; Halasyamani, P. S.; Monteiro, J. H. S. K.; Bettencourt-dias, A. De; Stoll, S. L. Luminescence and Nonlinear Optical Properties in Copper(I) Halide Extended Networks. **2016**, No. I. https://doi.org/10.1021/acs.inorgchem.6b01879.

(150) Cammarota, R. C.; Clouston, L. J.; Lu, C. C. Leveraging Molecular Metal–Support Interactions for H2 and N2 Activation. *Coordination Chemistry Reviews*. Elsevier B.V. March 1, 2017, pp 100–111. https://doi.org/10.1016/j.ccr.2016.06.014.

(151) Krogman, J. P.; Thomas, C. M. Metal–Metal Multiple Bonding in C3-Symmetric Bimetallic Complexes of the First Row Transition Metals. *Chemical Communications* **2014**, *50* (40), 5115–5127. https://doi.org/10.1039/c3cc47537a.

(152) Pye, D. R.; Mankad, N. P. Bimetallic Catalysis for C-C and C-X Coupling Reactions. *Chem Sci* **2017**, *8* (3), 1705–1718. https://doi.org/10.1039/c6sc05556g.

(153) Wing-Wah Yam, V.; Kam-Wing Lo, K.; Kit-Ma, W.; Wang, C.-R. *Design of Luminescent Poi[Ynuclear Copper(I) and Sitver(t) Complexes with Chalcogenides and Ace~ylides as the Bridging Iigand s*.

(154) Wang, J. J.; Chen, C.; Chen, W. G.; Yao, J. S.; Yang, J. N.; Wang, K. H.; Yin, Y. C.; Yao, M. M.; Feng, L. Z.; Ma, C.; Fan, F. J.; Yao, H. Bin. Highly Luminescent Copper Iodide Cluster Based Inks with Photoluminescence Quantum Efficiency Exceeding 98%. *J Am Chem Soc* **2020**, *142* (8), 3686–3690. https://doi.org/10.1021/jacs.9b12908.

(155) Lotito, K. J.; Peters, J. C. Efficient Luminescence from Easily Prepared Three-Coordinate Copper (I) Arylamidophosphines w. **2010**, 3690–3692. https://doi.org/10.1039/c000818d.

(156) Wei, W.; Lu, Y.; Chen, W.; Chen, S. One-Pot Synthesis, Photoluminescence, and Electrocatalytic Properties of Subnanometer-Sized Copper Clusters. *J Am Chem Soc* **2011**, *133* (7), 2060–2063. https://doi.org/10.1021/ja109303z.

(157) Lotito, K. J.; Peters, J. C. Efficient Luminescence from Easily Prepared Three-Coordinate Copper (I) Arylamidophosphines w. **2010**, 3690–3692. https://doi.org/10.1039/c000818d.

(158) Olaru, M.; Rychagova, E.; Ketkov, S.; Shynkarenko, Y.; Yakunin, S.; Kovalenko, M. V; Yablonskiy, A.; Andreev, B.; Kleemiss, F.; Beckmann, J.; Vogt, M. A Small Cationic Organo-Copper Cluster as Thermally Robust Highly Photo- And Electroluminescent Material. *J Am Chem Soc* **2020**, *142* (1), 373–381. https://doi.org/10.1021/jacs.9b10829.

(159) Igawa, S.; Hashimoto, M.; Kawata, I.; Yashima, M.; Hoshino, M.; Osawa, M. Highly Efficient Green Organic Light-Emitting Diodes Containing Luminescent Tetrahedral

Copper(i) Complexes. *J Mater Chem C Mater* **2013**, *1* (3), 542–551. https://doi.org/10.1039/c2tc00263a.

(160) Trowbridge, L.; Averkiev, B.; Sues, P. E. Palladium Complexes Bearing Calixpyrrole Ligands with Pendant Hydrogen Bond Donors: Synthesis, Structural Characterization, Electrochemistry and Dihydrogen Evolution. *Polyhedron* **2022**, *225*. https://doi.org/10.1016/j.poly.2022.116046.

(161) Trowbridge, L.; Averkiev, B.; Sues, P. E. Electrocatalytic Hydrogen Evolution Using a Nickel-Based Calixpyrrole Complex: Controlling the Secondary Coordination Sphere on an Electrode Surface. *Chemistry - A European Journal* **2023**, *29* (65). https://doi.org/10.1002/chem.202301920.

(162) Somachandra, M. S.; Averkiev, B.; Sues, P. E. Unsymmetric Co-Facial "Salixpyrrole" Hydrogen Evolution Catalysts: Two Metals Are Better than One. *Inorg Chem* **2024**, *63* (29), 13346–13357. https://doi.org/10.1021/acs.inorgchem.4c01101.

(163) Cuesta, L.; Gross, D.; Lynch, V. M.; Ou, Z.; Kajonkijya, W.; Ohkubo, K.; Fukuzumi, S.; Kadish, K. M.; Sessler, J. L. Design and Synthesis of Polymetallic Complexes Based on Meso-Calix[4]Pyrrole: Platforms for Multielectron Chemistry. *J Am Chem Soc* **2007**, *129* (38), 11696–11697. https://doi.org/10.1021/ja075613r.

(164) Veauthier, J. M.; Tomat, E.; Lynch, V. M.; Sessler, J. L.; Mirsaidov, U.; Markert, J. T. Calix[4]Pyrrole Schiff Base Macrocycles: Novel Binucleating Ligands for Cu(I) and Cu(II). *Inorg Chem* **2005**, *44* (19), 6736–6743. https://doi.org/10.1021/ic050690d.

(165) Love, J. B.; Blake, A. J.; Wilson, C.; Reid, S. D.; Novak, A.; Hitchcock, P. B. The Syntheses and Structures of Group 1 Expanded Dipyrrolides: The Formation of a 12-Rung Amidolithium Circular Ladder. *Chemical Communications* **2003**, *3* (14), 1682–1683. https://doi.org/10.1039/b303611a.

(166) Reid, S. D.; Blake, A. J.; Wilson, C.; Love, J. B. Syntheses and Structures of Dinuclear Double-Stranded Helicates of Divalent Manganese, Iron, Cobalt, and Zinc. *Inorg Chem* **2006**, *45* (2), 636–643. https://doi.org/10.1021/ic051433b.

(167) Wu, D.; Sedgwick, A.; Gunnlaugsson, T.; Akkaya, E. U.; Yoon, J.; James, T. D. Fluorescent Chrmosensors: The Past, the Present and Future. *Chem Soc Rev* **2017**, *46* (23), 7105. https://doi.org/10.1039/c7cs00240h.

(168) Lakshmanan, R.; Shivaprakash, N. C.; Sindhu, S. Orange Fluorescent Ru(III) Complexes Based on 4′-Aryl Substituted 2,2′:6′,2″-Terpyridine for OLEDs Application. *J Fluoresc* **2018**, *28* (1), 173–182. https://doi.org/10.1007/s10895-017-2180-5.

(169) Feng, X.; Yang, J. G.; Miao, J.; Zhong, C.; Yin, X.; Li, N.; Wu, C.; Zhang, Q.; Chen, Y.; Li, K.; Yang, C. Au···H−C Interactions Support a Robust Thermally Activated Delayed Fluorescence (TADF) Gold(I) Complex for OLEDs with Little Efficiency Roll-Off and Good Stability. *Angewandte Chemie - International Edition* **2022**, *61* (40). https://doi.org/10.1002/anie.202209451.

(170) Leitl, M. J.; Küchle, F. R.; Mayer, H. A.; Wesemann, L.; Yersin, H. Brightly Blue and Green Emitting Cu(I) Dimers for Singlet Harvesting in OLEDs. *Journal of Physical Chemistry A* **2013**, *117* (46), 11823–11836. https://doi.org/10.1021/jp402975d.

(171) Jankus, V.; Data, P.; Graves, D.; McGuinness, C.; Santos, J.; Bryce, M. R.; Dias, F. B.; Monkman, A. P. Highly Efficient TADF OLEDs: How the Emitter-Host Interaction Controls Both the Excited State Species and Electrical Properties of the Devices to Achieve near 100% Triplet Harvesting and High Efficiency. *Adv Funct Mater* **2014**, *24* (39), 6178–6186. https://doi.org/10.1002/adfm.201400948.

(172) Kandasamy, N.; Keerthi, N.; Jeyasekaran, J. Mixed Ligand Copper(I) Complexes as Emitters Enable Higher OLED Device Performance for Energy-Harvesting Applications. *ACS Appl Electron Mater* **2023**, *5* (9), 4805–4815. https://doi.org/10.1021/acsaelm.3c00604.

(173) Stollenz, M.; Raymond, J. E.; Pérez, L. M.; Wiederkehr, J.; Bhuvanesh, N. Highly Luminescent Linear Complex Arrays of up to Eight Cuprous Centers. *Chemistry - A European Journal* **2016**, *22* (7), 2396–2405. https://doi.org/10.1002/chem.201503869.

(174) Trose, M.; Nahra, F.; Cazin, C. S. J. Dinuclear N-Heterocyclic Carbene Copper(I) Complexes. *Coordination Chemistry Reviews*. Elsevier B.V. January 15, 2018, pp 380–403. https://doi.org/10.1016/j.ccr.2017.10.013.

(175) Tsuge, K.; Chishina, Y.; Hashiguchi, H.; Sasaki, Y.; Kato, M.; Ishizaka, S.; Kitamura, N. Luminescent Copper(I) Complexes with Halogenido-Bridged Dimeric Core. *Coordination Chemistry Reviews*. Elsevier January 1, 2016, pp 636–651. https://doi.org/10.1016/j.ccr.2015.03.022.

(176) Mensah, A.; Shao, J. J.; Ni, J. L.; Li, G. J.; Wang, F. M.; Chen, L. Z. Recent Progress in Luminescent Cu(I) Halide Complexes: A Mini-Review. *Frontiers in Chemistry*. Frontiers Media S.A. January 25, 2022. https://doi.org/10.3389/fchem.2021.816363.

(177) Curcio, M.; Pankhurst, J. R.; Sproules, S.; Mignard, D.; Love, J. B. Triggering Redox Activity in a Thiophene Compound: Radical Stabilization and Coordination Chemistry. *Angewandte Chemie - International Edition* **2017**, *56* (27), 7939–7943. https://doi.org/10.1002/anie.201703576.